Design, Synthesis and Characterization of Zinc-sensitive or Dual-modal Probes for Optical and Magnetic Resonance Imaging

Design, Synthese und Charakterizierung von zinkempfindlichen oder dual-modalen Sonden für die Optische und Magnetresonanztomographie

Dissertation

der Mathematisch-Naturwissenschaftlichen Fakultät

der Eberhard Karls Universität Tübingen

zur Erlangung des Grades eines

Doktors der Naturwissenschaften

(Dr. rer. nat.)

vorgelegt von

Gaoji Wang

aus Gansu/China

Tübingen

2020

Gedruckt mit Genehmigung der Mathematisch-Naturwissenschaftlichen Fakultät der Eberhard Karls Universität Tübingen.

Tag der mündlichen Qualifikation:	11.03.2021
Stellvertretender Dekan:	Prof. Dr. József Fortágh
1. Berichterstatter:	Prof. Dr. Klaus Scheffler
2. Berichterstatter:	Priv.–Doz. Dr. Goran Angelovski

This doctoral thesis was carried out at the Research Group of MR Neuroimaging Agents of the Max Planck Institute for Biological Cybernetics, Tübingen under the supervision of Priv.–Doz. Dr. Goran Angelovski and Prof. Dr. Klaus Scheffler during the period from October 2016 to October 2020 and in partial collaboration with Prof. Dr. Carlos Platas-Iglesias at the Centro de Investigacións Científicas Avanzadas (CICA) and Departamento de Química, Facultade de Ciencias, Universidade da Coruña, A Coruña, Spain.

Here I declare the fact that I am writing this work and no different than the indicated aids have been used.

Tübingen, December, 2020

Acknowledgements

First and foremost, I would like to express my special thanks to my principal supervisor Priv.–Doz. Dr. Goran Angelovski who paid patience during my PhD study and research for providing advice, encouragement and motivation. Specially, his methodical mind inspired me a lot. He managed group journal club and progress reports and let us share and discuss our research, as well as funny life stories.

Then, I would like to thank Prof. Dr. Klaus Scheffler, who generously provided some experimental equipment for us, making my research quite convenient. I am very glad to have him to be my second supervisor.

I would like to thank my first project collaborator, Prof. Dr. Carlos Platas-Iglesias who did DFT calculations for my luminescent probes and push the study to a deeper understanding. I am very impressed with his always positive and professional suggestions and a broad horizon in his research.

I wish to express my deepest thanks to all my colleagues in Goran's group: Giuseppe, Tanja, Liam, Yulia and Djordje, as well as the visiting members Ben, Rosa and Irene. During my Ph.D. study, we enjoyed talking about our research and questions. We had much nice lunchtime and great BBQ parties. All these different experiences in Germany comparing life in China broadened my horizon and enriched my life. This will be a treasure in my future life.

I would like to thank the friends in Tuebingen, especially Chenghao, Yapeng, Min, Yuan, Milan, Jia, Haokai and friends at MPI like Kengo, Philip and Katya.

I would like to thank Petra Krüger and Dr. Dorothee Wistuba at Tuebingen University for elemental analysis and high-resolution mass measurements. I also thank Michael, Hildegard, Vincent and Conchy at MPI.

The financial support of the Max-Planck Society and the China Scholarship Council (CSC, Ph.D. fellowship) is gratefully acknowledged.

Finally, I thank all my family for their support throughout my Ph.D. study. Especially, I thank my wife Yuhan for her love, understanding, encouragement and support.

Table of Contents

Abbreviations

Boc	*tert*-butoxycarbonyl
Bn	Benzyl
Bn-DO1A	(1,4,7,10-Tetraaza-cyclododec-1-yl)-acetic acid benzyl ester
BOLD	Blood-oxygen-level dependent
CA	Contrast agent
Cbz	Carboxybenzyl
CEST	Chemical exchange saturation transfer
CT	Computed tomography
DBU	1,8-Diazabicycloundec-7-ene
DA18C6	1,10-Diaza-18-crown-6
DFT	Density-functional theory
DO3A	1,4,7,10-Tetraazacyclododecane-1,4,7-trisacetic acid
DOTA	1,4,7,10-Tetraazacyclododecane-1,4,7,10-tetraacetic acid
DOTAM	1,4,7,10-Tetrakis(carbamoylmethyl)-1,4,7,10-tetraazacyclododecane
DPA	Di-(2-picolyl)amine
DTPA	Diethylenetriaminepentaacetic acid
Eq	Equation
Equiv	Equivalent
ESI-MS	Electrospray ionization mass spectrometry
FDA	U.S. food and drug administration
GBCA	Gadolinium-based contrast agents
Gly	Glycine
HATU	Hexafluorophosphate azabenzotriazole tetramethyl uronium
HEPES	4-(2-Hydroxyethyl)-1-piperazineethanesulfonic acid
HOMO	Highest occupied molecular orbital
HPLC	High-performance liquid chromatography
HSA	Human serum albumin
IC-MS	Low resolution mass spectrometry
J	Coupling constant
k_{ex}	Water exchange rate
Ln	Lanthanide

LUMO	Lowest unoccupied molecular orbital
m	Multiplet (NMR)
MI	Molecular imaging
MR	Magnetic resonance
MRI	Magnetic resonance imaging
MWCO	Molecular weight cutoff
m/z	Mass/charge ratio
NMR	Nuclear magnetic resonance
OI	Optical Imaging
PBS	Phosphate-buffered saline
PET	Positron emission tomography
PiET	Photoinduced electron transfer
pK_a	Acid dissociation constant
POA	Phenoxyacetic acid
q	Number of coordinated water molecules
r_1	Longitudinal relaxivity rate
r_2	Transverse relaxivity rate
RF	Radiofrequency
SCA	Smart contrast agent
SPECT	Single-photon emission tomography
SNR	Signal-to-noise ratio
T_1	Longitudinal relaxivity time
T_2	Transverse relaxivity time
*t*Bu	*tert*-butyl
TFA	Trifluoroacetic acid
Tyr	Tyrosine
US	Ultrasound
δ	Chemical shift
$\Delta\omega$	Chemical shift difference

Abstrakt

Optische Bildgebung (OI) und Magnetresonanztomographie (MRT) sind zwei leistungsstarke molekulare Bildgebungstechniken sowohl für die Biomedizin als auch für die Neurowissenschaften. Bisher wurden verschiedene molekulare Sensoren mit Bildkontrast stärken Funktion entwickelt, um die funktionelle und anatomische Visualisierung von Körperstrukturen und Flüssigkeiten zu verbessern. Zn(II) gilt als ein grundlegendes Element in vielen wesentlichen biologischen Prozessen. Die nicht-invasive Bestimmung der Zn(II)-Schwankungen von der Konzentration hält man für große Bedeutung, weil es dazu beiträgt, die biologische Rolle von Zn(II) zu verstehen und die Früherkennung von Krankheiten zu verbessern. Die vorhandenen/aktuellen relevanten Veröffentlichungen haben die kombinierten OI/MRT-Bildsensoren wenig untersucht. Die vorliegende Arbeit dokumentiert, wie es in meiner Forschung versucht wird, mit kombinierten OI/MRT-Bildsensoren Ln(III)-basierten Sonden, die gegenüber Zn(II) für die dualmodale MRT/OI-Bildgebung empfindlich sind, herzustellen. Die Zielsetzung dieser Forschungsprojekt ist den aktuellen Forschungstand weiter zu bringen.

Der erste Projekt beschäftigt sich mit der nicht reagierenden optischen Sonden **EuL$^{1-2}$**, die aus einer DO3A-basierten Berichtseinheit bestehen und die an ein von Tyrosin abgeleitetes Chromophor gebunden ist. Weitere strukturelle Modifikationen von **EuL$^{1-2}$** umfassten die Einführung einer Zn-sensitiven DPA-Einheit. Sie ergeben die Zn-sensitiven Sonden **EuL$^{3-4}$**. Im Vergleich zum untersuchten Kationen zeigten neuen Sonden außergewöhnliche starke Selektivität für Zn(II), und eine 7-fachen Lumineszenz Verstärkung. Die induzierte Lumineszenzänderung ermöglicht es, **EuL$^{3-4}$** als lebensfähige Zn-Chemosensoren für biologische Anwendungen zu etablieren.

Im zweitenTeil wurden die Gd(III)-Analoga von **EuL$^{3-4}$**, **GdL$^{3-4}$**, hergestellt und sie mittels NMR bewertet. Das Ergebnis ergab, dass beide Komplexe eine vernachlässigbare Empfindlichkeit gegenüber Zn(II) in der r_1-Relaxivität zeigten. Um die Empfindlichkeit zu verbessern, wurden die **GdL$^{3-4}$** weiteren Modifikationen unterzogen. Die eingeführten chemischen Umwandlungen implizierten die Umwandlung der phenolischen OH-Gruppe in Phenoxyessigsäure, um **GdL$^{5-6}$** bereitzustellen. Diese Modifikationen führten zu einer starken Verbesserung der r_1-Relaxivität (~ 280%) bei Zugabe von Zn(II) unter physiologisch relevanten

Bedingungen. Die Bewertung von **GdL$^{5\text{-}6}$** mit Hilfe verschiedener NMR-Studien in HEPES, PBS, HSA und Serum in Begleitung von MRT-Phantomen zeigte ihre hervorragende Empfindlichkeit gegenüber Zn(II). Dies macht die **GdL$^{5\text{-}6}$**-Wirkstoffe zu künftiger Sondenentwicklung für biologische Anwendungen aus.

Im dritten Projekt konzentrierte ich mich auf die Entwerfen und Synthetisieren von trimakrocyclischer Chelator **L^7**, der von der DA18C6-Einheit überbrückt wird. **L^7**s zweikerniger Eu(III)-Komplex **Eu$_2$L^7** zeigte einen für EuDOTAM-Gly typischen CEST-Effekt. Bei der Metallierung des verbleibenden DA18C6-Chelators mit Tb(III) wandelte sich der Komplex **Eu$_2$L^7** in ein hetero-mehrkerniges Komplex **Eu$_2$L^{7}Tb** um. Dieser gemischte Lanthanoidkomplex zeigte interessante Emissionseigenschaften bei verschiedenen Anregungswellenlängen. Insgesamt weid dieses System einen Weg zur Entwicklung von bimodalen Bildgebungssonden anbieten.

Abstract

Optical imaging (OI) and magnetic resonance imaging (MRI) are powerful molecular imaging techniques widely used in biomedicine and neuroscience. To date, various image-contrast-enhancing molecular sensors have been developed to improve the functional and anatomical visualization of body structures and fluids. Zn(II) plays a fundamental role in many essential biological processes. The non-invasive determination of Zn(II) concentration fluctuations is of paramount importance for understanding its biological role and improve early-stage disease detection. To the best of our knowledge, the OI/MRI combined imaging sensors are much less studied. Aiming to expand research in this field, the efforts towards preparing Ln(III)-based probes sensitive to Zn(II) for MRI/OI dual-modal imaging are described in this thesis.

The first part of this thesis begins with an introduction of non-responsive optical probes **EuL$^{1-2}$** consisting of a DO3A-based reporting moiety linked to a Tyr-derived chromophore. Further structural modifications of **EuL$^{1-2}$** include the introduction of a Zn-sensitive DPA moiety, resulting in the Zn-sensitive probes **EuL$^{3-4}$**. These novel compounds exhibited strong selectivity to Zn(II) over other studied cations, and demonstrated an up to 7-fold luminescence enhancement. The induced luminescence change enables establishing **EuL$^{3-4}$** as viable Zn-chemosensors for biological applications.

Based on the first project on optical probes, the Gd(III) analogues of **EuL$^{3-4}$**, **GdL$^{3-4}$**, were prepared and evaluated by means of NMR. It showed that both complexes displayed negligible sensitivity to Zn(II) in r_1 relaxivity. In order to improve the sensitivity, **GdL$^{3-4}$** were subjected to further modifications. Thus, the phenolic OH group was converted into phenoxyacetic acid providing **GdL$^{5-6}$**. These modifications led to a large r_1 relaxivity enhancement (~280%) upon the addition of Zn(II) under physiologically relevant conditions. The detailed evaluation of **GdL$^{5-6}$** properties by means of various NMR experiments in HEPES, PBS, HSA and serum accompanied by MRI phantoms, evidenced their outstanding sensitivity to Zn(II). This makes **GdL$^{5-6}$** complexes potential agents for biological applications.

In the third part, I focused on combining two different OI and MRI modalities into one entity. Thus, a trimacrocyclic chelator **L^{7}** bridged by DA18C6 moiety was designed and synthesized. Its dinuclear Eu(III) complex **Eu$_2$L^{7}** displayed a CEST

effect, which is typical for EuDOTAM-Gly. Upon metalation of the remaining DA18C6 chelator with Tb(III), the complex converted into a hetero-multinuclear **Eu_2L^7Tb**. This mixed lanthanide complex showed interesting emission properties at different excitation wavelengths. Overall, this system paves the way towards the development of bimodal imaging probes with controlled properties.

1. Introduction

1.1. Molecular imaging and imaging probes

Molecular imaging (MI) as an imaging technique was developed 30 years ago, which focuses on imaging molecules of medical interest within living patients. In stark contrast to conventional techniques such as histology, which is used to obtain molecular information from *ex vivo* samples, MI allows a non-invasive visualization of desired biomarkers in patients.[1] With the purpose to better understand fundamental biochemical processes within living organisms, MI, is constantly gaining in its popularity within the scientific community. In a broad sense, MI enables the study of cells in their natural microenvironment. Meanwhile, the real-time data can be acquired from the same experiment. Specifically, this method can trace cell movements/migration that give information on important biological processes, provide a thorough insight into mechanistic aspects of metabolic events, allow early diagnosis of various diseases, and monitor treatment progress. At present, MI techniques most used as diagnostic tools in clinics are US, OI, MRI, PET, SPECT and CT.[2, 3]

Table 1. Some of the most commonly applied imaging modalities and their properties.[3]

Technique	Reporting unit	Spatial resolution	Depth	Temporal resolution	Type of molecular probe
MRI	Gd^{3+}, Mn^{2+} or Fe^{3+} complexes	25-100 µm	no limit	minutes to hours	activatable
OI	Fluorochromes, Ln^{3+} complexes	2-5 mm	< 2 cm	seconds to minutes	activatable
US	Microbubbles	50-500 µm	0.1-10 cm	seconds to minutes	limited activatable
CT	Iodinated molecules	50-200 µm	no limit	minutes	maybe possible
PET	^{18}F, ^{64}Cu or ^{11}C radioisotopes	1-2 mm	No limit	seconds to minutes	radiolabeled
SPECT	^{99}Tc or ^{111}In radioisotopes	1-2 mm	No limit	minutes	radiolabeled

The different imaging modalities have their associated strengths and drawbacks, including the resolution of the images, the sensitivity of the technique, its penetration limit, scanning time and cost. None of the existing imaging modalities can provide information on all aspects of tissue structure and function. In respect to the type of molecular transducer, a wide variety of imaging modalities were coupled to detect signals in response to desired biomarkers. For example, recent interest has emerged on the development of multimodal imaging, unifying two or three different modalities into a single instrument. OI modality is a traditional method with advantages such as low cost, great sensitivity at the cellular and sub-cellular levels, and rapid multichannel readout. However, the OI is heavily limited by the low depth of tissue penetration. One alternative way to overcome this impairment is *via* the utilization of dual-modal chemosensors. Owing to the much better depth of penetration, MRI is considered as the second desirable imaging modality. In other words, the bimodal imaging technique with OI and MRI (OI-MRI) offers deep tissue penetration of MRI and excellent sensitivity of OI.[4, 5]

Currently, researchers in the molecular imaging field are focused on three branches: 1) the development of imaging methods for detecting previously undetectable types of molecules, 2) the expansion of the number and types of available probes, and 3) the development of functional probes that noninvasively visualize the various activities that cells and tissues perform in both health and disease.[1]

In a general sense, an imaging probe or CA is either an endogenous or exogenous substance used to help distinguish tissues. By injecting such reporting unit (for example, a metal ion chelate, or a fluorochrome) into live tissue, a corresponding imaging modality (for example, MRI, or OI) is applied to track its movement in the body. In OI, CAs enhance luminescence (e.g. photoluminescence (fluorescence, phosphorescence), chemiluminescence) in a target tissue or structure. Unlike the probes for OI, which are directly detected, in the case of MRI, CAs shorten the relaxation times of water protons within body tissues in order to alter the contrast of an image. CAs are commonly used to improve the visibility of blood vessels and the gastrointestinal tract. Several types of CA are in use in medical imaging and they can roughly be classified based on the imaging modalities used for their detection.

1.2. Optical imaging probes

Photophysical processes such as absorption, scattering and emission of light can be used for optical imaging and analyzing the interaction of light with biological tissues, to get an insight into specific cells or tissues. Usually, the photons emitted as a result of the excitation of fluorescent molecules, or as a consequence of a biochemical reaction that takes place in the body, are recorded.

Organic materials or fluorophores, as conventional optical probes, were developed to evaluate the concentration of target stimuli within a region of interest, with strong luminescence.[6] However, these organic probes are often associated with drawbacks such as short fluorescent lifetime and short Stokes shift, which limits their applications in biochemical research.

To overcome the aforementioned drawbacks, lanthanide-based probes were gradually developed. Compared to the typical organic fluorescence compounds, the Ln(III)-based complexes feature larger Stokes shifts (>200 nm) and display longer emission lifetimes (in the range of milliseconds), which is desirable to design the moieties for novel approaches.[7] The most important ions in the context of OI are Eu(III) and Tb(III) due to their narrow emission spectra and visible luminescence with red and green colours, respectively.[1, 8, 9] Unfortunately, Ln(III) are toxic to the human body. To efficiently coordinate the Ln(III) and decrease their toxicity, macrocyclic ligands like DO3A (1,4,7,10-tetraazacyclododecane-1,4,7-trisacetic acid) are widely used as a motif to develop the target or specific probes.[10, 11] Given the high stability and water solubility of DO3A-based Ln(III) complexes, their properties such as luminescence and magnetic behavior have been extensively studied.[12-16]

However, the luminescence intensities of such LnDO3A derivatives are very weak due to their inefficient direct excitation caused by the f-f transitions forbidden of the lanthanide ions. The f-f transition, the transition of an electron from an f orbital which is lower in energy to an f orbital which is higher, is a typical property of Ln(III) ions.[8] While f-f transitions are symmetry forbidden (Laporte-forbidden), transition metals or chromophores make use of vibronic coupling to break this rule. It has been noted that the colours of lanthanide complexes originate mostly from charge transfer interactions between metal and the ligand. Hence, the performance of Ln(III)-based

luminescent probes may often be enhanced by excitation of the Ln(III) *via* a sensitizing chromophore.[17] Interestingly, aromatics and their derivatives are often used as a chromophore motif for such probes.[15, 18] In this work, Tyr, as a nonessential amino acid, was carefully considered to be a chromophore for target probes, owing to its functional groups including phenol, carboxylic acid and amine which can be modified further to meet the proposed requirements. In detail, the Tyr chromophore is the excited from the ground state to excited state, followed by energy transfer to the Ln(III), resulting in the improved luminescent performance of the Ln(III)-based probes.

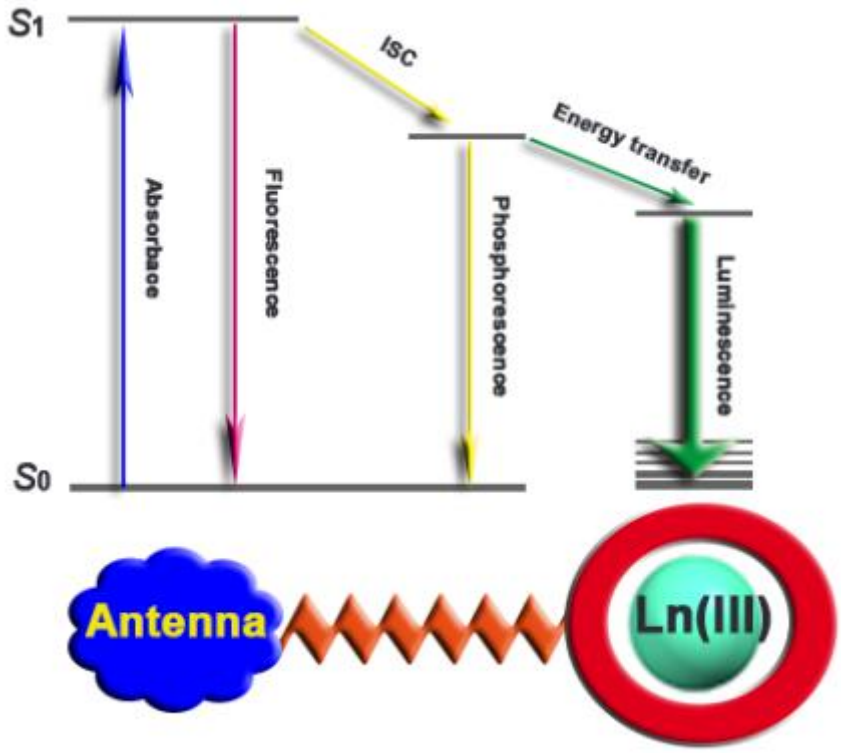

Figure 1. Simplified Jablonski diagram showing the main energy paths during sensitization of lanthanide luminescence *via* its antenna ligand. [7, 8, 17, 19] ISC = intersystem crossing

1.3. MR imaging agents

MRI is one of the most versatile and promising methods in modern diagnostic medicine, as it acquires 3D images of tissues and organs enabling identification of anatomic anomalies, and some assessment of physiological function. Its further perspective is monitoring of metabolic processes at cellular and molecular levels by using agents with high specificity and high relaxivity. Since the images acquired by

MRI are featured with high spatiotemporal resolution and unlimited penetration depth, this strategy is ideal for studying many diseases *in vivo*.[2, 4]

The MRI images generated by taking advantage of differences in longitudinal relaxation of diverse tissues are termed as T_1-weighed images. The T_1-weighed images are obtained by using short repetition times, and generally provide very bright spots of fat-based tissues due to their short relaxation times, while water-based tissues and fluids appear as mid-grey and very dark, respectively. In addition, differences concerning T_2 relaxation time are also exploited to generate contrast by using the appropriate pulse sequences with long echo time. In T_2-weighed images, tissues with short T_2 are observed as dark regions. MR imaging is based on the relaxation mechanism of NMR. Figure 2 demonstrates a magnetic resonance process, accompanying the recovery (T_1) and decay (T_2) of excited magnetization.

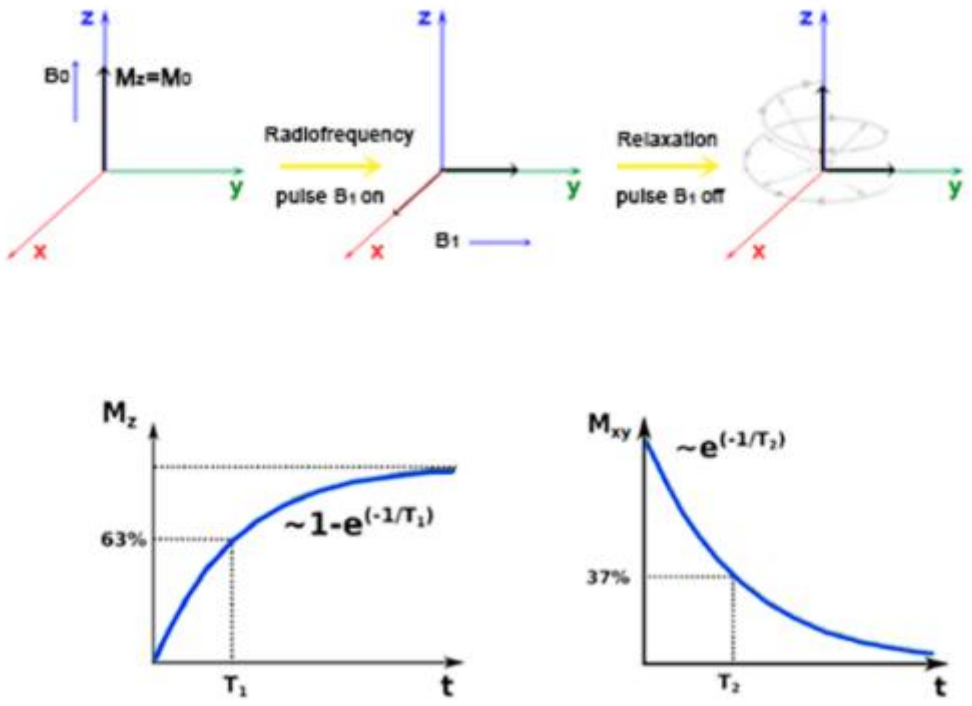

Figure 2. Acquisition of a magnetic resonance experiment and T_1, T_2 relaxation processes.

The paramagnetic gadolinium(III) ion, compared to other paramagnetic metal ions, is the most commonly employed candidate to generate MRI CAs. Generally, the Gd(III) based CAs, are used as T_1-weighted agents.[20] To efficiently coordinate the Gd(III) ion and decrease its toxicity, which means *increasing* the thermodynamic and kinetic stabilities of its complexes, various linear and macrocyclic ligands are

widely used to chelate it. Common Gd(III) coordination number is 9. Such ligands provide 7 or 8 donor atoms to chelate Gd(III) while leaving 2 or 1 binding position for water molecules, respectively. In other words, a majority of these chelators are heptadentate or octadentate leaving enough space for the coordination of one or two water molecule(s) in the inner sphere of Gd(III). At a wide range of magnetic fields, the number of bound water molecules (q) is the parameter that mostly determines relaxivity r_1, although the parameters such as the exchange rate of the coordinated water molecule(s) with bulk water (k_{ex}), rotational correlation time of the complex (τ_R), the Gd-H effective mean distance of the coordinated water molecules (r_H) and the longitudinal and transverse electronic spin relaxation times T_{1e} and T_{2e} of the metal ion are also important. Commonly, most Gd-based complexes are monohydrated. Despite the higher q could result in less satisfactory complex stabilities and lead to a risk of free Gd(III) leaking which will increase the toxicity, the reasonably designed q = 2 Gd-based systems still show acceptable thermodynamic stabilities and exhibit increased relaxivities. Therefore, the change of coordinated water molecule number (q) was properly considered in many cases to design so-called smart T_1-weighted agents, which can be turned “on” or “off” upon interaction with the target event.[10, 21]

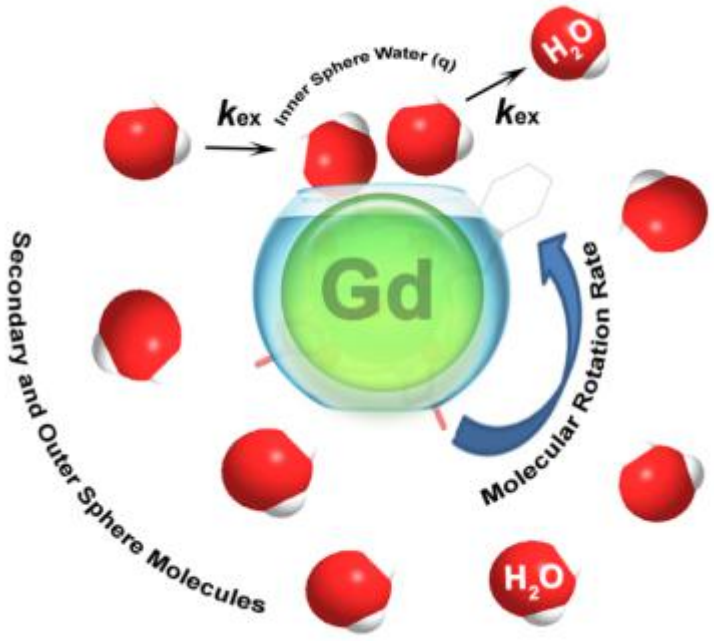

Figure 3. Schematic representation of a Gd-based complex with one or two inner sphere water molecules in exchange with bulk water and the parameters influencing the relaxation.[22]

So far, an increasing number of MRI CAs are designed to exploit the so-called CEST effect. The CEST effect generates a decrease in bulk water magnetisation based on proton exchange with a CEST agent. CEST agent gives certain advantages over conventional T_1-weighted GBCAs. Namely, the CEST modality enables an on/off response on request, accompanied by improved sensitivity.[11, 23] The magnitude of the magnetization transferred to the bulk water, namely the CEST effect, is calculated according to the following equation:[24]

$$\%CEST = (1 - M_s/M_0) \times 100\%, \quad (1)$$

Here M_s is the intensity of the magnetic resonance signal of the bulk water upon pre-saturation and M_0 is the intensity of the reference signal.

The CEST principle is best illustrated by the two pools of protons with a general requirement for frequency difference between the pools, $\Delta\omega$, must be $\geq k_{ex}$ (rate of exchange between the pools).[25] To observe the CEST effect, one pool of protons in slow-to intermediate exchange with bulk water protons must be pre-saturated by a frequency selective pulse. The saturated protons then exchange with the water protons, reducing the intensity of the bulk water MR signal. The illustration of the CEST mechanism is depicted in Figure 4.

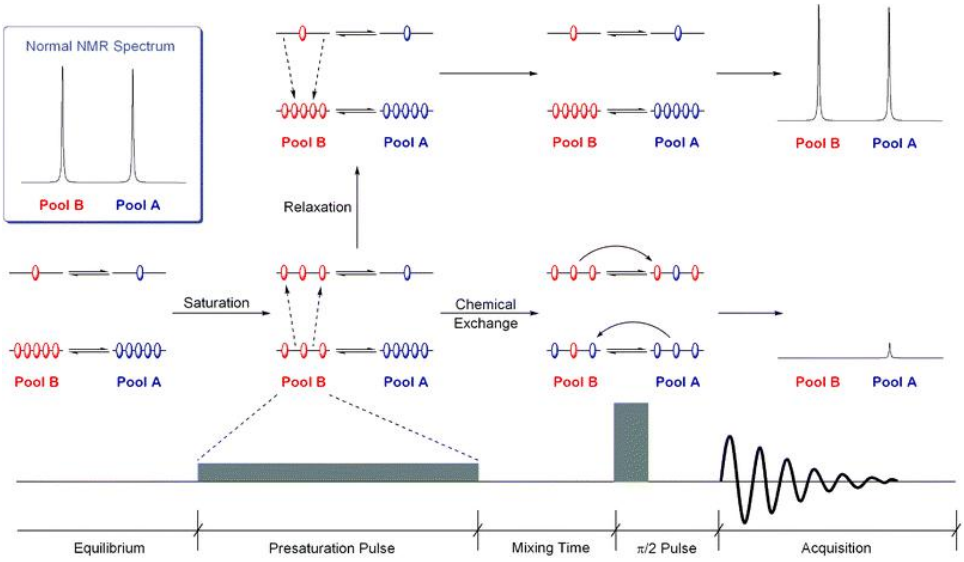

Figure 4. Illustration of the CEST mechanism. The saturated protons from pool B are passed to pool A through the process of chemical exchange, resulting in a signal decrease of protons in pool A.[26] (Adapted with permission from RSC)

The typical CEST CAs are comprised of ligand containing a pool of exchangeable protons, most commonly –NH (amide or amine) or –OH (alcohol or

phenol) groups.[16, 27] In addition, the CEST effect may also be produced by the water molecule which is directly coordinated to the paramagnetic metal ion. Application of a radiofrequency pulse at the spectral frequency of the ligated water results in the transfer of magnetization to the bulk water, hence the intensity of the bulk water signal is decreased (Figure 4). This CEST MRI was introduced around two decades ago by Ward, Aletras and Balaban.[23] The enhancement produced on the image is perceived as a negative contrast. Initially, it was used to detect different metabolites, so-called endogenous CAs (for example amino acids, proteins and nucleotides), present in the body that contains exchangeable protons.

Among the paramagnetic lanthanide ions, the Eu(III), Tb(III) and Yb(III) are known to considerably shift the signals of the exchangeable proton on the ligand or the coordinated water molecule. Their complexes are used to produce a CEST effect of the exchangeable proton or bound water molecule with bulk water and termed as paraCEST CAs.[15, 28] The typical Ln(III)-based paraCEST CAs are the EuDOTAM and EuDOTAM-Gly complexes.[23]

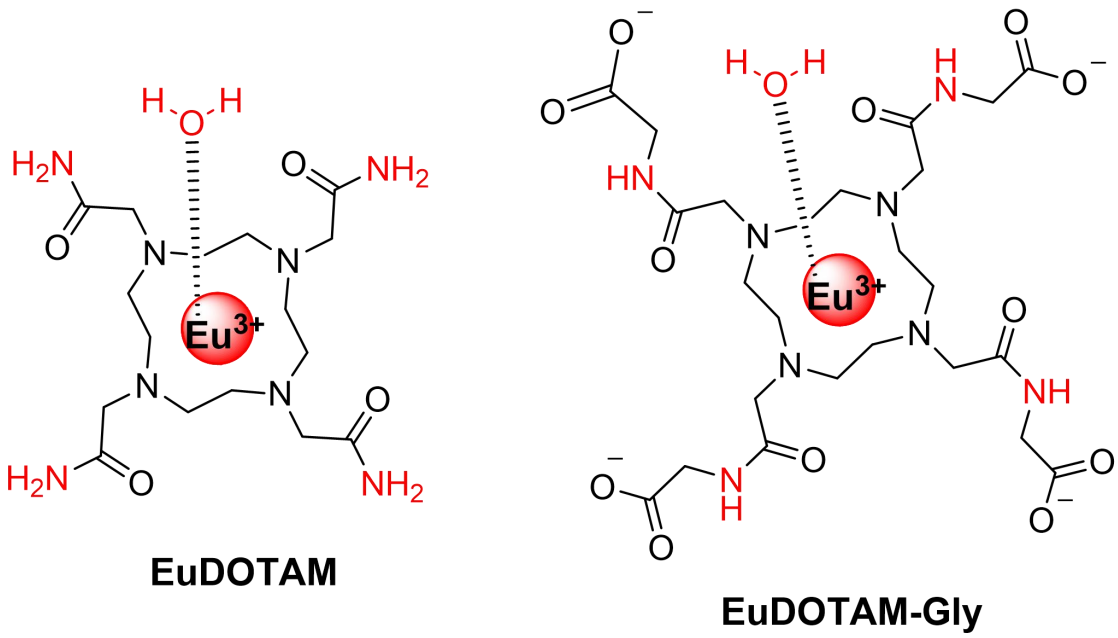

Figure 5. Typical lanthanide-based paraCEST CAs.

1.4. Smart probes sensitive to Zn(II)

Much effort has been invested in designing CAs capable of changing their MR properties upon a specific change in their microenvironment. As MRI is a particularly

attractive imaging modality, the smart contrast agents, also referred to as responsive or activatable CAs, were applied to monitor the changes of their MR properties upon a specific change in their microenvironment. The SCAs undergo conformational changes upon interaction with the target molecule, resulting in a change in their signal properties (for example, enhancing of luminescence or shortening of T_1 relaxation time) due to alteration of the parameter(s) that determine energy transfer or relaxivity. Considering the design of a T_1-weighted SCA, there must be a change of hydration number, rotational correlation time, water exchange rate, or the electron spin relaxation times. Given that a) the rotational correlation time is dependent on the magnetic field; b) water exchange rate is difficult to predict; and c) the electron spin relaxation times can only exert less influence, the predominant mechanism responsible for changes in relaxivity for SCAs at high magnetic fields is the change in hydration state of the complex. The observed signal change implies a change of CAs between “off” or “on” status that occurs only in the presence of a threshold concentration of the specific targets. CAs with high relaxivity provide high SNR while SCAs make high SNR difference. This makes SCAs ideal candidates for molecular imaging because they provide the highest SNR for molecular target identification.[29]

According to the stimuli that activate CAs, they are classified into pH-activated, enzyme-activated, metal ion responsive, redox CAs. For instance, a plethora of responsive CAs were developed to probe bivalent metal ions (such as Ca(II), Zn(II) or Fe(II), etc.), as they are important modulators of various biological processes. Besides, many diseases have been associated with altered metal ion concentration in the body and thus *in vivo* determination of metal ion distribution is highly desirable.

In the human body, Zn(II) takes part in various biochemical processes which are of essential importance for the normal functioning of the body.[30] It is the second most abundant trace metal in bodies after iron and it is the only metal which appears in all enzyme classes. Most Zn(II) is in the muscle, bone, liver and brain. In the brain, Zn(II) is stored in specific synaptic vesicles by glutamatergic neurons and can modulate neuronal excitability. It plays a key role in synaptic plasticity and in learning. Zn(II) homeostasis also plays a critical role in the functional regulation of the central nervous system.[31]

Symptoms associated with mild Zn(II) deficiency are diverse. Clinical outcomes include depression, impotence, delayed sexual maturation, eye and skin lesions, altered cognition, impaired immune functions, defects in carbohydrate utilization, and reproductive teratogenesis.[30] Although Zn(II) is an essential requirement for good health, excess zinc can be harmful. For instance, excessive absorption of Zn(II) suppresses copper and iron absorption. Therefore, determination of concentration fluctuations of Zn(II), in a non-invasive manner, is of paramount importance to understand its biological role and improve early-stage disease detection.[32-35]

Figure 6. Illustration of responsive mechanism and examples of zinc responsive SCAs.

To evaluate the Zn(II) concentrations in the body, DPA is the most used moiety to build Zn-responsive probes. The DPA chelator, first reported in 1964, is known to form stable complexes with Zn(II).[36] Combining the DPA moiety with either luminescent or MRI molecular sensors, can result in Zn(II)-responsive probes for optical or MR imaging, respectively. Specifically, appending the DPA moiety to a chemosensor makes it a luminescent probe sensitive to Zn(II), while appending the DPA to a lanthanide motif makes the complex an MRI CA sensitive to Zn(II). A variety of imaging probes selective to Zn(II) were developed including those used for *in vitro* or *in vivo* experiments. Especially, the optical probes and MRI CAs were abundantly developed to reach ideal probes sensitive to Zn(II).[10]

1.5. Optical/MR dual-modal imaging CAs

OI techniques, especially fluorescence microscopy, have a high spatiotemporal resolution but limited depth of penetration. However, MRI is benefited by unlimited penetration depth. Thus, an exogenous dual-modal CA which can transduce

interactions with stimuli into signals detectable by both MRI and fluorescence imaging techniques would be a perfect imaging agent characterized by high spatiotemporal resolution and non-limited penetration depth.[5, 22, 37-40] 'Two is better than one.'[41]

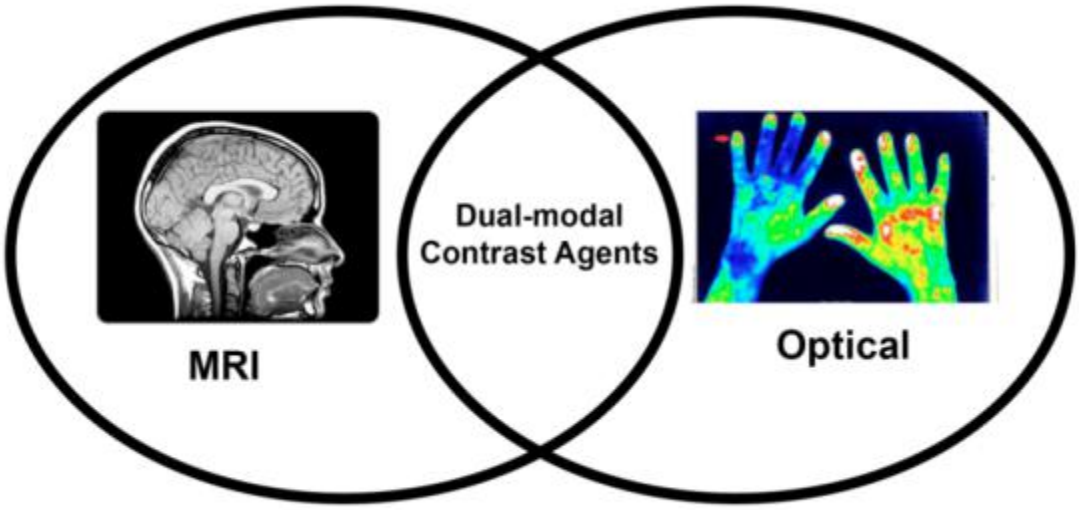

Figure 7. Dual-modal contrast agents combining optical and MR imaging properties.

The first MRI-fluorescent dual-modal probes were reported by Meade and co-workers in 1998, which contains both a Gd(III) chelate and a fluorophore tetramethylrhodamine.[40] Interestingly, complexes incorporating two different Ln(III) ions can provide such dual-properties, enabling the design of dual-modal probes, for instance, the luminescent and MRI imaging probe. The activatable dual-modal probes are rarely reported, Aime and co-workers reported a Tm(III)/Gd(III)-based lipoCEST CA, in which the CEST response is activated by quenching T_1 contrast through reductive cleavage of Gd-based moieties.[42] In addition, polynuclear complexes have also been widely studied.[22, 43-47] For example, in 2003, Faulkner and co-workers synthesized a hetero-trimetallic lanthanide complex using a DTPA-like cage to bridge two kinetically stable Tb-complexes, resulting in a probe with terbium-sensitized ytterbium luminescence.[48] Therefore, combining two or more different types of Ln(III) ions in one molecule can pave the way to synthesize multi-modal probes for future imaging of the interested stimuli.

1.6. Motivation and objectives of the thesis

Given OI and MRI techniques are powerful diagnostic tools utilised in clinics, the application of CAs pushed them to visualize biological processes in a dynamic manner. Zn(II) involves in many such essential processes and both its deficiency and excess states can result in symptoms. Therefore visualization of Zn(II) fluctuations by such techniques is of paramount importance to understand its biological role and improve early-stage disease detection. To this end, this Ph.D. thesis is focusing on the synthesis and characterization of OI and MRI probes sensitive to zinc ions. The research, as an attempt to explore dual-modal imaging probes, was gradually developed from two non-smart optical probes to two Zn-sensitive optical probes by adding a Zn-sensitive moiety DPA. Then, the research was proceeded continuously from two non-smart T_1-weighted MRI CAs to two Zn-sensitive T_1-weighted MRI CAs by converting a phenol group to a phenoxyacetic acid group. Additionally, a hetero-nuclear trimacrocyclic derivative appending a DA18C6 moiety was designed and synthesized, towards a potential optical and MR dual-modal imaging probe. In other words, getting closer to the final goal of Zn-sensitive OI/MRI dual-modal agents, the efforts were devoted step by step from non-smart optical probes to Zn-specific probes, from non-smart T_1-weighted MRI CAs to Zn-specific agents, and from the non-smart but hetero-polynuclear dual-modal probe, to explore the potential way towards the development of OI/MRI probes for zinc ions detection.

2. List of publications and declaration

1. Europium(III) Macrocyclic Chelates Appended with Tyrosine-based Chromophores and Di-(2-picolyl)amine-based Receptors: Turn-On Luminescent Chemosensors Selective to Zinc(II) Ions. *ChemPlusChem* **2020**, 85, 806-814
2. Highly Potent MRI Contrast Agent Displaying Outstanding Sensitivity to Zinc Ions. *Angew. Chem. Int. Ed.* **2020** DOI: 10.1002/anie.202014431
3. Macrocyclic Chelates Bridged by a Diaza-crown Ether: Towards Multinuclear Bimodal Molecular Imaging Probes. *Molecules* **2020**, 25, 5019.

Nr.	**1**	**2**	**3**
Publication status	published	submitted	published
List of authors	3	2	2
Candidate position	1	1	1
Scientific ideas %	75	80	65
Data generation %	85	90	95
Analysis & interpretation %	75	80	85
Paper writing %	65	70	75

I confirm that the above-stated is correct.

Date, Signature of the candidate

I/We certify that the above-stated is correct.

Date, Signature of the doctoral committee or the supervisor

3. Results and discussion

3.1. Zn(II)-specific luminescent probes

Zn(II) plays a fundamental role in many essential biological processes. Either an excess or deficiency of Zn(II) can induce symptoms and pathologies.[31] The luminescent probes sensitive to Zn(II) would be significant assets to investigate the biological role of Zn(II) and provide early-stage disease diagnosis. To this end, probes **EuL$^{3-4}$** were developed to specifically recognize Zn(II) over other metal ions. First, Tyr was considered to build the basic ligand block and to start the gradually developed system in this thesis thanks to its functional groups including one phenol, one carboxylic acid and one amine unit which can be modified further to meet the proposed requirements.[12, 49] For example, the phenol unit can react with aldehyde and amine in a Mannich reaction resulting in aminoalkylphenol derivatives at the ortho position.[50, 51]

Here, to chelate lanthanide ions and decrease their toxicity, DO3A is used to build the chelator, leaving one remaining secondary amine for further functional modification. Upon appending the previously mentioned Tyr to the DO3A chelator, two free ligands were synthesized, either bearing an amino acid (**H_3L^1**) or an amino acid methyl ester (**H_3L^2**) in the Tyr group.[52] Their Eu(III) complexes **EuL$^{1-2}$** were made and both of them behaved as typical chromophore probes. Namely, the chromophore Tyr was excited at 320 nm and absorbed energy at the first stage.[53, 54] Then, Tyr transferred its energy to Eu(III) because the LUMO of Eu(III) is lower than that of Tyr. In other words, the rule of f-f forbidden transition of Eu(III) was broken, resulting in characteristic emission peaks of Eu(III) at 580 nm, 596 nm, 617 nm, 655 nm and 702 nm from $^5D_0 \rightarrow {}^7F_J$ (J = 0 to 4) transitions. The emission intensity of **EuL$^{1-2}$** showed no obvious changes upon addition of the studied metal ions, suggesting they are non-sensitive probes.

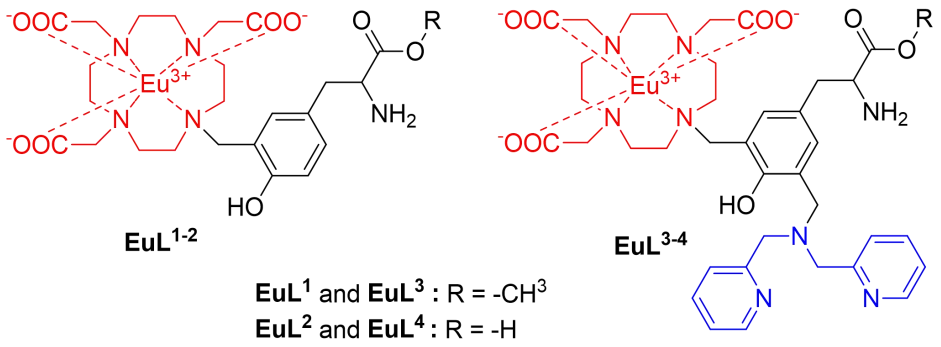

Figure 8. Chemical structures of **EuL$^{1-4}$** discussed in this project. The part in red is the luminescence center EuDO3A while the part in blue is the zinc sensitive DPA.

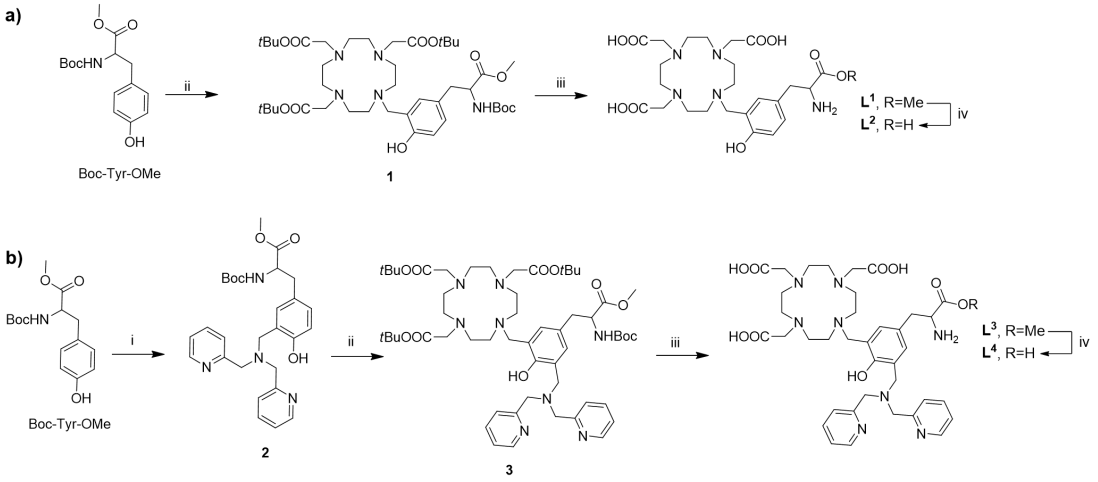

Scheme 1. Synthesis route of complex **EuL$^{1-4}$**.

To build a zinc-responsive probe, DPA as the most-used zinc-chelator was considered and appended to complexes **EuL$^{1-2}$**, providing smart probes **EuL$^{3-4}$**. For the synthesis of **L$^{1-2}$**, protected Tyr reacted with protected DO3A, resulting in the precursor **1**. The precursor **1** was treated with TFA and converted to **L^1**. **L^1** was further treated with LiOH and converted to L^2. For the synthesis of **L$^{3-4}$**, in the first step, DPA was coupled to the protected Tyr, providing compound DPA-Boc-Tyr-OMe **2**. Then the alkylation reaction of protected DO3A with Boc-Tyr-OMe was performed at 110 ^{o}C, which results in precursor **3**. Similarly, TFA treatment of precursor **3** results in **L^3** while further LiOH treatment results in **L^4**. After HPLC purifications, europium salt was introduced to the obtained final ligands respectively, giving corresponding complexes. Most importantly, here DPA acted as an electron-rich center/donor to achieve a “turn-on” process upon the addition of Zn(II). Specifically, in the absence of Zn(II), the “interception” of the energy absorbed by Tyr has occurred, induced by the nitrogen lone pair in DPA, namely the PiET process,

resulting in luminescence quenching of complexes **EuL$^{3-4}$**. In other words, the DPA moiety can intercept/capture the excited electron which is coming from the chromophore, which will transfer to Ln(III), giving a quenched luminescence.[55] Upon addition of Zn(II), the nitrogen lone pair was involved in complexation with Zn(II), which prevented the PiET process and made the energy transfer from Tyr to europium ion possible, resulting in luminescence enhancement.

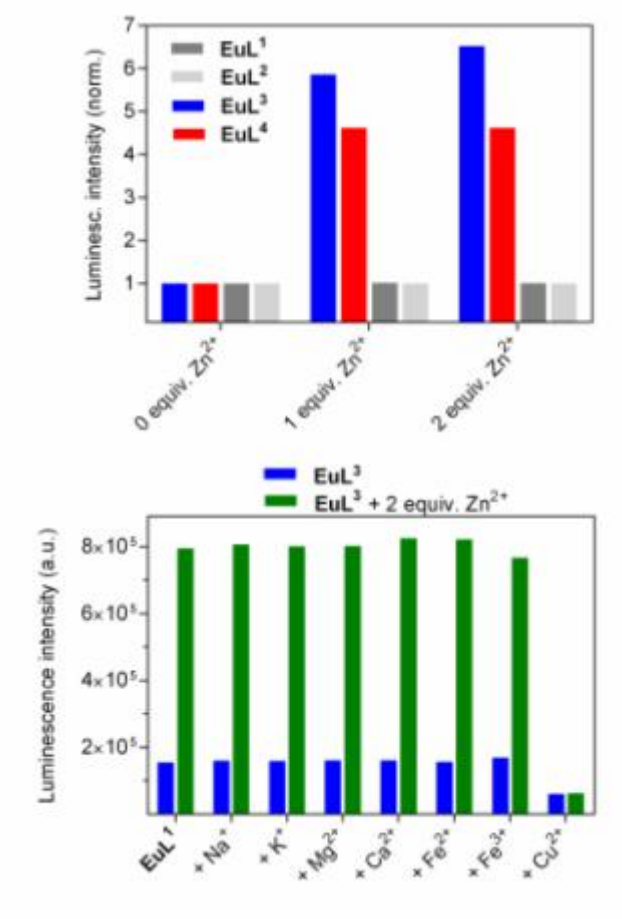

Figure 9. a) Luminescence changes of **EuL$^{1-4}$** (50 μM) upon addition of Zn(II). All data were recorded in HEPES buffer (50 mM, pH 7.4) with λ_{ex}=322 nm and λ_{em}=617 nm; intensity was estimated by the peak height at λ_{em}=617 nm. b) Luminescence variations of **EuL^3** (50 μM) to Zn(II) in the presence of different metal ions. Blue bars indicate the luminescence intensity of **EuL^3** in the presence of various metal ions (3 equiv.). Green bars indicate luminescence intensity of **EuL^3** after the subsequent addition of Zn(II) (3 equiv.).

At the same conditions (50 μM complex, 50 mM HEPES buffer, pH 7.4 and 25 ^{o}C), the ion selectivity of these two complexes were tested with biologically relevant ions such as Na(I), K(I), Mg(II), Ca(II), Fe(II), Fe(III), Cu(II). As shown in Figure 9, the results demonstrated the specificity of **EuL$^{3-4}$** towards Zn(II) over other metal ions except for Cu(II). However, this ion can be omitted because its amount is very low in

the body.[56] The proved ion selectivity of these complexes guaranteed the luminescence enhancement measurements upon the addition of Zn(II). In the Zn(II) titration experiment, luminescence was enhanced 7-fold for **EuL^3** and 5-fold for **EuL^4** upon Zn(II) addition, by monitoring the emission intensity at 617 nm. The Job's plots for both **EuL$^{3-4}$** were measured to demonstrate the binding relationship between the complexes and Zn(II). The results revealed complex **EuL^3** bound two Zn(II), while **EuL^4** bound one. The only structural difference between these two complexes is the amino acid Tyr moiety: either amino acid group was esterified or not. This difference resulted in different luminescence enhancement. The expected reason is that the amino acid was formed as a zwitterion while the amino acid methyl ester has interacted with Zn(II) at physiological pH. The additional Zn(II) binding induced further luminescence enhancement than complex **EuL^4**.

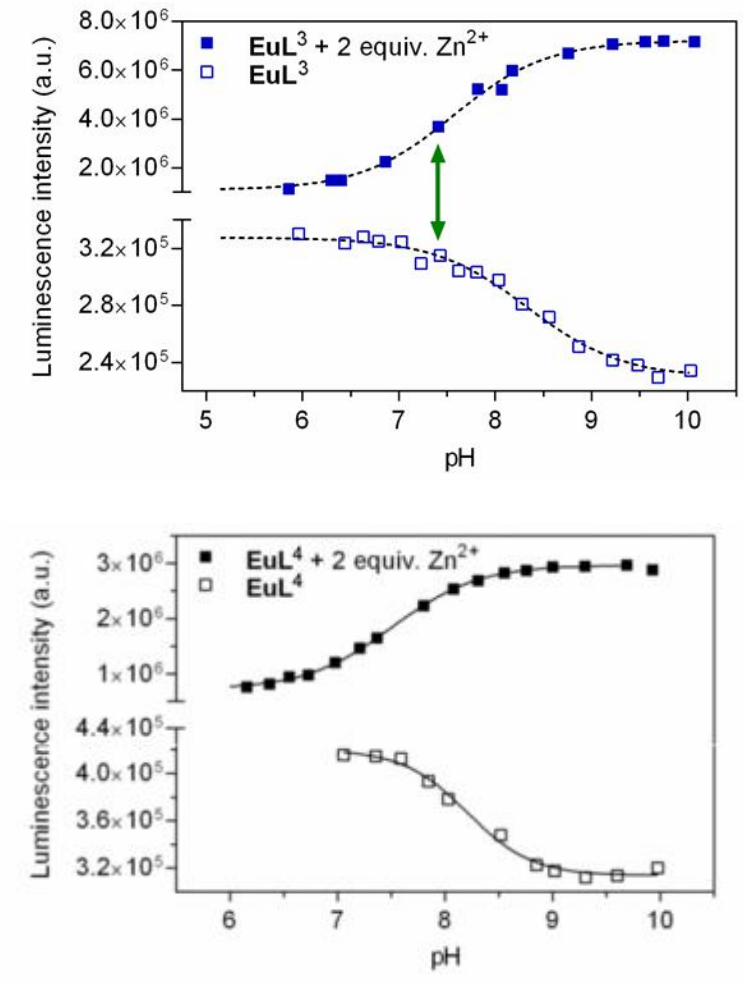

Figure 10. Luminescence emission intensity variations with pH changes of a) **EuL^3** (open symbols) and **EuL^{3}Zn** (filled symbols), b) **EuL^4** (open symbols) and **EuL^{4}Zn** (filled symbols) in water (50 μM complex, 100 mM KCl as the electrolyte, λ_{ex}=322 nm; intensity was estimated by the peak height at λ_{em}=617 nm).

To understand the mechanism responsible for the “turn-on” response to Zn(II), the pH dependences of the emission intensity of **EuL$^{3-4}$** and **EuL$^{3-4}$Zn** were investigated, respectively. The fitted equilibrium constants log*K* determined for the association of **EuL$^{3-4}$** with Zn(II) are close to values 8.3 (Figure 10), indicating that nearly all **EuL$^{3-4}$** were converted to **EuL$^{3-4}$Zn** at pH 7.4. For **EuL$^{3-4}$Zn**, the fitted equilibrium constants are near to values 7.5, involving the protonation/deprotonation of the phenol unit. To confirm the aforementioned insights, further UV-Vis studies with the investigated complexes were performed. The results showed that both **EuL$^{3-4}$** are responsive to 1 equivalent of Zn(II), causing the decline of absorption intensity at ~250 nm, which confirms the complexation of Zn(II) with the DPA moiety of the ligand. Furthermore, the absorbance variation of **EuL^{3}** was studied at different pH values. The band at 303 nm decreases by increasing pH, accompanying the development of a new band at 335 nm. The fitting of the absorbance changes at 335 nm provides an equilibrium constant log*K* = 9.4 ± 0.5, which confirms the protonation/deprotonation processes of phenol moiety.

Furthermore, DFT calculations of **EuL^{3}** and **EuL^{3}Zn** were carried out by Prof. Dr. Carlos Platas-Iglesias, which rationalized the observed results. Herein, **EuL^{3}** are responsive PiET probes in which the HOMO of the lone pair of the amine nitrogen in DPA has higher energy than the europium center in the absence of the Zn(II). Once the chromophore unit Tyr is excited, an electron transfers from the HOMO of the donor to the HOMO of the DPA moiety, quenching the emission of the probes. Upon coordination of Zn(II) with the DPA moiety, the energy level of the HOMO of the donor is reduced, making the energy transfer to europium ion feasible. As a result, the overall luminescence of **EuL^{3} Zn** is enhanced.

3.2. Zn(II)-specific T_1-weighted CAs

In this project, firstly, the gadolinium analogues of **EuL$^{3-4}$**, **GdL$^{3-4}$**, were synthesized and their T_1-relaxivity versus Zn(II) concentrations were measured at 25 ^{o}C, pH 7.4.[52] In detail, both complexes **GdL$^{3-4}$** have high initial r_1 values (~ 7.5 mM^{-1}s^{-1}), suggesting the presence of monohydrated complexes in both cases. The high r_1 values for both complexes are in line with monohydrated GdDO3A-type derivatives with similar size.[57] The relaxometric titrations of **GdL$^{3-4}$** with Zn(II) induce only a less than 10% enhancement in relaxivity upon the addition of up to 3 equivalents of Zn(II)

ions. The small relaxivity changes reveal that the phenolic OH of the complexes were bound to the gadolinium ion either with or without Zn(II) present, corresponding to the UV-Vis studies of **EuL^3** depicted in the previous project.

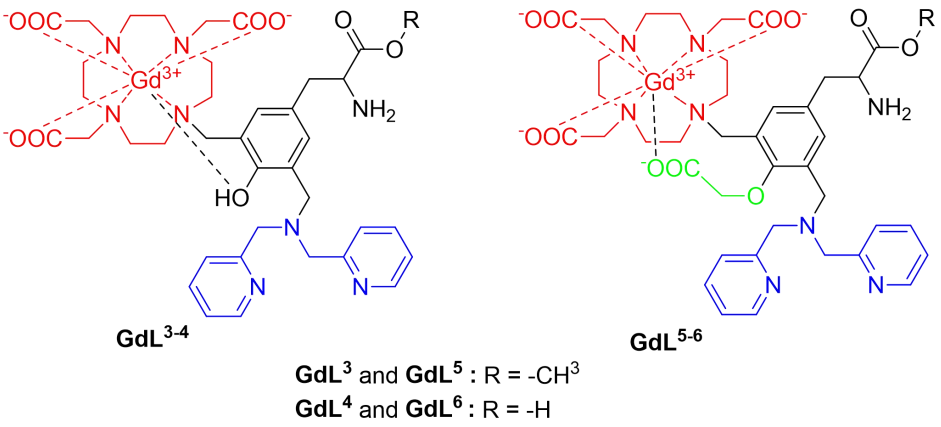

Figure 11. Chemical structures of **GdL$^{3-6}$**.

Changing the bound water molecule number is the most important method to change the relaxivity in small molecules,[58, 59] which is the key concerning for the project described here. Therefore, to build a zinc-responsive T_1-weighted MRI CA, the phenolic OH of **GdL$^{3-4}$** was modified further (Figure 11). Specifically, the phenol unit was alkylated and converted to a POA unit. The POA unit was proposed to chelate gadolinium in the absence of zinc ions whilst converting from Gd(III) to Zn(II) coordination upon zinc ion addition. The POA group as a "flipping" arm can result in the change of bound water molecule number *q* and provide the "turn-on" mechanism of the relaxivity of the complex. Therefore, the desired ligand **H$_4$L^5** and its complex **GdL^5** were prepared. The synthesis details of discussed complexes are depicted in scheme 2. Starting from compound **3** established in the first project, the alkylation of its phenol OH results in precursor **4**. On the other hand, the alkylation of compound **3** with ^{13}C-labeled compound **5** resulted in the isotopic precursor **4***. Both precursors were treated with TFA to give ligand **L^5** and **L^{5*}**. Then the corresponding lanthanide complexes were prepared by treating the ligands with $EuCl_3 \cdot 6H_2O$ or $TbCl_3 \cdot 6H_2O$ in water while maintaining the pH at ~7. To demonstrate the aforementioned mechanism, a series of ^{1}H NMR proof-of-principle studies were performed to describe the process of relaxivity changes of this complex and push the complex to be a highly potent MRI agent specific to Zn(II).

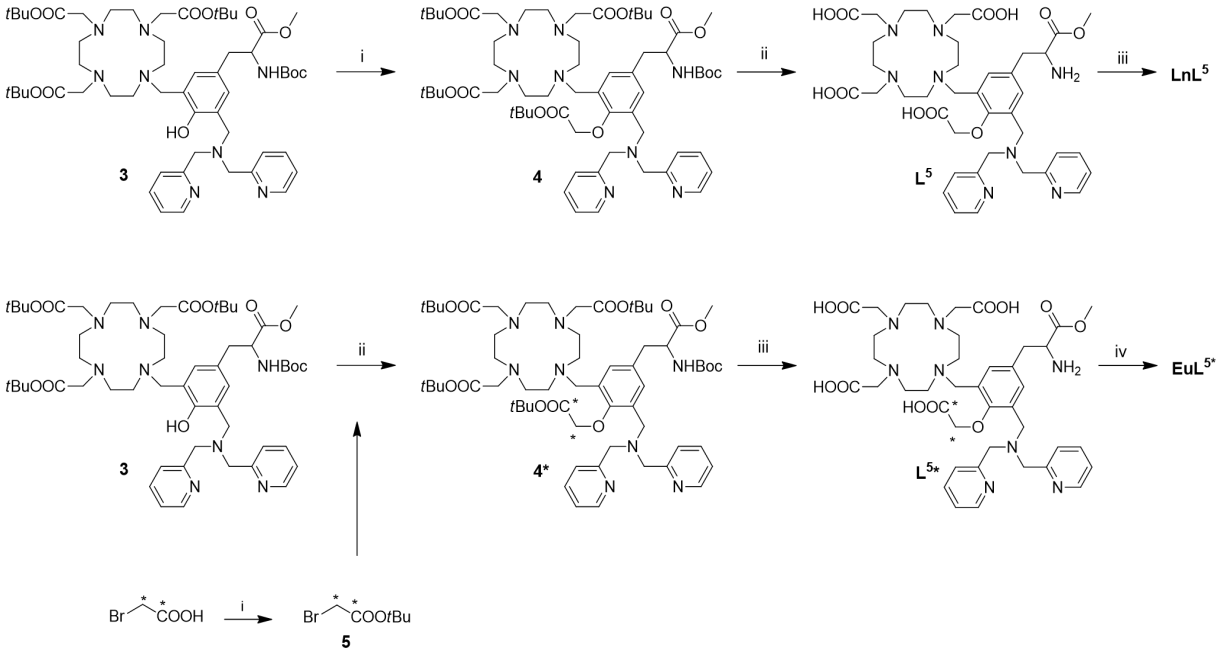

Scheme 2. Synthesis route of complex **LnL^5** (Ln = Gd, Tb) and **GdL^{5*}**

Following the assumption that the POA will be pulled away from paramagnetic ion by added Zn(II) , ^{1}H NMR relaxometric titrations were firstly performed at 7 T and 25 ^{o}C in 50 mM HEPES or PBS buffer, to evaluate the relaxivity response of **GdL^5** towards Zn(II). Both r_1 and r_2 were measured after every addition of Zn(II). The results shown an ~400% enhancement in r_1 relaxivity upon saturation with 1 equivalent of Zn(II) in HEPES (Figure 12a). Instead, when the PBS buffer was used, the overall r_1 enhancement is ~300% at 25 ^{o}C, indicating the formation of small amounts of ternary complexes between the phosphates and Gd(III). Surprisingly, this performance is still outstanding. Additional Zn(II) did not trigger either quenching or enhancement of r_1 relaxivity and confirmed the strong 1:1 binding between Zn(II) and the POA group. Then, the selectivity of **GdL^5** towards Zn(II) was tested in separate experiments with Mg(II), Ca(II) and Cu(II). As showed in Figure 12c, no obvious relaxivity response of **GdL^5** towards Mg(II) and Ca(II) was observed, with the exception of Cu(II). However, the very low quantities of Cu(II) in the human body is not likely a big issue for Zn(II) (~0.1 g and ~4 g for Cu(II) and Zn(II), respectively).[56, 60]

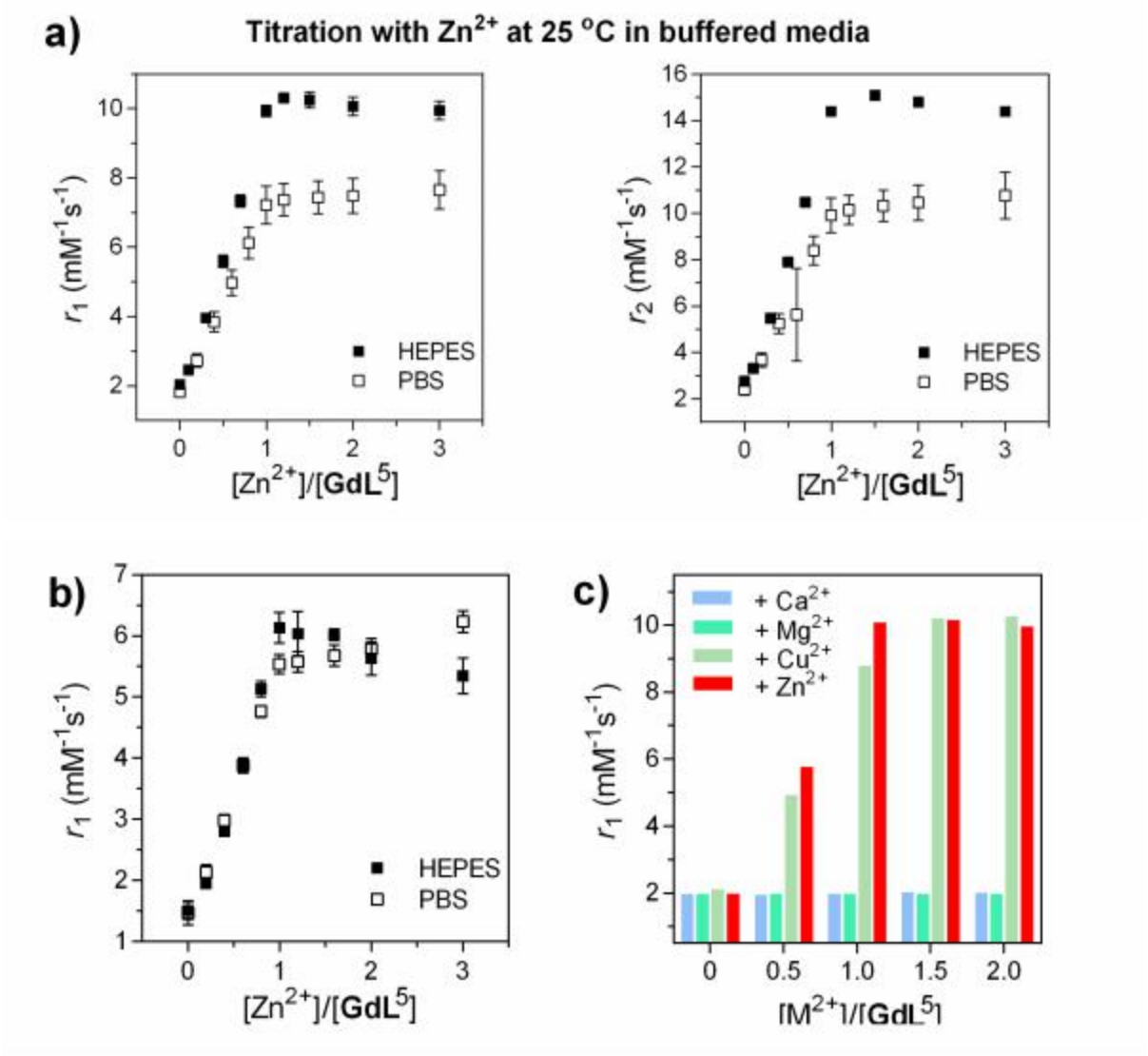

Figure 12. Longitudinal relaxivity r_1 of **GdL^5** at 7 T. a-b) r_1 in the presence of various concentrations of $ZnCl_2$ in HEPES (50 mM) or PBS (50 mM) at pH 7.4, a) 25 °C or b) 37 °C; c) r_1 in the presence of different quantities of Ca(II), Mg(II), Cu(II) or Zn(II) (50 mM HEPES, pH 7.4 and 25 °C).

Given the inspiring results of longitudinal relaxivity studies, to shed light on the binding pattern of **GdL^5** with Zn(II), its Eu(III) analogue **EuL^{5*}** was prepared with the ^{13}C-labeled POA group. As a paramagnetic ion, Eu(III) can strongly shift and reduce the signals of atoms with non-zero spin nucleus such as ^{1}H and ^{13}C (with a spin quantum number of 1/2), depending on the relative distance between them. Following the previously reported procedures by Meade and coworkers,[61, 62] a series of ^{13}C NMR spectra of 15 mM **EuL^{5*}** were recorded with adding $ZnCl_2$ (Figure 13). In the Zn-free state, only two broad and shifted signals at 93.5 ppm and 211.7 ppm were observed, indicating coordination of the POA group to the paramagnetic Eu(III).

Gradually adding Zn(II) conducts the attenuation and disappearance of these two broad peaks, accompanying the appearance and enhancement of two sharp doublets at 71.7 ppm and 175.6 ppm. This specific experiment strongly suggests the different behaviors of the POA group in the absence and presence of Zn(II). Namely, the addition of Zn(II) causes the formation of a Zn(II) complex with the DPA moiety, triggered the POA group to "flips" away from Eu(III) (Figure 13b). As a result, the ^{13}C NMR signals of the POA carbons recover to the status as free **L^{5*}** ligand. Therefore, this study illuminates the structural status changes of paramagnetic metal ion, which were selectively triggered by Zn(II).

Additionally, the coordination properties of this system were also assessed by testing the luminescence lifetimes of **EuL^{5*}** and **TbL^{5}** in D_2O or H_2O with and without Zn(II) at pH 7.4 and 25 ^{o}C. The hydration number *q* of Eu(III) or Tb(III) center was calculated from luminescence lifetimes in the absence and presence of Zn(II). In the Zn-free state, both complexes showed a *q* value of 0. This non-hydrated state matches the shifted and reduced signals of labeled carbon in ^{13}C NMR spectrum of **EuL^{5*}** and explains the very low initial r_1 value of **GdL^{5}**. Once the complex and Zn(II) interact, the calculated *q* values are increased to 1.4 and 1.5 for **EuL^{5*}** and **TbL^{5}**, respectively. This higher hydration matches the dramatically increased r_1 value of **GdL^{5}** upon Zn(II) binding and the recovery of signals of labeled carbons observed in ^{13}C NMR spectra of **EuL^{5*}**. The hydration number investigation and ^{13}C NMR study confirm the assumption that the non-hydrated Gd(III) leads to a very low relaxivity while higher hydration of Gd(III) caused by Zn(II) gives rise to a dramatically high relaxivity.

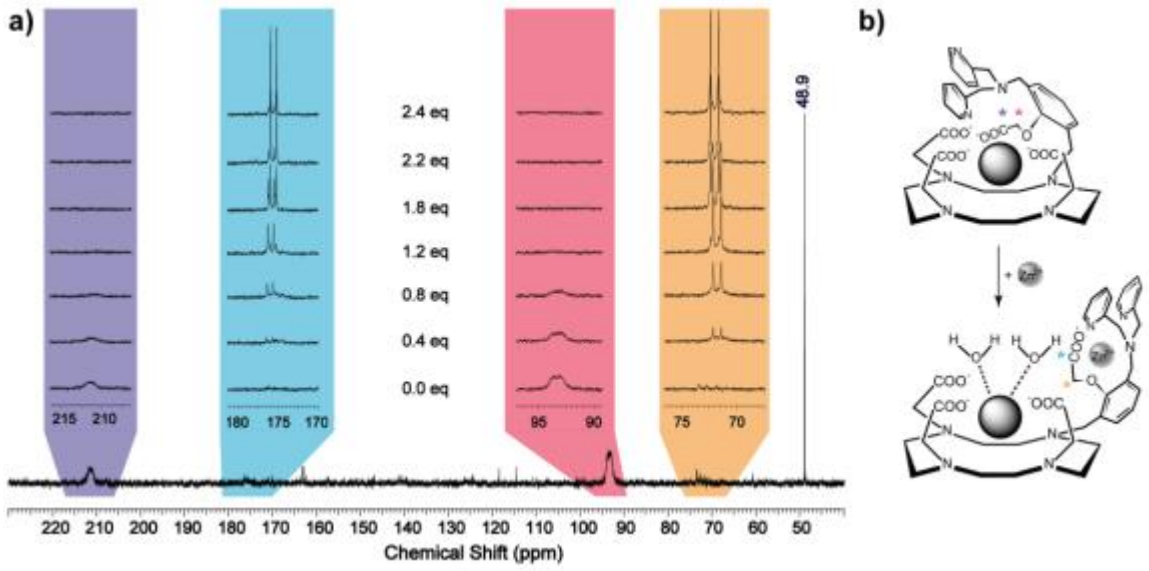

Figure 13. a) ^{13}C NMR spectra of **EuL^{5*}** in the presence of 0-2.4 equiv. of Zn(II) at 25 ^{o}C and 75 MHz (note: 48.9 ppm is the reference signal of $^{13}CH_3OH$). b) Proposed interaction of the phenoxyacetate group with the paramagnetic metal center (up) and Zn(II) (down), which leads to an increase in hydration number and the "turn-on" response.

In general terms, the relaxivity value is influenced by temperature. With the increase of temperature, the relaxivity will decrease at all magnetic field ranges due to the thermal activation of motion of water molecules surrounding the gadolinium complex.[63] Whilst the r_1 of **GdL^5** in PBS buffer increased from 1.47 to 5.58 $mM^{-1}s^{-1}$ at the physiological temperature 37 ^{o}C, the overall relaxivity enhancement still remained as high as ~280%, suggesting the potential of this complex to be a Zn(II) specific MRI CA (Figure 14b). Subsequently, the stability of **GdL^5** was assessed in a transmetalation reaction against Zn(II) at 25 ^{o}C and 37 ^{o}C, respectively. The "thermodynamic index" resulted in values 90%, 81% and 75% at 37 ^{o}C after 24 h, 72 h and 120 h, respectively. This experiment confirmed the investigated complex is a highly stable SCA.

Generally, the potential of a new complex to serve as a T_1-weighted SCA is further demonstrated 1) in HSA and serum medium in the ^{1}H NMR relaxometric titrations with Zn(II), and 2) *in vitro* in an MRI experiment on phantoms. HSA, known as a chelator for aromatic groups or Zn(II), may reduce the hydration of the complex then decrease its relaxivity. To evaluate the possibility of this investigated complex to be a candidate for *in vivo* application, the relaxometry of **GdL^5** with Zn(II) in the presence of either HSA or human serum were studied at 37 ^{o}C, 7 T. The experiment results showed the HSA binding affected the relaxivity of this complex but still

induced a ~200% relaxivity enhancement at the high magnetic field and physiological temperature (Figure 14a, left). To the best of our knowledge, this is the highest enhancement in the presence of HSA at the high magnetic field (> 1T) so far. On the other hand, the relaxivity enhancement is less impressive (~50%) in human serum (Figure 14a, right). It is proposed that bicarbonate, which is abundant in human serum (HCO_3^-, 20-30 mM),[64] is involved in the formation of a ternary complex between HCO_3^- and Gd(III). As reported in many research, bicarbonate possesses a relatively high affinity for these types of q = 1 or q = 2 complexes.[65, 66 64] To find out if the relaxivity quenching is caused by bicarbonate, the ^{1}H NMR relaxometric response of **GdL^5** towards Zn(II) was recorded in PBS buffer containing 25 mM HCO_3^- at 7 T and 37 ^{o}C (Figure 14c). The r_1 relaxivity enhancement is ~40%, which confirmed the bicarbonate in serum occupied the hydrated water molecules. Although the bicarbonate is involved in complexation with **GdL^5**, this relaxivity enhancement in serum is still better than published CAs so far.

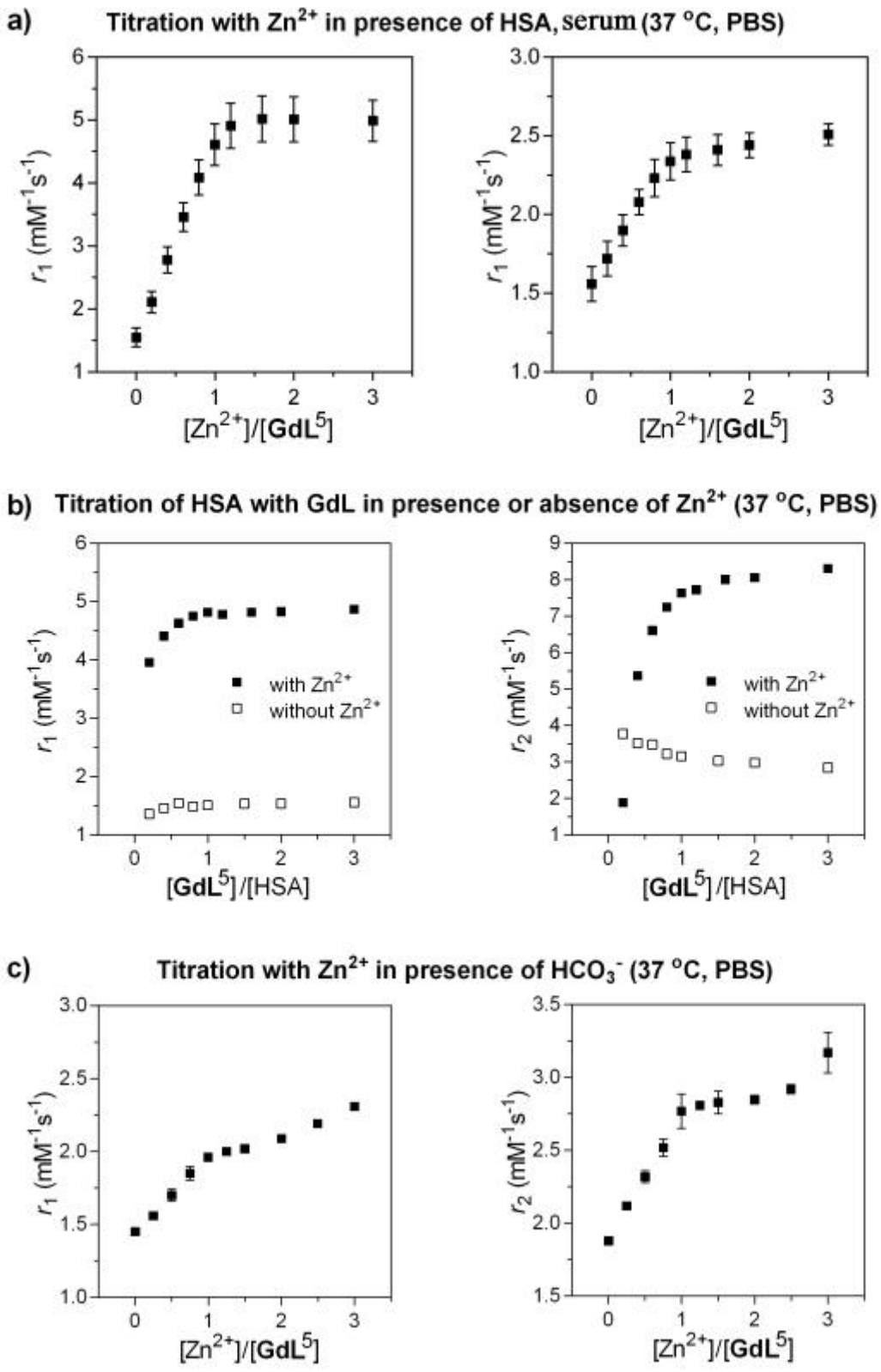

Figure 14. Relaxivities r_1 and r_2 of **GdL^5** in different media. a) 1.0 mM **GdL^5** in 0.6 mM HSA (left) or in serum (right) with various concentrations of $ZnCl_2$; b) in 0.6 mM HSA and 50mM PBS medium with various concentrations of **GdL^5**; c) 1.0 mM **GdL^5** in 25 mM $NaHCO_3$ and 50mM PBS with various concentrations of $ZnCl_2$ (pH 7.4 and 25 °C or 37 °C).

Subsequently, a series of different samples of **GdL^5** were imaged, to assess the potential of this complex as a T_1-weighted SCA. In the MRI phantom imaging experiment, six vials containing **GdL^5** alone, **GdL^5** with added 1 equivalent of Mg(II), 1 equivalent of Ca(II), 0.5 equivalent of Zn(II), 1 equivalent of Zn(II) and 1 equivalent of Zn(II) were imaged in a 7 T MRI scanner at room temperature by Dr. Tanja Gambino. In Figure 15, comparing the control image of the tube with **GdL^5** alone, tubes with **GdL^5** and 0.5 or 1.0 equivalent of Zn(II) show a great signal enhancement, whereas tubes where Ca(II) or Mg(II) were added just display similar contrast, confirming that a selective "turn-on" response of **GdL^5** can be visualized in a Zn-rich condition.

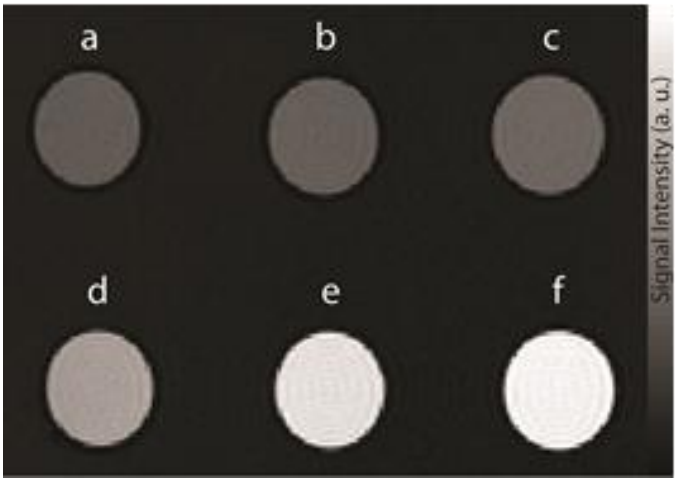

Figure 15. *T*1-weighted MR images of tube phantoms at 7 T of a 1 mM solution of **GdL^5** in 50 mM HEPES buffer (pH 7.4 and ~22 ^{o}C). The tubes were positioned in the following order: a) **GdL^5** only, b) +1.0 equiv. Mg(II), c) +1.0 equiv. Ca(II), d) +0.5 equiv. Zn(II), e) +1.0 equiv. Zn(II), f) +2.0 equiv. Zn(II).

The conversion of amino acid methyl ester to free amino acid in the Tyr group of **GdL^5** afforded complex **GdL^6**. At 25 ^{o}C, this new complex has a lower relaxivity enhancement (~200) than complex **GdL^5** in HEPES buffer but a similar enhancement (~290%) in PBS buffer. At 37 ^{o}C, the relaxivity enhancements of **GdL^6** in serum or bicarbonate medium are the same as **GdL^5**, owing to both complexes having similar coordination environments of the metal ions in the absence and presence of zinc ions (Figure 16). To collect more information on **GdL^6** upon the conversion of amino acid methyl ester to free amino acid in the Tyr group, a further step in the investigation of the detailed effect could be necessary.

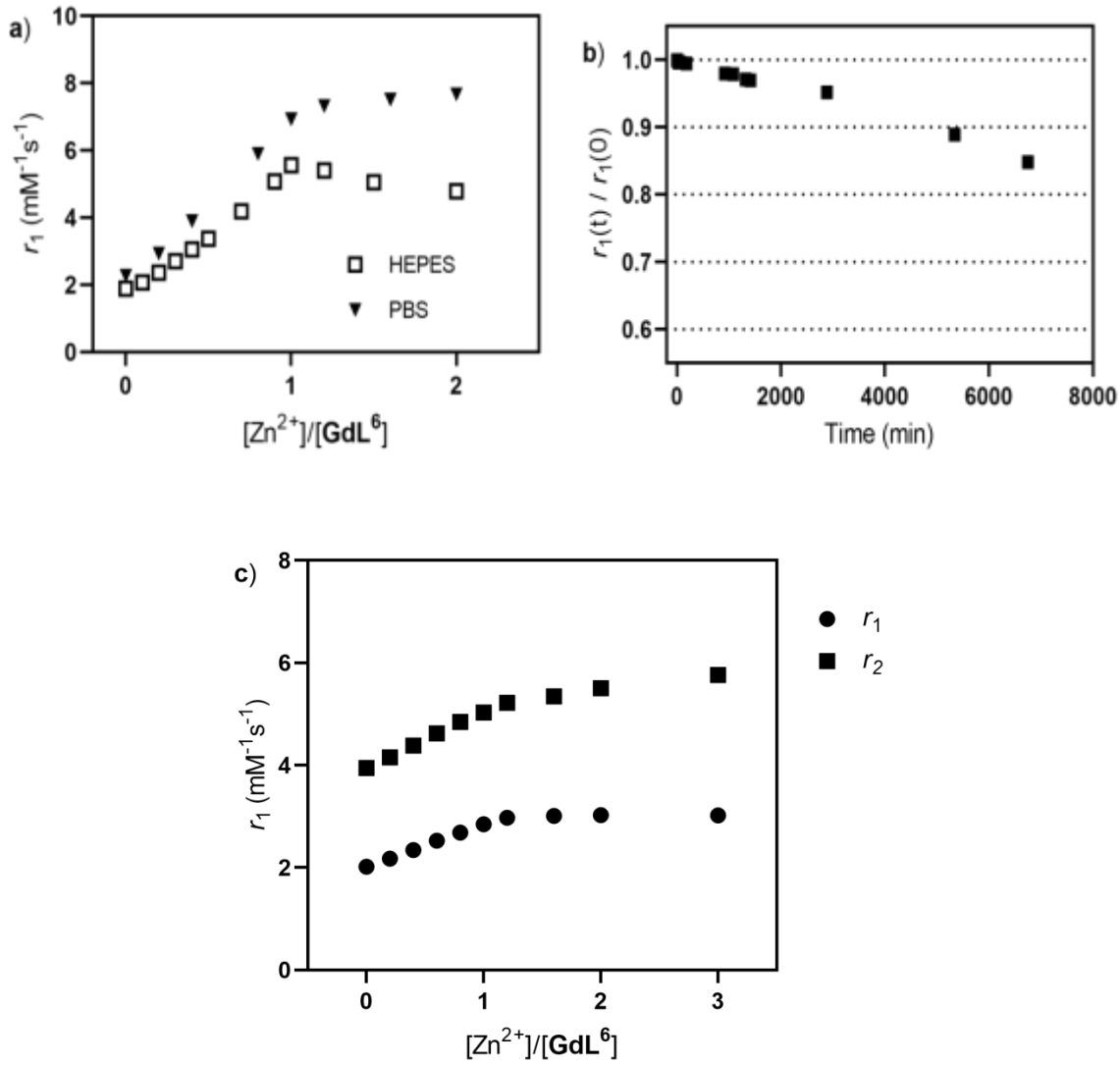

Figure 16. a) Relaxivity r_1 of 3.0 mM **GdL^6** in HEPES and PBS buffers with various concentrations of $ZnCl_2$ at 37 ^oC; b) Relaxivity rate variation of 3.0 mM **GdL^6** in 50 mM HEPES with Zn(II) versus time at 25 ^oC; c) Relaxivities r_1 and r_2 of 3.0 mM **GdL^6** in human serum with various concentrations of $ZnCl_2$ at 37 ^oC.

3.3. CEST/optical dual-modal probe.

Hetero-multinuclear agents make dual-/multi-modal imaging possible. By coupling different metal ions, the new agent will possess potential dual-modal sensing properties. For further extension of the first optical probes project and second T_1-weighted MRI project, in the third project, given that EuDOTAM-Gly is famous as a typical paraCEST agent,[67-69] the DOTAM-Gly block was considered to build up a trimacrocyclic derivative **L^7** appending a DA18C6 moiety, intending to explore a multi-nuclear dual-modal probe for CEST/optical imaging. First, the CEST

effects of the dinuclear europium complex **Eu_2L^7** were studied. Then, the hetero-trinuclear complex **Eu_2L^7Tb** was prepared and its luminescence properties were characterized.

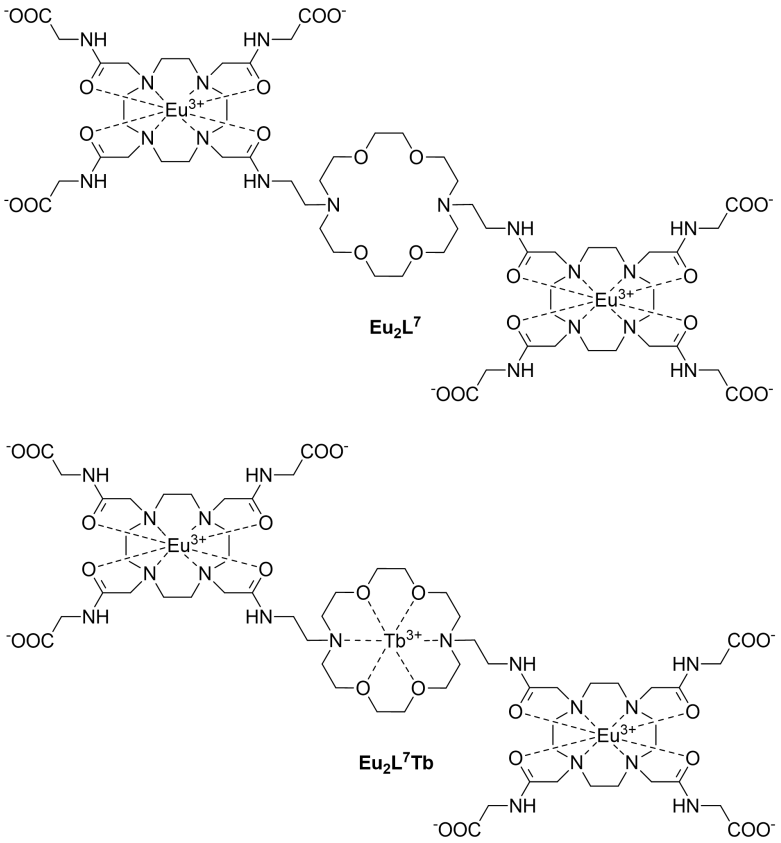

Figure 17. The chemical structures of **Eu_2L^7** and **Eu_2L^7Tb** investigated in this project.

Details for the ligand synthesis, starting from DA18C6 and mono-Bn-protected DO1A, are shown in Scheme 3. Two blocks for chelating Eu(II) and Tb(III) were synthesized separately. Europium chelator block was started from the alkylation of polyamine **6** with bromide **7**. The afforded macrocycle **8** was hydrogenated in DMF, providing the compound **9** with one free carboxylic acid. Terbium chelator block was started from the alkylation of DA18C6 with Cbz-protected compound **10**. The hydrogenation of the Cbz protecting group catalyzed by Pd/C formed compound **12** with two primary amines. The combination of two blocks **9** and **12** was catalyzed by HATU, resulting in the trimacrocyclic compound **13**. After deprotection by base hydrolysis, the free ligand **L^7** was purified by HPLC. The dinuclear complex **Eu_2L^7** was made at room temperature, adjusting pH ~7 using 0.1 M NaOH solution. Finally, the complex **Eu_2L^7** was treated with $TbCl_3$ solution, providing hetero-multinuclear complex **Eu_2L^7Tb**.

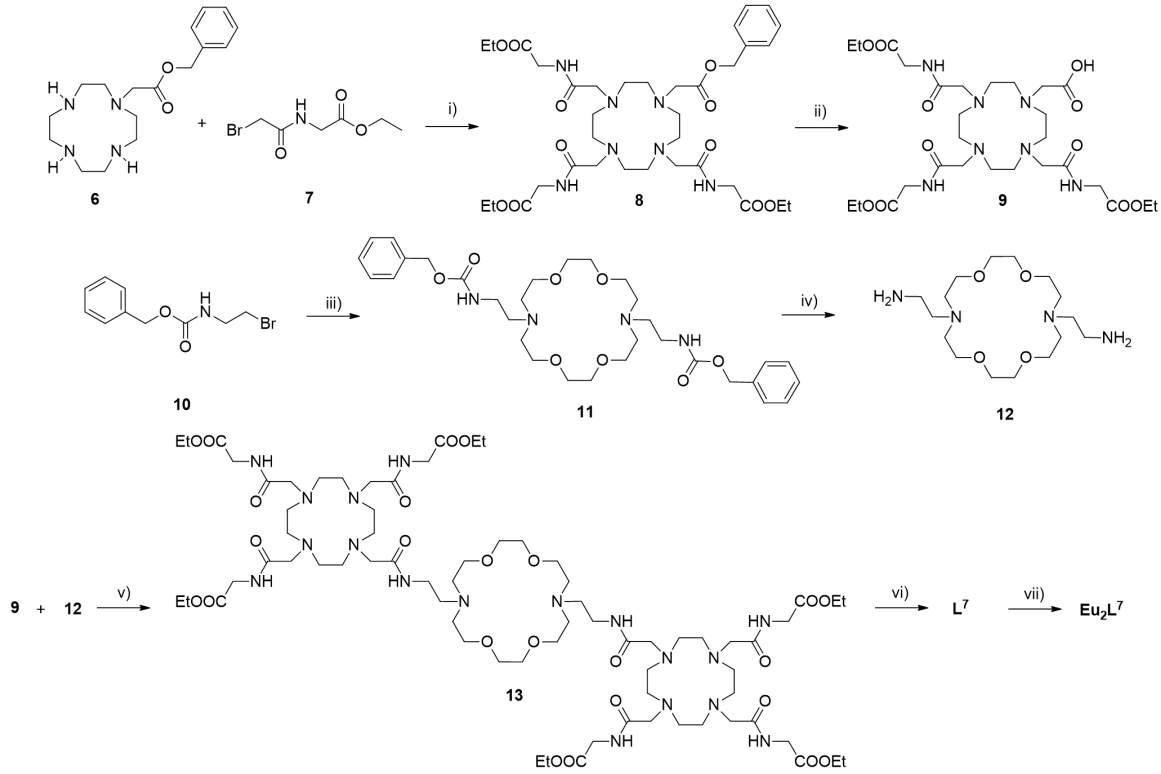

Scheme 3. Synthesis route of complex **Eu_2L^7**. Reagents and conditions: (i) Na_2CO_3, DCM, r.t. 12 h; (ii) H_2/Pt, DMF, r.t., 12 h; (iii) MeCN, Cs_2CO_3 , 65 ºC, 4.5 h; (iv) H_2/Pt, EtOH, r.t., 4 h; (v) HATU, DMF, r.t., 6 h; (vi) LiOH, MeOH, r.t., 12 h; (vii) $EuCl_3 \cdot 6H_2O/H_2O$, 50 °C, 12 h

Firstly, the CEST effects of **Eu_2L^7** were studied at 25 °C. The CEST spectra of the 5 mM complex were recorded with 10 s pre-saturation times and variable saturation power B_1 at pH 7.4, as depicted in Figure 18. Given a series of paraCEST derivatives of EuDOTAM-Gly show a CEST signal at ~50 ppm,[67-69] the signal of **Eu_2L^7** similarly appeared at 51 ppm, which is attributed to the proton exchange of Eu(III)-bound water with the bulk water molecules. With the increase of saturation power B_1 from 2.5 μT to 30 μT, the CEST effects are strongly affected.[70] The CEST effect enhancement reaches ~40% for the increase in saturation power from 5 μT to 30 μT.

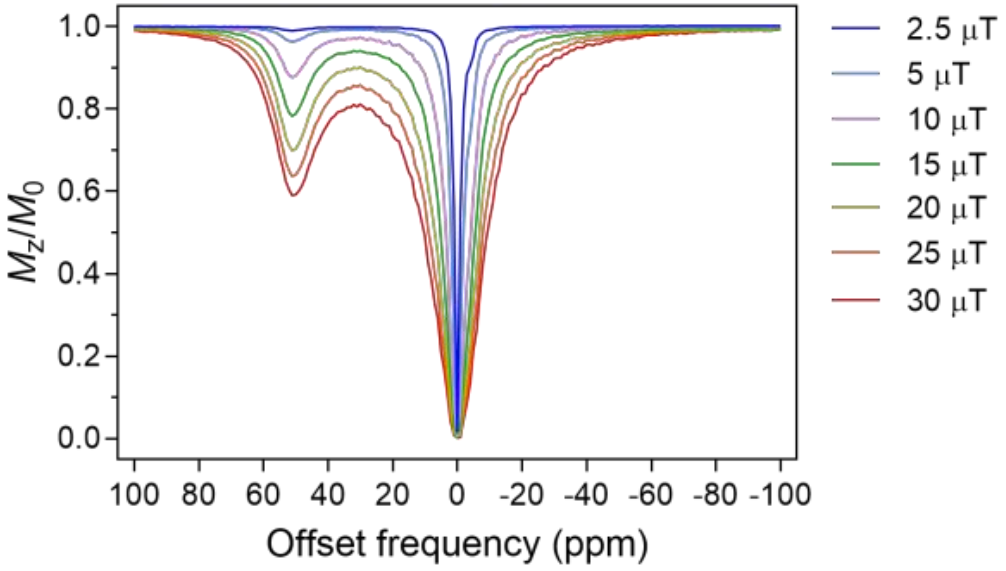

Figure 18. The CEST spectra of the complex **Eu_2L^7** (5 mM, irradiation time 10 s, in 50 mM HEPES with pH 7.4, 25 °C) recorded at different B_1.

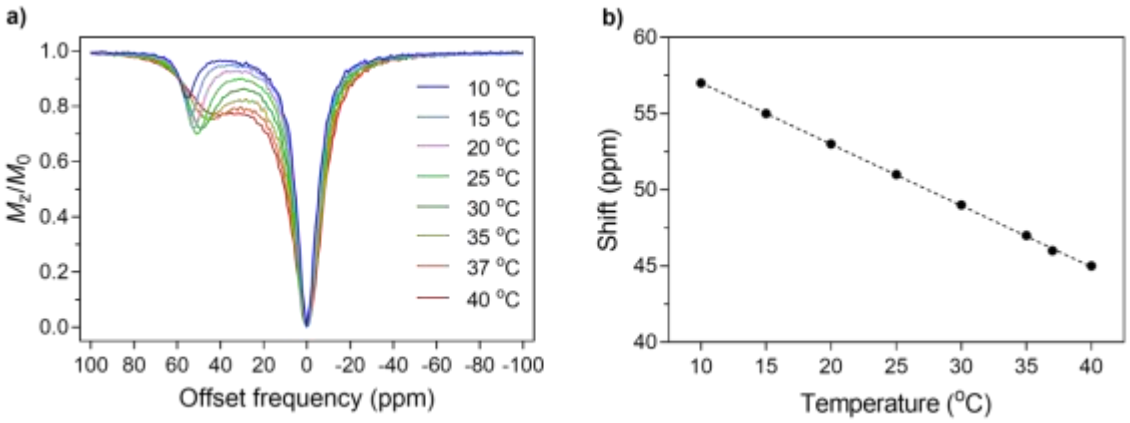

Figure 19. a): The CEST spectra of 5 mM **Eu_2L^7** at different temperatures. b): The dependence of the chemical shift of the bound water protons on temperature (pH = 7.4, B_0 = 7 T, saturation power B_1= 20 μT, TS 10 s).

Then, the aforementioned CEST studies were repeated at different temperatures. As expected, the CEST spectra registered pronounced differences both in the chemical shift of the bound water pool and the saturation efficiency of the bulk water (Figure 19). Along with the increase in temperature from 10 °C to 40 °C, the chemical shift of the bound water pool shifted upfield from 57 ppm to 45 ppm. A linear fitting was performed and the results showed that the shift of signal is linear to temperature (Figure 19b). The calculated temperature sensitivity is 0.4 ppm/°C, having a similar value to that of EuDOTAM-Gly.[71] Additionally, the signal shape of

both bound and bulk water were also affected by temperature (Figure 19 a). As the higher temperature is applied, the shapes of the two water peaks broaden, owing to more rapid exchange.

Subsequently, the Bloch–McConnell equations, modified for chemical exchange, namely the quantitative CEST methods,[72] were used to extract the water exchange rates, k_{ex}, at different temperatures. The longitudinal and transversal relaxation times, T_1 and T_2, were measured using the inversion-recovery and Carr-Purcell-Meiboom-Gill pulse sequences respectively and used to fit these data. As depicted in Figure 20, the k_{ex} assumed from a three-pool fitting model is dependent on temperature.[73, 74] At 25 °C, the value is 10 kHz, comparable to the value reported for the EuDOTAM-Gly.[75] All the discussed properties make **Eu_2L^7** to be a good candidate for future use as a paraCEST agent.

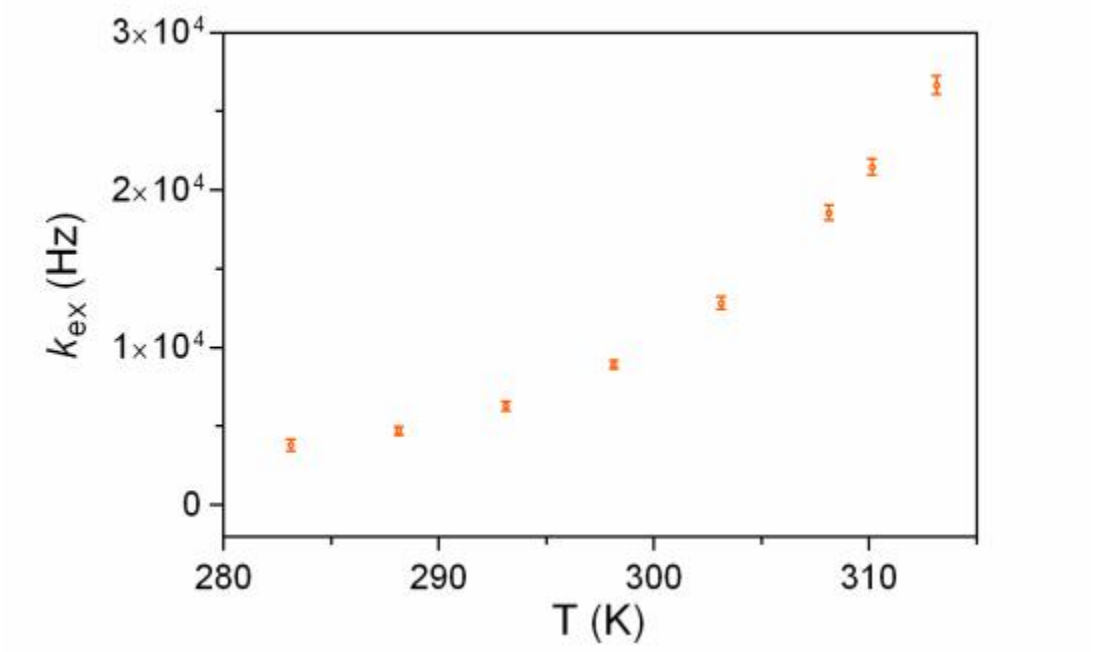

Figure 20. The k_{ex} values of bound water molecule (5 mM complex **Eu_2L^7**) dependent on temperature. Each temperature experiment was recorded at pH 7.4, with an irradiation time of 10 s and different B_1 (5, 10, 15, 20, 25 and 30 μT). The corresponding k_{ex} value was calculated using the quantitative CEST (qCEST) method.

To extend the complex **Eu_2L^7** to be a dual-modal probe, the remaining DA18C6 moiety was used to chelate another type of Ln(III) ion, albeit rather weakly. Namely, the stability constant of DA18C6-based Ln-complexes is small ($\log K_a < 3$),[76, 77] But interestingly, the afforded hetero-trinuclear complex **Eu_2L^7Tb** showed mixed emission spectra including both characteristic peaks of terbium and europium ions.

In Figure 21, the emission spectra of **Eu_2L^7Tb** were recorded at different excitation wavelengths from 225 nm to 395 nm, displaying fluctuations of the peaks either from Eu(III) ($^5D_0 \rightarrow {}^7F_J$) or from Tb(III) ($^5D_4 \rightarrow {}^7F_J$). The emission excited at 225 nm exhibited only four characteristic peaks of Tb(III) ion, with the strongest one at 545 nm ($^5D_4 \rightarrow {}^7F_5$). While the emission excited at 395 nm resulted in only four characteristic peaks of Eu(III) ion, with the strongest one at 616 nm ($^5D_0 \rightarrow {}^7F_2$).[78, 79] Additionally, excitations at 265 nm, 283 nm and 305 nm cause the combined peaks from both Eu(III) and Tb(III) ions.[80]

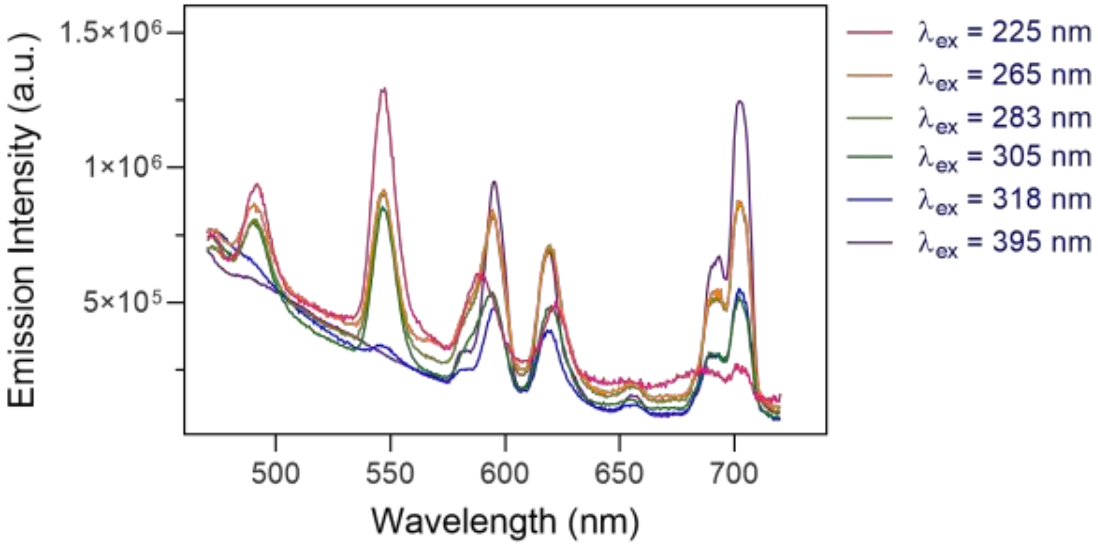

Figure 21. Luminescence spectra of 0.2 mM **Eu_2L^7Tb** versus excitation wavelength values at 25 °C, pH 7.4.

Upon the formation of **Eu_2L^7Tb**, the potential of this molecule for the detection of anions was investigated. Owing to the coordinatively unsaturated nature, the effects of small endogenous anions to **Eu_2L^7Tb** are studies, which is similar to previously investigated cyclen-based Ln(III) chelates.[18, 81] In these cases, the unsaturated Eu(III) or Tb(III) ions have binding site(s) for water molecules. The bound water molecule(s) are O–H oscillators with high energy, which can efficiently quench the luminescence.[82, 83] By contrast, displacement of a water molecule by anions can suppress the non-radiative energy quenching, providing stronger emission. Here, the luminescence of trimacrocyclic host **Eu_2L^7Tb** was assessed in solution with biologically important anions. A series of **Eu_2L^7Tb** solutions with F^-, Br^-, I^-, HCO_3^-, HPO_4^{2-}, OAc^- and SO_4^{2-}, respectively, were excited at 285 nm and their emission intensities were monitored in the range between 540 nm and 630 nm. As shown in

Figure 22, only anions HCO_3^- and OAc^- significantly enhanced the emission intensities. In a single emission spectrum, HCO_3^- induces stronger emission of Eu(III), while the OAc^- strengthens the emission of Tb(III), suggesting that bicarbonates preferentially displace bound waters in cyclen-derived chelates, whereas the acetates dominantly replace Tb-bound water molecules. On the other hand, the emission of Tb(III) is definitely quenched by anions F^- and HPO_4^{2-}, remaining unaffected emission of Eu(III).

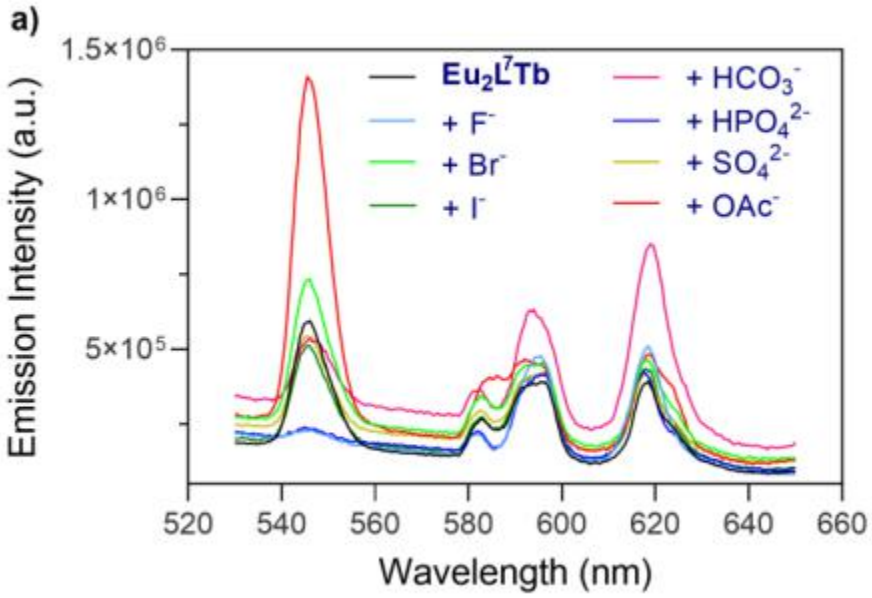

Figure 22. Luminescence selectivity studies of 0.2 mM **Eu_2L^7Tb** at 25 °C, pH 7.4. Excitation = 285 nm, 2 eq. of anions, monitored range from 540-630 nm.

4. Conclusions and outlook

Zn(II) is a fundamentally important metal ion which appears in all enzyme classes. Its deregulation is associated with diverse symptoms. Therefore, to understand its biological role and improve early-stage disease detection, in a non-invasive manner like OI and MRI, is of paramount importance. Here, this thesis describes the design, synthesis and characterization of lanthanide-based chelates, contributing to work in the field of MR or optical probes sensitive to zinc ions, and dual-modal probes with MR/optical imaging modalities, which paves the way to build dual-modal agents for zinc ion detection by means of optical/MR imaging. Towards such a final aim, many efforts have been undertaken.

a) Two Zn-sensitive optical probes **EuL$^{3\text{-}4}$** were developed from two non-sensitive optical probes. These novel probes exhibited strong selectivity to Zn(II) over other studied cations, leading to a 5- or 7-fold enhancement in luminescence intensity. The induced luminescence change establishes **EuL$^{3\text{-}4}$** as viable Zn-chemosensors for biological applications.

b) Two Zn-sensitive T_1-weighted MR agents **GdL$^{5\text{-}6}$** were developed from two non-sensitive T_1-weighted agents. Especially **GdL^{5}** showed ~400% relaxivity enhancement. Luminescence lifetime studies, ITC studies and ^{13}C NMR spectra measurements were conducted to explain the "turn-on" mechanism. The transmetalation studies, selectivity tests, performance evaluation in media like HSA or human serum and MRI phantoms, all the results evidenced the outstanding sensitivity of this complex to Zn(II) for potential biological applications

c) A polynuclear lanthanide complex as a dual-modal probe was developed. By combing the MRI CEST effects and luminescence properties into one platform, this probe paves the way to develop further potential dual-modal MRI/luminescence probes.

To conclude, the work conducted here describes gradually developed approaches towards the development of dual-modal agents for zinc ion detection by means of optical/MR imaging. Looking to the future, based on the third project and combining the aforementioned another two projects, the final aim can be achieved by coupling the Zn-sensitive optical probe with the Zn-sensitive MRI agent, which will result in a dual-model probe **EuL^{1}-GdL^{5}** for zinc ions detection by OI/MRI. For further

steps, such a dual-model probe can be modified by attaching a ^{19}F moiety. To this end, the multi-modal optical/^{19}F/T_1-weighted agent **EuL^1-GdL^5-^{19}F** can be established towards monitoring of zinc ion levels *in vivo*.

5. References/Cited Sources

1. Long, N. J.; Wong, W.-T., *The Chemistry of Molecular Imaging*. Wiley: Hoboken, New Jersey, 2015; p xii, 395 pages. 24 pages of plates.
2. Hogemann, D.; Basilion, J. P.; Weissleder, R., Molecular Imaging Techniques in Magnetic Resonance Imaging and Nuclear Imaging. *Radiologe* **2001,** 41, (2), 116-120.
3. Massoud, T. F.; Gambhir, S. S., Molecular Imaging in Living Subjects: Seeing Fundamental Biological Processes in a New Light. *Genes & Development* **2003,** 17, (5), 545-580.
4. Knight, J. C.; Edwards, P. G.; Paisey, S. J., Fluorinated Contrast Agents for Magnetic Resonance Imaging; a Review of Recent Developments. *RSC Advances* **2011,** 1, (8), 1415-1425.
5. Zhao, J. H.; Chen, J. W.; Ma, S. N.; Liu, Q. Q.; Huang, L. X.; Chen, X. N.; Lou, K. Y.; Wang, W., Recent Developments in Multimodality Fluorescence Imaging Probes. *Acta Pharmaceutica Sinica B* **2018,** 8, (3), 320-338.
6. Liu, J. J.; Liu, C.; He, W., Fluorophores and Their Applications as Molecular Probes in Living Cells. *Current Organic Chemistry* **2013,** 17, (6), 564-579.
7. Crosby, G. A.; Whan, R. E.; Freeman, J. J., Spectroscopic Studies of Rare Earth Chelates. *Journal of Physical Chemistry* **1962,** 66, (12), 2493-2499.
8. Dehorrocks, W.; Albin, M., Lanthanide Ion Luminescence in Coordination Chemistry and Biochemistry. *Progress in Inorganic Chemistry* **1983,** 31, 1-104.
9. Binnemans, K., Interpretation of Europium(III) Spectra. *Coordination Chemistry Reviews* **2015,** 295, 1-45.
10. Bonnet, C. S., Zn^{2+} Detection by MRI Using Ln^{3+}-Based Complexes: The Central Role of Coordination Chemistry. *Coordination Chemistry Reviews* **2018,** 369, 91-104.
11. Wahsner, J.; Gale, E. M.; Rodriguez-Rodriguez, A.; Caravan, P., Chemistry of Mri Contrast Agents: Current Challenges and New Frontiers. *Chemical Reviews* **2019,** 119, (2), 957-1057.
12. Akiba, H.; Sumaoka, J.; Komiyama, M., Binuclear Terbium(III) Complex as a Probe for Tyrosine Phosphorylation. *Chemistry-a European Journal* **2010,** 16, (17), 5018-5025.
13. Roger, M.; Regueiro-Figueroa, M.; Ben Azzeddine, C.; Patinec, V.; Bonnet, C. S.; Platas-Iglesias, C.; Tripier, R., Lanthanide Complexes with Heteroditopic Ligands as Fluorescent Zinc Sensors. *European Journal of Inorganic Chemistry* **2014,** 2014, (6), 1072-1081.
14. Pope, S. J.; Laye, R. H., Design, Synthesis and Photophysical Studies of an Emissive, Europium Based, Sensor for Zinc. *Dalton Transactions* **2006**, (25), 3108-13.
15. Heffern, M. C.; Matosziuk, L. M.; Meade, T. J., Lanthanide Probes for Bioresponsive Imaging. *Chemical Reviews* **2014,** 114, (8), 4496-4539.
16. Rodríguez-Rodríguez, A.; Zaiss, M.; Esteban-Gómez, D.; Angelovski, G.; Platas-Iglesias, C., Paramagnetic Chemical Exchange Saturation Transfer Agents and Their Perspectives for Application in Magnetic Resonance Imaging. *International Reviews in Physical Chemistry* **2020,** 40, (1), 51-79.
17. Moore, E. G.; Samuel, A. P. S.; Raymond, K. N., From Antenna to Assay: Lessons Learned in Lanthanide Luminescence. *Accounts of Chemical Research* **2009,** 42, (4), 542-552.
18. Aletti, A. B.; Gillen, D. M.; Gunnlaugsson, T., Luminescent/Colorimetric Probes and (Chemo-) Sensors for Detecting Anions Based on Transition and Lanthanide Ion Receptor/Binding Complexes. *Coordination Chemistry Reviews* **2018,** 354, 98-120.
19. Cable, M. L.; Levine, D. J.; Kirby, J. P.; Gray, H. B.; Ponce, A., Luminescent Lanthanide Sensors. *Advances in Inorganic Chemistry, Vol 63: Inorganic Photochemistry* **2011,** 63, 1-45.

20. Caravan, P.; Ellison, J. J.; McMurry, T. J.; Lauffer, R. B., Gadolinium(III) Chelates as MRI Contrast Agents: Structure, Dynamics, and Applications. *Chemical Reviews* **1999,** 99, (9), 2293-2352.
21. Helm, L.; Merbach, A. E.; Tóth, E. v., *The Chemistry of Contrast Agents in Medical Magnetic Resonance Imaging*. 2ed.; John Wiley & Sons Inc.: Hoboken, NJ, 2013; p xvi, 496 pages.
22. Debroye, E.; Parac-Vogt, T. N., Towards Polymetallic Lanthanide Complexes as Dual Contrast Agents for Magnetic Resonance and Optical Imaging. *Chemical Society Reviews* **2014,** 43, (23), 8178-8192.
23. Ward, K. M.; Aletras, A. H.; Balaban, R. S., A New Class of Contrast Agents for MRI Based on Proton Chemical Exchange Dependent Saturation Transfer (CEST). *Journal of Magnetic Resonance* **2000,** 143, (1), 79-87.
24. Murase, K.; Tanki, N., Numerical Solutions to the Time-Dependent Bloch Equations Revisited. *Magnetic Resonance Imaging* **2011,** 29, (1), 126-131.
25. Evbuomwan, O. M.; Terreno, E.; Aime, S.; Sherry, A. D., CEST and ParaCEST Agents for Molecular Imaging. In *The Chemistry of Molecular Imaging*, Long, N.; Wong, W. T., Eds. 2014; pp 224-243.
26. Woods, M.; Donald, E. W. C.; Sherry, A. D., Paramagnetic Lanthanide Complexes as Paracest Agents for Medical Imaging. *Chemical Society Reviews* **2006,** 35, (6), 500-511.
27. Yang, X.; Yadav, N. N.; Song, X. L.; Banerjee, S. R.; Edelman, H.; Minn, I.; van Zijl, P. C. M.; Pomper, M. G.; McMahon, M. T., Tuning Phenols with Intra-Molecular Bond Shifted Hydrogens (IM-SHY) as DiaCEST MRI Contrast Agents. *Chemistry-a European Journal* **2014,** 20, (48), 15824-15832.
28. Zhang, S. R.; Merritt, M.; Woessner, D. E.; Lenkinski, R. E.; Sherry, A. D., ParaCEST Agents: Modulating MRI Contrast via Water Proton Exchange. *Accounts of Chemical Research* **2003,** 36, (10), 783-790.
29. Que, E. L.; Chang, C. J., Responsive Magnetic Resonance Imaging Contrast Agents as Chemical Sensors for Metals in Biology and Medicine. *Chemical Society Reviews* **2010,** 39, (1), 51-60.
30. Mills, C. F., *Zinc in Human Biology*. Springer-Verlag: London ; New York, 1988; p xix, 388 p.
31. Maret, W.; Li, Y., Coordination Dynamics of Zinc in Proteins. *Chemical Reviews* **2009,** 109, (10), 4682-4707.
32. Jiang, P. J.; Guo, Z. J., Fluorescent Detection of Zinc in Biological Systems: Recent Development on the Design of Chemosensors and Biosensors. *Coordination Chemistry Reviews* **2004,** 248, (1-2), 205-229.
33. Kikuchi, K.; Komatsu, K.; Nagano, T., Zinc Sensing for Cellular Application. *Current Opinion in Chemical Biology* **2004,** 8, (2), 182-191.
34. De Leon-Rodriguez, L.; Lubag, A. J., Jr.; Sherry, A. D., Imaging Free Zinc Levels *in vivo* - What Can Be Learned? *Inorganica Chimica Acta* **2012,** 393, 12-23.
35. Carter, K. P.; Young, A. M.; Palmer, A. E., Fluorescent Sensors for Measuring Metal Ions in Living Systems. *Chemical Reviews* **2014,** 114, (8), 4564-4601.
36. Biniecki, S.; Kabzinska, S., [Synthesis of Bis-(Pyridylmethyl)-Amines]. *Annales pharmaceutiques françaises* **1964,** 22, 685-687.
37. Frullano, L.; Meade, T. J., Multimodal MRI Contrast Agents. *Journal of Biological Inorganic Chemistry* **2007,** 12, (7), 939-949.
38. Li, K.; Ding, D.; Huo, D.; Pu, K. Y.; Ngo, N. P. T.; Hu, Y.; Li, Z.; Liu, B., Conjugated Polymer Based Nanoparticles as Dual-Modal Probes for Targeted *in vivo* Fluorescence and Magnetic Resonance Imaging. *Advanced Functional Materials* **2012,** 22, (15), 3107-3115.
39. Ding, D.; Wang, G.; Liu, J. Z.; Li, K.; Pu, K. Y.; Hu, Y.; Ng, J. C. Y.; Tang, B. Z.; Liu, B., Hyperbranched Conjugated Polyelectrolyte for Dual-Modality Fluorescence and Magnetic Resonance Cancer Imaging. *Small* **2012,** 8, (22), 3523-3530.

40. Huber, M. M.; Staubli, A. B.; Kustedjo, K.; Gray, M. H. B.; Shih, J.; Fraser, S. E.; Jacobs, R. E.; Meade, T. J., Fluorescently Detectable Magnetic Resonance Imaging Agents. *Bioconjugate Chemistry* **1998,** 9, (2), 242-249.
41. Jennings, L. E.; Long, N. J., 'Two Is Better Than One'-Probes for Dual-Modality Molecular Imaging. *Chemical Communications* **2009**, (24), 3511-3524.
42. Terreno, E.; Boffa, C.; Menchise, V.; Fedeli, F.; Carrera, C.; Delli Castelli, D.; Digilio, G.; Aime, S., Gadolinium-Doped Lipocest Agents: A Potential Novel Class of Dual ^{1}H-MRI Probes. *Chemical Communications* **2011,** 47, (16), 4667-4669.
43. Placidi, M. P.; Villaraza, A. J.; Natrajan, L. S.; Sykes, D.; Kenwright, A. M.; Faulkner, S., Synthesis and Spectroscopic Studies on Azo-Dye Derivatives of Polymetallic Lanthanide Complexes: Using Diazotization to Link Metal Complexes Together. *Journal of the American Chemical Society* **2009,** 131, (29), 9916-9917.
44. Sorensen, T. J.; Tropiano, M.; Blackburn, O. A.; Tilney, J. A.; Kenwright, A. M.; Faulkner, S., Preparation and Study of an F,F,F',F" Covalently Linked Tetranuclear Hetero-Trimetallic Complex - a Europium, Terbium, Dysprosium Triad. *Chemical Communications* **2013,** 49, (8), 783-785.
45. Mamedov, I.; Parac-Vogt, T. N.; Logothetis, N. K.; Angelovski, G., Synthesis and Characterization of Dinuclear Heterometallic Lanthanide Complexes Exhibiting MRI and Luminescence Response. *Dalton Transactions* **2010,** 39, (24), 5721-5127.
46. Jones, J. E.; Amoroso, A. J.; Dorin, I. M.; Parigi, G.; Ward, B. D.; Buurma, N. J.; Pope, S. J. A., Bimodal, Dimetallic Lanthanide Complexes That Bind to DNA: The Nature of Binding and Its Influence on Water Relaxivity. *European Journal of Inorganic Chemistry* **2011,** 47, (12), 3374-3376.
47. Belina, M. F.; Freire, R. O.; Galembeck, A.; de Sa, G. F.; de Farias, R. F.; Alves, S., A New Eu(III)/Tb(III) Binuclear Coordination Compound with Crown Ethers and Bridging 4,4 '-Dipyridyl. *Journal of Luminescence* **2010,** 130, (10), 1946-1951.
48. Faulkner, S.; Pope, S. J., Lanthanide-Sensitized Lanthanide Luminescence: Terbium-Sensitized Ytterbium Luminescence in a Trinuclear Complex. *Journal of the American Chemical Society* **2003,** 125, (35), 10526-10527.
49. Kohlmeier, M., *Tyrosine*. acdemic press: 2003; p 321-328.
50. Torelli, S.; Belle, C.; Gautier-Luneau, I.; Pierre, J. L.; Saint-Aman, E.; Latour, J. M.; Le Pape, L.; Luneau, D., pH-Controlled Change of the Metal Coordination in a Dicopper(II) Complex of the Ligand H-BPMP: Crystal Structures, Magnetic Properties, and Catecholase Activity. *Inorganic Chemistry* **2000,** 39, (16), 3526-3536.
51. Shieh, W. C.; Dell, S.; Repic, O., 1,8-Diazabicyclo[5.4.0]Undec-7-Ene (DBU) and Microwave-Accelerated Green Chemistry in Methylation of Phenols, Indoles, and Benzimidazoles with Dimethyl Carbonate. *Organic Letters* **2001,** 3, (26), 4279-4281.
52. Wang, G.; Platas-Iglesias, C.; Angelovski, G., Europium(III) Macrocyclic Chelates Appended with Tyrosine-Based Chromophores and Di-(2-Picolyl)Amine-Based Receptors: Turn-on Luminescent Chemosensors Selective to Zinc(II) Ions. *ChemPlusChem* **2020,** 85, (5), 806-814.
53. Fornander, L. H.; Feng, B.; Beke-Somfai, T.; Norden, B., UV Transition Moments of Tyrosine. *The Journal of Physical Chemistry B* **2014,** 118, (31), 9247-9257.
54. Antosiewicz, J. M.; Shugar, D., UV-Vis Spectroscopy of Tyrosine Side-Groups in Studies of Protein Structure. Part 1: Basic Principles and Properties of Tyrosine Chromophore. *Biophysical Reviews* **2016,** 8, (2), 151-161.
55. Escudero, D., Revising Intramolecular Photoinduced Electron Transfer (PET) from First-Principles. *Accounts of Chemical Research* **2016,** 49, (9), 1816-1824.
56. Zhang, S.; Adhikari, R.; Fang, M.; Dorh, N.; Li, C.; Jaishi, M.; Zhang, J.; Tiwari, A.; Pati, R.; Luo, F. T.; Liu, H., Near-Infrared Fluorescent Probes with Large Stokes Shifts for Sensing Zn(II) Ions in Living Cells. *Acs Sensors* **2016,** 1, (12), 1408-1415.
57. Regueiro-Figueroa, M.; Gündüz, S.; Patinec, V.; Logothetis, N. K.; Esteban-Gómez, D.; Tripier, R.; Angelovski, G.; Platas-Iglesias, C., Gd^{3+}-Based Magnetic Resonance Imaging Contrast Agent Responsive to Zn^{2+}. *Inorganic Chemistry* **2015,** 54, (21), 10342-10350.

58. Helm, L.; Merbach, A. E.; Tóth, E. v., *The Chemistry of Contrast Agents in Medical Magnetic Resonance Imaging*. 2ed.; John Wiley & Sons Inc.: Hoboken, NJ, 2013; p 496.
59. Angelovski, G., What We Can Really Do with Bioresponsive MRI Contrast Agents. *Angewandte Chemie International Edition* **2016,** 55, (25), 7038-46.
60. Osredkar, J.; Sustar, N., Copper and Zinc, Biological Role and Significance of Copper/Zinc Imbalance. *Journal of Clinical Toxicology* **2011,** S3, (1), 1-18.
61. Major, J. L.; Boiteau, R. M.; Meade, T. J., Mechanisms of Zn^{ii}-Activated Magnetic Resonance Imaging Agents. *Inorganic Chemistry* **2008,** 47, (22), 10788-10795.
62. Matosziuk, L. M.; Leibowitz, J. H.; Heffern, M. C.; MacRenaris, K. W.; Ratner, M. A.; Meade, T. J., Structural Optimization of Zn(II)-Activated Magnetic Resonance Imaging Probes. *Inorganic Chemistry* **2013,** 52, (21), 12250-12261.
63. Reichenbach, J. R.; Hacklander, T.; Harth, T.; Hofer, M.; Rassek, M.; Modder, U., ^1H T_1 and T_2 Measurements of the MR Imaging Contrast Agents Gd-DTPA and Gd-DTPA BMA at 1.5T. *European Radiology* **1997,** 7, (2), 264-274.
64. Giardiello, M.; Lowe, M. P.; Botta, M., An Esterase-Activated Magnetic Resonance Contrast Agent. *Chemical Communications* **2007**, (39), 4044-4046.
65. Burai, L.; Hietapelto, V.; Kiraly, R.; Toth, E.; Brucher, E., Stability Constants and ^1H Relaxation Effects of Ternary Complexes Formed between Gd-DTPA, Gd-DTPA-BMA, Gd-DOTA, and Gd-EDTA and Citrate, Phosphate, and Carbonate Ions. *Magnetic Resonance in Medicine* **1997,** 38, (1), 146-150.
66. Aime, S.; Barge, A.; Botta, M.; Howard, J. A. K.; Kataky, R.; Lowe, M. P.; Moloney, J. M.; Parker, D.; de Sousa, A. S., Dependence of the Relaxivity and Luminescence of Gadolinium and Europium Amino-Acid Complexes on Hydrogencarbonate and pH. *Chemical Communications* **1999**, (11), 1047-1048.
67. Zhang, S.; Winter, P.; Wu, K.; Sherry, A. D., A Novel Europium(III)-Based MRI Contrast Agent. *Journal of the American Chemical Society* **2001,** 123, (7), 1517-1518.
68. Evbuomwan, O. M.; Kiefer, G.; Sherry, A. D., Amphiphilic Eudota-Tetraamide Complexes Form Micelles with Enhanced Cest Sensitivity. *European Journal of Inorganic Chemistry* **2012,** 2012, (12), 2126-2134.
69. Cakic, N.; Verbic, T. Z.; Jelic, R. M.; Platas-Iglesias, C.; Angelovski, G., Synthesis and Characterisation of Bismacrocyclic DO3A-Amide Derivatives - an Approach Towards Metal-Responsive Paracest Agents. *Dalton Transactions* **2016,** 45, (15), 6555-6565.
70. van Zijl, P. C. M.; Yadav, N. N., Chemical Exchange Saturation Transfer (CEST): What Is in a Name and What Isn't? *Magnetic Resonance in Medicine* **2011,** 65, (4), 927-948.
71. Zhang, S.; Malloy, C. R.; Sherry, A. D., MRI Thermometry Based on Paracest Agents. *Journal of the American Chemical Society* **2005,** 127, (50), 17572-17573.
72. Zaiss, M.; Angelovski, G.; Demetriou, E.; McMahon, M. T.; Golay, X.; Scheffler, K., Quesp and Quest Revisited - Fast and Accurate Quantitative CEST Experiments. *Magnetic Resonance in Medicine* **2018,** 79, (3), 1708-1721.
73. Meiboom, S.; Gill, D., Modified Spin-Echo Method for Measuring Nuclear Relaxation Times. *Review of Scientific Instruments* **1958,** 29, (8), 688-691.
74. Carr, H. Y.; Purcell, E. M., Effects of Diffusion on Free Precession in Nuclear Magnetic Resonance Experiments. *Physical Review* **1954,** 94, (3), 630-638.
75. Dixon, W. T.; Ren, J.; Lubag, A. J.; Ratnakar, J.; Vinogradov, E.; Hancu, I.; Lenkinski, R. E.; Sherry, A. D., A Concentration-Independent Method to Measure Exchange Rates in Paracest Agents. *Magnetic Resonance in Medicine* **2010,** 63, (3), 625-632.
76. Suarez, S.; Mamula, O.; Scopelliti, R.; Donnio, B.; Guillon, D.; Terazzi, E.; Piguet, C.; Bunzli, J. C. G., Lanthanide Luminescent Mesomorphic Complexes with Macrocycles Derived from Diaza-18-Crown-6. *New Journal of Chemistry* **2005,** 29, (10), 1323-1334.
77. Sazonov, P. K.; Stolyarenko, V. Y.; Shtern, M. M.; Beletskaya, I. P., Unexpected Lanthanide Cation Selectivity of Bis-B-Ketovinylated Diaza-18-Crown-6 and Open-

Chain Diamines: Cooperative Effect of the Second Keto Group. *Journal of Inclusion Phenomena and Macrocyclic Chemistry* **2014,** 79, (1-2), 193-203.
78. Zhang, H. X.; Chen, Z. H.; Liu, X.; Zhang, F., A Mini-Review on Recent Progress of New Sensitizers for Luminescence of Lanthanide Doped Nanomaterials. *Nano Research* **2020,** 13, (7), 1795-1809.
79. Kaczmarek, M., Lanthanide-Sensitized Luminescence and Chemiluminescence in the Systems Containing Most Often Used Medicines; a Review. *Journal of Luminescence* **2020,** 222, 117174.
80. Gao, C. J.; Kirillov, A. M.; Dou, W.; Tang, X. L.; Liu, L. L.; Yan, X. H.; Xie, Y. J.; Zang, P. X.; Liu, W. S.; Tang, Y., Self-Assembly Synthesis, Structural Features, and Photophysical Properties of Dilanthanide Complexes Derived from a Novel Amide Type Ligand: Energy Transfer from Tb(III) to Eu(III) in a Heterodinuclear Derivative. *Inorganic Chemistry* **2014,** 53, (2), 935-942.
81. Parker, D.; Dickins, R. S.; Puschmann, H.; Crossland, C.; Howard, J. A., Being Excited by Lanthanide Coordination Complexes: Aqua Species, Chirality, Excited-State Chemistry, and Exchange Dynamics. *Chemical Reviews* **2002,** 102, (6), 1977-2010.
82. Kropp, J. L.; Windsor, M. W., Luminescence and Energy Transfer in Solutions of Rare Earth Complexes. II. Studies of the Solvation Shell in Europium(III) and Terbium(III) as a Function of Acetate Concentration. *The Journal of Physical Chemistry* **1967,** 71, (3), 477-482.
83. Horrocks, W. D.; Sudnick, D. R., Lanthanide Ion Probes of Structure in Biology - Laser-Induced Luminescence Decay Constants Provide a Direct Measure of the Number of Metal-Coordinated Water-Molecules. *Journal of the American Chemical Society* **1979,** 101, (2), 334-340.

6. Appendix

Chapter 3.1

G. Wang, C. Platas-Iglesias, G. Angelovski*. Europium(III) Macrocyclic Chelates Appended with Tyrosine-based Chromophores and Di-(2-picolyl)amine-based Receptors: Turn-On Luminescent Chemosensors Selective to Zinc(II) Ions. *ChemPlusChem* **2020**, 85, 806-814.

Chapter 3.2

G. Wang, G. Angelovski*. Highly Potent MRI Contrast Agent Displaying Outstanding Sensitivity to Zinc Ions. *Angew. Chem. Int. Ed.* **2020**, DOI: 10.1002/anie.202014431

Chapter 3.3

G. Wang, G. Angelovski*. Macrocyclic Chelates Bridged by a Diaza-crown Ether: Towards Multinuclear Bimodal Molecular Imaging Probes. *Molecules* **2020**, 25, 5019

G. Castro, **G. Wang**, T. Gambino, D. Esteban-Gómez, L. Valencia, G. Angelovski, C. Platas-Iglesias*, P. Pérez-Lourido. Lanthanide(III) Complexes Based on a 18-Membered Macrocycle Containing Acetamide Pendants. Structural Characterization and paraCEST Properties. *Inorg. Chem.* (Submitted)

ChemPlusChem

A Multidisciplinary Journal Centering on Chemistry

Chemistry Europe

European Chemical Societies Publishing

Front Cover:

G. Angelovski and co-workers

Europium(III) Macrocyclic Chelates Appended with Tyrosine-based Chromophores and Di-(2-picolyl)amine-based Receptors: Turn-On Luminescent Chemosensors Selective to Zinc(II) Ions

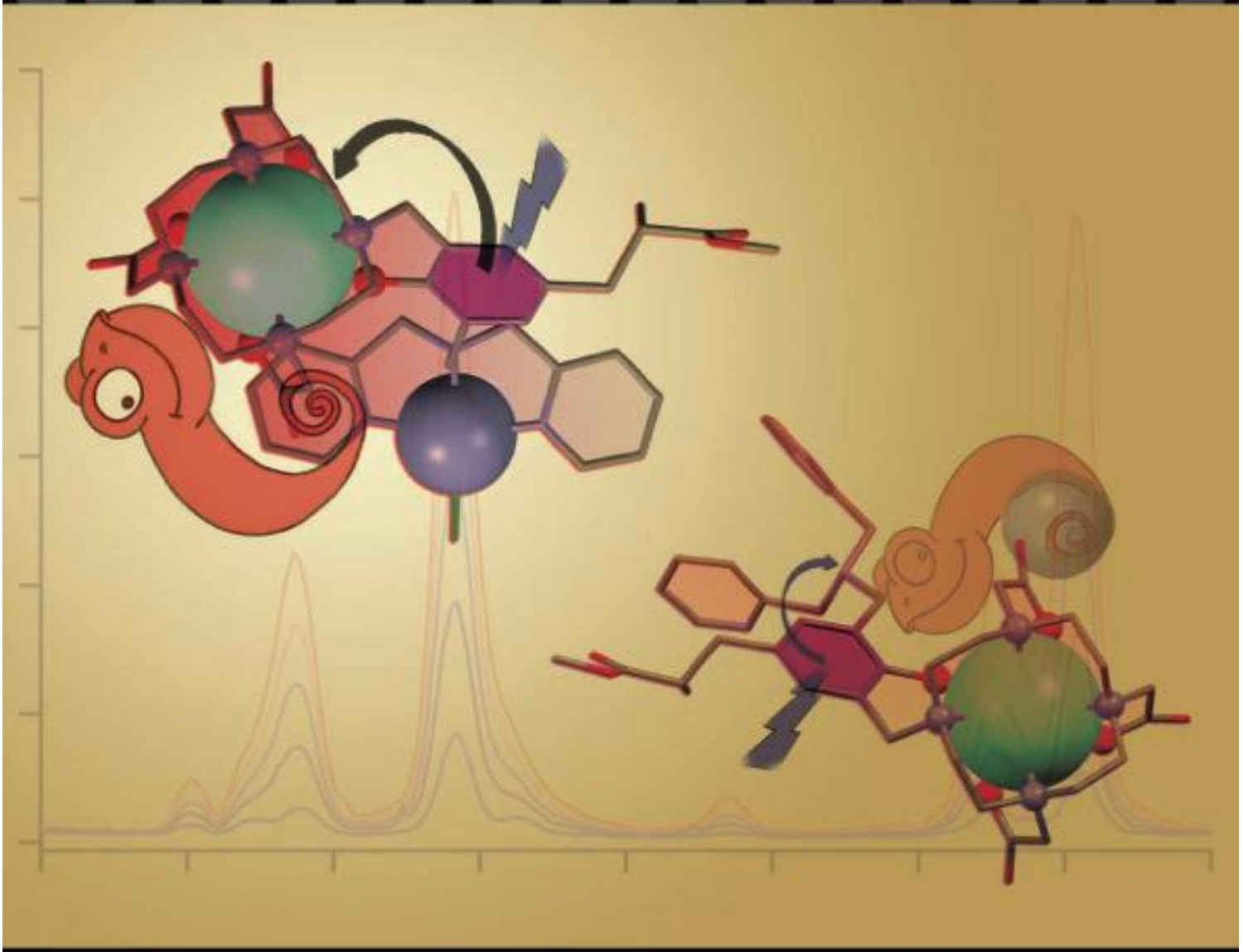

05/2020

WILEY-VCH

Europium(III) Macrocyclic Chelates Appended with Tyrosine-based Chromophores and Di-(2-picolyl)amine-based Receptors: Turn-On Luminescent Chemosensors Selective to Zinc(II) Ions

Gaoji Wang,[a] Carlos Platas-Iglesias,[b] and Goran Angelovski*[a]

Zinc ions play an important role in many biological processes in the human body. To selectively detect Zn^{2+}, two EuDO3A-based complexes (DO3A − 1,4,7,10-tetraazacyclododecane-1,4,7-tricarboxylic acid) appended with tyrosine as a chromophore and di-(2-picolyl)amine (DPA) as the Zn^{2+} recognition moiety were developed as suitable luminescent sensors. Their luminescence intensity is affected by the photoinduced electron transfer mechanism. Upon addition of Zn^{2+}, both probes display an up to sevenfold enhancement in Eu^{3+} emission. Competition experiments demonstrated their specificity toward Zn^{2+} over other metal ions, while also revealing the nonspecificity of the derivatives lacking the DPA-moiety, thus confirming the essential role of the DPA for the recognition of Zn^{2+}. The induced emission changes of Eu^{3+} allow for precise quantitative analysis of Zn^{2+}, establishing these lanthanide-based complexes as viable chemosensors for biological applications.

Introduction

Zinc ions are the second most abundant transition metal ions in the human body. They play a fundamental role in living systems as they are involved in many essential biological processes, including enzyme activity, signaling and gene transcription.[1] In vivo, Zn^{2+} is present in the free and protein-bound form. The abundance of Zn^{2+} is particularly important in the brain, breast, prostate and pancreas.[2] While it is not redox active under physiological conditions, Zn^{2+} deficiency is known to cause increased oxidative stress contributing to the development of different pathologies, such as cancer.[3] Therefore, its concentration in healthy organs is highly regulated by the cells through transporters and metallochaperones.[1c] Thus, imaging Zn^{2+} by non-invasive techniques is of paramount importance to understand its biological role and improve early-stage disease detection.[1c]

Due to low cost and high instrument sensitivity, a large number of optical probes and related toolboxes have been developed for the detection of Zn^{2+} in the last few decades.[1d,4] One of the commonly used chelators for sensing of Zn^{2+} is di-(2-picolyl)amine (DPA),[5] which is known to form stable complexes with Zn^{2+}, providing the molecular recognition complexes known as Zn-DPA.[6] Furthermore, combining the Zn-DPA moiety with a luminescent center can result in Zn^{2+}-responsive optical imaging probes. In 2009, the Zn^{2+} sensor Zinpyr-1 was synthesized and studied by Lippard and coworkers.[7] Zinpyr-1, bearing the DPA moiety, can respond to Zn^{2+} coordination through fluorescence quenching by photo-induced electron transfer (PET)[8] occurring in the absence of Zn^{2+}. The presence of Zn^{2+} results in an enhancement in the fluorescence emission intensity. The three nitrogen atoms of DPA strongly coordinate Zn^{2+}, with a dissociation constant (K_d) in water media of around 10^{-10} M, giving rise to the 'turn-on' fluorescence response of Zinpyr-1.[7] However, this probe also presents some disadvantages such as a small Stokes shift, low water solubility, short lifetime and broad spectra of the emission, limiting its application as an organic fluorescein compound.[1a,6d]

Due to larger Stokes shifts (> 200 nm), a longer emission lifetime in the order of milliseconds and a higher water solubility compared to the typical organic fluorescence compounds, the complexes of lanthanide trivalent ions (Ln^{3+}) such as Eu^{3+} or Tb^{3+} have been employed as Zn^{2+}-selective sensors.[4b,9] In 2004, Nagano and coworkers developed a Eu^{3+}-based chemosensor appending a DPA arm for Zn^{2+} recognition.[1a] The quinolyl moiety was applied as a chromophore to achieve a longer excitation wavelength (~ 320 nm). Upon addition of Zn^{2+}, the luminescence can be strongly enhanced. To efficiently coordinate the Ln^{3+} ions, DO3A (1,4,7,10-tetraazacyclododecane-1,4,7-triacetic acid) is widely and successfully used as a backbone for the development of

[a] G. Wang, Dr. G. Angelovski
MR Neuroimaging Agents,
Max Planck Institute for Biological Cybernetics,
Max-Planck-Ring 11, 72076 Tübingen (Germany)
E-mail: goran.angelovski@tuebingen.mpg.de
[b] Prof. Dr. C. Platas-Iglesias
Centro de Investigacións Científicas Avanzadas (CICA)
and Departamento de Química
Facultade de Ciencias
Universidade da Coruña
A Coruña, Galicia (Spain)

Supporting information for this article is available on the WWW under https://doi.org/10.1002/cplu.201900731

This article is part of a Special Collection on "Fluorescent Biomolecules and their Building Blocks".

ligands. Given the high stability of DO3A-based Ln^{3+} complexes, their properties such as luminescence and magnetic behavior have been extensively studied.[9a,b,10] However, the luminescence intensities of such LnDO3A complexes are very weak due to their inefficient direct excitation (the *f-f* transitions of the ions are Laporte-forbidden). Hence, the performance of Ln^{3+}-based luminescent probes may often be enhanced by excitation of the Ln^{3+} via a sensitizing chromophore. This moiety is included in the structure of the ligand giving the so-called chromophore-luminophore complex.[10a,11] By combining Ln^{3+} complexes and antenna moieties, the Laporte-forbidden transitions can be circumvented. The natural amino acid tyrosine (Tyr), bearing a phenol group can serve as a good antenna.[9a,12] Once it is excited by UV light, radiationless energy is transferred from tyrosine to the Ln^{3+} center, resulting in the characteristic luminescence of this metal ion.

To build upon the previous studies and prepare a potent Zn^{2+} luminescence lanthanide-based sensor, we designed, synthesized and investigated two Eu^{3+} probes, **EuL^1** and **EuL^2**, functionalized with Tyr as a chromophore and DPA as the Zn^{2+} recognition moiety (Figure 1). The Tyr unit was incorporated into the ligand designed to serve as an antenna, transferring energy efficiently to Eu^{3+}, and also as a molecular linker that connects the Eu^{3+} and Zn^{2+} chelating units. These two probes were anticipated to show an enhancement of luminescence upon Zn^{2+} addition with a long wavelength Eu^{3+}-centered emission (617 nm). Hence the large apparent Stokes shift between the excitation and emission wavelengths of the antenna and the lanthanide metal ion, respectively (~300 nm), combined with the high water-solubility typically expected for such complexes, could potentially be utilized for practical applications. Furthermore, two additional complexes **EuL^3** and **EuL^4** lacking the DPA-moiety were synthesized and utilized for comparative studies (Figure 1), expecting to highlight the effect of the Zn^{2+}-sensitive chelator on the final properties of the complexes.

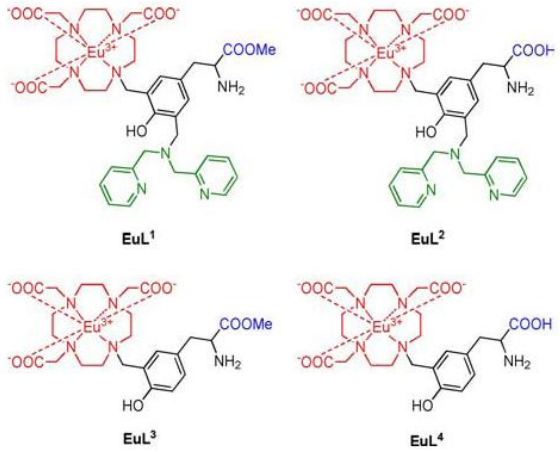

Figure 1. Chemical structures of **EuL$^{1-4}$** discussed in this work.

Results and Discussion

Design and synthesis of EuL$^{1-4}$

The probes **EuL$^{1-4}$** were synthesized in a stepwise manner, starting from the protected amino acid Boc-Tyr-OMe (Scheme 1). Firstly, DPA was coupled to Boc-Tyr-OMe to give **1** following a previously reported literature procedure.[13] Subsequently, this molecule was coupled to the DO3A moiety by reacting **1** with *t*BuDO3A in the presence of paraformaldehyde at 110 °C to afford macrocycle **2**.[14] The ligand L^1 was obtained by treating **2** with TFA in CH_2Cl_2, followed by HPLC purification. Subsequently, basic hydrolysis of the methyl ester of L^1 was achieved with LiOH giving L^2 (Scheme 1a). In parallel, the ligands $L^{3,4}$ were prepared directly by combining the amino acid Boc-Tyr-OMe and the *t*BuDO3A to give the macrocycle **3**

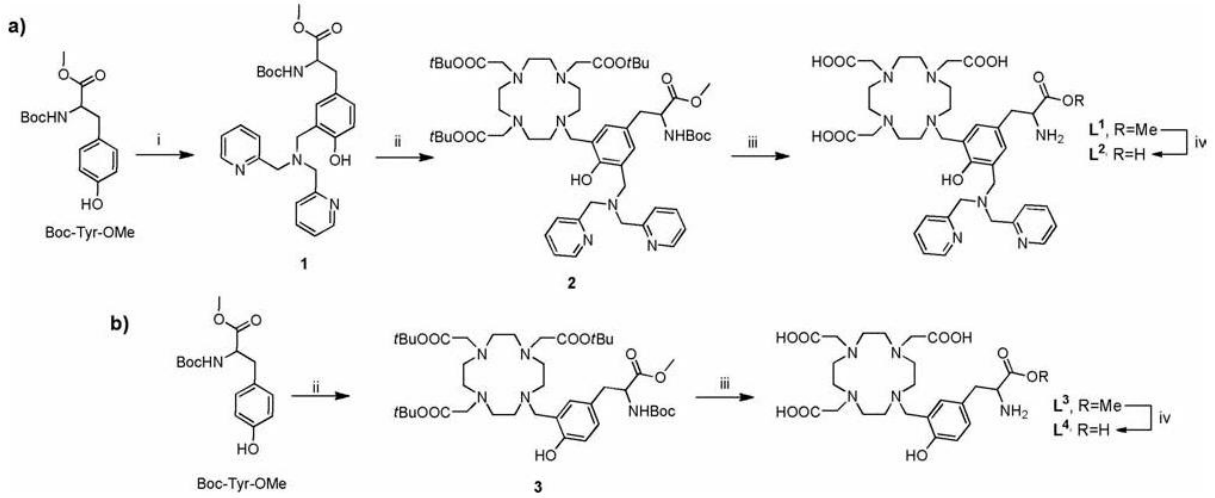

Scheme 1. The synthetic routes to ligands a) $L^{1,2}$ and b) $L^{3,4}$. Reagents and conditions: i) MeOH, di-(2-picolyl)amine, $(CH_2O)_2$, 65 °C, 5 h; ii) DBU, $(CH_2O)_2$, toluene, 110 °C, 6 h for **2** and 65 °C, 3 h for **3**; iii) TFA, CH_2Cl_2, 18 h; iv) LiOH, MeOH, 18 h.

(Scheme 1b). Acid hydrolysis with TFA resulted in the ligand L^3, which was further subjected to basic hydrolysis with LiOH to provide the ligand L^4. Finally, all the complexes **EuL$^{1-4}$** were prepared by treating the ligands with $EuCl_3 \cdot 6H_2O$ in water, while maintaining the pH at ~7.

Luminescence properties of EuL$^{1-4}$

Competition with biologically relevant cations

The **EuL$^{1-4}$** complexes present weak luminescence upon excitation through the ligand bands at 322 nm (HEPES buffer, pH 7.4). Due to such weak emission, no luminescence lifetime values could be determined to evaluate the hydration number (q) of each complex. Instead, estimation of the hydration state of the studied complexes was based on the results obtained from the relaxometric studies of the Gd^{3+} analogues (see below).

The addition of Zn^{2+} has quite different effects on the luminescence emission intensity for these complexes. Specifically, both **EuL^1** and **EuL^2** exhibit an increase in emission intensity upon the addition of one equivalent of Zn^{2+}, while another equiv. of Zn^{2+} causes a further but smaller increase in emission for **EuL^1** only. Meanwhile, both **EuL^{3,4}** remain insensitive to the addition of Zn^{2+}, confirming that the presence of the DPA moiety is essential to affect the luminescence emission (Figure 2a).

The selectivity of **EuL^{1,2}** was further tested by addition of metal ions commonly found in biological systems. Chloride salts of K^+, Na^+, Ca^{2+}, Mg^{2+}, Fe^{2+} and Fe^{3+} (3 equiv.) do not provoke significant changes in the intensity of the Eu^{3+} $^5D_0 \rightarrow {}^7F_J$ transitions ($J=0$ to 4),[15] while Cu^{2+} almost completely quenches the Eu^{3+}-based luminescence. Subsequent addition of Zn^{2+} (3 equiv.) results in a dramatic enhancement of the emission intensity in the presence of K^+, Na^+, Ca^{2+}, Mg^{2+}, Fe^{2+} and Fe^{3+}, indicating the selective response of **EuL^{1,2}** to Zn^{2+} in the presence of these competing metal ions (Figures 2b and S1 in the Supporting Information). Only Cu^{2+} was found to compete efficiently with Zn^{2+} among the metal ions examined in this study. This is however expected considering the higher affinity of DPA for Cu^{2+} compared with Zn^{2+},[16] and the known ability of Cu^{2+} to quench the emission of organic chromophores due to its partially occupied 3d shell.[17] However, the luminescence quenching effect of Cu^{2+} is not likely to be a significant problem for practical applications because free copper ions in living cells are present in very low quantities.[18] As expected, **EuL^{3,4}** exhibit weak and random luminescence changes toward all of these studied ions. The high selectivity toward Zn^{2+} suggested that probes **EuL^{1,2}** can be useful for potential biological applications.

Titrations with Zn^{2+}. Since **EuL^1** and **EuL^2** exhibited different responses to the addition of Zn^{2+}, we conducted more detailed studies with these two systems. Increasing amounts of Zn^{2+} were added to an aqueous solution of **EuL^1** (50 μM) and the steady-state emission spectra were recorded from 560 to 720 nm using the same excitation wavelength (322 nm). By following the most intense $^5D_0 \rightarrow {}^7F_2$ transition, the titration profile presents two inflection points close to 1:1 and ~1:2 (Eu^{3+}:Zn^{2+}) stoichiometry ratios, reaching a plateau with further Zn^{2+} addition of up to 4 equiv. (Figure 3). The emission intensity of **EuL^1** increased significantly (about 7-fold at 617 nm) upon the addition of two equiv. of Zn^{2+}, with a large apparent Stokes shift (295 nm). These results indicate the presence of two different Zn^{2+} binding sites: the initial increase of luminescence intensity should be ascribed to the complexation between DPA and Zn^{2+}, while the second should be related to the weak interaction between the amino acid methyl ester of tyrosine and Zn^{2+} (Figure 3 inset). The emission spectra of **EuL^1** were analyzed to a model including the formation of both 1:1 and 1:2 (Eu^{3+}:Zn^{2+}) species, affording association constants of $\log K_{11} = 7.15 \pm 0.03$ and $\log K_{12} = 4.59 \pm 0.02$ (Figure S2 in the Supporting Information). Obviously, the binding of the first equivalent of Zn^{2+} is very strong, while the second binding process is weaker. The first association constant is virtually identical to that determined for $[Zn(DPA)]^{2+}$ at pH 7.0 ($\log K_{11} = 7.15$).[19]

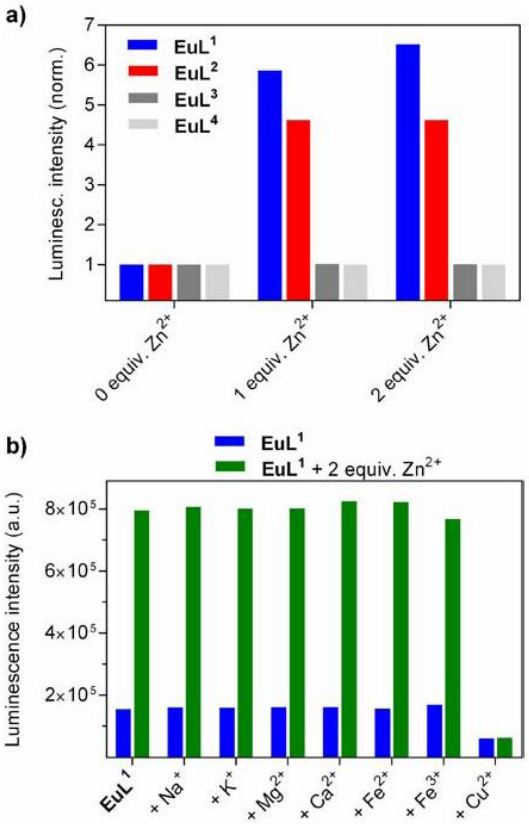

Figure 2. a) Luminescence changes of **EuL$^{1-4}$** (50 μM) upon addition of Zn^{2+}. All data were recorded in HEPES buffer (50 mM, pH 7.4) with $\lambda_{ex} = 322$ nm and $\lambda_{em} = 617$ nm; intensity was estimated by the peak height at $\lambda_{em} = 617$ nm. b) Luminescence variations of **EuL^1** (50 μM) to Zn^{2+} in the presence of different metal ions. Blue bars indicate luminescence intensity of **EuL^1** in the presence of various metal ions (3 equiv.). Green bars indicate luminescence intensity of **EuL^1** after the subsequent addition of Zn^{2+} (3 equiv.).

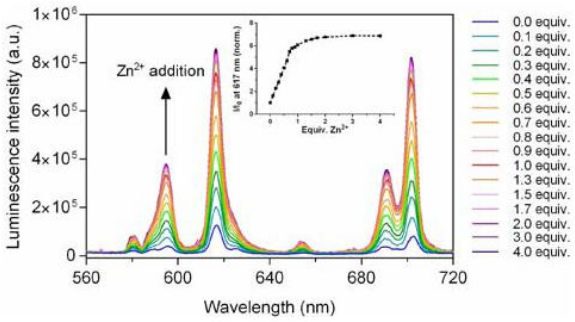

Figure 3. Luminescence emission spectral variations of **EuL**^{1} (50 μM, $\lambda_{ex}=322$ nm, $\lambda_{em}=617$ nm) upon titration with Zn^{2+} (50 mM HEPES, pH 7.4, 25°C). Inset: normalized emission intensities of **EuL**^{1} as a function of Zn^{2+} concentration.

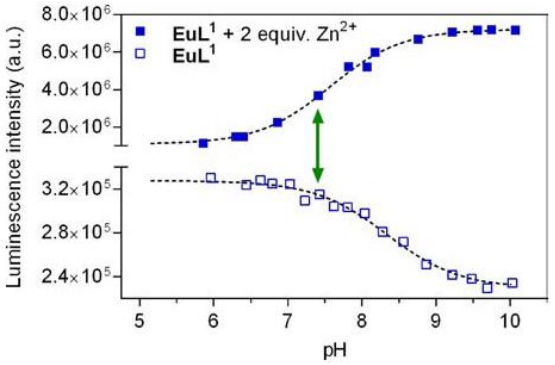

Figure 4. Luminescence emission intensity variations with pH changes of **EuL**^{1} (open symbols) and **EuL**^{1}**Zn** (filled symbols) in water (50 μM complex, 100 mM KCl as the electrolyte, $\lambda_{ex}=322$ nm; intensity was estimated by the peak height at $\lambda_{em}=617$ nm). The dashed lines represent fitted values as described in the Experimental section, while the green arrow shows the luminescence emission change at pH 7.4.

Further insights into the behavior of these systems were obtained by repeating the titration experiments with **EuL**^{2}, which bears a carboxylic acid on the Tyr moiety instead of a methyl ester group as in **EuL**^{1} (Figure S3 in the Supporting Information). The luminescence changes were investigated upon addition of Zn^{2+} within the same concentration range (0–4 equiv.). Here, the emission intensity increases 5-fold and only up to the addition of one equiv. of Zn^{2+}. The analysis of the data according to a 1:1 binding model resulted in an association constant with a value of $\log K_{11}=7.1\pm0.1$, indicating strong binding of Zn^{2+} to the DPA-tyrosine moiety (Figure S2 in the Supporting Information). We hypothesize that the amino acid of **EuL**^{2} exists as a zwitterion at physiological pH,[20] which consequently induces the observed luminescence increase with only one equiv. of Zn^{2+}. The situation is slightly different in **EuL**^{1}, where the DPA-tyrosine moiety dominates the turn-on response of luminescence; however, the positively charged Tyr moiety in the form of a methyl ester interacts with the second equiv. of Zn^{2+}, thus further promoting the luminescence emission.

Luminescence pH titrations

The pH dependence of the emission intensity of **EuL**^{1} and **EuL**^{1}**Zn** was investigated to shed light into the mechanism responsible for the turn-on response to Zn^{2+} (Figure 4). For **EuL**^{1}, in the absence of Zn^{2+}, the luminescence is gradually quenched by increasing pH. This is a result of photoinduced electron transfer (PET) caused by the lone pair of electrons from the DPA moiety.[21] Protonation of the amine nitrogen atom of the DPA moiety decreases the energy of the nitrogen lone pair, thus preventing the PET process. The fitting of the pH titration profile provides a pK_a of 8.3 ± 0.1, indicating that the DPA group is largely protonated under physiological conditions.

For **EuL**^{1}**Zn** (**EuL**^{1} with 2 equiv. Zn^{2+}), the luminescence is gradually enhanced with increasing pH, providing a pK_a of 7.6 ± 0.1. The relatively high equilibrium constant determined for the association of **EuL**^{1} with Zn^{2+} (see above) indicates that nearly all Zn^{2+} present in solution is already bound to the DPA moiety at pH 7.4. Subsequently, the pH dependent changes in luminescence emission observed for **EuL**^{1}**Zn** should be ascribed to a protonation process that does not involve the DPA moiety, but is likely related to the protonation/deprotonation of the phenol unit. This pK_a is considerably lower than that determined in the absence of Zn^{2+} ($pK_a=9.4\pm0.5$, see below), which opens the question of whether the phenol group remains coordinated to the lanthanide ion upon protonation. Indeed, Sherry et al. showed that a GdDO3A derivative containing a methylene nitrophenol pendant arm provided a relaxivity response to pH, as protonation of the phenol group provokes its dissociation from the lanthanide center, resulting in an increase of the number of coordinated water molecules.[22]

Similarly to **EuL**^{1}, the **EuL**^{2} and **EuL**^{2}**Zn** complexes show similar pH titration profiles (Figure S4 in the Supporting Information). Here, the pK_a values are almost identical to those of the **EuL**^{1}/**EuL**^{1}**Zn** pair, resulting in values of 8.2 ± 0.1 and 7.5 ± 0.1 for **EuL**^{2} and **EuL**^{2}**Zn**, respectively. This provides additional evidence that the pK_a observed for the **EuL**^{1}**Zn** complex can be associated to the protonation of the phenol group from the Tyr moiety. Indeed, the similar pK_a values of the **EuL**^{1,2}/**EuL**^{1,2}**Zn** systems suggest that both groups experiencing protonation (amine and phenol groups of the DPA and phenol moieties, respectively) are not affected significantly by the different functional groups of the amino acid part of Tyr, i.e. the ester and free acid in **EuL**^{1} and **EuL**^{2}, respectively. The carboxyl group, being either protected as an ester or not, is apparently sufficiently isolated from the remaining part of the DPA-Tyr moiety to influence the protonation processes of groups substantially involved in the luminescence emission.

UV-Vis studies of EuL^{1,2}. Further studies with the investigated complexes were performed by means of UV-Vis spectrophotometry, in order to reveal new insights that could not be obtained with the luminescence emission experiments.

Firstly, UV-Vis absorption spectra of solutions of **EuL**^{1,2} (50 μM) at pH 7.4 were recorded in the presence of various concentrations of Zn^{2+} (0–3 equiv). The spectra are dominated

by an intense absorption around 250 nm attributable to the pyridyl units of the DPA moiety,[23] and a second broad band with a maximum around 305 nm characteristic of the phenol group.[24] Addition of 1 equiv. of Zn^{2+} causes a slight blue shift of the band of **EuL**^{1} with maximum at 305 nm to 295 nm (Figure 5), whereas the same type of shift from 306 nm to 296 nm takes place for **EuL**^{2} (Figure S5 in the Supporting Information). Further addition of Zn^{2+} did not induce noticeable changes. This is consistent with the previously observed luminescence effects: binding of Zn^{2+} to the amine group of Tyr does not affect the UV spectrum of **EuL**^{1}, while **EuL**^{2} already exhibited insensitivity towards Zn^{2+} beyond 1 equiv. added (see above). Furthermore, the band with a maximum at 250 nm and 248 nm for **EuL**^{1} and **EuL**^{2}, respectively, experiences a dramatic intensity decrease upon Zn^{2+} addition, which confirms the binding of the metal ion to the DPA moiety of the ligand. No UV-Vis absorbance changes were found for **EuL**^{3} or **EuL**^{4} (50 μM) at pH 7.4 in the presence and absence of Zn^{2+}.

UV-Vis absorption of **EuL**^{1} (50 μM) was also studied at different pH values to find out whether the phenol group of tyrosine is involved in binding to Eu^{3+}. The absorption spectra were recorded from pH ~ 4.0 to ~ 11.0 (Figure 6). Increasing the pH provokes a decrease of the band at 303 nm while a new maximum at 335 nm develops. Conversely, the band at 250 nm remains nearly unaffected by pH. The analysis of the absorbance changes at 335 nm provides a $pK_a = 9.4 \pm 0.5$. These results

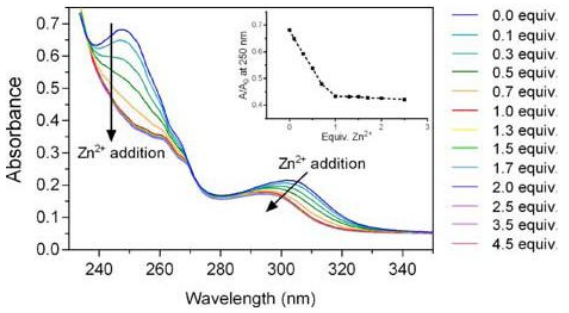

Figure 5. UV-Vis absorption titrations of **EuL**^{1} (50 μM) with Zn^{2+} (50 mM HEPES buffer at pH 7.4). Inset: absorption intensity variations at 250 nm with Zn^{2+} addition.

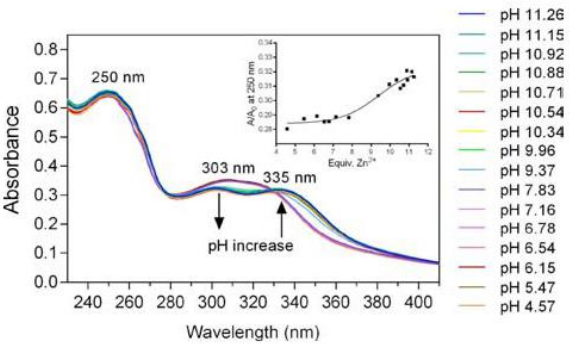

Figure 6. Changes in the UV-Vis absorbance of **EuL**^{1} (50 μM in water) upon variations in pH. Inset: absorption intensity variations at 335 nm with pH changes.

suggest that the phenol group is involved in protonation/deprotonation processes, specifically being protonated at physiological pH.

Finally, to confirm the binding relationship of Zn^{2+} with **EuL**^{1,2}, a method of continuous variation was applied on both complexes and Job's plots were obtained (Figure S6 in the Supporting Information).[25] The experiments were performed with the total concentration of $[Zn^{2+}]+[\mathbf{EuL}^{1,2}] = 50\ \mu M$ and their result confirmed that **EuL**^{1} possesses two Zn^{2+}-binding sites, as it presents a maximum close to $x_{Zn2+} = 0.60$.[26] The same experiment performed for **EuL**^{2} indicates a 1:1 ratio of binding to Zn^{2+}, matching the obtained results from the luminescence titration experiments (see above).

Longitudinal relaxivity of Gd^{3+} complexes

The coordination properties of the studied systems were also assessed by preparing highly paramagnetic Gd^{3+} analogues of **EuL**^{1,2} and testing their relaxometric response in the presence of Zn^{2+}. The synthesis of **GdL**^{1,2} was performed in the same manner as for **EuL**^{1,2} by chelating Gd^{3+} in the form of the chloride hydrate with the respective ligand **L**^{1,2}. Subsequently, the longitudinal relaxivity, r_1, was determined for both complexes in the absence or presence of different concentrations of Zn^{2+} (Figure S7 in the Supporting Information). Initial r_1 values for both complexes are high (7.35 and 7.95 mM $^{-1}$s $^{-1}$ for **GdL**^{1} and **GdL**^{2}, respectively), which suggests the presence of monohydrated complexes in both cases. Addition of Zn^{2+} to **GdL**^{1} causes a rather small increase in relaxivity of ~10% (r_1 = 8.21 mM $^{-1}$s $^{-1}$ upon addition of 5 equiv. of Zn^{2+}). This small relaxivity enhancement is not compatible with a change in the hydration number of the complex, but rather to some effect on the rotational dynamics of the complex in the presence of two Zn^{2+} ions or a change in the water exchange. Additionally, the relaxometric titrations of **GdL**^{2} with Zn^{2+} resulted in negligible relaxivity changes, with the r_1 value remaining in the range 7.9–8.0 mM $^{-1}$s $^{-1}$, confirming that the hydration number of the complex remains unchanged when Zn^{2+} is added to the solution. Moreover, r_1 values for both complexes are very similar to those recorded under identical conditions for monohydrated GdDO3A-type derivatives with similar size.[27] This suggests that the phenolate group remains coordinated to the metal ion upon protonation, and that the electron withdrawing effect of the nitro substituent at position 4 of the phenol group in the complex reported by Woods et al. is responsible for its dissociation when protonated.[22]

DFT calculations

DFT calculations were carried out to aid the rationalization of the observed results. The optimized structure of the **EuL**^{1} complex supports octadentate binding of the ligand to the Eu^{3+} ion, with average Eu–N and Eu–$O_{carboxylate}$ distances of 2.67 and 2.38 Å, respectively. The Eu–O_{phenol} distance of 2.56 Å is relatively long, and decreases to 2.34 Å upon deprotonation.

Calculations were also performed on the EuL^1ZnCl_2 system, in which two chloride anions were included to complete the square-pyramidal coordination of Zn^{2+} observed for DPA derivatives of this metal ion in the presence of Cl^-.[28] The experimental data were obtained using 100 mM KCl as background electrolyte, and thus Cl^- coordination is expected.

The coordination of Zn^{2+} to the DPA moiety provokes little changes in the Eu^{3+} coordination environment (Figure 7), but significant changes in the frontier molecular orbitals. Indeed, the HOMO of EuL^1 is mainly located on the amine nitrogen atom of the DPA moiety, with some contribution of the lone pairs of the pyridyl nitrogen atoms. Conversely, the LUMO is comprised of π orbitals of the pyridyl and phenol groups. The HOMO of the EuL^1ZnCl_2 system is predicted to be centered on one of the carboxylate groups of the DO3A unit, while the main contributions to the LUMO are provided by π orbitals of the pyridyl groups. Both the HOMO and the LUMO are significantly stabilized upon Zn^{2+} coordination (Figure 7). These results are in line with a PET mechanism being responsible for the turn-on luminescence response of EuL^1 to Zn^{2+}.[9b] PET sensors are responsive electron donor-acceptor probes in which the HOMO of the donor (the lone pair of the amine N atoms in this case) presents a higher energy than the acceptor in the absence of the target analyte. As a result, excitation of the LUMO results in an electron transfer from the HOMO of the donor to the HOMO of the acceptor, quenching the emission of the probe. Coordination of Zn^{2+} to the DPA moiety reduces the energy of the HOMO of the donor, enhancing the overall luminescence.

Conclusion

We studied a series of EuDO3A-based complexes as potential luminescence chemosensors for the detection of Zn^{2+}. All complexes were appended with tyrosine as a chromophore, while only two that contained DPA as a recognition moiety for Zn^{2+} exhibited properties suitable for the desired luminescent sensors. In the absence of Zn^{2+}, only weak luminescence of each probe was observed due to quenching of luminescence caused by the PET mechanism involving the deprotonated amine group of DPA. Upon the addition of Zn^{2+}, both DPA-containing probes displayed large increases in Eu^{3+}-centered luminescent emission, which reached up to sevenfold enhancement. The ion selectivity experiments demonstrated the specificity of these probes toward Zn^{2+} over other biologically relevant metal ions. The two complexes without a DPA-moiety did not show any obvious luminescent enhancement for any of the studied metal ions, emphasizing the essential role of DPA for the recognition of Zn^{2+}. Extensive luminescence, UV-Vis and relaxometric studies that involved pH and Zn^{2+} titrations or theoretical DFT calculations revealed the major properties of the chemosensors in aqueous solution. They also provided essential mechanistic insights of their interaction with Zn^{2+} and the consequence of this interaction on the subsequent luminescence emission. For future studies, it would be desirable to design a complex in which both protonation constants (of the amine of DPA and phenol on Tyr units) are lowered, thus promoting greater change in the luminescence intensity upon Zn^{2+} addition by: a) achieving greater quenching by the DPA group/free electron pair in the absence of Zn^{2+}, and b) further enhancing the signal by deprotonating the phenol group upon Zn^{2+} addition. Overall, the results reported in this work allowed for precise quantitative analysis of the interaction of Eu^{3+} luminescent complexes together with Zn^{2+} as the target analyte. It also provided important insights which can assist further in establishing Ln^{3+}-based complexes as useful chemosensors for potential biological applications that range from the development of different bioassays to medical optical imaging.

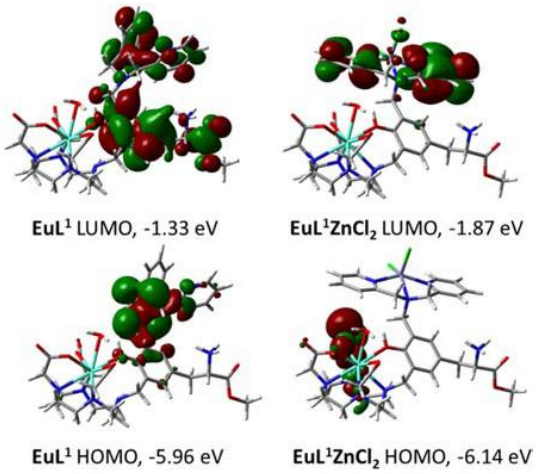

Figure 7. Views of the frontier molecular orbitals of EuL^1 and EuL^1ZnCl_2 obtained with DFT calculations.

Experimental Section

General

The reagents were purchased from Aldrich and were used without further purification. Compound 1 was synthesised following a previously published procedure.[13] Purification of synthesized compounds was performed using silica gel 60 (0.03–0.2 mm) from Carl Roth (Germany). The buffer solution (0.1 M HEPES, pH 7.4) was prepared by dissolving solid HEPES in HPLC grade water. After the solution became clear, aqueous NaOH (1 M) was added to adjust the pH to the desired value. The buffer solution was used without degassing. All UV-vis absorption and fluorescence spectra were recorded on an Agilent Cary 60 UV-Vis Spectrophotometer and a QuantaMaster™ 3 PH fluorescence spectrometer from Photon Technology International, Inc. (USA), respectively. Low resolution mass spectra were recorded on an ion trap SL 1100 system Agilent with an electrospray ionization source. High resolution mass spectra were recorded on a Bruker Daltonics APEX II (FT-ICR-MS) with an electrospray ionization source. MALDI-TOF-MS analysis was performed by The Scripps Center for Mass Spectrometry, La Jolla, CA. ^1H and ^{13}C NMR spectra were recorded on a Bruker Avance III 300 MHz spectrometer at 25 °C. Processing was performed using TopSpin 2.1 (Bruker GmbH) and ACD/SpecManager 9.0 (Advanced Chemistry Development, Inc.). The concentration of Gd^{3+} and Eu^{3+}

in analyzed solutions was determined using the bulk magnetic susceptibility shift (BMS).[29]

Synthetic procedures

3-[3-[(Bis-pyridin-2-ylmethyl-amino)-methyl]-4-hydroxy-5-(4,7,10-tris-*tert*-butoxycarbonylmethyl-1,4,7,10tetraaza-cyclododec-1-ylmethyl)-phenyl]-2-*tert*-butoxycarbonylamino-propionic acid methyl ester (2): DO3A-*t*Bu (1.544 g, 3.00 mmol) and paraformaldehyde (0.198 g, 6.6 mmol) in 10 mL toluene were stirred at 60 °C until the solution became clear. Then, compound **1** (3.040 g, 6.00 mmol) was added to the reaction mixture and a few drops of DBU were added shortly afterwards, followed by stirring for 6 h at 110 °C. Upon reaction completion, the reaction mixture was evaporated and purified by silica gel column chromatography using DCM/MeOH (v/v, 20:1) as the eluent, affording 1.333 g (43%) of compound **2** as a light yellow oil. **^{1}H NMR** ($CDCl_3$, 300MHz): δ (ppm): 1.40, 1.42 (s, 36H, CCH_3); 2.22–3.49 (br, 24H, NCH_2); 3.69 (s, 3H, OCH_3); 3.81 (s, 6H, NCH_2C); 4.39–4.58 (m, 1H, NHCH); 6.83–6.96 (m, 2H, phOH); 7.09–8.72 (m, 8H, pyridyl). **^{13}C NMR** ($CDCl_3$, 75MHz): δ (ppm): 27.8, 28.1 (12C, CCH_3); 37.3 (1C, $phCH_2CH$); 51.4, 51.6, 51.7, 51.9, 52.6, 52.7 (8C, NCH_2CH_2); 53.5 (1C, OCH_3); 55.6, 56.1 (3C, NCH_2CO); 54.7 (2C, $phCH_2N$); 57.3 (1C, NH_2CH); 60.1 (2C, $pyCH_2$); 80.5, 82.2 (4C, CCH_3); 121.7, 122.7 (4C, CCHCH, NCHCH); 123.2, 125.2 (2C, HOCCH); 128.7 (2C, CCHC); 129.9 (1C, CHCCH); 136.3 (2C, CCHCH); 148.8 (2C, NCHCH); 149.1 (1C, OHC); 155.7 (1C, NHCCO); 160.0 (2C, NCCH); 170.8, 171.1, 172.5 (4C, CO). ESI-TOF/MS: (*m/z*) $[M+H]^+$ calcd. for $C_{55}H_{85}N_8O_{11}^+$: 1033.6332; found: 1033.6325.

2-Amino-3-[3-[(bis-pyridin-2-ylmethyl-amino)-methyl]-4-hydroxy-5-(4,7,10-tris-carboxymethyl-1,4,7,10tetraaza-cyclododec-1-ylmethyl)-phenyl]-propionic acid methyl ester (L^1): Compound **2** (1.033 g, 1.00 mmol) was dissolved in 5 mL TFA/DCM (v/v 50/50) and the solution was stirred at room temperature overnight. After purification by HPLC, pure H_3L^1 (0.604 g, 79%) was obtained. **^{1}H NMR** (D_2O, 300MHz): δ (ppm): 2.81–3.49 (br, 24H, NCH_2); 3.67 (s, 8H, NCH_2Ar); 3.73 (s, 3H, OCH_3); 4.26–4.42 (m, 1H, NH_2CH); 6.77, 7.31 (s, 2H, ph); 7.19 (d, $J=7.2$ Hz, 2H, NCHCH); 7.21 (d, $J=7.0$ Hz, 2H, NCCH); 7.63 (t, $J=7.7$ Hz, 2H, CHCHCH); 8.32 (d, $J=4.5$ Hz, 2H, NCHCH). **^{13}C NMR** (D_2O, 75MHz): δ (ppm): 34.6 (1C, $phCH_2CH$); 48.5–50.7 (8C, NCH_2CH_2); 53.4 (1C, OCH_3); 53.6 (1C, NH_2CH); 55.6, 56.3, 56.8 (3C, NCH_2CO); 55.9 (2C,, $phCH_2N$); 59.3 (2C, $pyCH_2$); 123.3, 123.6 (4C, CCHCH); 124.4, 126.4 (2C, HOCCH); 130.8 (1C, CHCCH); 132.4 (2C, CCHC); 138.2 (2C, CCHCH); 148.2 (2C, NCCH); 154.0 (1C, OHC); 156.0 (2C, NCHCH); 170.7 (4C, CO). ESI-TOF/MS: (*m/z*) $[M-H]^-$ calcd. for $C_{38}H_{51}N_8O_9^-$: 763.3785; found: 763.3785.

2-Amino-3-[3-[(bis-pyridin-2-ylmethyl-amino)-methyl]-4-hydroxy-5-(4,7,10-tris-carboxymethyl-1,4,7,10tetraaza-cyclododec-1-ylmethyl)-phenyl]-propionic acid (L^2): Compound L^1 (0.306 g, 0.40 mmol) was dissolved in 5 mL methanol and LiOH was added. Then the mixture was stirred at room temperature overnight. After filtering, the methanol was evaporated. The crude mixture was dissolved in water and the pH was adjusted to 7. The mixture was then purified by HPLC to yield 0.222 g (74%) of H_3L^2 as a light yellow powder. **^{1}H NMR** (D_2O, 300MHz): δ (ppm): 2.61–3.49 (br, 24H, NCH_2); 3.53–3.87 (br, 8H, NCH_2Ar); 3.95–4.05 (m, 1H, NH_2CH); 6.83, 6.96 (s, 2H, phOH); 7.02–7.39 (m, 4H, NCHCH, NCCH); 7.64 (t, $J=7.3$ Hz, 2H, CHCHCH); 8.24 (d, $J=4.3$ Hz, 2H, NCHCH). **^{13}C NMR** (D_2O, 75MHz): δ (ppm): 34.8 (1C, $phCH_2CH$); 47.7, 50.7 (8C, NCH_2CH_2); 52.6 (1C, NH_2CH); 53.4, 54.5 (3C, NCH_2CO); 56.7 (2C, $phCH_2N$); 58.7 (2C, $pyCH_2$); 126.4, 127.5 (4C, CCHCH); 127.9 (2C, HOCCH); 134.3 (2C, CCHC); 134.8 (1C, CHCCH); 141.5 (2C, CCHCH); 146.5 (2C, NCCH); 151.9 (2C, NCHCH); 152.7 (1C, OHC); 163.0, 162.6 (2C, NCCH); 173.3 (4C, CO). ESI-TOF/MS: (*m/z*) $[M-H]^-$ calcd. for $C_{37}H_{49}N_8O_9^-$: 749.3628; found: 749.3631.

2-*tert*-Butoxycarbonylamino-3-[4-hydroxy-3-(4,7,10-tris-*tert*-butoxycarbonylmethyl-1,4,7,10tetraazacyclododec-1-ylmethyl)-phenyl]-propionic acid methyl ester (3): DO3A-*t*Bu (1.029 g, 2.00 mmol) and paraformaldehyde (0.132 g, 4.40 mmol) were stirred in 5 mL toluene at 65 °C until the solution became clear. Then, Boc-Tyrosine-OMe (1.299 g, 4.40 mmol) was added to the reaction mixture and a few drops of DBU were added shortly afterwards, followed by stirring for 3 h at 65 °C. Upon reaction completion, the reaction mixture was evaporated and purified by silica gel column chromatography using DCM/MeOH (v/v, 20:1) as the eluent to yield 1.217 g (74%) of **3** as light yellow oil. **^{1}H NMR** ($CDCl_3$, 300MHz): δ (ppm): 1.01–1.17 (br, 36H, CCH_3), 1.79–2.78 (br, 26H, NCH_2), 3.35 (s, 3H, OCH_3), 4.65 (m, 1H, NHCH), 6.47 (d, $J=7.9$ Hz, 1H, HOC=CH), 6.61 (s, 1H, C=CH=C); 6.85–7.00 (m, 1H, C=CH=CH). **^{13}C NMR** ($CDCl_3$, 75MHz): δ (ppm): 27.8, 28.1 (12C, CH_2CH_3); 36.9 (1C, $phCH_2$); 46.3 (1C, OCH_3); 49.5, 49.6 (8C, NCH_2CH_2); 51.9 (1C, $phCH_2N$); 53.7, 55.2, 55.8 (3C, NCH_2CO); 54.6 (1C, $NHCH_2$); 79.5, 82.0, 82.1, (4C, $C(CH_3)_3$); 117.9, 123.7, 126.7, 129.3, 132.7 (5C, ph); 154.3 (1C, OHC); 154.7 (1C, NHCO); 171.9 (3C, CH_2CO); 172.4 (1C, CHCO). ESI-TOF/MS: (*m/z*) $[M+H]^+$ calcd. for $C_{42}H_{72}N_5O_{11}^+$: 822.5223, found: 822.5225.

2-Amino-3-[4-hydroxy-3-(4,7,10-tris-carboxymethyl-1,4,7,10tetraaza-cyclododec-1-ylmethyl)-phenyl]-propionic acid methyl ester (L^3): Compound **3** (1.200 g, 1.46 mmol) was dissolved in 6 mL TFA/DCM (v/v 50/50) and the solution was stirred at room temperature overnight. Pure H_3L^3 (0.671 g, 83%) was obtained by HPLC. **^{1}H NMR** (D_2O, 300MHz): δ (ppm): 2.99–3.49 (br, 24H, NCH_2, $phCH_2CH$), 3.58 (s, 3H, OCH_3), 3.94 (s, 2H, $phCH_2N$), 3.98–4.13 (m, 1H, NH_2CH), 6.78–6.93 (br, 1H, C=CH=CH), 7.12 (d, 1H, $J=6.6$ Hz, HOC=CH), 7.21 (s, 1H, C=CH=CH). **^{13}C NMR** (D_2O, 75MHz): δ (ppm): 34.7 (1C, $phCH_2$); 46.7 (1C, OCH_3); 47.8 (1C, NH_2CH); 51.6 (1C, $phCH_2N$); 52.1, 53.5, 54.1, 54.5 (8C, NCH_2CH_2); 55.5 (3C, NCH_2CO); 116.13, 126.1, 133.2, 133.5 (5C, ph); 154.7 (1C, OHC); 169.3, 169.9 (3C, CH_2CO); 173.6 (1C, CHCO). ESI-TOF/MS: (*m/z*) $[M-H]^-$ calcd. for $C_{25}H_{38}N_5O_9^-$ *m/z* 552.2675; found: 552.2677.

2-Amino-3-[4-hydroxy-3-(4,7,10-tris-carboxymethyl-1,4,7,10tetraaza-cyclododec-1-ylmethyl)-phenyl]-propionic acid (L^4): Compound L^3 (0.277 g, 0.50 mmol) was dissolved in 5 mL methanol and LiOH was added. Then the mixture was stirred at room temperature overnight. After filtering, methanol was evaporated. The crude mixture was dissolved in water and the pH was adjusted to 7. Then the mixture was purified by HPLC to yield 0.129 g (71%) of H_3L^4 as a white powder. **^{1}H NMR** (D_2O, 300MHz): δ (ppm): 2.80–3.39 (br, 24H, NCH_2, $phCH_2CH$), 3.72 (s, 2H, $phCH_2N$), 4.22–4.42 (m, 1H, NH_2CH), 6.65–6.85 (br, 2H, C=CH=CH), 6.95–7.11 (br, 1H, HOC=CH), 7.13–7.30 (m, 1H, C=CH=CH). **^{13}C NMR** (D_2O, 75MHz): δ (ppm): 34.6, 35.2, 35.7 (1C, $phCH_2CH$); 53.5, 53.8 (1C, $phCH_2N$); 55.0, 55.2 (8C, NCH_2CH_2); 55.5, 55.7 (3C, NCH_2CO); 56.5, 56.6 (1C, NH_2CH); 116.7, 126.1, 127.1, 128.1, 131.5, 131.9, 133.2 (5C, ph); 153.9, 154.1 (1C, OHC); 170.4, 172.8, 173.8 (4C, CO). ESI-TOF/MS: (*m/z*) $[M-H]^-$ calcd. for $C_{24}H_{36}N_5O_9^-$: 538.2519; found: 538.2519.

General procedure for the preparation of the Eu^{3+} and Gd^{3+} complexes: The introduction of the europium (for L^{1-4}) or gadolinium (for L^{1-2}) ions into the macrocyclic framework was carried out at pH ~7.0 adjusted by 0.1 M NaOH solution. To a stirred aqueous solution of ligand, a solution of $EuCl_3 \cdot 6H_2O$ or $GdCl_3 \cdot 6H_2O$ was prepared in water and was added dropwise to the ligand solution in 1:1 molar ratios. The reaction mixture was heated to 50 °C and stirred overnight. The pH of the solution was periodically adjusted to 7.0 by addition of 0.1 M NaOH solution. The reaction mixture was then cooled to room temperature. The yellow solid compound was obtained by lyophilization. The formation of the metal complexes EuL^{1-4} was confirmed by mass spectrometry.

EuL^1: ESI-LRMS: (*m/z*) $[M+H]^+$ calcd. for $C_{38}H_{50}EuN_8O_9^+$: 915.3; found: 915.3.

GdL^1: ESI-LRMS: (*m/z*) $[M-H]^-$ calcd. for $C_{38}H_{48}GdN_8O_9^-$: 918.3; found: 918.3.

EuL^2: ESI-LRMS: (*m/z*) $[M-H]^-$ calcd. for $C_{37}H_{46}EuN_8O_9^-$: 899.3; found: 899.3.

GdL^2: ESI-LRMS: (*m/z*) $[M-H]^-$ calcd. for $C_{37}H_{46}GdN_8O_9^-$: 904.3; found: 904.3.

EuL^3: ESI-LRMS: (*m/z*) $[M+H]^+$ calcd. for $C_{25}H_{37}EuN_5O_9^+$: 704.2; found: 704.2.

EuL^4: ESI-LRMS: (*m/z*) $[M-H]^-$ calcd. for $C_{24}H_{33}EuN_5O_9^-$: 688.1; found: 688.1.

UV/Vis spectroscopy: UV-Vis spectra of complexes **EuL$^{1-4}$** (50 μM) in 50 mM HEPES buffer at pH 7.4 were obtained at 25 °C on a Cary Varian double beam spectrophotometer (Cary). The pH effect on absorptions of **EuL^1** (50 μM) was studied with changes of pH values from 4.57 to 11.26. Zn^{2+}-sensitive absorptions of **EuL^{1,2}** were studied with the addition of various concentrations of Zn^{2+} (0–3 mM).

Luminescence studies: The Zn^{2+}-sensitive luminescence spectra of 50 μM complex in 50 mM HEPES buffer at pH 7.4 were measured at 25 °C (excitation at 322 nm), with the addition of various concentrations of Zn^{2+} (0–4.0 equiv. of Zn^{2+}). The pH effect on luminescence of **EuL^{1,2}** and **EuL^{1,2}Zn** was studied with changes of pH values from 4 to 12, respectively. The pK_a values were fitted by a Boltzmann-type sigmoid.[30] Association constants were determined by analysing the emission spectra in the range 560–720 nm with the HYPERQUAD 2008 (HypSpec) program.[31]

Zn^{2+}-binding titrations: All the Zn^{2+}-binding titrations were measured in 50 mM HEPES buffer at pH 7.4 at 25 °C. The total molar concentration of complex and Zn^{2+} was 50 μM.

Metal ion selectivity: For metal ion selectivity experiments, stock solutions (0.05 M) of NaCl, KCl, $CaCl_2$, $MgCl_2$, $FeCl_2$, $FeCl_3$, $CuCl_2$ and $ZnCl_2$ were prepared. The appropriate concentrations (50 μM) of Eu^{3+} complex were prepared by the dilution method using HPLC grade water and HEPES buffer. All data were recorded in HEPES buffer (50 mM, pH 7.4); excitation wavelength at 322 nm; slit widths were 1 nm for both excitation and emission.

Relaxometric Titrations: Proton longitudinal relaxometric titrations with Zn^{2+} were performed at 7.0 T, 25 °C, and pH 7.4 (50 mM HEPES buffer) using inversion recovery (T_1) pulse sequences. A $ZnCl_2$ solution of known concentration was added stepwise to the **GdL$^{1-2}$** solution (starting concentration 3.0 mM Gd^{3+}), and measurements of T_1 were performed after each addition of the analyte. The longitudinal relaxivities, r_1, were calculated from Eq. 1 where $T_{1,obs}$ is the measured T_1, T_{1d} is the diamagnetic contribution of the solvent, and [Gd] is the actual Gd^{3+} concentration at each point of the titration.

$$1/T_{1,obs} = T_{1d} + r_1 \times [Gd] \quad (1)$$

DFT calculations: Geometry optimizations and analytical frequency calculations of the **EuL^1** and **EuL^{1}ZnCl$_2$** systems were carried out using the Gaussian 09 program package.[32] The frequency analysis confirmed that the optimized geometries corresponded to local energy minima in all cases. In these calculations we used the hybrid meta generalized gradient approximation (hybrid meta-GGA) with the TPSSh exchange-correlation functional.[33] Relativistic effects were considered using the large-core effective core potential of Dolg et al.[34] for Eu, in combination with the associated (7s6p5d)/[5s4p3d] GTO valence basis. The 6-31G(d,p) basis set was used for all other atoms. The TPSSh functional in combination with the large-core approximation was found to provide good results in studies focusing on the structures and energetics of lanthanide complexes.[35] The quality of the integration grid was increased from the default values using the integral=ultrafine keyword in Gaussian 09.

Acknowledgements

The financial supports of the China Scholarship Council (PhD fellowship to Gaoji Wang) and the German Research Foundation (DFG, grant AN 716/7-1) for this research are acknowledged. C.P.-I. acknowledges the support of Centro de Supercomputación de Galicia (CESGA).

Keywords: lanthanides · luminescence · photoinduced electron transfer · tyrosine · zinc

[1] a) K. Hanaoka, K. Kikuchi, H. Kojima, Y. Urano, T. Nagano, *J. Am. Chem. Soc.* **2004**, *126*, 12470–12476; b) W. Maret, Y. Li, *Chem. Rev.* **2009**, *109*, 4682–4707; c) C. S. Bonnet, *Coord. Chem. Rev.* **2018**, *369*, 91–104; d) K. P. Carter, A. M. Young, A. E. Palmer, *Chem. Rev.* **2014**, *114*, 4564–4601; e) P. N. Basa, S. Antala, R. E. Dempski, S. C. Burdette, *Angew. Chem. Int. Ed.* **2015**, *54*, 13027–13031.
[2] L. De Leon-Rodriguez, A. J. M. Lubag, A. D. Sherry, *Inorg. Chim. Acta* **2012**, *393*, 12–23.
[3] D. J. Eide, *Metallomics* **2011**, *3*, 1124–1129.
[4] a) P. J. Jiang, Z. J. Guo, *Coord. Chem. Rev.* **2004**, *248*, 205–229; b) K. Kikuchi, K. Komatsu, T. Nagano, *Curr. Opin. Chem. Biol.* **2004**, *8*, 182–191; c) T. Gunnlaugsson, T. C. Lee, R. Parkesh, *Org. Biomol. Chem.* **2003**, *1*, 3265–3267; d) G. J. Stasiuk, F. Minuzzi, M. Sae-Heng, C. Rivas, H. P. Juretschke, L. Piemonti, P. R. Allegrini, D. Laurent, A. R. Duckworth, A. Beeby, G. A. Rutter, N. J. Long, *Chem. Eur. J.* **2015**, *21*, 5023–5033.
[5] a) S. Biniecki, S. Kabzinska, *Ann. Pharm. Fr.* **1964**, *22*, 685–687; b) J. R. Johnson, H. Jiang, B. D. Smith, *Bioconjugate Chem.* **2008**, *19*, 1033–1039.
[6] a) E. R. Milaeva, D. B. Shpakovsky, Y. A. Gracheva, S. I. Orlova, V. V. Maduar, B. N. Tarasevich, N. N. Meleshonkova, L. G. Dubova, E. F. Shevtsova, *Dalton Trans.* **2013**, *42*, 6817–6828; b) E. J. O'Neil, H. Jiang, B. D. Smith, *Supramol. Chem.* **2013**, *25*, 315–322; c) B. Roy, A. S. Rao, K. H. Ahn, *Org. Biomol. Chem.* **2011**, *9*, 7774–7779; d) S. A. Yoon, J. Lee, M. H. Lee, *Sens. Actuators B* **2018**, *258*, 50–55.
[7] B. A. Wong, S. Friedle, S. J. Lippard, *J. Am. Chem. Soc.* **2009**, *131*, 7142–7152.
[8] a) J. Fan, X. Peng, Y. Wu, E. Lu, J. Hou, H. Zhang, R. Zhang, X. Fu, *J. Lumin.* **2005**, *114*, 125–130; b) A. P. de Silva, T. S. Moody, G. D. Wright, *Analyst* **2009**, *134*, 2385–2393; c) M. J. Culzoni, A. M. de la Pena, A. Machuca, H. C. Goicoechea, R. Brasca, R. Babiano, *Talanta* **2013**, *117*, 288–296; d) D. Escudero, *Acc. Chem. Res.* **2016**, *49*, 1816–1824.
[9] a) H. Akiba, J. Sumaoka, M. Komiyama, *Chem. Eur. J.* **2010**, *16*, 5018–5025; b) M. Roger, M. Regueiro-Figueroa, C. Ben Azzeddine, V. Patinec, C. S. Bonnet, C. Platas-Iglesias, R. Tripier, *Eur. J. Inorg. Chem.* **2014**, *2014*, 1072–1081; c) O. Reany, T. Gunnlaugsson, D. Parker, *J. Chem. Soc. Perkin Trans. 2* **2000**, 1819–1831; d) K. Hanaoka, K. Kikuchi, H. Kojima, Y. Urano, T. Nagano, *Angew. Chem. Int. Ed.* **2003**, *42*, 2996–2999; e) M. L. Aulsebrook, B. Graham, M. R. Grace, K. L. Tuck, *Tetrahedron* **2014**, *70*, 4367–4372.
[10] a) S. J. A. Pope, R. H. Laye, *Dalton Trans.* **2006**, 3108–3113; b) S. Shuvaev, M. Starck, D. Parker, *Chem. Eur. J.* **2017**, *23*, 9974–9989.
[11] S. Shuvaev, M. A. Fox, D. Parker, *Angew. Chem. Int. Ed.* **2018**, *57*, 7488–7492.
[12] a) L. H. Fornander, B. B. Feng, T. Beke-Somfai, B. Norden, *J. Phys. Chem. B* **2014**, *118*, 9247–9257; b) J. M. Antosiewicz, D. Shugar, *Biophys. Rev. Lett.* **2016**, *8*, 151–161.
[13] R. G. Hanshaw, E. J. O'Neil, M. Foley, R. T. Carpenter, B. D. Smith, *J. Mater. Chem.* **2005**, *15*, 2707–2713.
[14] W. C. Shieh, S. Dell, O. Repic, *Org. Lett.* **2001**, *3*, 4279–4281.
[15] K. Binnemans, *Coord. Chem. Rev.* **2015**, *295*, 1–45.
[16] V. Hlinova, A. Jaros, T. David, I. Cisarova, J. Kotek, V. Kubicek, P. Hermann, *New J. Chem.* **2018**, *42*, 7713–7722.

[17] L. Fabbrizzi, M. Licchelli, P. Pallavicini, *Acc. Chem. Res.* **1999**, *32*, 846–853.
[18] S. W. Zhang, R. Adhikari, M. X. Fang, N. Dorh, C. Li, M. Jaishi, J. T. Zhang, A. Tiwari, R. Pati, F. T. Luo, H. Y. Liu, *ACS Sens.* **2016**, *1*, 1408–1415.
[19] G. K. Walkup, S. C. Burdette, S. J. Lippard, R. Y. Tsien, *J. Am. Chem. Soc.* **2000**, *122*, 5644–5645.
[20] N. Q. Jie, J. H. Yang, X. R. Huang, W. Y. Ma, *Anal. Proc.* **1995**, *32*, 427–429.
[21] B. Daly, J. Ling, A. P. de Silva, *Chem. Soc. Rev.* **2015**, *44*, 4203–4211.
[22] M. Woods, G. E. Kiefer, S. Bott, A. Castillo-Muzquiz, C. Eshelbrenner, L. Michaudet, K. McMillan, S. D. K. Mudigunda, D. Grin, G. Tircso, S. R. Zhang, P. Zhao, A. D. Sherry, *J. Am. Chem. Soc.* **2004**, *126*, 9248–9256.
[23] I. Carreira-Barral, T. Rodriguez-Blas, C. Platas-Iglesias, A. de Bias, D. Esteban-Gomez, *Inorg. Chem.* **2014**, *53*, 2554–2568.
[24] O. A. Blackburn, M. Tropiano, L. S. Natrajan, A. M. Kenwright, S. Faulkner, *Chem. Commun.* **2016**, *52*, 6111–6114.
[25] W. Likussar, D. F. Boltz, *Anal. Chem.* **1971**, *43*, 1265–1272.
[26] J. S. Renny, L. L. Tomasevich, E. H. Tallmadge, D. B. Collum, *Angew. Chem. Int. Ed.* **2013**, *52*, 11998–12013.
[27] M. Regueiro-Figueroa, S. Gündüz, V. Patinec, N. K. Logothetis, D. Esteban-Gómez, R. Tripier, G. Angelovski, C. Platas-Iglesias, *Inorg. Chem.* **2015**, *54*, 10342–10350.
[28] a) Y. P. Zhang, Z. Y. Ma, C. Y. Gao, X. Qiao, J. L. Tian, W. Gu, X. Liu, J. Y. Xu, J. Z. Zhao, S. P. Yan, *New J. Chem.* **2016**, *40*, 7513–7521; b) Y. I. Kim, Y. S. Lee, H. J. Seo, J. Y. Lee, S. K. Kang, *Acta Crystallogr. Sect. E* **2007**, *63*, M2810-U1669.
[29] D. M. Corsi, C. Platas-Iglesias, H. van Bekkum, J. A. Peters, *Magn. Reson. Chem.* **2001**, *39*, 723–726.
[30] J. Aguiar, P. Carpena, J. A. Molina-Bolivar, C. C. Ruiz, *J. Colloid Interface Sci.* **2003**, *258*, 116–122.
[31] P. Gans, A. Sabatini, A. Vacca, *Talanta* **1996**, *43*, 1739–1753.
[32] M. J. Frisch, G. W. Trucks, H. B. Schlegel, G. E. Scuseria, M. A. Robb, J. R. Cheeseman, G. Scalmani, V. Barone, B. Mennucci, G. A. Petersson, H. Nakatsuji, M. Caricato, X. Li, H. P. Hratchian, A. F. Izmaylov, J. Bloino, G. Zheng, J. L. Sonnenberg, M. Hada, M. Ehara, K. Toyota, R. Fukuda, J. Hasegawa, M. Ishida, T. Nakajima, Y. Honda, O. Kitao, H. Nakai, T. Vreven, J. A. Montgomery, J. E. Peralta, F. Ogliaro, M. Bearpark, J. J. Heyd, E. Brothers, K. N. Kudin, V. N. Staroverov, R. Kobayashi, J. Normand, K. Raghavachari, A. Rendell, J. C. Burant, S. S. Iyengar, J. Tomasi, M. Cossi, N. Rega, J. M. Millam, M. Klene, J. E. Knox, J. B. Cross, V. Bakken, C. Adamo, J. Jaramillo, R. Gomperts, R. E. Stratmann, O. Yazyev, A. J. Austin, R. Cammi, C. Pomelli, J. W. Ochterski, R. L. Martin, K. Morokuma, V. G. Zakrzewski, G. A. Voth, P. Salvador, J. J. Dannenberg, S. Dapprich, A. D. Daniels, Farkas, J. B. Foresman, J. V. Ortiz, J. Cioslowski, D. J. Fox in *Gaussian 09, Revision B.01, Vol.* Gaussian, Inc., Wallingford CT, **2009**.
[33] J. M. Tao, J. P. Perdew, V. N. Staroverov, G. E. Scuseria, *Phys. Rev. Lett.* **2003**, *91*, 146401.
[34] M. Dolg, H. Stoll, A. Savin, H. Preuss, *Theor. Chim. Acta* **1989**, *75*, 173–194.
[35] a) M. Regueiro-Figueroa, D. Esteban-Gómez, A. de Blas, T. Rodríguez-Blas, C. Platas-Iglesias, *Chem. Eur. J.* **2014**, *20*, 3974–3981; b) M. Regueiro-Figueroa, C. Platas-Iglesias, *J. Phys. Chem. A* **2015**, *119*, 6436–6445.

Manuscript received: December 13, 2019
Revised manuscript received: January 8, 2020

ChemPlusChem

Supporting Information

Europium(III) Macrocyclic Chelates Appended with Tyrosine-based Chromophores and Di-(2-picolyl)amine-based Receptors: Turn-On Luminescent Chemosensors Selective to Zinc(II) Ions

Gaoji Wang, Carlos Platas-Iglesias, and Goran Angelovski*

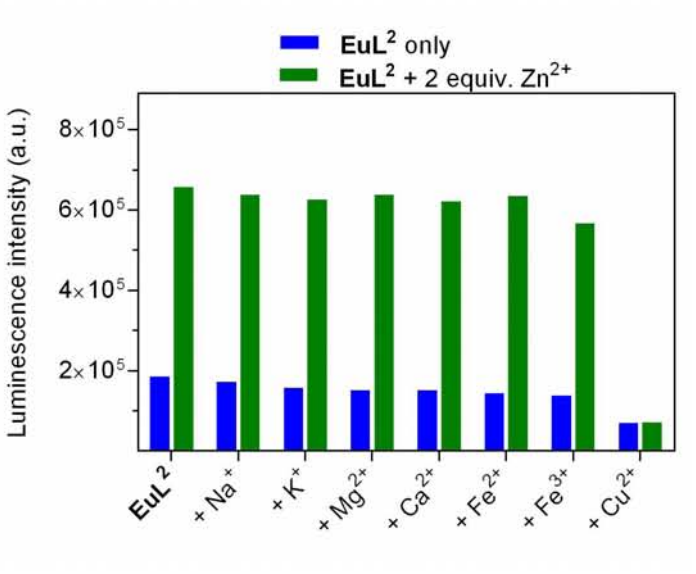

Figure S1. Luminescence variation of **EuL^2** (50 μM) to Zn^{2+} in the presence of other metal ions Na^+, K^+, Ca^{2+}, Mg^{2+}, Fe^{2+}, Fe^{3+} and Cu^{2+}. Blue bars indicate luminescence intensity of probe **EuL^2** in the presence of various metal ions (3 equiv., respectively). Green bars indicate luminescence intensity of probe **EuL^2** containing various metal ions after the subsequent addition of Zn^{2+} (3 equiv.).

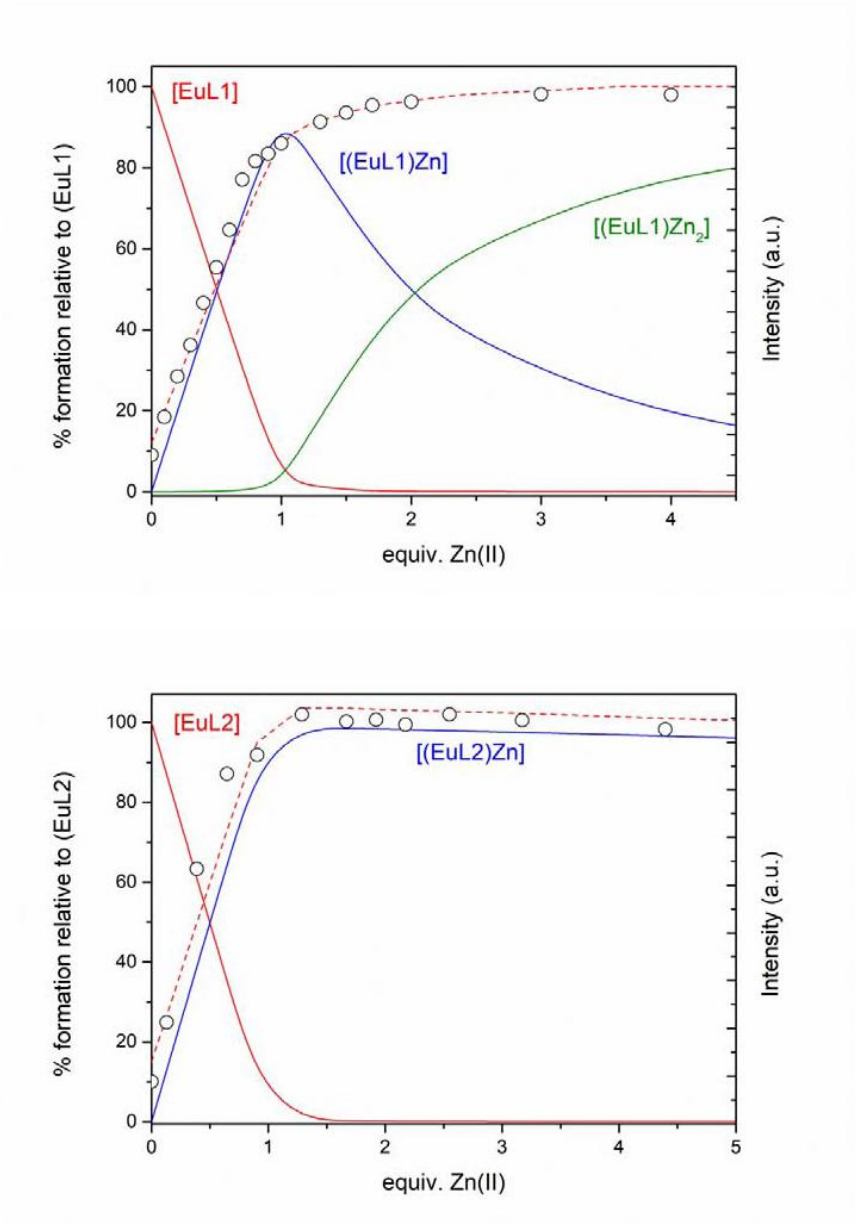

Figure S2. Titration profiles of **EuL**^{1} and **EuL**^{2} with Zn^{2+} at 617 nm, fitted data (dashed lines) and speciation diagrams. The total concentration of complex and Zn^{2+} was 50 μM. All data were recorded in 50 mM HEPES buffer at pH 7.4.

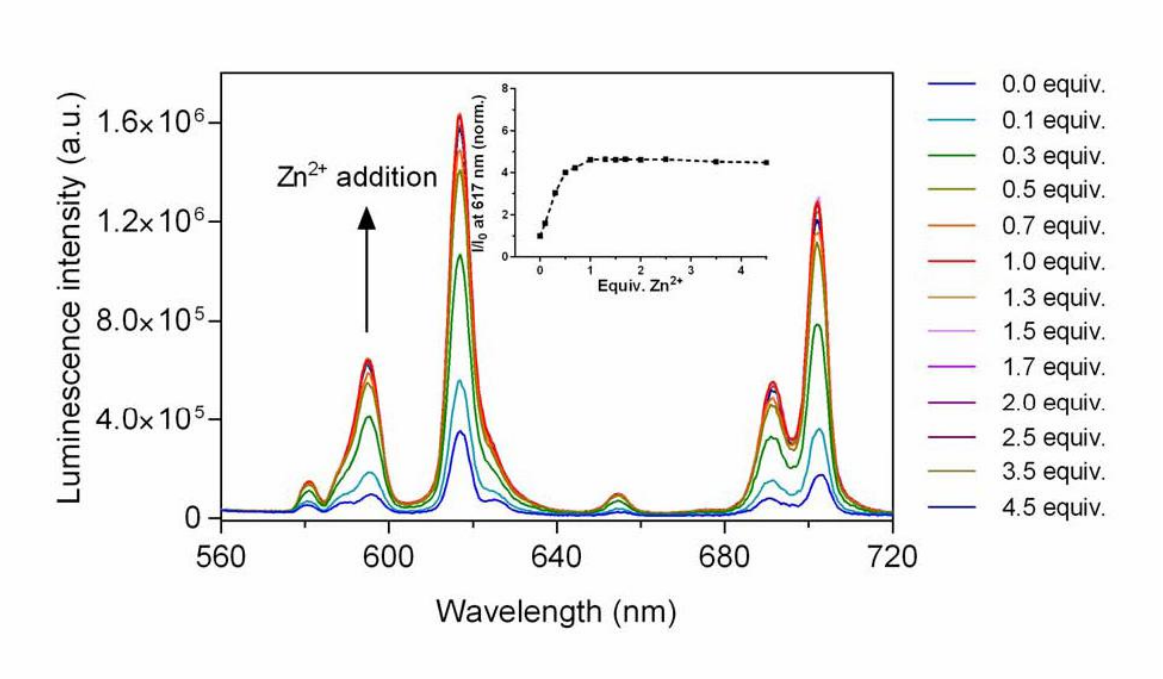

Figure S3. Luminescence emission spectral variations of **EuL^2** (50 μM, λ_{ex} = 322 nm, λ_{em} = 617 nm) upon titration with Zn^{2+} (50 mM HEPES, pH 7.4, 25 °C). Inset: normalized emission intensities of **EuL^2** as a function of Zn^{2+} concentration.

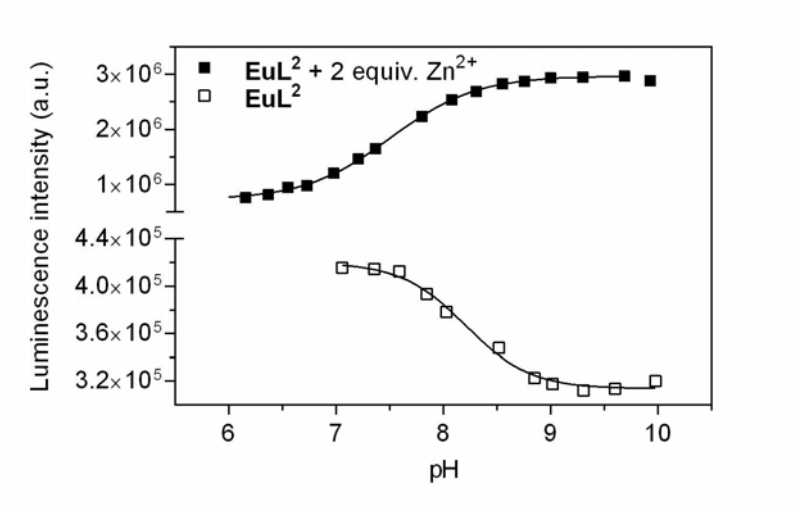

Figure S4. Luminescence intensity changes of the buffered **EuL^2** (50 μM) upon titration with Zn^{2+} (λ_{ex} = 322 nm, λ_{em} = 617 nm) at various pH.

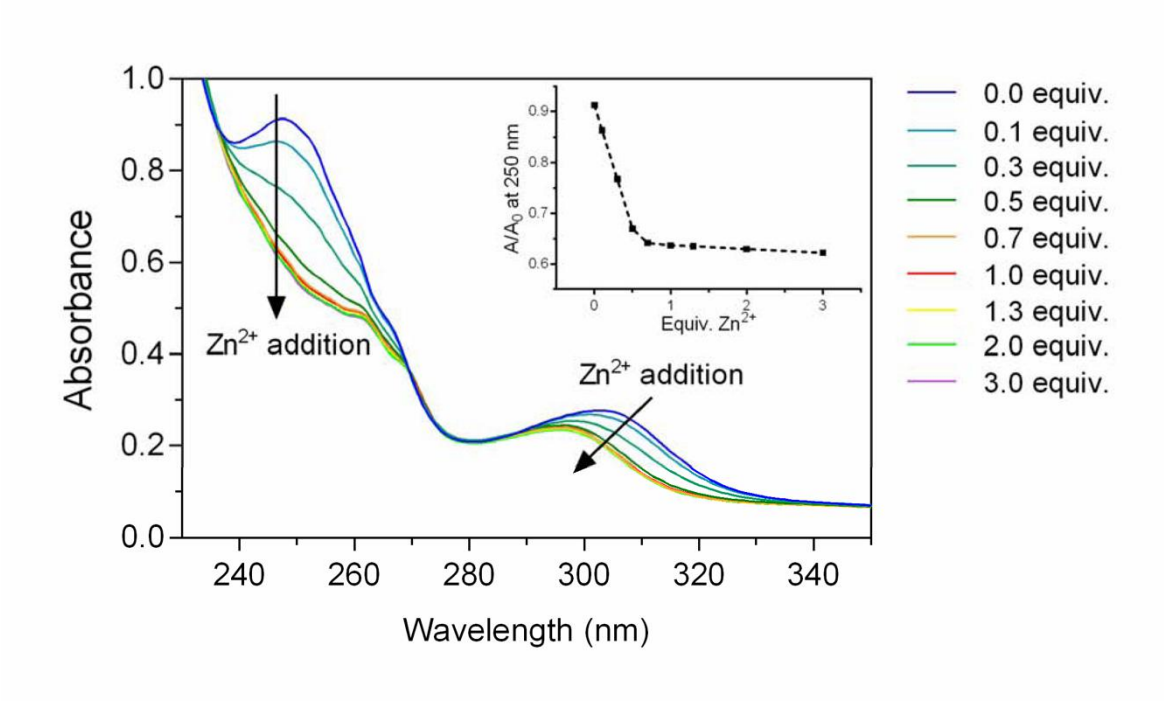

Figure S5. UV-Vis absorbance variation of buffered **EuL^2** (50 μM) upon Zn^{2+} addition at 25 ºC and pH 7.4 (50 mM HEPES).

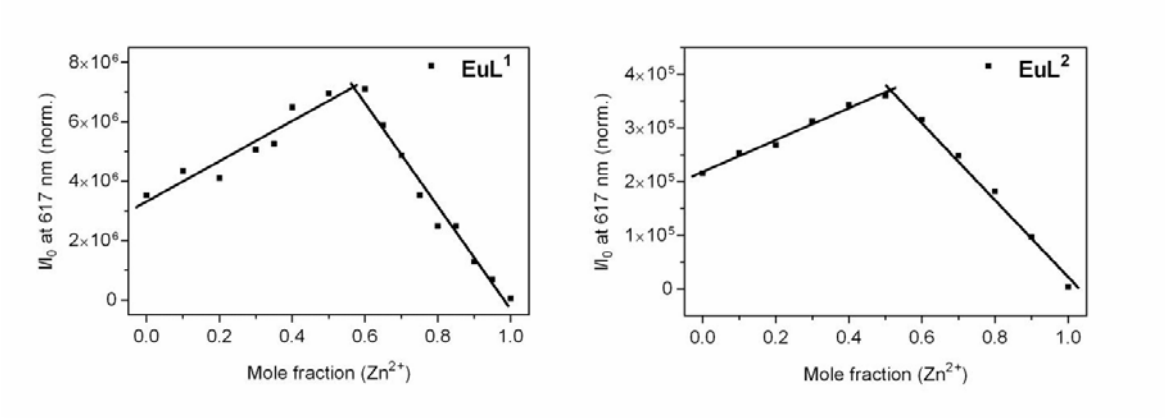

Figure S6. Job's plot for the binding event of **EuL^2** with Zn^{2+}. The total concentration of complex and Zn^{2+} was 50 μM. All data were recorded in 50 mM HEPES buffer at pH 7.4 (λ_{ex} = 322 nm, λ_{em} = 617 nm).

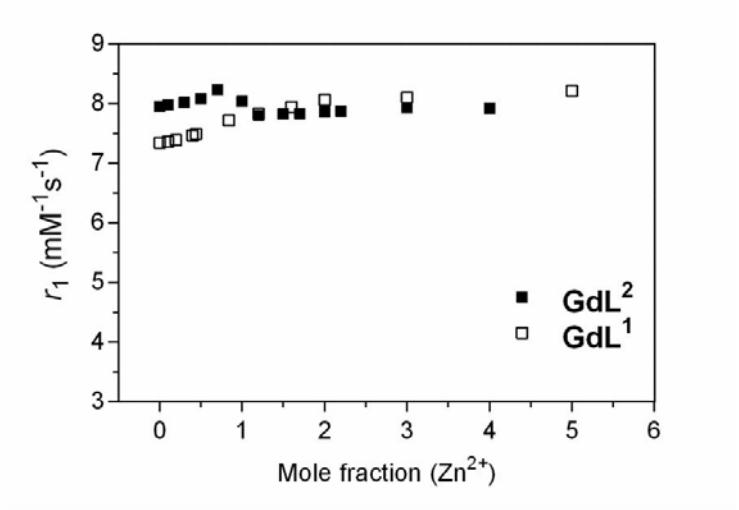

Figure S7. Changes in the r_1 longitudinal relaxivity of **GdL^1** and **GdL^2** (3.0 mM) upon addition of Zn^{2+} at 7.0 T, 25°C, and pH 7.4 (50 mM HEPES).

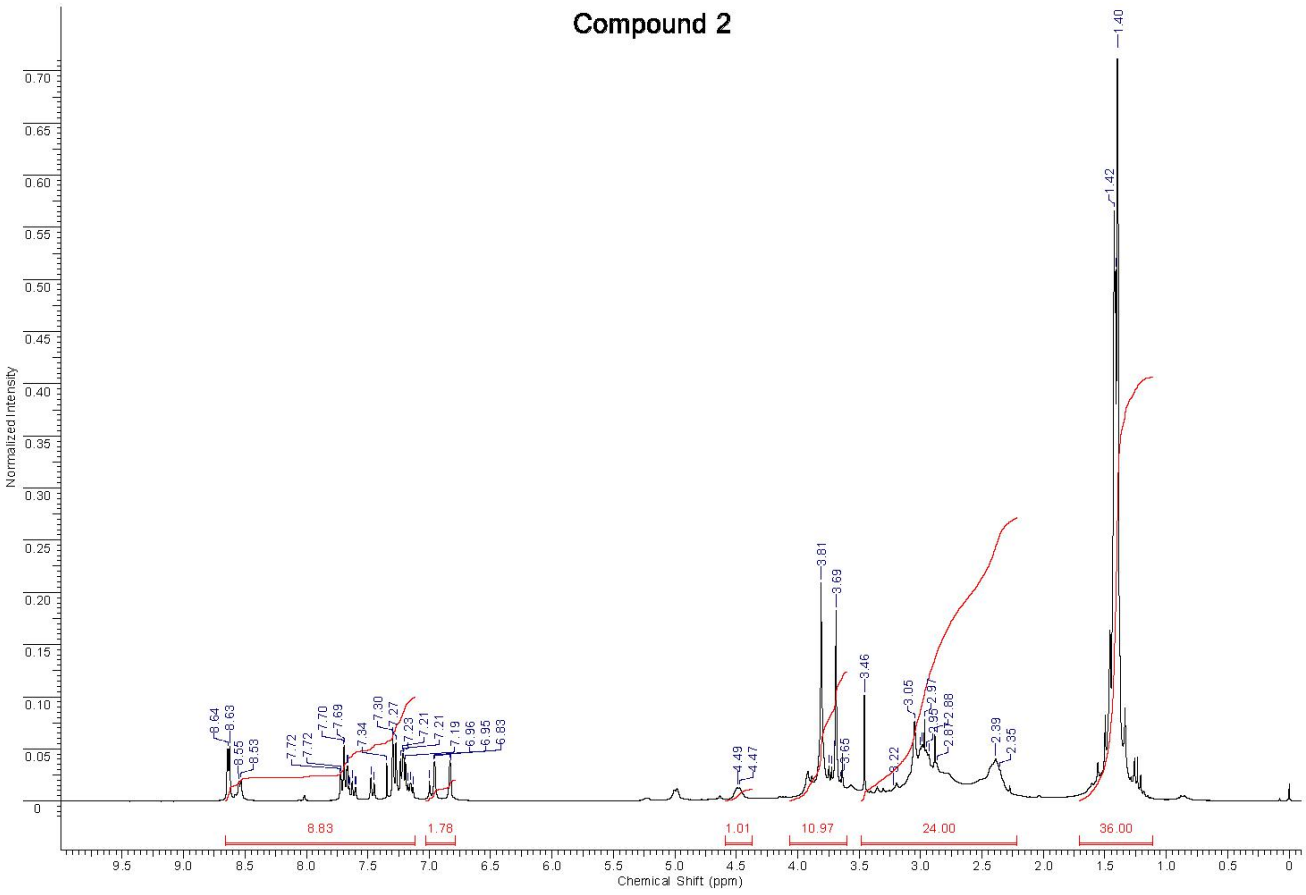
Compound 2
Normalized Intensity
Chemical Shift (ppm)
8.64
8.63
8.55
8.53
7.72
7.72
7.70
7.69
7.34
7.30
7.27
7.23
7.21
7.21
7.19
6.96
6.95
6.83
4.49
4.47
3.81
3.69
3.65
3.46
3.22
3.05
2.97
2.88
2.87
2.39
2.35
1.42
1.40
8.83
1.78
1.01
10.97
24.00
36.00

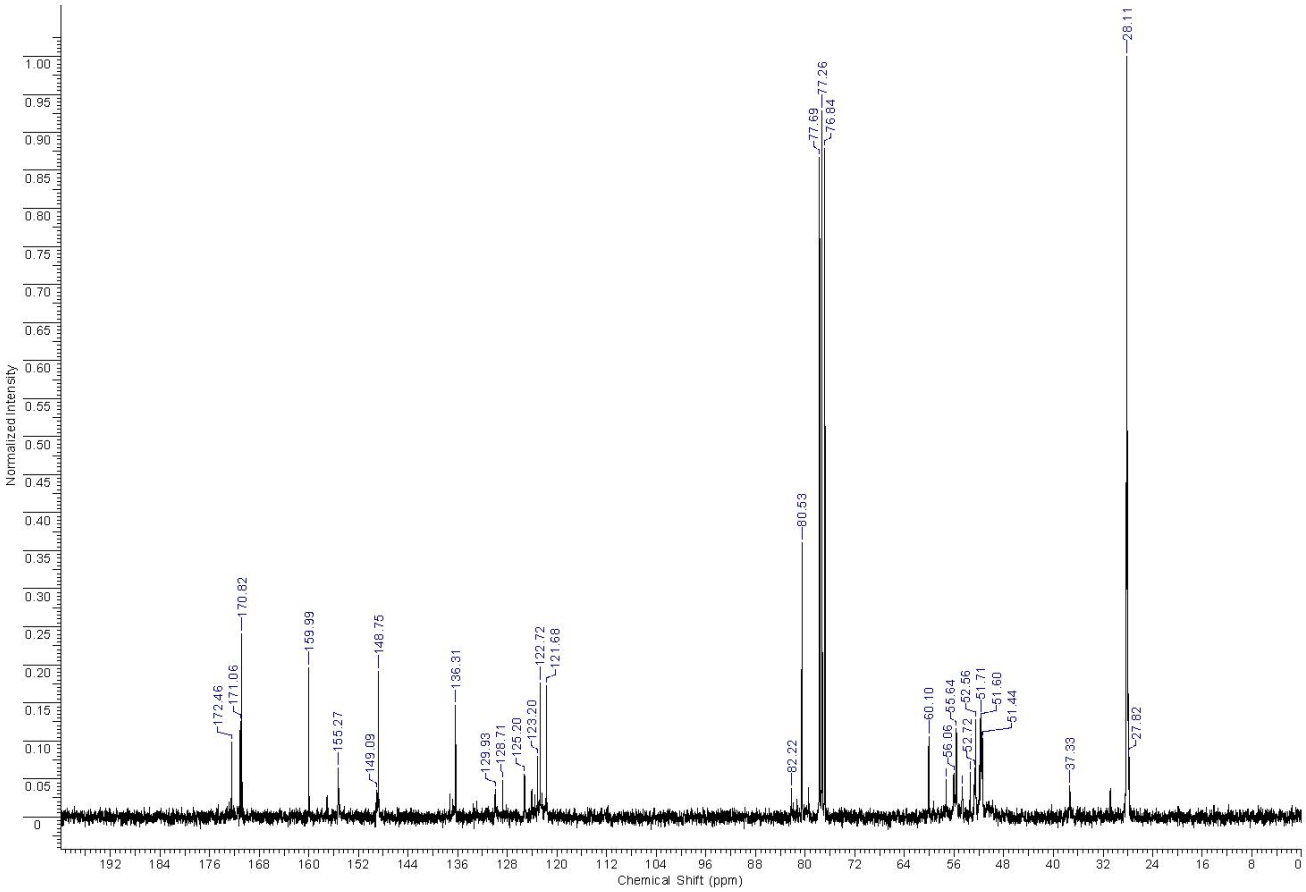
Normalized Intensity
Chemical Shift (ppm)
172.46
171.06
170.82
159.99
155.27
149.09
148.75
136.31
129.93
128.71
125.20
123.20
122.72
121.68
82.22
80.53
77.69
77.26
76.84
60.10
56.06
55.64
52.72
52.56
51.71
51.60
51.44
37.33
28.11
27.82

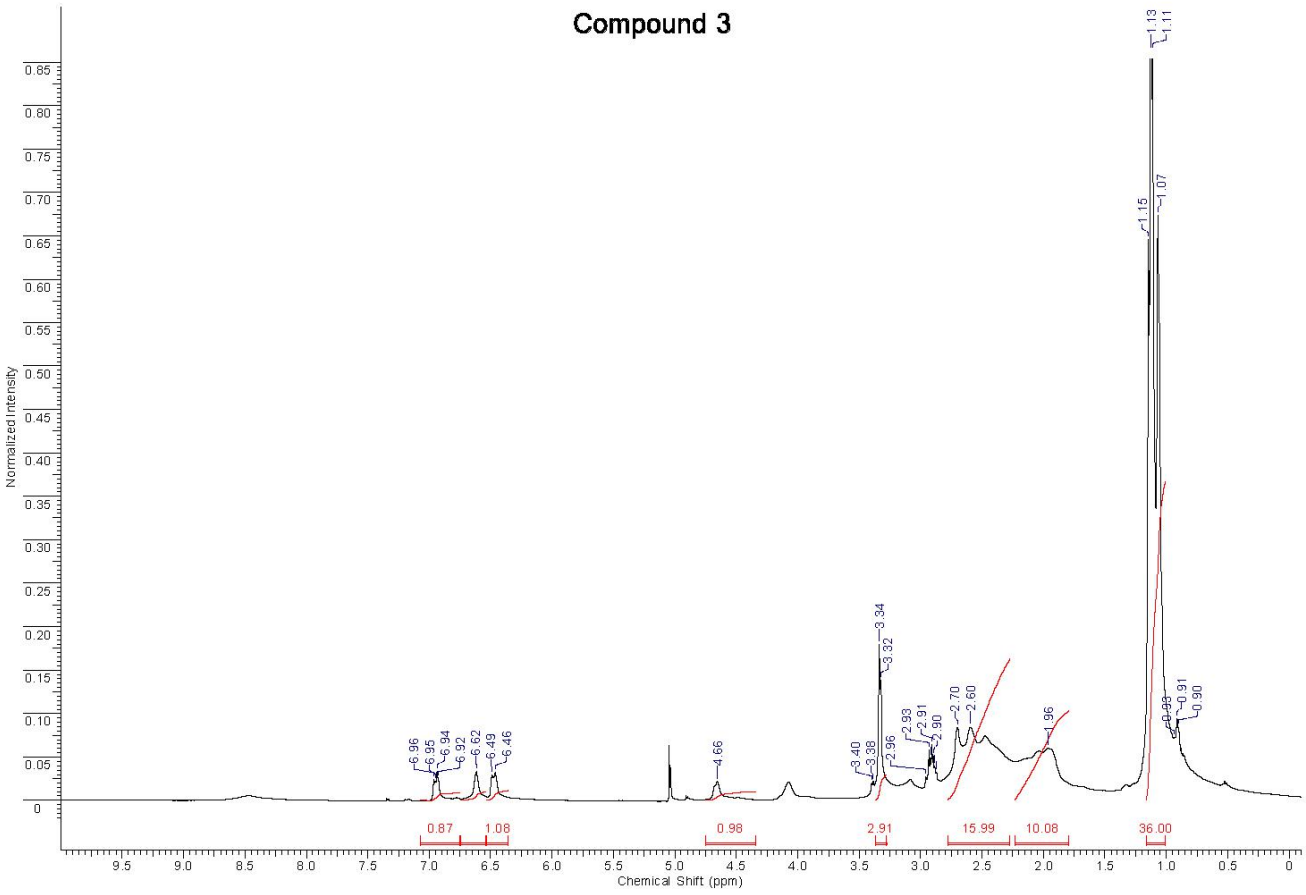
Compound 3
Normalized Intensity
Chemical Shift (ppm)
6.96
6.95
6.94
6.92
6.62
6.49
6.46
4.66
3.40
3.38
3.34
3.32
2.96
2.93
2.91
2.90
2.70
2.60
1.96
1.15
1.13
1.11
1.07
0.93
0.91
0.90
0.87
1.08
0.98
2.91
15.99
10.08
36.00

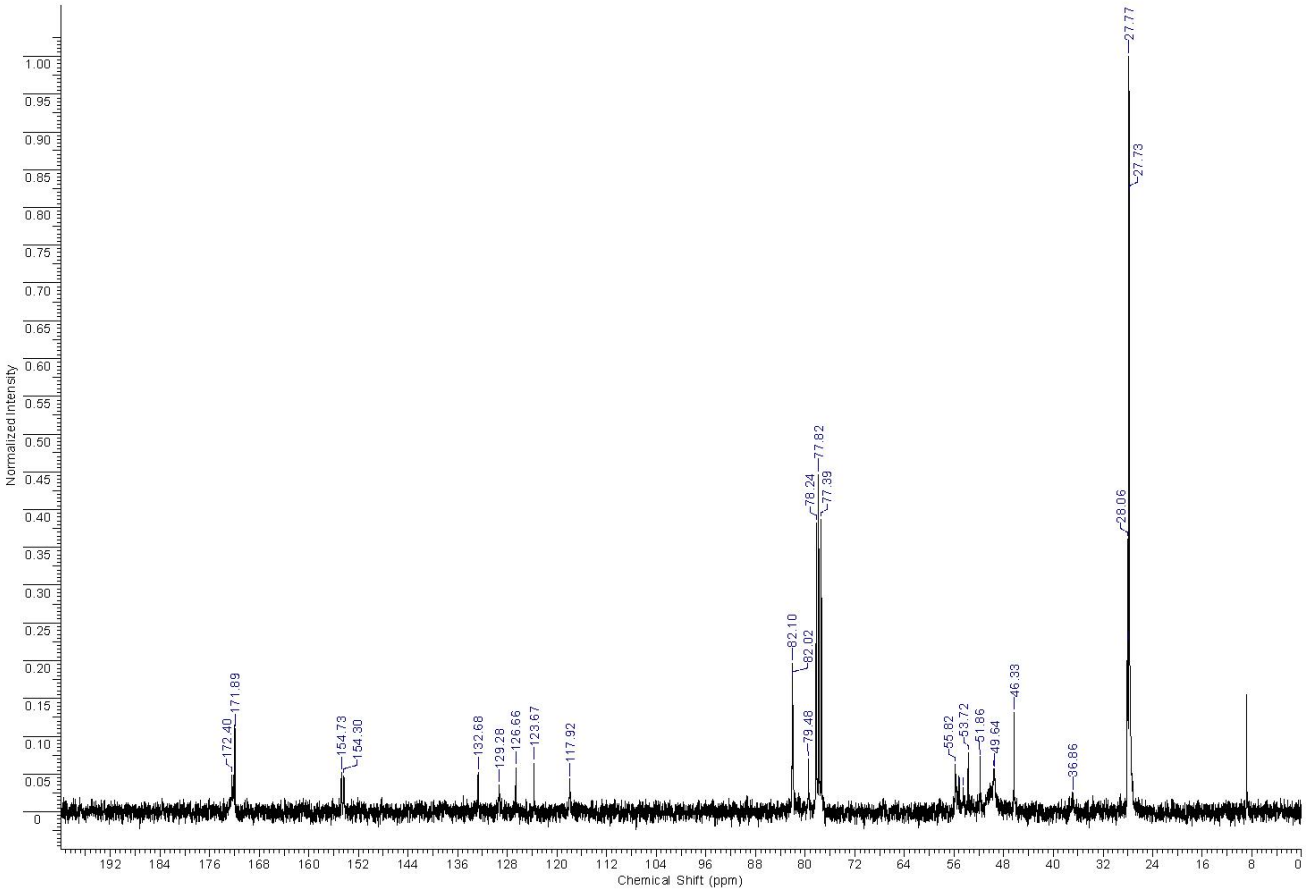
Normalized Intensity
Chemical Shift (ppm)
172.40
171.89
154.73
154.30
132.68
129.28
126.66
123.67
117.92
82.10
82.02
79.48
78.24
77.82
77.39
55.82
53.72
51.86
49.64
46.33
36.86
28.06
27.77
27.73

Compound L^1

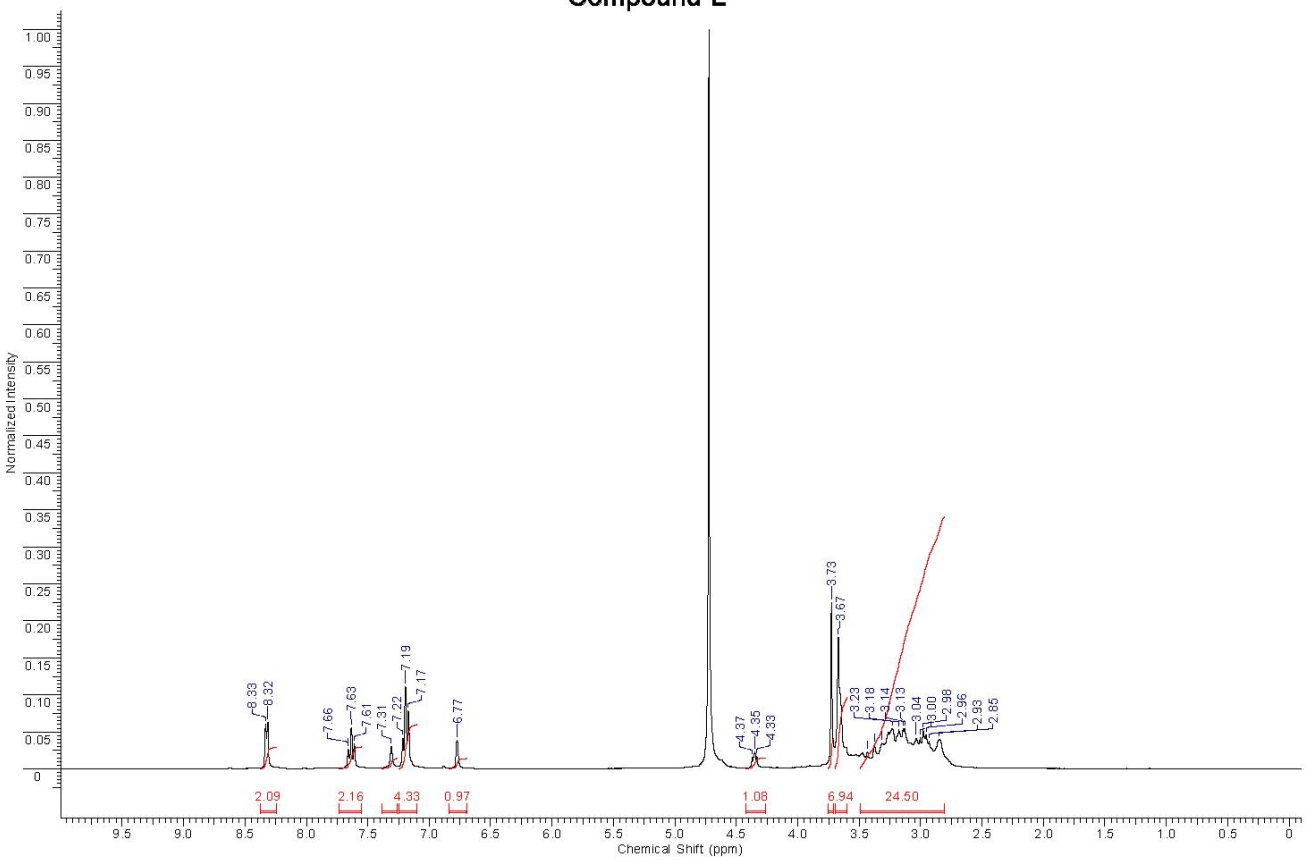
Normalized Intensity
Chemical Shift (ppm)
8.33
8.32
7.66
7.63
7.61
7.31
7.22
7.19
7.17
6.77
4.37
4.35
4.33
3.73
3.67
3.23
3.18
3.14
3.13
3.04
3.00
2.98
2.96
2.93
2.85
2.09
2.16
4.33
0.97
1.08
6.94
24.50

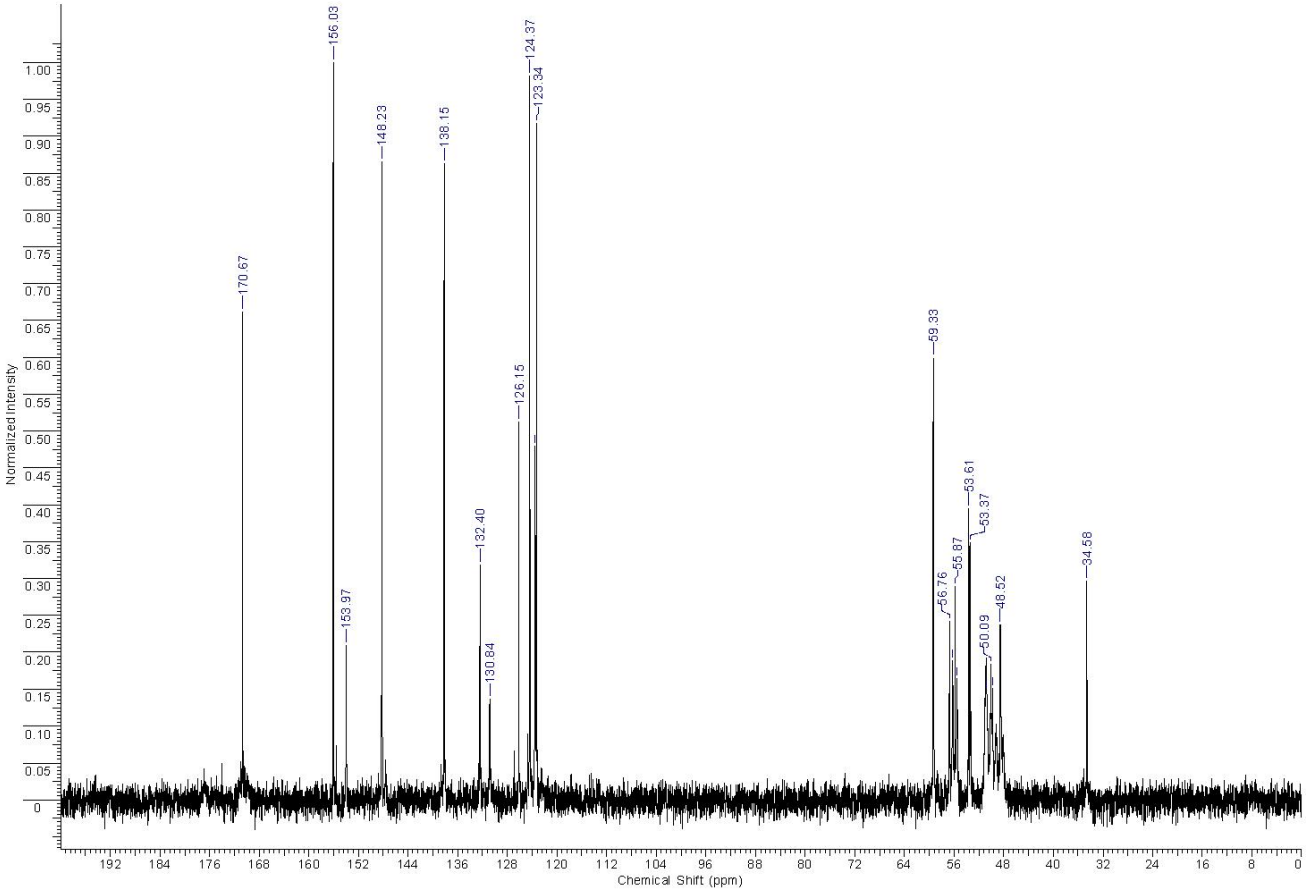
Normalized Intensity
Chemical Shift (ppm)
170.67
156.03
153.97
148.23
138.15
132.40
130.84
126.15
124.37
123.34
59.33
56.76
55.87
53.61
53.37
50.09
48.52
34.58

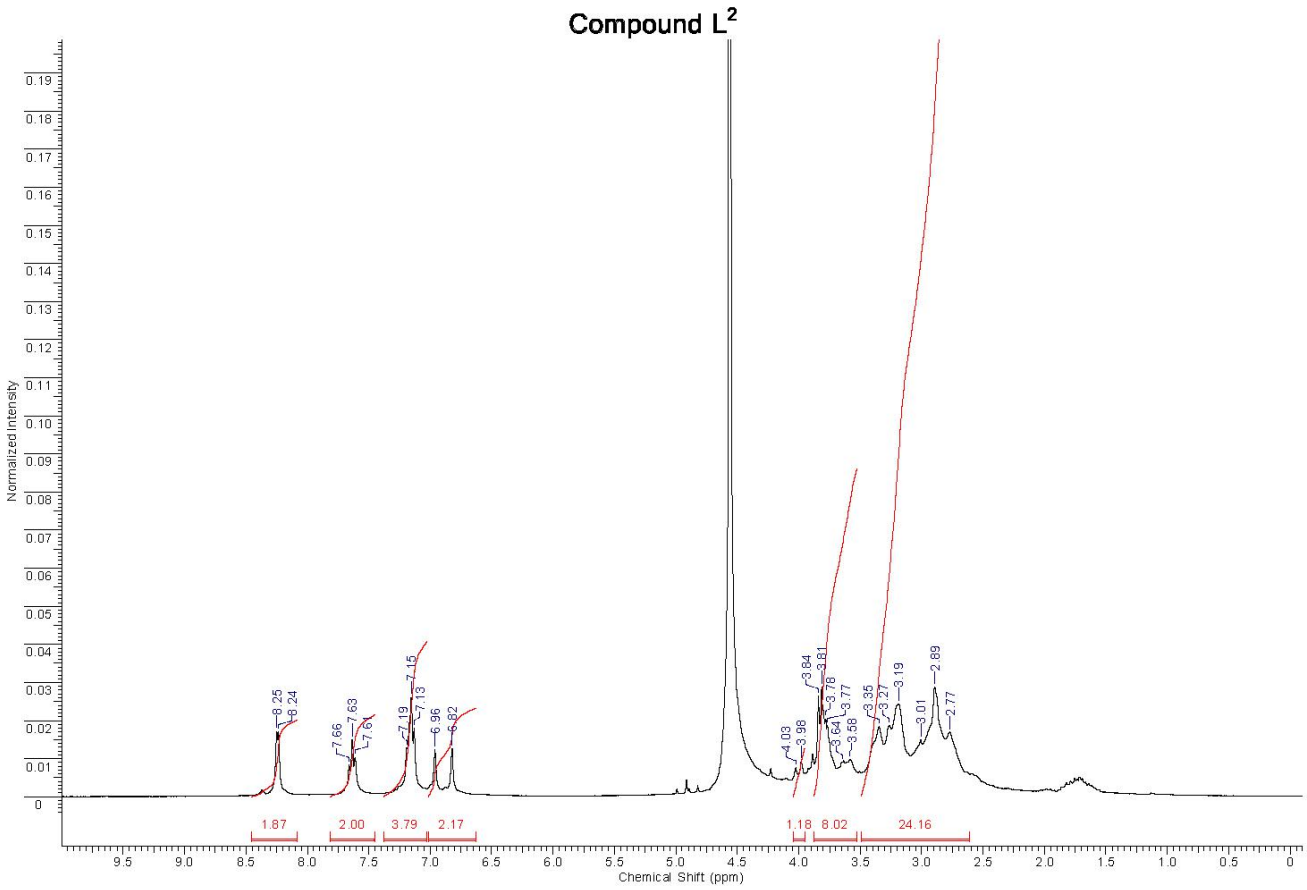
Compound L2
Normalized Intensity
Chemical Shift (ppm)
8.25
8.24
7.66
7.63
7.61
7.19
7.15
7.13
6.96
6.82
4.03
3.98
3.84
3.81
3.78
3.77
3.64
3.58
3.35
3.27
3.19
3.01
2.89
2.77
1.87
2.00
3.79
2.17
1.18
8.02
24.16

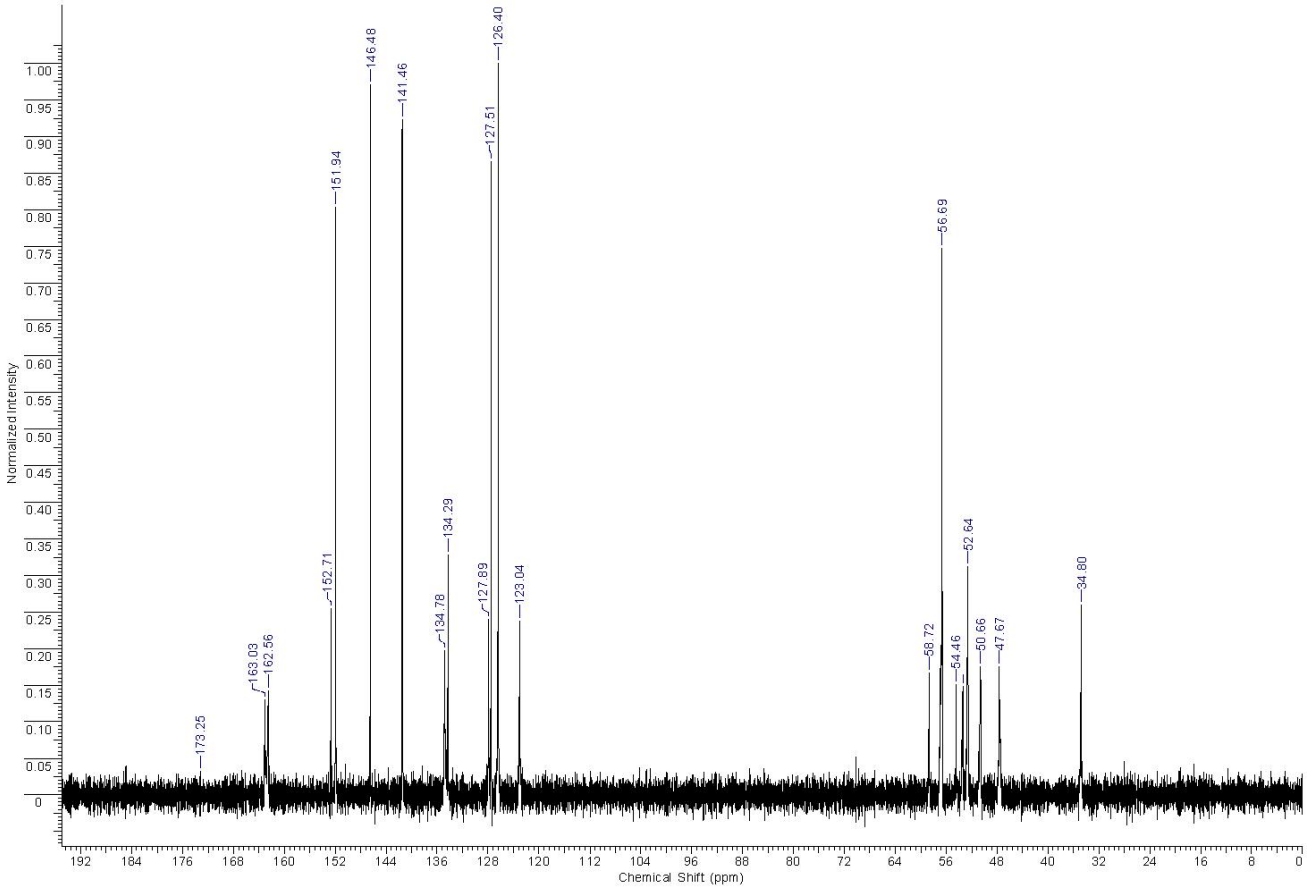
Normalized Intensity
Chemical Shift (ppm)
173.25
163.03
162.56
152.71
151.94
146.48
141.46
134.78
134.29
127.89
127.51
126.40
123.04
58.72
56.69
54.46
52.64
50.66
47.67
34.80

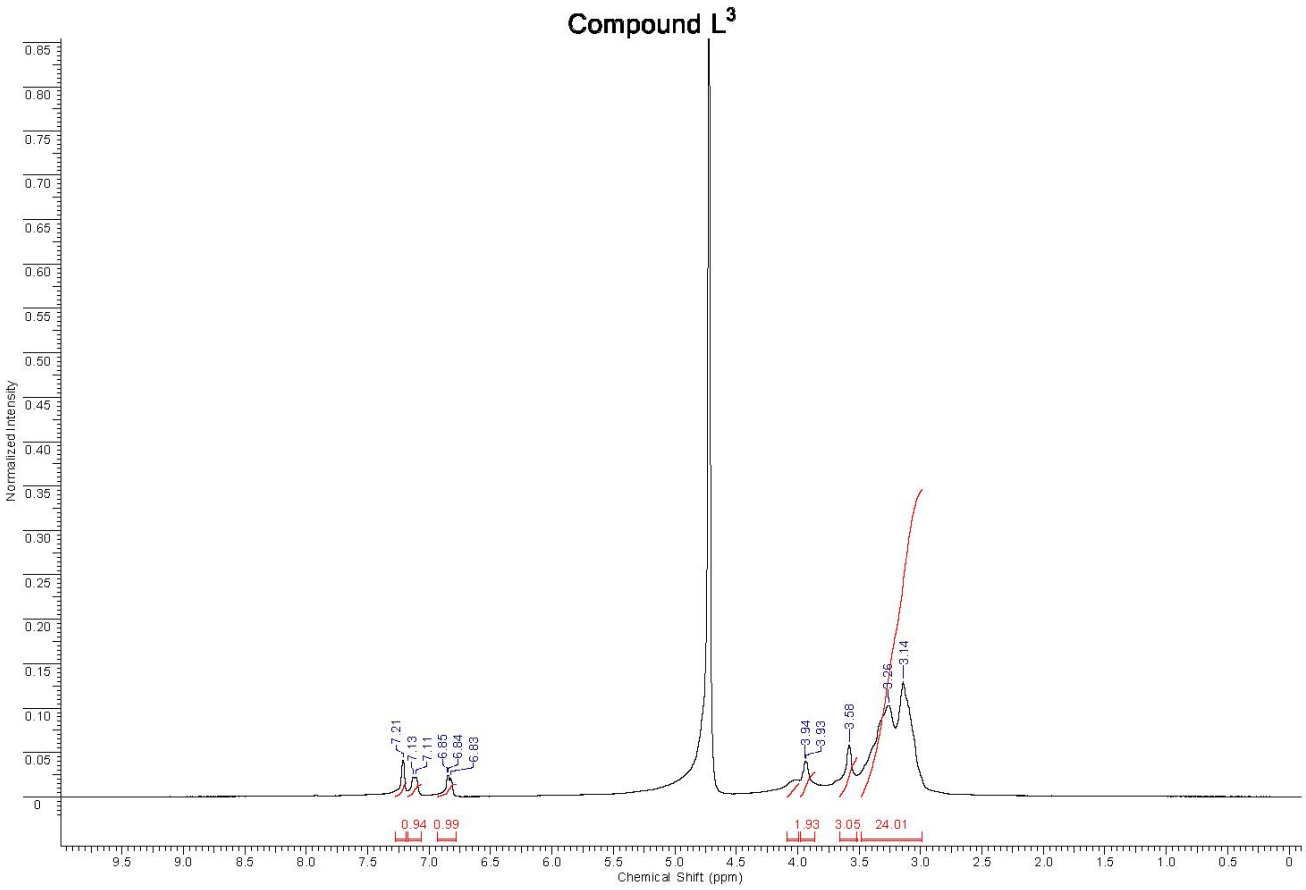
Compound L3
Normalized Intensity
Chemical Shift (ppm)
7.21
7.13
7.11
6.85
6.84
6.83
3.94
3.93
3.58
3.26
3.14
0.94
0.99
1.93
3.05
24.01

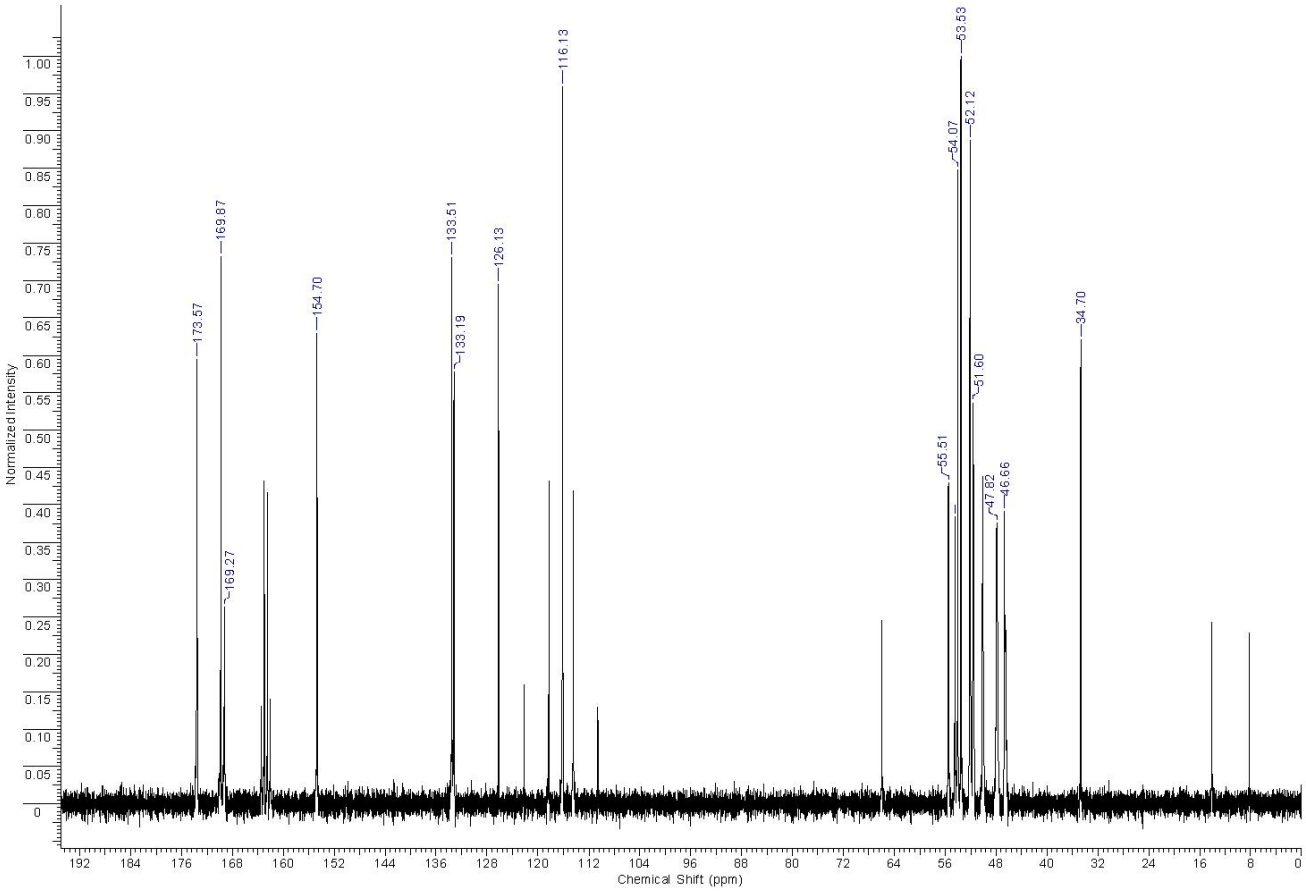
Normalized Intensity
Chemical Shift (ppm)
173.57
169.87
169.27
154.70
133.51
133.19
126.13
116.13
53.53
54.07
52.12
51.60
55.51
47.82
46.66
34.70

Compound L^4

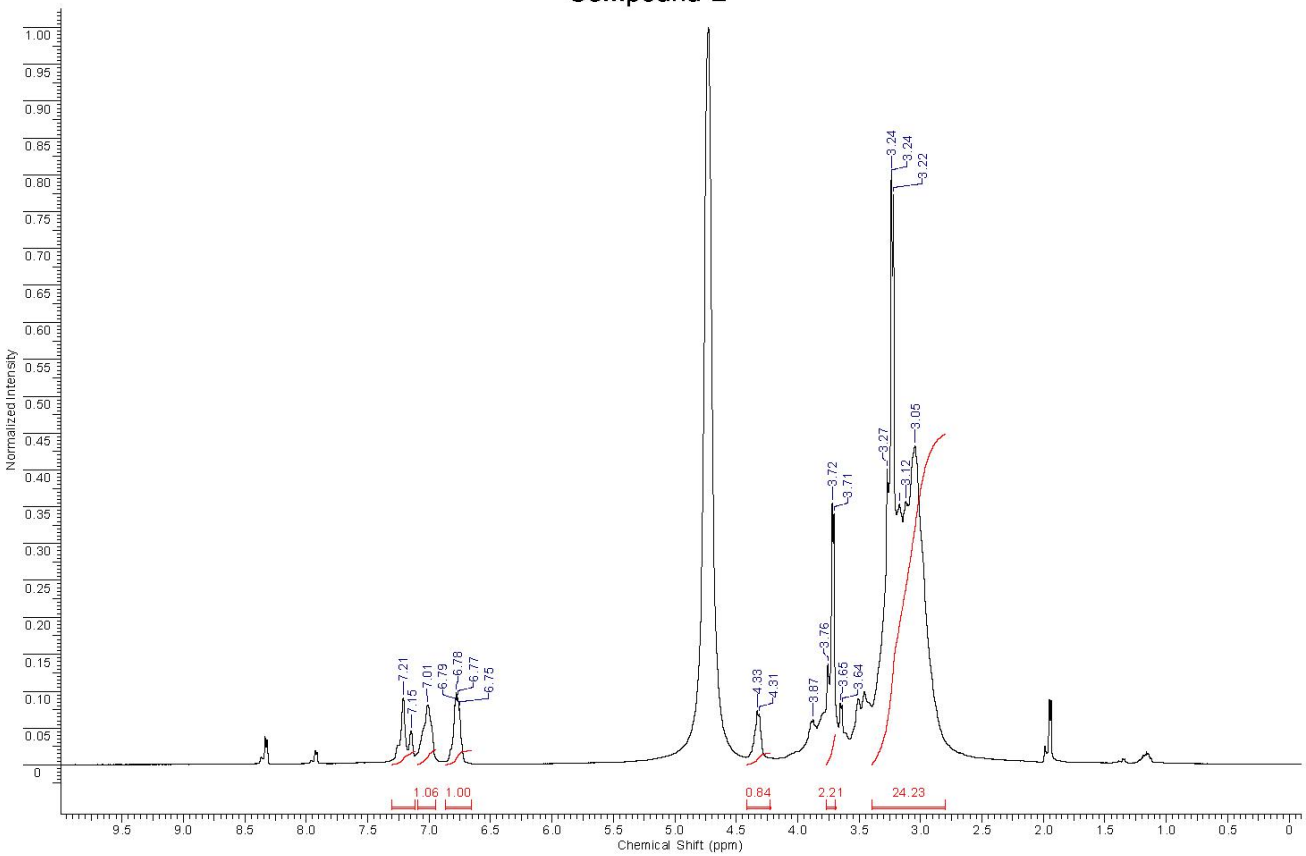
Normalized Intensity
Chemical Shift (ppm)
7.21
7.15
7.01
6.79
6.78
6.77
6.75
4.33
4.31
3.87
3.76
3.72
3.71
3.65
3.64
3.27
3.24
3.24
3.22
3.12
3.05
1.06
1.00
0.84
2.21
24.23

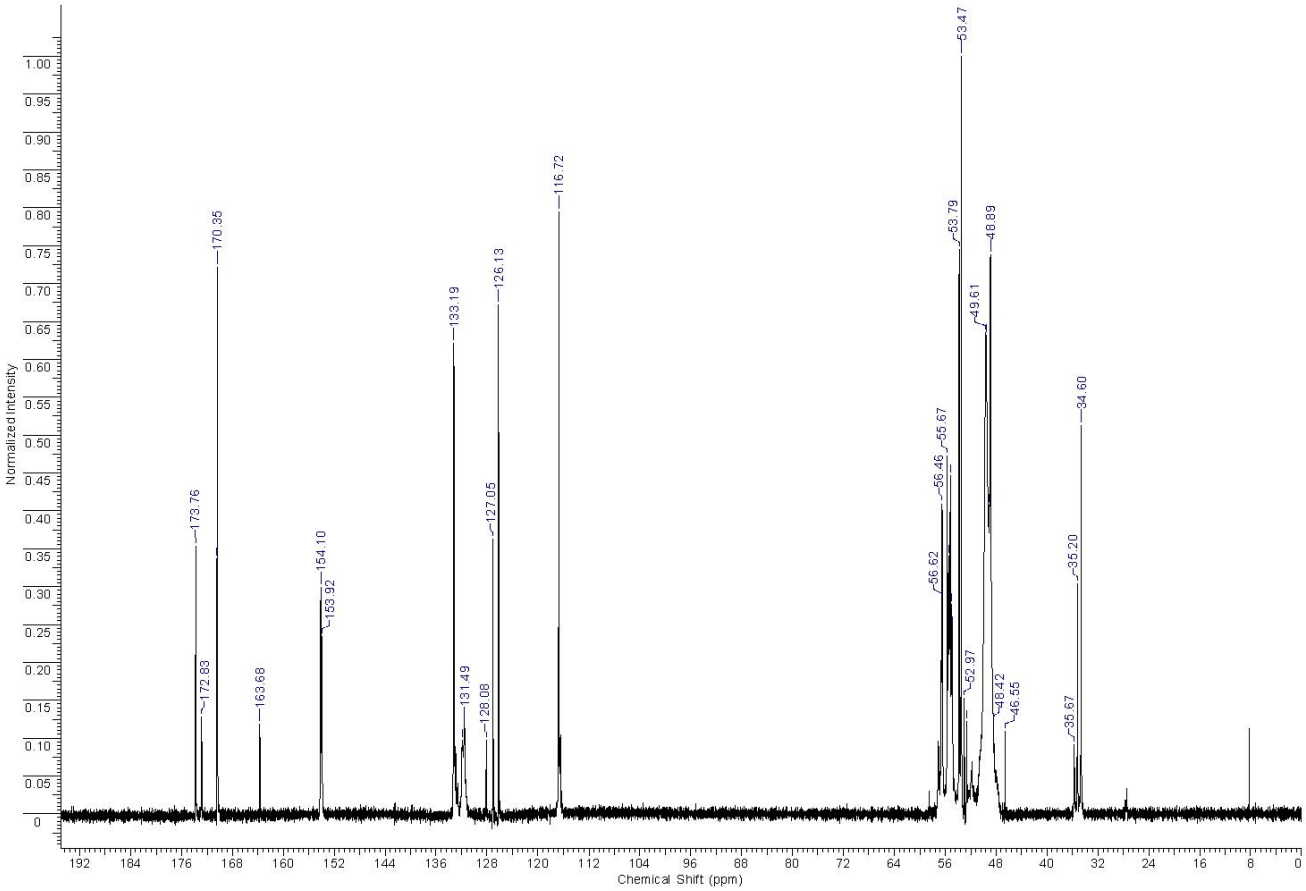
Normalized Intensity
Chemical Shift (ppm)
173.76
172.83
170.35
163.68
154.10
153.92
133.19
131.49
128.08
127.05
126.13
116.72
63.47
63.79
56.62
56.46
55.67
52.97
49.61
48.89
48.42
46.55
35.67
35.20
34.60

Table S1. Optimized Cartesian coordinates (Å) of the $[EuHL^1]^+$ system (0 imaginary frequencies)

Center Number	Atomic Number	Coordinates (Angstroms) X	Y	Z
1	7	-3.012206	0.235701	-2.403316
2	6	-4.238985	0.862347	-2.976049
3	6	-5.526911	0.368653	-2.324219
4	7	-5.561956	0.645810	-0.862440
5	6	-6.587560	-0.204309	-0.191185
6	6	-6.109799	-1.633833	0.043799
7	7	-4.871331	-1.675152	0.864353
8	6	-4.167012	-2.977041	0.697800
9	6	-3.385327	-3.057659	-0.607045
10	7	-2.267203	-2.073649	-0.700021
11	6	-1.847855	-1.964641	-2.126325
12	6	-2.817833	-1.128657	-2.959401
13	6	-1.855135	1.108466	-2.715711
14	6	-1.821876	2.369938	-1.830711
15	8	-2.571635	2.331459	-0.770739
16	8	-1.072225	3.296345	-2.160590
17	6	-5.881822	2.069740	-0.593555
18	6	-5.552570	2.468038	0.856671
19	8	-4.689787	1.699780	1.463344
20	8	-6.074135	3.479745	1.331637
21	6	-5.176191	-1.480784	2.301926
22	6	-3.916273	-1.158167	3.122674
23	8	-2.896805	-0.723574	2.430540
24	8	-3.952001	-1.284612	4.348540
25	1	-0.929062	0.556923	-2.527371
26	1	-1.847214	1.399582	-3.774757
27	1	-5.261947	2.697673	-1.240365
28	1	-6.934055	2.293720	-0.812529
29	1	-5.846131	-0.622359	2.407107
30	1	-5.682913	-2.357211	2.727601
31	63	-3.216597	0.299754	0.264120
32	6	-1.140721	-2.557300	0.174316
33	1	-1.037391	-3.644820	0.058913
34	1	-1.435481	-2.352690	1.209070
35	1	-4.145423	1.941921	-2.837233
36	1	-4.289420	0.680013	-4.059129
37	1	-5.632205	-0.710274	-2.463759
38	1	-6.385135	0.837295	-2.826500
39	1	-7.514814	-0.221429	-0.781004
40	1	-6.824661	0.268152	0.765169
41	1	-6.914391	-2.209447	0.523226
42	1	-5.899938	-2.122594	-0.910840
43	1	-3.491247	-3.098621	1.547297
44	1	-4.886924	-3.807155	0.734406
45	1	-2.994274	-4.079067	-0.725947
46	1	-4.056674	-2.881117	-1.450250
47	1	-0.855344	-1.511281	-2.150578
48	1	-1.751015	-2.960354	-2.583333

49	1	-3.796004	-1.612968	-3.007975
50	1	-2.441674	-1.078068	-3.991479
51	6	0.210377	-1.934722	-0.099897
52	6	1.287682	-2.738773	-0.482939
53	6	0.438301	-0.558046	0.055346
54	6	2.561172	-2.196494	-0.706646
55	1	1.121810	-3.805115	-0.613037
56	6	1.691091	0.028898	-0.170861
57	6	2.741595	-0.815538	-0.552185
58	1	3.705018	-0.357990	-0.754721
59	8	-0.662998	0.208553	0.390913
60	6	1.873587	1.535033	-0.078044
61	1	1.450143	1.989606	-0.981549
62	1	1.284408	1.939603	0.768621
63	7	3.279791	1.944243	0.026350
64	6	3.415976	3.365128	-0.363466
65	1	2.864154	3.496995	-1.298757
66	1	2.963386	4.027543	0.394379
67	6	3.792975	1.686831	1.381766
68	1	3.587004	2.528109	2.064004
69	1	3.243760	0.827874	1.786815
70	6	5.271151	1.343942	1.475243
71	6	6.024042	0.897704	0.382400
72	6	7.354921	0.528324	0.586757
73	1	5.576483	0.880118	-0.604571
74	6	7.062801	1.077406	2.898377
75	6	7.890437	0.613780	1.873646
76	1	7.962740	0.184583	-0.245033
77	1	7.444198	1.167946	3.913729
78	1	8.919565	0.338595	2.079256
79	6	4.848013	3.793483	-0.613979
80	6	5.529150	4.622547	0.285143
81	6	6.665425	3.729040	-2.024641
82	6	6.842233	5.002682	-0.002261
83	1	5.037544	4.960568	1.192261
84	6	7.427711	4.544098	-1.182363
85	1	7.086266	3.362377	-2.958919
86	1	7.393064	5.643017	0.679836
87	1	8.443755	4.812811	-1.451785
88	7	5.781830	1.437414	2.719018
89	7	5.403832	3.356853	-1.762788
90	6	3.724371	-3.084504	-1.098568
91	1	3.418115	-3.827797	-1.839638
92	1	4.526067	-2.486948	-1.543488
93	6	4.289599	-3.884392	0.101495
94	1	3.527315	-4.546982	0.511042
95	6	5.538077	-4.673352	-0.288134
96	8	6.660789	-4.322992	0.039120
97	8	5.227136	-5.720976	-1.037427
98	6	6.354661	-6.508719	-1.518566
99	1	5.907568	-7.301173	-2.112973
100	1	7.006613	-5.879586	-2.125027
101	1	6.902736	-6.914869	-0.668092
102	7	4.726737	-2.955431	1.203068
103	1	4.680237	-3.405652	2.121575
104	1	5.711246	-2.693848	1.039453

105	1	4.138474	-2.113600	1.233274
106	8	-1.998941	1.713670	2.112365
107	1	-2.179094	0.949766	2.709637
108	1	-2.762121	2.309217	2.232525
109	1	-0.429983	1.039958	0.847042

E(RTPSSh) = -2705.3082566 Hartree
Zero-point correction = 0.904148
Thermal correction to Energy = 0.959267
Thermal correction to Enthalpy = 0.960211
Thermal correction to Gibbs Free Energy = 0.812387
Sum of electronic and zero-point Energies = -2704.404109
Sum of electronic and thermal Energies = -2704.348989
Sum of electronic and thermal Enthalpies = -2704.348045
Sum of electronic and thermal Free Energies = -2704.495870

Table S2. Optimized Cartesian coordinates (Å) of the **[EuL^1]** system (0 imaginary frequencies)

Center Number	Atomic Number	Coordinates (Angstroms) X	Y	Z
1	7	-2.981597	-0.821506	-2.432435
2	6	-4.375066	-0.467747	-2.814855
3	6	-5.393603	-0.790818	-1.728443
4	7	-5.099603	-0.096355	-0.452705
5	6	-5.851103	-0.732481	0.659882
6	6	-5.201735	-2.022893	1.140026
7	7	-3.806956	-1.804467	1.588397
8	6	-3.065670	-3.091158	1.590995
9	6	-2.607551	-3.490789	0.194104
10	7	-1.646648	-2.527950	-0.398394
11	6	-1.529174	-2.778592	-1.856461
12	6	-2.740069	-2.269866	-2.636706
13	6	-2.057478	-0.002897	-3.248642
14	6	-2.073061	1.474502	-2.810541
15	8	-2.608787	1.713992	-1.658551
16	8	-1.563550	2.312565	-3.572334
17	6	-5.477378	1.332616	-0.508877
18	6	-4.894051	2.123590	0.678504
19	8	-3.908072	1.554323	1.301574
20	8	-5.373282	3.236555	0.936295
21	6	-3.772695	-1.224729	2.947578
22	6	-2.369660	-0.701154	3.303649
23	8	-1.589823	-0.479686	2.297173
24	8	-2.099938	-0.501609	4.499085
25	1	-1.037692	-0.368094	-3.103939
26	1	-2.297109	-0.074094	-4.320229
27	1	-5.054846	1.772255	-1.416370
28	1	-6.569192	1.463668	-0.537787
29	1	-4.450336	-0.366514	2.977411
30	1	-4.105563	-1.948508	3.706024
31	63	-2.423528	0.042652	0.086309

32	6	-0.326851	-2.689798	0.301628
33	1	-0.133365	-3.763260	0.453658
34	1	-0.451186	-2.228489	1.287955
35	1	-4.393319	0.603723	-3.023269
36	1	-4.661610	-0.983236	-3.744245
37	1	-5.399652	-1.866557	-1.531110
38	1	-6.400263	-0.532077	-2.093012
39	1	-6.890479	-0.934976	0.358346
40	1	-5.888224	-0.014158	1.481593
41	1	-5.810209	-2.457296	1.948323
42	1	-5.187824	-2.758460	0.331355
43	1	-2.201230	-2.977896	2.248290
44	1	-3.689238	-3.895552	2.010682
45	1	-2.160818	-4.497524	0.236930
46	1	-3.473109	-3.560237	-0.469252
47	1	-0.625616	-2.275357	-2.205307
48	1	-1.398915	-3.852857	-2.063660
49	1	-3.642406	-2.805876	-2.329792
50	1	-2.592683	-2.494409	-3.704618
51	6	0.877891	-2.088594	-0.384230
52	6	2.033015	-2.857802	-0.507046
53	6	0.856995	-0.728611	-0.836507
54	6	3.211616	-2.342041	-1.073990
55	1	2.015453	-3.889648	-0.158091
56	6	2.040995	-0.213052	-1.448812
57	6	3.182445	-1.018268	-1.540439
58	1	4.067083	-0.606164	-2.026823
59	8	-0.224811	-0.000058	-0.714354
60	6	2.078808	1.176204	-2.050346
61	1	2.726283	1.148869	-2.933961
62	1	1.068164	1.460497	-2.384993
63	7	2.648327	2.203277	-1.144015
64	6	3.027637	3.408312	-1.899474
65	1	3.616404	3.077921	-2.762457
66	1	2.151057	3.956564	-2.289611
67	6	1.722376	2.504024	-0.038506
68	1	1.594093	3.591597	0.051078
69	1	0.733353	2.081347	-0.244612
70	6	2.175089	1.991394	1.316178
71	6	3.518702	1.739127	1.618271
72	6	3.855451	1.321123	2.905876
73	1	4.261049	1.885410	0.841059
74	6	1.530284	1.427831	3.469792
75	6	2.842303	1.158836	3.855689
76	1	4.891619	1.125306	3.166913
77	1	0.705245	1.300477	4.165855
78	1	3.059375	0.830577	4.866467
79	6	3.883117	4.358166	-1.082889
80	6	3.427920	5.640379	-0.750592
81	6	5.884403	4.733116	-0.005259
82	6	4.255105	6.488870	-0.010183
83	1	2.442377	5.965052	-1.070738
84	6	5.513863	6.027079	0.373268
85	1	6.861081	4.341087	0.272456
86	1	3.921965	7.486360	0.259855
87	1	6.194424	6.646905	0.947558

88	7	1.196623	1.837889	2.233118
89	7	5.101408	3.907681	-0.715836
90	6	4.473311	-3.169361	-1.154632
91	1	4.266269	-4.206313	-1.433793
92	1	5.155876	-2.755397	-1.904455
93	6	5.211075	-3.230430	0.212563
94	1	4.606819	-3.768115	0.943022
95	6	6.595479	-3.853505	0.083719
96	8	7.621180	-3.190074	0.102509
97	8	6.514660	-5.165158	-0.099899
98	6	7.781644	-5.850333	-0.312137
99	1	7.514537	-6.894408	-0.453926
100	1	8.272655	-5.445334	-1.197483
101	1	8.416849	-5.722256	0.564814
102	7	5.431821	-1.835814	0.730960
103	1	5.439037	-1.796437	1.753460
104	1	6.352175	-1.508045	0.400487
105	1	4.682742	-1.213992	0.387660
106	8	-1.340972	2.138134	1.085614
107	1	-0.512391	1.997162	1.624222
108	1	-2.089207	2.307012	1.687116

E(RTPSSh) = -2704.8533309 Hartree
Zero-point correction = 0.891804
Thermal correction to Energy = 0.946490
Thermal correction to Enthalpy = 0.947434
Thermal correction to Gibbs Free Energy = 0.802132
Sum of electronic and zero-point Energies = -2703.961527
Sum of electronic and thermal Energies = -2703.906841
Sum of electronic and thermal Enthalpies = -2703.905897
Sum of electronic and thermal Free Energies = -2704.051199

Table S3. Optimized Cartesian coordinates (Å) of the **[EuHL^{1}ZnCl$_2$]$^+$** system (0 imaginary frequencies)

Center Number	Atomic Number	Coordinates (Angstroms) X	Y	Z
1	7	2.979924	0.380508	-2.509018
2	6	4.163077	-0.272173	-3.141562
3	6	5.478639	0.060635	-2.444896
4	7	5.486022	-0.356755	-1.015406
5	6	6.576287	0.343138	-0.274198
6	6	6.218181	1.780912	0.088641
7	7	4.984183	1.849124	0.914873
8	6	4.379355	3.209583	0.861303
9	6	3.594942	3.449507	-0.421911
10	7	2.414083	2.548880	-0.582038
11	6	1.962998	2.607171	-2.002271
12	6	2.868661	1.800791	-2.932222
13	6	1.767735	-0.383702	-2.891480

14	6	1.633178	-1.698947	-2.100141
15	8	2.400326	-1.808288	-1.057758
16	8	0.794841	-2.525508	-2.478928
17	6	5.691282	-1.820400	-0.879525
18	6	5.318303	-2.326051	0.526317
19	8	4.531206	-1.540611	1.211353
20	8	5.736767	-3.424939	0.896265
21	6	5.269287	1.511489	2.329500
22	6	3.984462	1.219290	3.120984
23	8	2.935162	0.940068	2.392006
24	8	4.022516	1.224577	4.352666
25	1	0.879697	0.216169	-2.671196
26	1	1.752266	-0.595902	-3.968963
27	1	5.031227	-2.335832	-1.582970
28	1	6.724976	-2.104245	-1.115863
29	1	5.872246	0.599199	2.360436
30	1	5.839406	2.307883	2.826166
31	63	3.183664	0.076222	0.138715
32	6	1.339423	2.999226	0.372431
33	1	1.321587	4.096881	0.397331
34	1	1.631795	2.644137	1.366522
35	1	3.990740	-1.350454	-3.110053
36	1	4.233943	0.012103	-4.201131
37	1	5.661139	1.137809	-2.479466
38	1	6.304272	-0.417781	-2.990472
39	1	7.503847	0.334843	-0.863589
40	1	6.768953	-0.230554	0.635583
41	1	7.065979	2.242221	0.614593
42	1	6.053273	2.370000	-0.817088
43	1	3.721725	3.313959	1.727037
44	1	5.159262	3.978826	0.952079
45	1	3.268493	4.499513	-0.450338
46	1	4.246426	3.299913	-1.285565
47	1	0.945653	2.214326	-2.047599
48	1	1.916703	3.646676	-2.357426
49	1	3.875045	2.225743	-2.951242
50	1	2.477539	1.873638	-3.957018
51	6	-0.067555	2.531821	0.061993
52	6	-1.057756	3.486178	-0.177208
53	6	-0.433349	1.171614	0.049844
54	6	-2.389555	3.119909	-0.416230
55	1	-0.770567	4.534301	-0.185435
56	6	-1.748855	0.751648	-0.209641
57	6	-2.705207	1.758997	-0.433592
58	1	-3.721142	1.458195	-0.675572
59	8	0.609443	0.279233	0.225911
60	6	-2.179084	-0.701686	-0.406082
61	1	-2.934361	-0.697601	-1.197450
62	1	-1.350617	-1.312127	-0.777710
63	6	-3.452433	4.163453	-0.702520
64	1	-3.170639	4.775869	-1.564369
65	1	-4.401106	3.675650	-0.946639
66	6	-3.670740	5.150368	0.466878
67	1	-2.756472	5.702759	0.684409
68	6	-4.818205	6.117068	0.172997
69	8	-5.908582	6.018024	0.713116

70	8	-4.470327	7.007525	-0.743039
71	6	-5.513501	7.944846	-1.140547
72	1	-5.046615	8.580065	-1.888586
73	1	-6.356604	7.395038	-1.559395
74	1	-5.830300	8.523903	-0.272901
75	7	-4.075430	4.420182	1.721520
76	1	-3.771870	4.913440	2.566760
77	1	-5.106949	4.375346	1.746604
78	1	-3.678942	3.474571	1.751221
79	8	1.884929	-1.380558	1.908212
80	1	2.104426	-0.657068	2.544279
81	1	2.648365	-1.990077	1.958114
82	30	-3.988522	-3.182021	-0.033177
83	17	-4.755647	-4.048176	2.000916
84	7	-2.052355	-3.917386	0.014501
85	7	-2.780577	-1.436542	0.752809
86	7	-5.280404	-1.563235	-0.231119
87	6	-1.652034	-5.047545	-0.600071
88	6	-0.445918	-5.671020	-0.298122
89	6	0.370990	-5.103697	0.682237
90	6	-0.037417	-3.926462	1.310248
91	6	-1.256367	-3.354759	0.945492
92	6	-1.799039	-2.105395	1.621325
93	6	-3.807743	-0.675546	1.483418
94	6	-5.069306	-0.563749	0.648790
95	6	-5.982542	0.479550	0.805374
96	6	-7.138948	0.489482	0.024352
97	6	-7.344795	-0.539543	-0.897230
98	6	-6.392501	-1.549483	-0.991286
99	1	-2.340338	-5.439483	-1.341568
100	1	-0.159838	-6.577932	-0.817926
101	1	1.315321	-5.566051	0.950218
102	1	0.577793	-3.443031	2.059613
103	1	-0.976609	-1.453384	1.945408
104	1	-2.325522	-2.415280	2.530774
105	1	-4.049085	-1.244973	2.387768
106	1	-3.464021	0.318378	1.793357
107	1	-5.787326	1.264223	1.527960
108	1	-7.863132	1.290420	0.129780
109	1	-8.224075	-0.563329	-1.530247
110	1	-6.492360	-2.381578	-1.680275
111	17	-4.745253	-4.394421	-1.920480
112	1	0.344439	-0.565225	0.631312

E(RTPSSh) = -5404.9645913 Hartree
Zero-point correction= 0.910846
(Hartree/Particle)
Thermal correction to Energy= 0.971411
Thermal correction to Enthalpy= 0.972355
Thermal correction to Gibbs Free Energy= 0.814513
Sum of electronic and zero-point Energies= -5404.053746
Sum of electronic and thermal Energies= -5403.993181
Sum of electronic and thermal Enthalpies= -5403.992236
Sum of electronic and thermal Free Energies= -5404.150078

Table S4. Optimized Cartesian coordinates (Å) of the **[EuL^{1}ZnCl$_2$]** system (0 imaginary frequencies)

Center Number	Atomic Number	Coordinates (Angstroms) X	Y	Z
1	7	-2.283914	-2.230644	-2.165325
2	6	-3.645298	-2.383024	-2.743477
3	6	-4.676607	-2.823834	-1.712630
4	7	-4.790324	-1.863707	-0.590082
5	6	-5.466202	-2.505841	0.566851
6	6	-4.526365	-3.396417	1.367409
7	7	-3.352483	-2.646956	1.875931
8	6	-2.263589	-3.589904	2.239923
9	6	-1.516849	-4.102293	1.016603
10	7	-0.815158	-3.028234	0.270114
11	6	-0.452518	-3.534724	-1.078664
12	6	-1.643021	-3.559740	-2.030461
13	6	-1.500856	-1.335608	-3.044852
14	6	-1.995061	0.122409	-2.947389
15	8	-2.738269	0.393553	-1.924328
16	8	-1.635746	0.919192	-3.827871
17	6	-5.572037	-0.672911	-0.984910
18	6	-5.445828	0.455864	0.050878
19	8	-4.442534	0.345703	0.871147
20	8	-6.261437	1.385811	0.023553
21	6	-3.713894	-1.853724	3.071553
22	6	-2.614877	-0.840541	3.438868
23	8	-1.789940	-0.543492	2.486245
24	8	-2.613336	-0.364077	4.583566
25	1	-0.453352	-1.347845	-2.728807
26	1	-1.534339	-1.666897	-4.093426
27	1	-5.169785	-0.283368	-1.924229
28	1	-6.633695	-0.914738	-1.140740
29	1	-4.615615	-1.276684	2.847256
30	1	-3.926982	-2.500553	3.935023
31	63	-2.368961	-0.771315	0.158430
32	6	0.406340	-2.617137	1.053409
33	1	0.875714	-3.516750	1.479519
34	1	0.047135	-1.994244	1.879969
35	1	-3.934948	-1.416914	-3.161028
36	1	-3.630392	-3.104665	-3.574573
37	1	-4.399427	-3.796594	-1.297051
38	1	-5.648705	-2.960939	-2.211684
39	1	-6.332183	-3.096587	0.230773
40	1	-5.849366	-1.708872	1.207364
41	1	-5.082278	-3.859146	2.197225
42	1	-4.163387	-4.215177	0.740690
43	1	-1.574235	-3.062194	2.902483
44	1	-2.667074	-4.445609	2.802797
45	1	-0.798244	-4.875557	1.332281
46	1	-2.217874	-4.587579	0.333215
47	1	0.324454	-2.883579	-1.480999
48	1	-0.018774	-4.545235	-1.018075

49	1	-2.401773	-4.261488	-1.674241
50	1	-1.306389	-3.933784	-3.009994
51	6	1.437250	-1.873942	0.245521
52	6	2.679916	-2.458014	0.014175
53	6	1.099890	-0.607276	-0.333437
54	6	3.660510	-1.831992	-0.775637
55	1	2.865675	-3.447543	0.429770
56	6	2.121330	0.066501	-1.081062
57	6	3.349718	-0.571369	-1.303334
58	1	4.077163	-0.088188	-1.953931
59	8	-0.109327	-0.123476	-0.213898
60	6	1.820565	1.361837	-1.795446
61	1	2.296917	1.331190	-2.786278
62	1	0.741636	1.451747	-1.938579
63	6	4.944665	-2.537574	-1.168221
64	1	4.748933	-3.386511	-1.832526
65	1	5.595702	-1.846715	-1.714823
66	6	5.725050	-3.116331	0.034243
67	1	5.147514	-3.892083	0.536943
68	6	7.089638	-3.653264	-0.385240
69	8	8.128265	-3.051302	-0.159766
70	8	6.973259	-4.797752	-1.044228
71	6	8.217255	-5.362579	-1.549383
72	1	7.921615	-6.272606	-2.064938
73	1	8.687762	-4.656195	-2.233728
74	1	8.882687	-5.581439	-0.713851
75	7	6.003736	-2.027252	1.033224
76	1	6.061176	-2.382240	1.991821
77	1	6.916911	-1.605135	0.803593
78	1	5.259811	-1.316648	0.997240
79	8	-2.302802	1.733205	0.688723
80	1	-1.714171	2.081774	1.389928
81	1	-3.212502	1.680810	1.053088
82	30	1.242686	3.482155	0.642849
83	17	2.407105	5.532151	0.876256
84	7	2.709829	2.265812	1.494812
85	7	2.268765	2.653993	-1.146714
86	7	-0.055904	4.037742	-0.884693
87	6	2.761728	1.875482	2.783654
88	6	3.908159	1.331453	3.351717
89	6	5.047677	1.197008	2.552735
90	6	4.985809	1.575894	1.211327
91	6	3.792320	2.104212	0.711298
92	6	3.675848	2.630486	-0.705231
93	6	2.006513	3.747992	-2.109010
94	6	0.537358	4.107792	-2.094935
95	6	-0.148359	4.547502	-3.226162
96	6	-1.480905	4.942282	-3.095230
97	6	-2.086878	4.881901	-1.838885
98	6	-1.339913	4.419419	-0.758609
99	1	1.850271	2.029207	3.351657
100	1	3.910506	1.035096	4.394091
101	1	5.969372	0.803700	2.970184
102	1	5.849589	1.484565	0.560304
103	1	4.324600	2.064237	-1.382669
104	1	4.035541	3.665642	-0.695799

105	1	2.569219	4.627997	-1.777539
106	1	2.332955	3.492720	-3.125268
107	1	0.356285	4.579030	-4.185700
108	1	-2.036718	5.288459	-3.960434
109	1	-3.119006	5.179547	-1.694762
110	1	-1.760231	4.332161	0.235921
111	17	-0.290135	3.384696	2.461522

E(RTPSSh) = -5404.5143545 Hartree
Zero-point correction = 0.896978
Thermal correction to Energy = 0.957197
Thermal correction to Enthalpy = 0.958141
Thermal correction to Gibbs Free Energy = 0.801779
Sum of electronic and zero-point Energies = -5403.617376
Sum of electronic and thermal Energies = -5403.557157
Sum of electronic and thermal Enthalpies = -5403.556213
Sum of electronic and thermal Free Energies = -5403.712576

A Journal of the Gesellschaft Deutscher Chemiker
Angewandte
GDCh
International Edition
Chemie
www.angewandte.org

Accepted Article

Title: Highly Potent MRI Contrast Agent Displaying Outstanding Sensitivity to Zinc Ions

Authors: Gaoji Wang and Goran Angelovski

To be cited as: *Angew. Chem. Int. Ed.* 10.1002/anie.202014431

Link to VoR: https://doi.org/10.1002/anie.202014431

WILEY-VCH

10.1002/anie.202014431

COMMUNICATION

WILEY-VCH

Highly Potent MRI Contrast Agent Displaying Outstanding Sensitivity to Zinc Ions

Gaoji Wang[a] and Goran Angelovski*[a],[b]

[a] G. Wang, Priv.-Doz. Dr. G. Angelovski
MR Neuroimaging Agents
Max Planck Institute for Biological Cybernetics
Tuebingen, Germany
E-mail: goran.angelovski@tuebingen.mpg.de

[b] Priv.-Doz. Dr. G. Angelovski
Lab of Molecular and Cellular Neuroimaging
International Center for Primate Brain Research (ICPBR)
Center for Excellence in Brain Science and Intelligence Technology (CEBSIT)
Chinese Academy of Science (CAS)
Shanghai, PR China

Supporting information for this article is given via a link at the end of the document.

Abstract: Zinc ions play an important role in numerous crucial biological processes in the human body. The ability to image the function of Zn^{2+} would be a significant asset to biomedical research for monitoring various physiopathologies dependent on its fate. To this end, we developed a novel Gd^{3+} chelate that can selectively recognize Zn^{2+} over other abundant endogenous metal ions and alter its paramagnetic properties. More specifically, this lanthanide chelate displayed an extraordinary increase in longitudinal relaxivity (r_1) of over 400% upon interaction with Zn^{2+} at 7 T and 25 °C, which is the greatest r_1 enhancement observed for any of the metal ion-responsive Gd-based complexes at high magnetic field. A "turn-on" mechanism responsible for these massive changes was confirmed through NMR and luminescence lifetime studies on a ^{13}C-labeled Eu^{3+} analogue. This molecular platform represents a new momentum in developing highly suitable magnetic resonance imaging contrast agents for functional molecular imaging studies of Zn^{2+}.

Zinc ions are found in all cells in the human body, either in free or protein-bounded forms.[1] As the second most abundant transition metal ion, Zn^{2+} plays an important role in many essential biological processes.[2] For example, it is involved in numerous aspects of cellular metabolism such as the mediation of enzymes activity, the conveyance of neural signals and the transcription of genes. Both an excess and deficiency of Zn^{2+} causes different symptoms and pathologies, such as hair loss, brain or prostate cancer.[3] Therefore, it is essential for healthy organs that the concentration of Zn^{2+} is perfectly balanced by transporters and metallochaperones. Magnetic resonance imaging (MRI), a non-invasive technique with high spatial resolution, is one of the highly suitable methods for investigating the biological role of Zn^{2+} and providing early-stage disease detection, particularly in combination with the use of contrast agents (CA).[4]

Application of CAs in MRI guarantees higher contrast images through the shortening of the T_1 (spin-lattice) and T_2 (spin-spin) relaxation times of the water molecule that interact with the CA.[4a] Complexes of gadolinium with different polydentate chelating ligands are most frequently chosen for such purposes,[4a, 5] as they can shorten the T_1 and T_2 relaxation times of water protons by rapid exchange of inner-sphere water molecules with the bulk solvent and thus enhance the MR image contrast.[6] A variant of these complexes, so-called bioresponsive or "smart" contrast agents (SCAs), are well suitable for the visualization of numerous biological processes through functional MRI (fMRI) studies, as they can alter their signal upon interaction with the desired target (e.g. metal ion of interest).[4c, 7] To this end, development of SCAs to specifically distinguish Zn^{2+} over other metal ions was initiated in the pioneering studies from Nagano and coworkers in 2001.[8] Meanwhile, many approaches and a large number of SCAs sensitive to Zn^{2+} have been reported, based mainly on Gd^{3+} complexes,[4c, 9] while the Zn-responsive probes for other imaging modalities have also been developed.[10] Recently, significant progress in performing MRI *in vivo* to study the function of Zn^{2+} has been made by Sherry and coworkers. In these studies, the SCAs can only be trigged by Zn^{2+} and human serum albumin (HSA) together, resulting in a longitudinal r_1 relaxivity enhancement of ~60% at high magnetic field (9.4 T). A greater change in r_1 (~270%) can only be measured at low magnetic field (0.5 T).[9a] Nevertheless, the former level of changes in r_1 was sufficient to perform a set of important *in vivo* experiments to study the role of Zn^{2+} in β-cell function and insulin release at high field.[9a, 11]

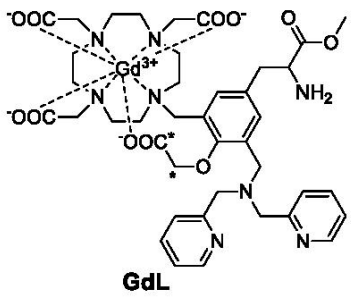

GdL

Figure 1. Chemical structure of **GdL**. Asterisks show the positions labeled with ^{13}C isotopes in the respective **EuL*** complex.

To push the limits of Zn^{2+} detection at high magnetic fields with SCAs, we approached the problem by using a structural motif we recently discovered, which shows an excellent turn-on luminescence emission response to Zn^{2+}.[12] The SCA molecule we designed was based on the di-(2-picolyl)amine (DPA) as the

Zn^{2+} recognition moiety, 1,4,7,10-tetraazacyclododecane-1,4,7-tricarboxylic acid (DO3A) as chelator for Gd^{3+} and a tyrosine (Tyr) unit as a spacer. Herein, we protected the carboxylate of Tyr as the methyl ester, and deliberately appended an acetate moiety on the phenolic oxygen, which can act as a bridge between the DPA moiety and the DO3A chelator. Positioned in such way, the phenoxyacetic acid can interact and coordinate with either Zn^{2+} or Gd^{3+}, thus playing an important role in potential alterations of relaxivity.

The preparation of the desired complex **GdL** (Figure 1) was done in analogy to the recently reported luminescence chemosensor.[12] Additionally, phenoxyacetate was installed by the alkylation of the phenolic -OH of **1** at room temperature to smoothly provide **2** within 12 h (Scheme S1 in SI). The chelator **H_4L** was obtained by treating **2** with TFA, followed by purification with HPLC (synthetic procedure in SI). In parallel, we prepared the chelator **H_4L***, labeled with ^{13}C isotopes on the phenoxyacetate group. Here, we used 1,2-^{13}C-*tert*-butyl bromoacetate in the alkylation step, instead of the molecule with normal isotope abundance. The final complexes **GdL**, **TbL** or **EuL*** were prepared by treating **H_4L**/**H_4L*** with the respective metal ion salt.

To evaluate the response of **GdL** toward Zn^{2+} and its potential as a MRI contrast agent, a series of ^1H NMR relaxometric titrations were performed at 7 T and 25 or 37 °C. Both r_1 and r_2 were measured after every addition of Zn^{2+}, resulting in an unprecedented change in r_1 relaxivity from 2.05 to 10.30 $mM^{-1}s^{-1}$ (~400 %) at 25 °C and 1.51 to 6.04 $mM^{-1}s^{-1}$ (~300 %) at 37 °C upon saturation with Zn^{2+} (Figure 2a and S1a in SI). Such a significant increase in r_1 upon the addition of 1 equiv. of Zn^{2+} is, to the best of our knowledge, the highest change reported thus far for a metal cation-sensitive Gd-based CA operating at the high magnetic fields. These observations seemingly indicate substantial changes in the coordination geometry around the Gd^{3+} center that lead to changes in the inner-sphere hydration (*vide infra*). Indeed, when the HEPES buffer was exchanged for PBS, the overall r_1 increased from 1.82 to 7.37 $mM^{-1}s^{-1}$ (~300 %) and 1.47 to 5.58 $mM^{-1}s^{-1}$ (~280 %) for 25 and 37 °C, respectively. These indicated still an outstanding r_1 response, however slightly affected by the formation of ternary complexes between the phosphates and Gd^{3+}.[13] The changes in r_2 values in both buffered media followed similar trends (Figure S1 in SI).

The selectivity of **GdL** towards Zn^{2+} was tested in separate experiments with metal ions commonly present in biological systems, such as Ca^{2+}, Mg^{2+} and Cu^{2+} (Figure 2b). No obvious response of **GdL** toward any other cation was observed, with the exception of Cu^{2+}. However, such potential competition can be omitted because the concentration of free Cu^{2+} in living cells is very low.[14]

Finally, the relaxometric behavior of **GdL** was probed in more complex environments at physiological pH and 37 °C. The r_1 enhancement in the presence of HSA (0.6 mM in PBS) exceeded 200 % upon saturation with $ZnCl_2$ (Figure 2c). The r_1 and r_2 titrations of HSA with **GdL** or **GdLZn** complex showed that interaction of **GdL** / **GdLZn** with the protein is not pronounced and is slightly notable only in the sub-equimolar amounts; however, the bicarbonates (25 mM) have remarkable influence on both r_1 and r_2 values, as expected (Figure S1b,c in SI). Nevertheless, the titration of **GdL** with $ZnCl_2$ in human serum resulted in the increase in r_1 of around 60 % (Figure 2d), which is the highest change observed so far for any of the Zn-sensitive SCA.[9a]

The specificity toward Zn^{2+} and its strong relaxivity enhancement, suggest that **GdL** could be a highly promising molecular probe for the imaging of this biomarker. We therefore performed additional characterization of the complex to assess its coordination properties and estimate its potential for MRI applications. The binding affinity of **GdL** towards Zn^{2+} was determined by means of isothermal titration calorimetry in both HEPES and PBS (Figure S2 in SI). The obtained dissociation constant resulted in the values $K_{d(GdZnL)}$ = 543 ± 39 and 552 ± 76 nM in HEPES and PBS, respectively. This is in line with the values we obtained

Figure 2. Longitudinal relaxivity of **GdL** at 7 T. a) r_1 in the presence of various concentrations of $ZnCl_2$ in HEPES (50 mM) or PBS (50 mM) (**[GdL]** = 3 mM, pH 7.4 and 37 °C); b) r_1 in the presence of different quantities of Ca^{2+}, Mg^{2+}, Cu^{2+} or Zn^{2+} (**[GdL]** = 3 mM, 50 mM HEPES, pH 7.4 and 25 °C). c-d) r_1 in the presence of various concentrations of $ZnCl_2$ in c) HSA (0.6 mM) or d) human serum (both **[GdL]** = 1 mM, pH 7.4 and 37 °C). Values in a), c) and d) represent the mean and standard deviation from 3 independent measurements.

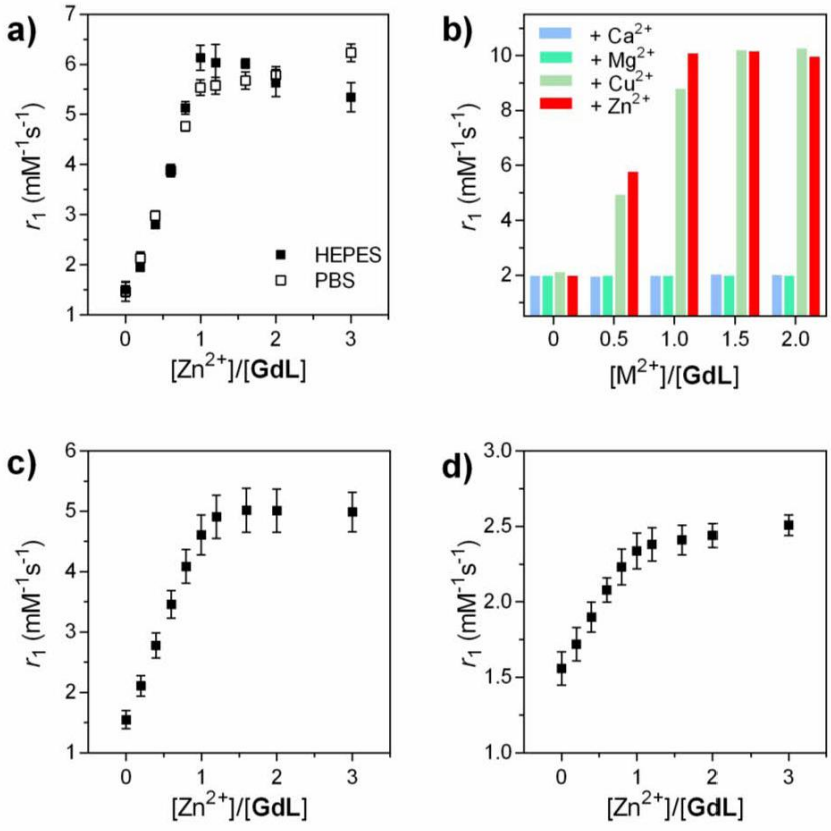

for the luminescence sensor with a similar structure;[12] also, the results indicate that the binding affinity is not affected by the ternary complex formation between the phosphates and Gd^{3+} (*vide supra*).

The stability of **GdL** was investigated in a transmetallation experiment against Zn^{2+}, a major potential competitor for the displacement of Gd^{3+}.[15] For this, **GdL** was exposed to 2 equiv. of Zn^{2+} in a phosphate buffer (50 mM, pH = 7.0) at 25 and 37 °C. The replacement of Gd^{3+} for Zn^{2+} was monitored by measuring the relaxation rate of the solution over a period of 120 h (Figure S3 in SI). Subsequently, a "thermodynamic index" was calculated as the ratio of the paramagnetic relaxation rate after a given period, compared with the starting value. For **GdL**, this index resulted in values 90, 81 and 75% after 24, 72 and 120 h for the temperature 37 °C, respectively, indicating high stability of the investigated SCA.

To confirm the binding pattern of Zn^{2+} with **GdL**, an analogous Eu^{3+} complex **EuL*** was prepared with the ^{13}C-labeled phenoxyacetate group (*vide supra*). Thereafter, a series of ^{13}C NMR spectra of 15 mM **EuL*** were recorded with increasing concentrations of $ZnCl_2$ (Figure 3a and S4 in SI), in analogy to the experiments previously conducted by Meade and coworkers.[16] In the absence of Zn^{2+}, the spectrum showed two broad signals at 93.5 ppm and 211.7 ppm. Once Zn^{2+} was gradually added to the sample, these signals slowly disappeared, while two sharp doublets at 71.7 ppm and 175.6 ppm appeared, owing to the coupling interactions with the neighboring isotopic carbon atom. After the addition of one equiv. of Zn^{2+}, the broader signals at 93.5 ppm and 211.7 ppm disappeared completely. Furthermore, the doublets at 71.7 ppm and 175.6 ppm experienced a small shift with further additions of Zn^{2+}, indicating the formation of the second type of species in the excess of Zn^{2+}; no further changes in ^{13}C NMR spectra were observed beyond the second equiv. of Zn^{2+}.

This specific experiment provided the strongest ground for the mechanism responsible for changes in the coordination around the paramagnetic metal ion that are caused by Zn^{2+}. Namely, broad and shifted signals in the Zn-free state indicated coordination of phenoxyacetate group to the paramagnetic Eu^{3+}. Moreover, the amplitude of the shifts (~36 and ~22 ppm for the carboxylate and methylene group, respectively), suggests the carboxylate being much closer to Eu^{3+}, hence the larger shift. Upon addition of Zn^{2+}, the phenoxyacetate group flips from Eu^{3+} to Zn^{2+}, forming a Zn^{2+} complex with the DPA moiety (Figure 3b). Consequently, the ^{13}C signals of the carbons in the phenylacetate recover in intensity, multiplicity and the usual frequency shift in ^{13}C NMR for the respective functional groups. Moreover, the minor change in the shift of doublets between 1-2 equiv. of Zn^{2+} indicates that **EuL***:Zn^{2+} stoichiometry likely moves from 1:1 to 1:2 complex formation, which was also observed in the case of the luminescent phenoxy analogue.[12] However, it is obvious that, irrespective of the type of formed species (1:1 or 1:2), already the first equiv. of Zn^{2+} causes the decoordination of the phenoxyacetate from the paramagnetic metal center. We note that ^{1}H NMR of **EuL*** at 25 °C displays sharp resonances, suggesting the existence of only one of the isomers, namely the twisted antisquare prismatic species (TSAP, Figure S5 in SI).

The coordination features of this system were also studied by means of the luminescence lifetime experiments. For this purpose, the luminescence lifetimes of **EuL*** and **TbL** in D_2O or H_2O with and without Zn^{2+} were measured at pH 7.4 and 25 °C. Subsequently, the number of the water molecules coordinated to the Eu^{3+}/Tb^{3+} center (q) was estimated (Table 1).

In the absence of Zn^{2+}, both **EuL*** or **TbL** are non-hydrated, explaining the very low initial r_1 value of **GdL** (*vide supra*). Upon Zn^{2+} addition, the estimated q values are 1.4 and 1.5 for **EuL*** and **TbL**, respectively. In parallel, the r_1 value of **GdL** upon Zn^{2+}

Figure 3. a) ^{13}C NMR spectra of **EuL*** (15 mM) in the presence of 0-2.4 equiv. of Zn^{2+} at 25 °C and 75 MHz (note: 48.9 ppm is the referent signal of $^{13}CH_3OH$). b) Proposed interaction of the phenoxyacetate group with the paramagnetic metal center (top) and Zn^{2+} (bottom), which leads to an increase in hydration number and the "turn-on" response.

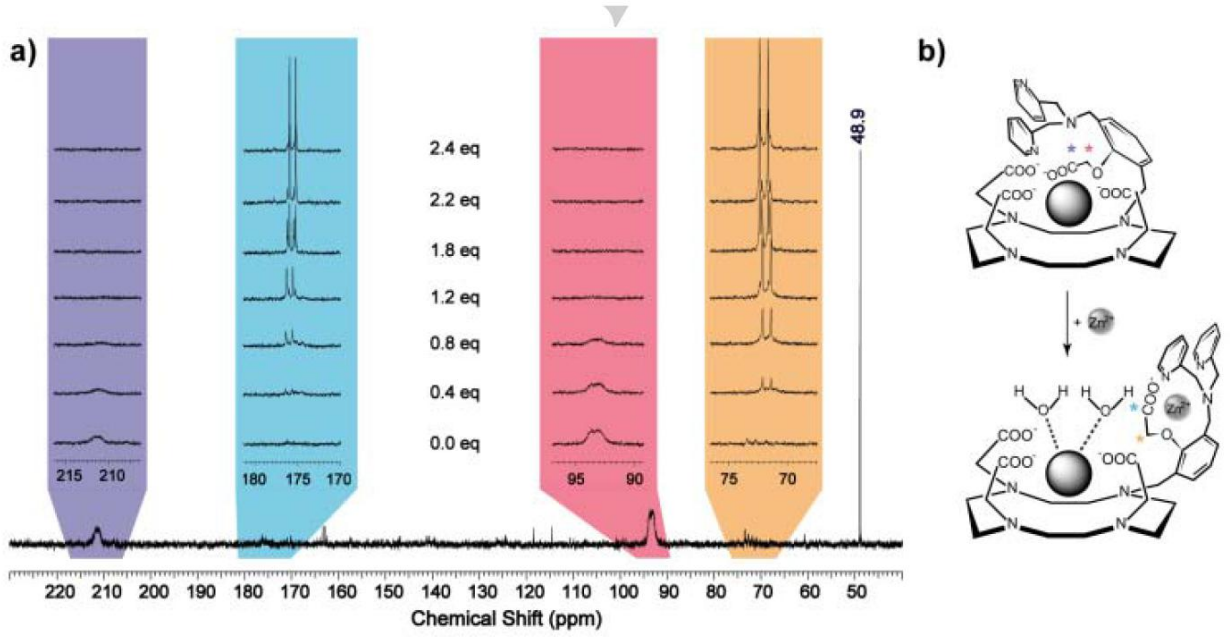

binding dramatically increases, which matches this observation. These results confirm the mechanism that assumes complete coordination of the Gd^{3+} with DO3A and DPA units, leading to q=0 in the absence of Zn^{2+}. Once Zn^{2+} is added, the whole DPA unit including the phenoxyacetate is involved in coordination with Zn^{2+}, giving rise to higher hydration of the paramagnetic chelate and therefore the boost in r_1 (Figure 3b). Additionally, this coordination probably causes a concurrent decrease in τ_R with an increase in the outer-sphere hydration, which contribute to the overall r_1, as previously observed on structurally similar systems that are Ca^{2+} sensitive. These also exhibited high r_1 values, while being monohydrated complexes.[17]

Table 1. Luminescence lifetimes of the **EuL*** (5 mM) and **TbL** (1 mM) in H_2O and D_2O with and without Zn^{2+}, and the calculated q values.

	LnL only			**LnL** + Zn^{2+} (2 equiv.)			
	τ_{H_2O}/ms	τ_{D_2O}/ms	q	τ_{H_2O}/ms	τ_{D_2O}/ms	q	Δq
EuL*	0.89	1.25	0.1	0.42	1.02	1.4	1.3
TbL	1.91	1.96	0.0	1.30	2.37	1.5	1.5

The potential of this complex to serve as a T_1-weighted SCA was demonstrated *in vitro* in an MRI experiment on tube phantoms. Eight tubes containing **GdL** alone, **GdL** with added Zn^{2+}, Mg^{2+}, Ca^{2+} or a HEPES buffer tube as a control were imaged in a 7 T MRI scanner. The results indicated a great enhancement in the MR signal intensity for tubes with **GdL** and 0.5 or 1.0 equiv. of Zn^{2+}, whereas no obvious difference was observed in tubes where Ca^{2+} or Mg^{2+} were added (Figure 4 and Table S1 in SI). The collected MR data also confirmed that a selective turn-on response of **GdL** can be visualized in a Zn-rich environment.

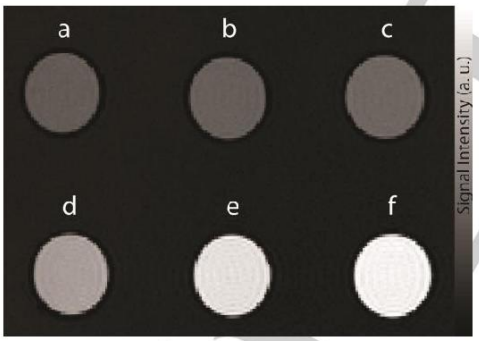

Figure 4. T_1-weighted MR images of tube phantoms at 7 T of a 1 mM solution of **GdL** in 50 mM HEPES buffer (pH 7.4 and ~22 °C). The tubes were positioned in the following order: a) **GdL** only, b) +1.0 equiv. Mg^{2+}, c) +1.0 equiv. Ca^{2+}, d) +0.5 equiv. Zn^{2+}, e) +1.0 equiv. Zn^{2+}, f) +2.0 equiv. Zn^{2+}.

In summary, we report a novel paramagnetic complex appended with DPA as a Zn^{2+} recognition moiety and phenoxyacetate as a trigger for the "turn-on" relaxometric response. The overall r_1 relaxivity enhancement reached 400% upon Zn^{2+} addition, which is, to the best of our knowledge, the highest r_1 change observed to date for this type of ion-sensitive SCA at high magnetic fields. The additional experiments demonstrated high binding affinity and specificity of the complex toward Zn^{2+} and confirmed the existence of the turn-on mechanism. Indeed, this system displays the most desirable properties for a SCA, which encompass high q modulation, followed by a massive increase in relaxivity. These features are highly preferred for the development of potent probes for the molecular imaging of biomarkers. With the new paramagnetic system presented in this work, the field of functional imaging of Zn^{2+} is receiving an important tool to enable substantial and faster progress.

Acknowledgements

We thank Drs. Tanja and Giuseppe Gambino for MRI tube phantom measurements. The financial support of China Scholarship Council (PhD fellowship to Gaoji Wang) and the German Federal Ministry of Education and Research (BMBF, e:Med program: FKZ: 01ZX1503) is gratefully acknowledged.

Keywords: Gadolinium • Magnetic resonance imaging • Responsive contrast agents • Zinc

[1] A. Krezel, W. Maret, *Arch. Biochem. Biophys.* **2016**, *611*, 3-19.
[2] a) B. L. Vallee, D. S. Auld, *Biochemistry* **1990**, *29*, 5647-5659; b) L. C. Costello, C. C. Fenselau, R. B. Franklin, *J. Inorg. Biochem.* **2011**, *105*, 589-599.
[3] C. F. Mills, *Zinc in human biology*, Springer-Verlag, London, **1988**.
[4] a) J. Wahsner, E. M. Gale, A. Rodríguez-Rodríguez, P. Caravan, *Chem. Rev.* **2019**, *119*, 957-1057; b) M. V. C. Jordan, S. T. Lo, S. W. Chen, C. Preihs, S. Chirayil, S. R. Zhang, P. Kapur, W. H. Li, L. M. De Leon-Rodriguez, A. J. M. Lubag, N. M. Rofsky, A. D. Sherry, *Proc. Natl. Acad. Sci. U.S.A.* **2016**, *113*, E5464-E5471; c) C. S. Bonnet, *Coord. Chem. Rev.* **2018**, *369*, 91-104.
[5] T. J. Clough, L. Jiang, K.-L. Wong, N. J. Long, *Nat. Commun.* **2019**, *10*, 1420.
[6] M. C. Heffern, L. M. Matosziuk, T. J. Meade, *Chem. Rev.* **2014**, *114*, 4496-4539.
[7] H. Li, T. J. Meade, *J. Am. Chem. Soc.* **2019**, *141*, 17025-17041.
[8] K. Hanaoka, K. Kikuchi, Y. Urano, T. Nagano, *J. Chem. Soc., Perkin Trans. 2* **2001**, 1840-1843.
[9] a) J. Yu, A. F. Martins, C. Preihs, V. C. Jordan, S. Chirayil, P. Y. Zhao, Y. K. Wu, K. Nasr, G. E. Kiefer, A. D. Sherry, *J. Am. Chem. Soc.* **2015**, *137*, 14173-14179; b) G. J. Stasiuk, F. Minuzzi, M. Sae-Heng, C. Rivas, H. P. Juretschke, L. Piemonti, P. R. Allegrini, D. Laurent, A. R. Duckworth, A. Beeby, G. A. Rutter, N. J. Long, *Chem. Eur. J.* **2015**, *21*, 5023-5033; c) J. L. Major, G. Parigi, C. Luchinat, T. J. Meade, *Proc. Natl. Acad. Sci. U.S.A.* **2007**, *104*, 13881-13886; d) X. A. Zhang, K. S. Lovejoy, A. Jasanoff, S. J. Lippard, *Proc. Natl. Acad. Sci. U.S.A.* **2007**, *104*, 10780-10785.
[10] a) K. L. Haas, K. J. Franz, *Chem. Rev.* **2009**, *109*, 4921-4960; b) R. McRae, P. Bagchi, S. Sumalekshmy, C. J. Fahrni, *Chem. Rev.* **2009**, *109*, 4780-4827; c) T. W. Price, G. Firth, C. J. Eling, M. Kinnon, N. J. Long, J. Sturge, G. J. Stasiuk, *Chem. Commun.* **2018**, *54*, 3227-3230.
[11] a) A. J. M. Lubag, L. M. De Leon-Rodriguez, S. C. Burgess, A. D. Sherry, *Proc. Natl. Acad. Sci. U.S.A.* **2011**, *108*, 18400-18405; b) A. F. Martins, V. C. Jordan, F. Bochner, S. Chirayil, N. Paranawithana, S. R. Zhang, S. T. Lo, X. D. Wen, P. Y. Zhao, M. Neeman, A. D. Sherry, *J. Am. Chem. Soc.* **2018**, *140*, 17456-17464.
[12] G. Wang, C. Platas-Iglesias, G. Angelovski, *ChemPlusChem* **2020**, *85*, 806-814.
[13] R. S. Dickins, S. Aime, A. S. Batsanov, A. Beeby, M. Botta, J. Bruce, J. A. K. Howard, C. S. Love, D. Parker, R. D.

Peacock, H. Puschmann, *J. Am. Chem. Soc.* **2002**, *124*, 12697-12705.
[14] S. W. Zhang, R. Adhikari, M. X. Fang, N. Dorh, C. Li, M. Jaishi, J. T. Zhang, A. Tiwari, R. Pati, F. T. Luo, H. Y. Liu, *ACS Sens.* **2016**, *1*, 1408-1415.
[15] S. Laurent, L. Vander Elst, C. Henoumont, R. N. Muller, *Contrast Media Mol. Imaging* **2010**, *5*, 305-308.
[16] a) J. L. Major, R. M. Boiteau, T. J. Meade, *Inorg. Chem.* **2008**, *47*, 10788-10795; b) L. M. Matosziuk, J. H. Leibowitz, M. C. Heffern, K. W. MacRenaris, M. A. Ratner, T. J. Meade, *Inorg. Chem.* **2013**, *52*, 12250-12261.
[17] K. D. Verma, A. Forgács, H. Uh, M. Beyerlein, M. E. Maier, S. Petoud, M. Botta, N. K. Logothetis, *Chem. Eur. J.* **2013**, *19*, 18011-18026.

10.1002/anie.202014431

Entry for the Table of Contents

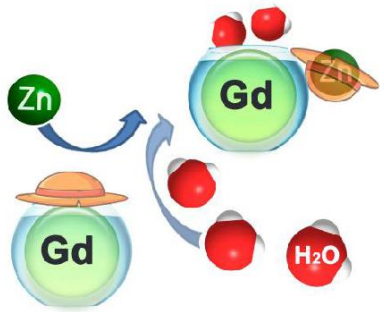

Highly potent MRI contrast agent based on paramagnetic Gd^{3+} was developed to selectively recognize Zn^{2+} over other abundant endogenous metal ions. The interaction with Zn^{2+} modulates the hydration of the complex, leading to significant increase in its longitudinal relaxivity. The new responsive platform is highly suitable for studying the Zn-related physiological processes at high magnetic fields.

Materials and instrumentation

The reagents were purchased from commercial sources and were used without further purification. Albumin from human serum and the human serum were purchased from Sigma-Aldrich Chemie GmbH, Germany (catalogue numbers A3782 and P2918, respectively). Compound **1** was synthesized following a previously published procedure.[1] Purification of synthesized compounds was performed using silica gel 60 (0.03–0.2 mm) from Carl Roth (Germany). The final ligand and metallated complexes were purified using preparative HPLC on a Varian PrepStar system equipped with the UV−vis detector model 335 and a binary pump model SD-1 manual injector, controlled by Star chromatography workstation version 6.3 software. All fluorescence spectra were recorded on a QuantaMaster™ 3 PH fluorescence spectrometer from Photon Technology International, Inc. (USA). Low resolution mass spectra were recorded on an ion trap SL 1100 system Agilent with an electrospray ionization source. High resolution mass spectra were recorded on a Bruker Daltonics APEX II (FT-ICR-MS) with an electrospray ionization source. ^{1}H and ^{13}C NMR spectra were recorded on a Bruker Avance III 300 MHz spectrometer at 25 °C. Processing was performed using TopSpin 2.1 (Bruker GmbH) and ACD/SpecManager 9.0 (Advanced Chemistry Development, Inc.). The NMR spectra were recorded using either $CDCl_3$ or D_2O and referenced to TMS/TSP. The concentration of Eu^{3+}, Gd^{3+} and Tb^{3+} in analyzed solutions were determined using the bulk magnetic susceptibility shift (BMS).[2] ^{1}H NMR relaxometric titrations were performed on the same instrument (Bruker Avance III 300 MHz spectrometer) at 25 or 37 °C. Isothermal titration calorimeter (ITC) experiments were performed on the MicroCal PEAQ-ITC (MicroCal™, Malvern Panalytical, UK). MRI experiments were performed on Bruker BioSpec 70/30 USR magnet (software version Paravision 5.1) using Bruker volume coil (RF RES 300 1H 075/040 QSN TR).

Synthetic procedures

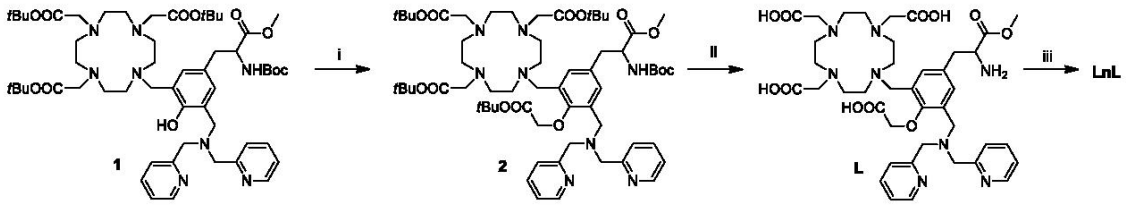

Scheme S1. The synthetic route for complexes **GdL** and **TbL**. Reagents and conditions: i) $BrCH_2COOtBu$, K_2CO_3, KI, MeCN, R.T., 12 h; ii) TFA, CH_2Cl_2, R.T., 6h; iii) $LnCl_3 \cdot 6H_2O$ (Ln = Tb^{3+}, Gd^{3+}), H_2O, 12 h.

3-[3-[(bis-pyridin-2-ylmethyl-amino)-methyl]-4-*tert*-butoxycarbonylmethoxy-5-(4,7,10-tris-*tert*-butoxycarbonylmethyl-1,4,7,10tetraaza-cyclododec-1-ylmethyl)-phenyl]-2-*tert*-butoxycarbonylamino-propionic acid methyl ester (2).

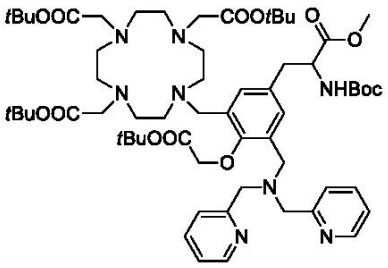

Compound **1** (0.517 g, 0.50 mmol) was added to a suspension of K_2CO_3 (0.138 g, 1.00 mmol) and KI (0.166 g, 1.00 mmol) in MeCN (3 mL). The mixture was stirred 10 min at room temperature. Then, *tert*-butyl bromoacetate (0.146 g, 0.75 mmol) was added to the reaction mixture, followed by stirring for 12 h at room temperature. Upon reaction completion, the reaction mixture was filtered and the filtrate was evaporated under vacuum. The crude residue was purified by silica gel column chromatography using CH_2Cl_2/MeOH (v/v, 20:1) as the eluent, affording 0.465 g (81%) of compound **2** as a light yellow oil. **^{1}H NMR** ($CDCl_3$, 300 MHz): δ (ppm): 1.09–1.55 (m, 45H, CC*H*$_3$); 2.08–3.25 (br, 24H, NC*H*$_2$); 3.34, 3.35, 3.36 (s, 3H, OC*H*$_3$); 3.76, 3.63 (s, 8H, NC*H*$_2$C); 4.29 (s, 2H, CC*H*$_2$O); 4.35–4.57 (m, 1H, NHC*H*); 5.70–5.98, 7.21–7.35 (br, 2H, phenolic); 7.03–7.20 (br, 2H, NCHC*H*), 7.36–7.56 (br, 2H, NCC*H*), 7.57–7.76 (br, 2H, CCHC*H*), 8.37–8.55 (br, 2H, NC*H*CH). **^{13}C NMR** ($CDCl_3$, 75 MHz): δ (ppm): 26.5–29.1 (15C, C*C*H$_3$); 37.3 (1C, phC*H*$_2$CH); 48.7, 49.2, 49.5, 51.9, 52.9, 55.9, 56.0, (12C); 57.0 (1C, NH$_2$*C*H); 59.4 (2C, py*C*H$_2$); 71.3 (1C, C=O*C*H$_2$O); 79.1; 82.0, 82.3 (5C, *C*CH$_3$); 121.9, 122.2, 122.6, 123.3 (4C, CCO*C*, NCH*C*H); 128.8 (C, CH$_2$*C*CH); 131.2, 131.8 (2C, C*C*HC); 132.8 (1C, CH*C*CH); 136.2, 136.9 (2C, CCH*C*H); 148.4, 148.8 (2C, N*C*HCH); 151.5 (1C, CH$_2$O*C*); 155.1 (1C, NH*C*O); 158.4 (2C, N*C*CH); 167.7 (1C, *C*=OCH$_2$O); 172.1, 172.3, 173.2 (4C, *C*O). ESI-TOF/MS: (*m/z*) $[M+H]^+$ calcd. for $C_{61}H_{95}N_8O_{13}^+$: 1147.7013; found: 1147.7000.

2-amino-3-[3-[(bis-pyridin-2-ylmethyl-amino)-methyl]-4-carboxymethoxy-5-(4,7,10-tris-carboxymethyl-1,4,7,10tetraaza-cyclododec-1-ylmethyl)-phenyl]- propionic acid methyl ester (L).

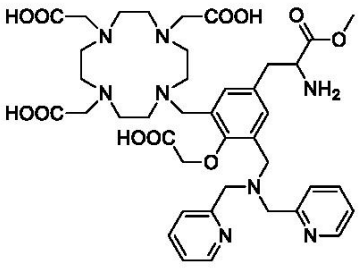

Compound **2** (0.275 g, 0.24 mmol) was dissolved in TFA/CH_2Cl_2 (2 mL, v/v 80/20) and the solution was stirred for 6 hours at room temperature. The reaction mixture was evaporated to

dryness and purified by HPLC using MeCN/H_2O as the eluent, affording 0.182 g (76%) of compound **L** as a light yellow oil. **^{1}H NMR** (D_2O, 300 MHz): δ (ppm): 2.69–3.54 (br, 24H, CH_2); 3.62–3.91 (br, 7H, CH_3, CH_2); 4.08 (s, 2H, ArO-CH_2); 4.29–4.46 (br, 5H, $CHNH_2$, CH_2); 7.05–7.23, 7.34–7.58, 7.76–8.00, 8.39–8.66 (br, 10H, Ar*H*). **^{13}C NMR** (D_2O, 75 MHz): δ (ppm): 32.6 (1C, ArCH_2CH); 45.7, 47.3 (2C, ArCH_2N); 46.2 (1C, CH_3); 46.6 (1C, $CHNH_2$); 48.2, 48.4, 49.5, 50.0, 51.6, 53.5, 53.8, 54.2, 54.4 (11C, NCH_2CH_2, NCH_2CO); 56.0 (2C, PyCH_2N); 71.3 (1C, ArOCH_2); 124.0, 130.0, 130.5, 131.4, 132.1 (5C, Ar); 123.2, 123.9, 138.3, 145.9, 149.1 (10C, Py); 154.1 (1C, *C*-OCH_2), 166.8, 168.0, 168.6, 173.8, 176.4 (5C, *C*O). ESI-TOF/MS: (*m/z*) $[M+H]^+$ calcd. for $C_{40}H_{55}N_8O_{11}^+$: 823.3985; found: 823.3973.

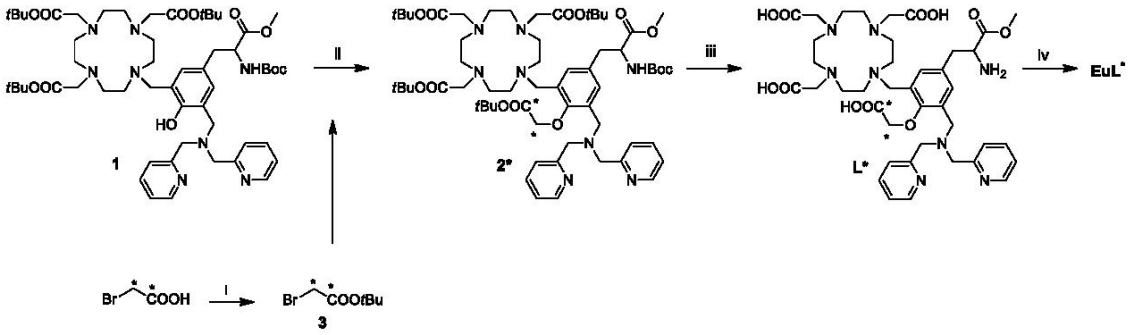

Scheme S2. The synthetic route for complex **EuL***. Reagents and conditions: i) H_2SO_4, $MgSO_4$, *t*BuOH, DCM, R.T., 15 h. ii) **3**, K_2CO_3, KI, MeCN, R.T., 12 h; iii) TFA, CH_2Cl_2, R.T., 6 h; iv) $EuCl_3$•$6H_2O$, H_2O, 12 h.

1,2-^{13}C-*tert*-Butyl bromoacetate (3)

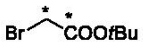

Concentrated H_2SO_4 (0.19 mL) was added slowly to a vigorously stirred suspension of $MgSO_4$ (1.300 g, 10.80 mmol) in CH_2Cl_2 (7 mL) The mixture was stirred for 20 minutes, after which the isotopically labeled 1,2-^{13}C-bromoacetic acid (0.507 g, 3.60 mmol) was added, followed by addition of *t*BuOH (1.5 mL). The mixture was stirred for 15 h at room temperature. The insoluble matter was removed by vacuum filtration. The filtrate was transferred to a separatory funnel and washed with water (10 mL) and saturated sodium bicarbonate (10 mL). The aqueous layer was extracted with CH_2Cl_2 (3× 3 mL). The combined organic layers were washed with brine and dried over anhydrous $MgSO_4$. The solvent was evaporated under reduced pressure to afford **3** as a light-yellow liquid (0.341 g, 48%). **^{1}H NMR** ($CDCl_3$, 300 MHz): δ (ppm): 1.48 (s, 9H, CCH_3); 3.49, 3.50, 3.99, 4.01 (d, J= 4.5 Hz, 2H, $BrCH_2$). **^{13}C NMR** ($CDCl_3$, 75 MHz): δ (ppm): 25.6–30.2 (4C, CCH_3, Br*C*); 82.8 (1C, CCH_3); 165.8, 166.6 (1C, *C*=O).

^{13}C-labeled 3-[3-[(Bis-pyridin-2-ylmethyl-amino)-methyl]-4-*tert*-butoxycarbonylmethoxy-5-(4,7,10-tris-*tert*-butoxycarbonylmethyl-1,4,7,10tetraaza-cyclododec-1-ylmethyl)-phenyl]-2-*tert*-butoxycarbonylamino-propionic acid methyl ester (2*).

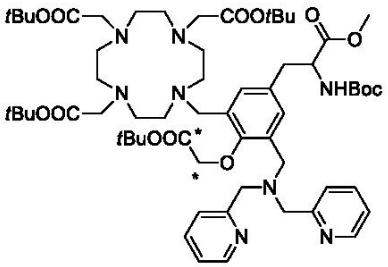

Procedure was the same as for compound **2**. Starting materials: compound **1** (0.238 g, 0.23 mmol), K_2CO_3 (0.064 g, 0.46 mmol), KI (0.076 g, 0.46 mmol) and compound **3** (0.054 g, 0.276 mmol). Yield: 0.185 g (70%) of compound **2*** as a light yellow oil. **^{1}H NMR** ($CDCl_3$, 300 MHz): δ (ppm): 1.20–1.55 (m, 45H, CC*H*$_3$); 2.22–3.33 (br, 24H, NC*H*$_2$); 3.44 (s, 3H, OC*H*$_3$); 3.62–3.94 (s, 10H, NC*H*$_2$C); 4.02–4.15, 4.39–4.54 (s, 2H, CC*H*$_2$O); 4.54–4.63 (m, 1H, NHC*H*); 6.92–7.31 (br, 2H, NCHC*H*; 1H, phenolic), 7.38–7.63 (br, 2H, NCC*H*; 1H, phenolic), 7.64–7.82 (br, 2H, CCHC*H*), 8.48–8.71 (br, 2H, NC*H*CH). **^{13}C NMR** ($CDCl_3$, 75 MHz): δ (ppm):): 27.7, 27.8, 28.0, 28.2 (15C, C*C*H$_3$); 37.6 (1C, phCH$_2$CH); 48.9–59.5 (15C); 70.7, 71.0, 71.9, 72.1 (1C, C=O^{13}*C*H$_2$O); 79.3; 82.2, 82.5 (5C, *C*CH$_3$); 122.1 (2C, NCH*C*H); 123.0 (2C, NC*C*H); 128.3, 128.9 (2C, C*C*HC); 131.1–133.2 (3C, ph*C*CH$_2$); 136.5 (2C, CCH*C*H); 148.8 (2C, N*C*HCH); 151.6 (1C, CH$_2$O*C*); 155.0, 155.4, 155.8 (1C, NH*C*O); 158.6 (2C, N*C*CH); 167.3, 167.98, 168.2, 168.6 (1C, ^{13}*C*=OCH$_2$O); 172.4, 173.3 (4C, *C*O). ESI-TOF/MS: (*m/z*) $[M+H]^+$ calcd. for $^{13}C_2C_{59}H_{95}N_8O_{13}^+$: 1149.7080; found: 1149.7063.

^{13}C-labeled 2-amino-3-[3-[(bis-pyridin-2-ylmethyl-amino)-methyl]-4-carboxymethyloxy-5-(4,7,10-tris-carboxymethyl-1,4,7,10tetraaza-cyclododec-1-ylmethyl)-phenyl]-propionic acid methyl ester (L*).

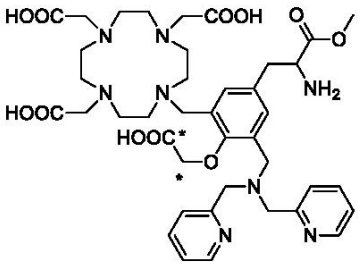

Procedure was the same as for compound **L**. The starting material compound **2*** (0.185 g, 0.161 mmol) afforded 0.090 g (68%) of compound **L*** as a light yellow oil. **^{1}H NMR** (D_2O, 300 MHz): δ (ppm): 2.96–3.60 (br, 24H, NC*H*$_2$); 3.63 (s, 3H, OC*H*$_3$); 3.85, 4.04, 4.11, 4.17, 4.22 (s, 8H, NC*H*$_2$C; m, 1H, NH$_2$C*H*); 7.39 (s, 2H, phenolic); 7.81–7.95 (br, 2H, NCC*H*); 7.96–8.10 (br, 2H, CCHC*H*); 8.38–8.50 (br, 2H, CCHC*H*); 8.59–8.70 (br, 2H, NC*H*CH). **^{13}C NMR** (D_2O, 75 MHz): δ (ppm): 34.8 (1C, phCH$_2$CH); 48.0–50.1, 52.5, 53.6, 54.9, 58.8, 59.6,

65.9 (15C); 70.6, 71.4 (1C, C=O^{13}*C*H$_2$O); 126.5, 127.1 (4C, CCO*C*, NCH*C*H); 130.1 (C, CH$_2$*C*CH); 132.5, 133.5 (2C, C*C*HC); 134.5 (1C, CH*C*CH); 141.4 (2C, CCH*C*H); 147.4 (2C, N*C*HCH); 152.2 (1C, CH$_2$O*C*); 155.8 (1C, NH*C*O); 169.3 (2C, N*C*CH) ; 170.1 (4C, *C*O); 171.1, 172.0 (1C, ^{13}*C*=OCH$_2$O). ESI-TOF/MS: (*m/z*) $[M+H]^+$ calcd. for $^{13}C_2C_{38}H_{55}N_8O_{11}^+$: 825.4052; found: 825.4054.

General procedure for the preparation of the Eu^{3+}, Gd^{3+} and Tb^{3+} complexes. The introduction of the gadolinium, terbium (for **L**) or europium (for **L***) ions into the macrocyclic framework was carried out at pH ~7.0 adjusted by 0.1 M NaOH solution. To a stirred aqueous solution of ligand, a solution of $EuCl_3$•$6H_2O$, $GdCl_3$•$6H_2O$ or $TbCl_3$•$6H_2O$ was prepared in water and was added dropwise to the ligand solution in 1:1 molar ratios. The pH of the solution was periodically adjusted to 7.0 by addition of 0.1 M NaOH solution. The reaction mixture was stirred at room temperature for 12 h then purified by HPLC, respectively. The yellow solid compound was obtained by lyophilization. The formation of the metal complexes **TbL**, **GdL** and **EuL*** were confirmed by mass spectrometry.

GdL. ESI- TOF/MS: (*m/z*) $[M]^-$ calcd. for $C_{40}H_{50}GdN_8O_{11}^-$: 976.2846; found: 976.2866.

EuL*. ESI-TOF/MS: (*m/z*) $[M+H]^+$ calcd. for $^{13}C_2C_{38}H_{52}EuN_8O_{11}^+$: 975.3040; found: 975.3050.

TbL. ESI-LRMS: (*m/z*) $[M]^-$ calcd. for $C_{40}H_{50}TbN_8O_{11}^-$: 977.3; found: 977.3.

NMR measurements

Relaxometric titrations: Proton longitudinal relaxometric titrations with Zn^{2+} were performed at 7 T, pH 7.4 (50 mM HEPES buffer) and 25 °C, using using inversion recovery (T_1) and Car–Purcell-Meiboom-Gill (T_2) pulse sequences. A $ZnCl_2$ solution of known concentration was added stepwise to the **GdL** solution (starting concentration 1.0 or 3.0 mM Gd^{3+}), and measurements of T_i (i=1, 2) were performed after each addition of the analyte. The longitudinal and transverse relaxivities were calculated from Eq. S1 where $T_{i,obs}$ is the measured T_i, $T_{i,d}$ is the diamagnetic contribution of the solvent, and [Gd] is the actual Gd^{3+} concentration at each point of the titration.

$$1/T_{i,obs} = T_{i,d} + r_i \times [Gd],\ i=1, 2 \qquad \text{Eq. S1}$$

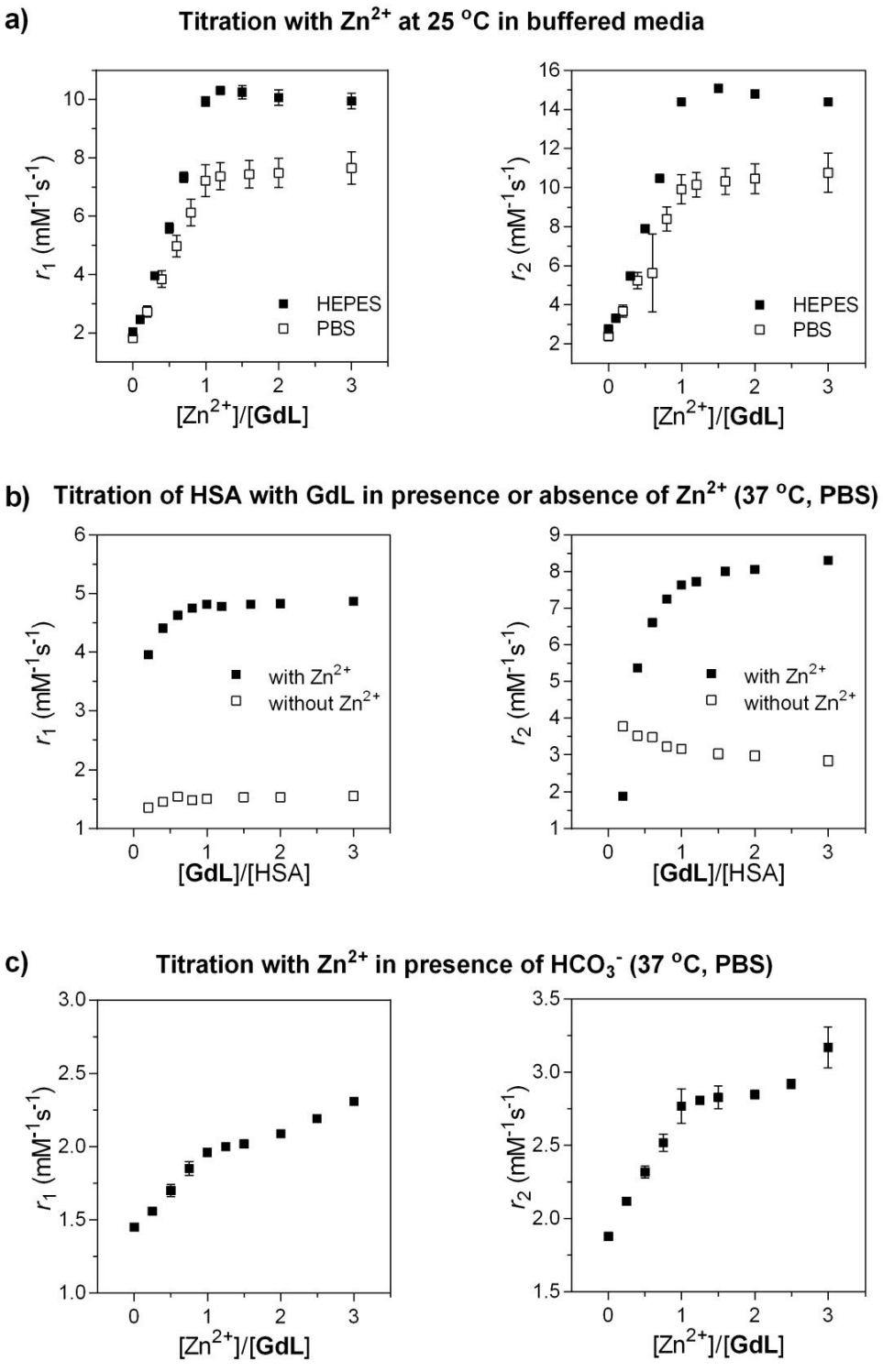

Figure S1. Longitudinal and transverse relaxivities of **GdL** at 7 T in the presence of various concentrations of $ZnCl_2$ in HEPES (50 mM) or PBS (50 mM) (pH 7.4 and 25 or 37 °C). Concentrations of **GdL** used: a) 3 mM, b-c) 1 mM.

Metal ion selectivity: For metal ion selectivity experiments, stock solutions (50 mM) of $CaCl_2$, $MgCl_2$, $CuCl_2$ and $ZnCl_2$ were prepared. The samples of **GdL** (3 mM) were prepared by the dilution method using HPLC grade water and HEPES buffer (50 mM, pH 7.4). The longitudinal relaxivities were performed in same way as described above after addition of 0, 0.5, 1.0, 1.5 and 2.0 equiv. of the respective metal ions to the solution of **GdL**.

ITC experiments

The experiments were carried out by placing **GdL** (50 μM) in the reaction cell and $ZnCl_2$ (300 μM) in the syringe. All data were recorded in HEPES or PBS (50 mM) at pH 7.4.

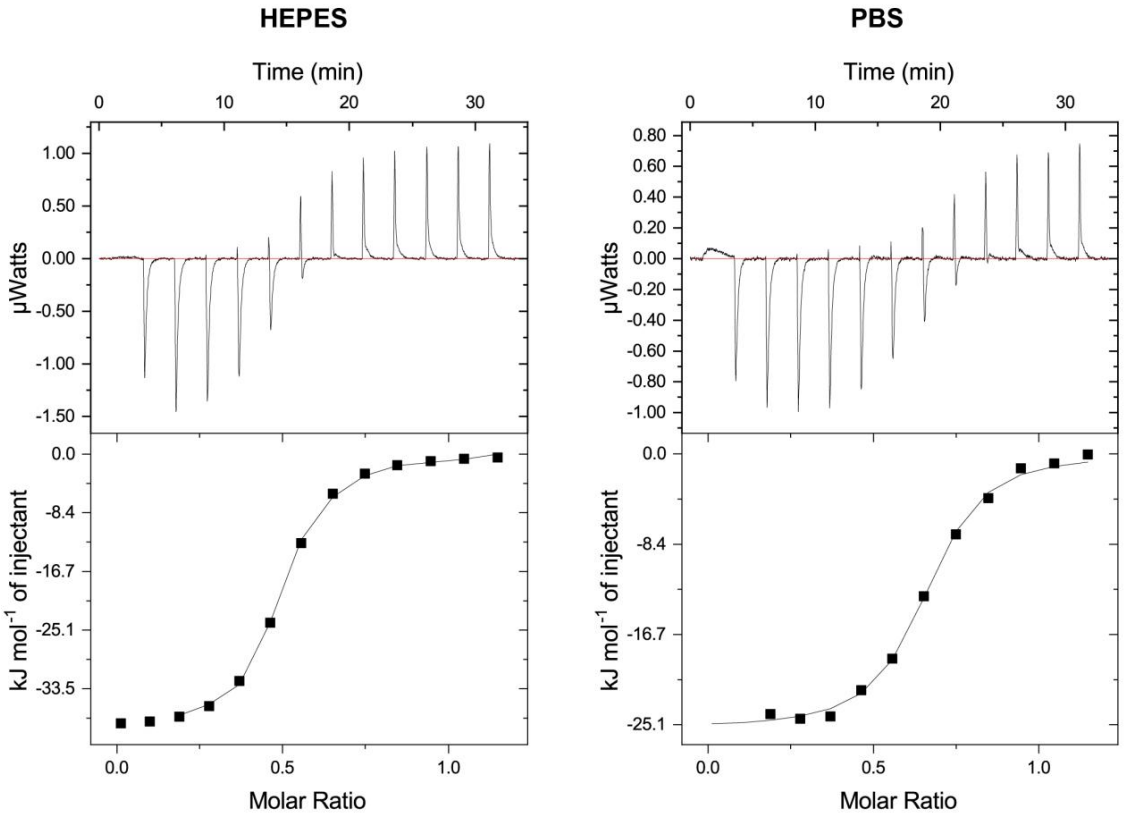

Figure S2. The raw thermogram (top) and the binding isotherm (bottom) obtained in the ITC experiment of **GdL** with Zn^{2+} in HEPES (left) and PBS (right).

Transmetalation study

The transmetalation with Zn^{2+} was performed in 50 mM phosphate buffer pH 7.0 at 25 °C. Stock solutions of the **GdL** (27 mM), and zinc chloride (250 mM) were prepared. Exact concentration of [Gd] was determined by BMS method. Calculated volumes were pipetted with calibrated pipettes into small glass vials to obtain these concentrations: 50 mM PBS, 3 mM **GdL**, 6 mM $ZnCl_2$. Deionized water was used to complete the volume to 350 µL. Thereafter, the longitudinal relaxation times were measured periodically over the period of 3 days.

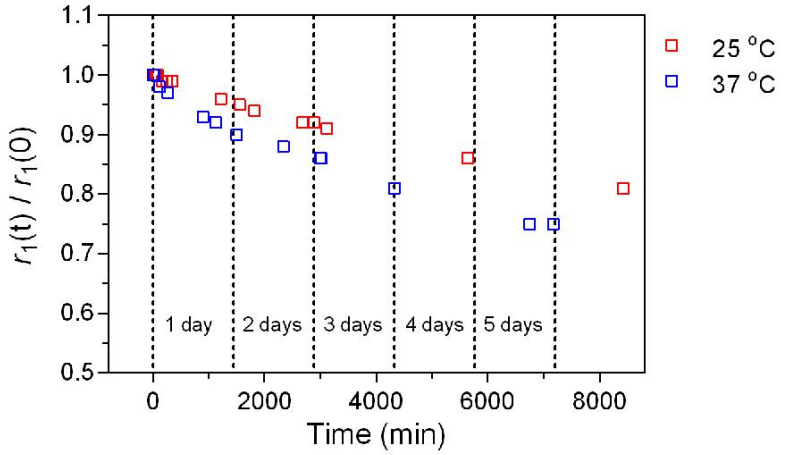

Figure S3. Relaxivity rate variation of **GdL** (3 mM) with Zn^{2+} versus time. All data were recorded in 50 mM PBS buffer at pH 7.0.

$^{1}H/^{13}C$ NMR spectroscopy of ^{13}C-labeled EuL*

^{13}C NMR spectra were measured with 15 mM **EuL*** in D_2O with 0 to 2.4 equiv. of Zn^{2+} (50 mM HEPES buffer, pH 7.4, 25 °C). A capillary filled with ^{13}C-labeled methanol was placed into the **EuL*** solution as an external reference. All measurements were performed under the same NMR parameters (receiver gain, number of scans). Twelve ^{13}C NMR experiments were performed by adding the following amount of Zn^{2+} (see Figure S4 top): 1: 0 equiv., 2: 0.2 equiv., 3: 0.4 equiv., 4: 0.6 equiv., 5: 0.8 equiv., 6: 1.0 equiv., 7: 1.2 equiv., 8: 1.4 equiv., 9: 1.8 equiv., 10: 2.0 equiv., 11: 2.2 equiv., and 12: 2.4 equiv.

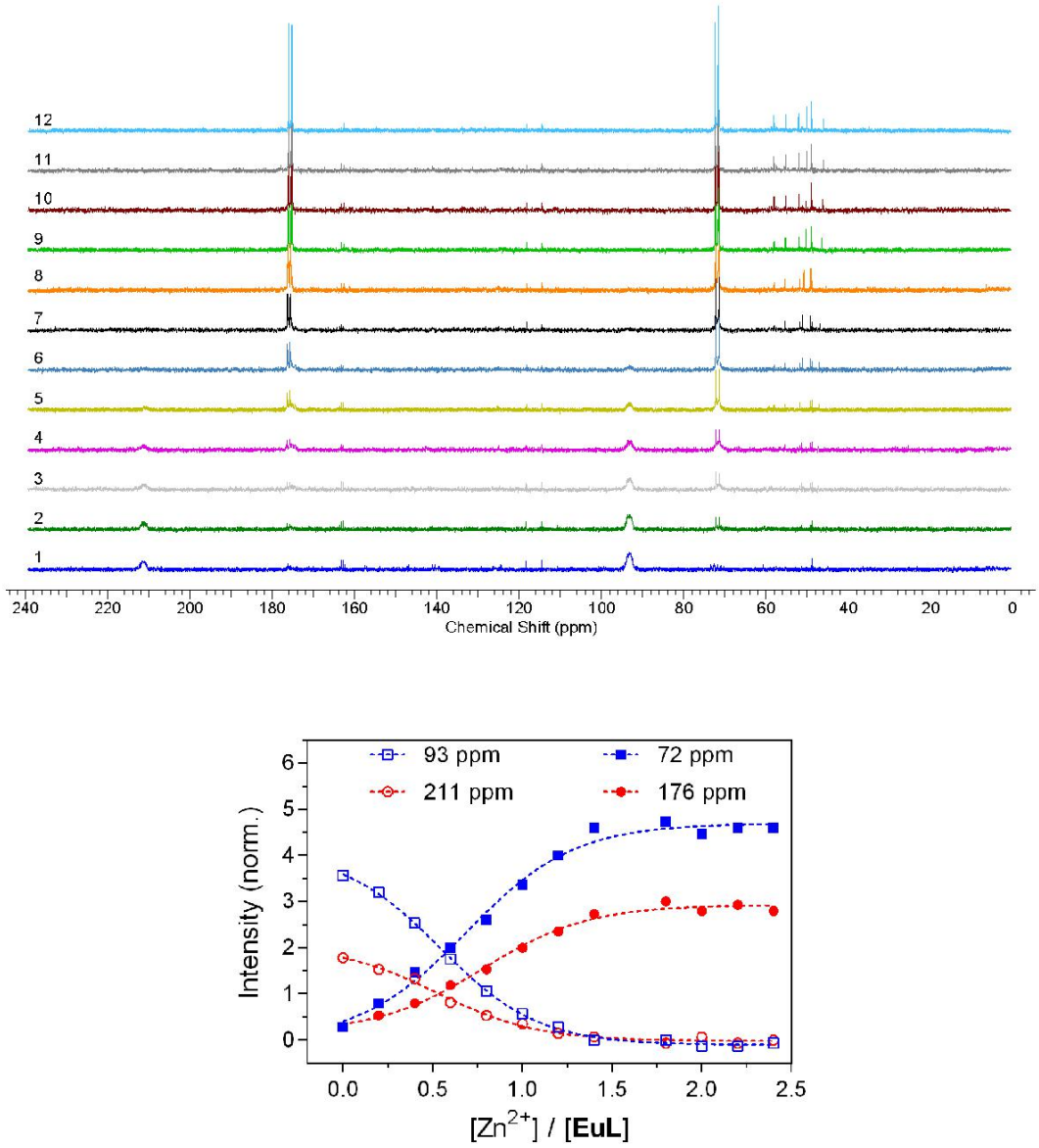

Figure S4. ^{13}C NMR spectra of **EuL*** (15 mM) in the presence of 0 to 2.4 equiv of Zn^{2+} (top) and the observed changes in ^{13}C NMR shifts with the additions of Zn^{2+} (bottom).

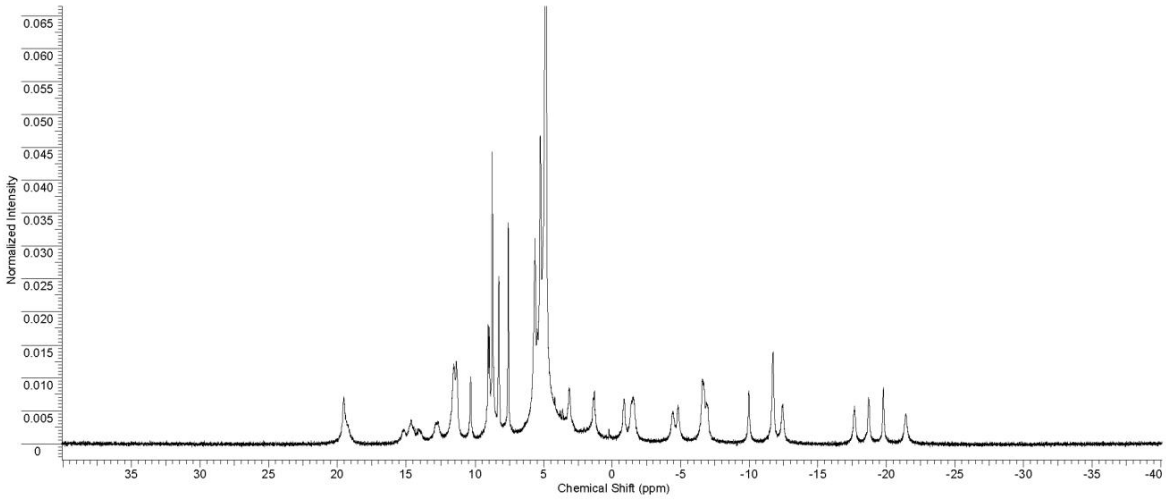

Figure S5. ^{1}H NMR spectrum of **EuL*** in D_2O at 25 °C.

Luminescence lifetime experiments

Luminescence lifetime measurements were performed with **TbL** (1 mM) or **EuL*** (5 mM) in D_2O and H_2O with and without Zn^{2+} (2 equiv.) at 25 °C (50 mM HEPES, pH 7.4). The Ln^{3+} ion was directly excited (λ_{ex} = 283 and 395 nm for Tb^{3+} and Eu^{3+}, respectively) and the emission intensity (λ_{max} = 546 and 615 nm for Tb^{3+} and Eu^{3+}, respectively) was recorded. The excitation and emission slits were set at 10 nm. In total, three independent measurements each with 15 scans were performed to obtain the data set. The obtained curves were fitted with a first order exponential decay with an $r^2 > 0.99$. The resulting q value, which denotes the hydration number of coordinated water molecules, was then calculated using the equation Eq. S2 for **EuL*** and Eq. S3 for **TbL**.[3]

$$q(\mathrm{Eu}) = 1.2 \times \left(\frac{1}{\tau_{H_2O}} - \frac{1}{\tau_{D_2O}} - 0.25\right) \qquad \text{Eq. S2}$$

$$q(\mathrm{Tb}) = 5 \times \left(\frac{1}{\tau_{H_2O}} - \frac{1}{\tau_{D_2O}} - 0.06\right) \qquad \text{Eq. S3}$$

MRI experiments

Tube phantoms studies: MRI phantoms were obtained using 6 x 400 μL vials, immersed in HEPES (50 mM, pH 7.4) solution. Apart from the first vial containing only 1 mM buffered (50 mM HEPES, pH 7.4) solution of the **GdL** complex, the rest vials were treated with $MgCl_2$ (1.0 equivalent), $CaCl_2$ (1.0 equivalent) and $ZnCl_2$ (0.5, 1.0, 2.0 equivqlents). The following parameters were used for MRI acquisition: FOV = 2.85 × 2.85 cm, MTX = 190 × 190, spatial resolution = 150 x 150 um, slice thickness = 0.5 mm, FA = 90°, TR = 20.0 ms, TE = 2.35 ms, TA= 3 m 10 s.

Table S1. Obtained SNR (signal-to-noise ratio) in T_1-weighted MRI of tube phantoms of different solutions with 1 mM of **GdL** (50 mM HEPES buffer, pH 7.4 and 298 K).

Sample	**GdL**	**GdL** + 1.0 eq Mg^{2+}	**GdL** + 1.0 eq Ca^{2+}
SNR	54.0	56.3	61.0
Sample	**GdL** + 0.5 eq Zn^{2+}	**GdL** + 1.0 eq Zn^{2+}	**GdL** + 2.0 eq Zn^{2+}
SNR	92.7	124.3	132.8

References

[1] G. Wang, C. Platas-Iglesias, G. Angelovski, *ChemPlusChem* **2020**, *85*, 806-814.

[2] D. M. Corsi, C. Platas-Iglesias, H. van Bekkum, J. A. Peters, *Magn. Reson. Chem.* **2001**, *39*, 723-726.

[3] A. Beeby, I. M. Clarkson, R. S. Dickins, S. Faulkner, D. Parker, L. Royle, A. S. de Sousa, J. A. G. Williams, M. Woods, *J. Chem. Soc., Perkin Trans. 2* **1999**, 493-503.

molecules

Article

Macrocyclic Chelates Bridged by a Diaza-Crown Ether: Towards Multinuclear Bimodal Molecular Imaging Probes

Gaoji Wang [1] and Goran Angelovski [1,2,*]

[1] MR Neuroimaging Agents, Max Planck Institute for Biological Cybernetics, Max-Planck-Ring 11, 72076 Tübingen, Germany; gaoji.wang@tuebingen.mpg.de
[2] Lab of Molecular and Cellular Neuroimaging, International Center for Primate Brain Research (ICPBR), Center for Excellence in Brain Science and Intelligence Technology (CEBSIT), Chinese Academy of Science (CAS), Shanghai 200031, China
* Correspondence: goran.angelovski@tuebingen.mpg.de

Academic Editor: Zoltan Kovacs
Received: 29 September 2020; Accepted: 27 October 2020; Published: 29 October 2020

Abstract: Bridged polymacrocyclic ligands featured by structurally different cages offer the possibility of coordinating multiple trivalent lanthanide ions, giving rise to the exploitation of their different physicochemical properties, e.g., multimodal detection for molecular imaging purposes. Intrigued by the complementary properties of optical and MR-based image capturing modalities, we report the synthesis and characterization of the polymetallic Ln(III)-based chelate comprised of two DOTA-amide-based ligands (DOTA—1,4,7,10-tetraazacyclododecane-1,4,7,10-tetraacetic acid) bridged via 1,10-diaza-18-crown-6 (DA18C6) motif. The DOTA-amide moieties and the DA18C6 were used to chelate two Eu(III) ions and one Tb(III) ion, respectively, resulting in a multinuclear heterometallic complex Eu_2LTb. The bimetallic complex without Tb(III), Eu_2L, displayed a strong paramagnetic chemical exchange saturation transfer (paraCEST) effect. Notably, the luminescence spectra of Eu_2LTb featured mixed emission including the characteristic bands of Eu(III) and Tb(III). The advantageous features of the complex Eu_2LTb opens new possibilities for the future design of bimodal probes and their potential applicability in CEST MR and optical imaging.

Keywords: diaza-crown ether; hetero-multinuclear complexes; lanthanide; luminescence; macrocyclic; paraCEST; water exchange

1. Introduction

In modern medicine, magnetic resonance imaging (MRI) is recognized as the method of choice for non-radiative and non-invasive imaging of soft body tissues [1–3]. Conventional MRI exploits the magnetic properties of water proton's spins to generate signal. However, it suffers from intrinsic insensitivity, which often requires the administration of contrast agents (CAs). Specifically, these mainly paramagnetic Ln(III)-based complexes improve specificity of the MRI scans through various contrast-generating mechanisms [3]. One of the recently introduced MRI strategies is based on the chemical exchange saturation transfer (CEST) effect, which possesses specific advantages over the conventional T_1-weighted MRI. Namely, the CEST MRI enables generation of the signal at will by using selected radiofrequency (RF) pre-saturation pulses, thus providing improved specificity in these MRI studies due to the absence of permanent background signal originating from the CEST agent [4,5]. The principle of CEST detection is based on the selective saturation of the pool of protons that are in slow to intermediate exchange rate on the NMR time-scale, with bulk water pool. Subsequently, the chemical exchange of the pre-saturated CEST proton pool with the

water protons reduces the intensity of the MR signal at the frequency of the bulk water protons. The general requirement for successful CEST is that the frequency difference between the two pools of protons ($\Delta\omega$) is greater than the corresponding exchange rate (k_{ex}) [6]. Moreover, the paramagnetic lanthanide(III) ions, such as Eu(III), Tb(III) or Yb(III), are known to induce chemical shifts (and hence $\Delta\omega$), which makes them perfect candidates for paramagnetic CEST (paraCEST) CAs [7–9]. As a general rule, the CEST effect is induced either by the exchangeable proton of the ligand or by the water molecule coordinated to Ln(III). Typically, Ln(III) complexes based on DOTAM (DOTA-tetraamide, DOTA—1,4,7,10-tetraazacyclododecane-1,4,7,10-tetraacetic acid) are characterized by an exchange rate suitable for CEST imaging [6]. Although the thermodynamic stability of the Ln(III)-DOTA-tetraamide complexes is considerably lower than that of the tetracarboxylate analogues, their kinetic inertness is extremely high, which makes them good candidates for potential in vivo applications [3,10–12].

Furthermore, Ln(III) ions, especially Eu(III) and Tb(III), have often been employed for optical sensing owing to their specific sharp line-like emission bands and long lifetimes, often being in the milliseconds range [13]. These features allow implementation of the time-gated techniques to increase the signal-to-noise ratio (SNR). Most importantly, lanthanide luminescence has large Stokes shifts (>200 nm) when compared to typical organic fluorescence compounds. Such unique photophysical properties circumvent the autofluorescence, as well as the light scattering from backgrounds of the biological samples, such as cell cultures or tissues [14]. Thus, besides suitable properties for optical imaging, complexes comprised of two different Ln(III) ions might provide properties suitable for dual-modal imaging, enabling the design of dual- and multi-modal probes [15–21].

In this work, we set out to investigate the possibility of developing a dual-modal agent that is suitable for CEST MR and optical imaging (Chart 1). We designed a molecule that consisted of two DOTAM-Gly macrocyclic moieties and a DA18C6 (DA18C6- 1,10-diaza-18-crown-6) azacrown moiety, intended for chelation of two different paramagnetic and luminescent Ln(III) ions. The DOTAM-Gly accommodated two Eu(III), giving rise to strong paraCEST signal of the generated dinuclear complex. The interaction of Tb(III) with the azacrown moiety resulted in the increase of the Tb-centered luminescence emission, showing the advantageous properties of the prepared multinuclear heterometallic complex as a potential dual-modal imaging probe.

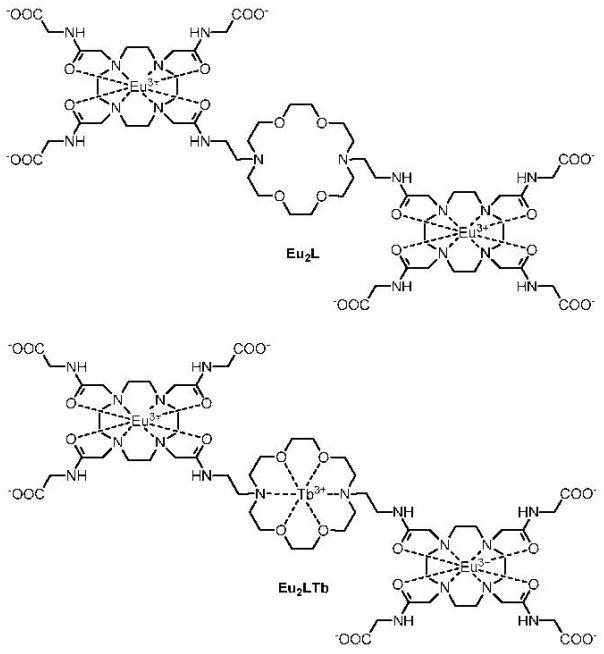

Chart 1. The chemical structures of **Eu_2L** and **Eu_2LTb** investigated in this work.

2. Results and Discussion

2.1. Synthesis of Complexes Eu_2L and Eu_2LTb

The desired trismacrocyclic ligand was synthesized in a stepwise manner, using glycine ethyl ester hydrochloride, bromoacetyl bromide, 2-bromoethylamine hydrogen bromide and benzyl chloroformate as starting compounds (Scheme 1). In the first step, the cyclic polyamine **1** was alkylated with three equiv. of the bromide **2** to provide the macrocycle **3**. Hydrogenation of **3** catalyzed by Pd/C in DMF afforded the acid **4** in high yield. In the second, azacrown fragment **7** was prepared in a three-step procedure. The commercially available 2-bromoethylamine hydrogen bromide was reacted with benzyl chloroformate to yield Cbz-protected amine **5** [22]. Then, two equiv. of **5** were reacted with 1,10-iaza-18-crown-6 to acquire azacrown dicarbamate **6**, which was then subjected to the catalytic deprotection of Cbz groups by hydrogenation in the presence of Pd/C in ethanol to afford the diamine **7**. Coupling of two equiv. of the acid **4** with the diamine **7** resulted in the thismacrocyclic precursor **8**. Finally, the base hydrolysis of **8** was achieved with LiOH to give the final ligand $\mathbf{H_6L}$. The obtained compounds were characterized by $^{1}H/^{13}C$-NMR and mass spectrometry. The bimetallic complex $\mathbf{Eu_2L}$ was prepared by treating the final ligand $\mathbf{H_6L}$ with $EuCl_3{\cdot}6H_2O$ in water, while maintaining the pH at ~7. Subsequently, complex $\mathbf{Eu_2LTb}$ was prepared by treating $\mathbf{Eu_2L}$ with one equiv. of $TbCl_3$ aqueous solution and was characterized by LC-MS spectrometry.

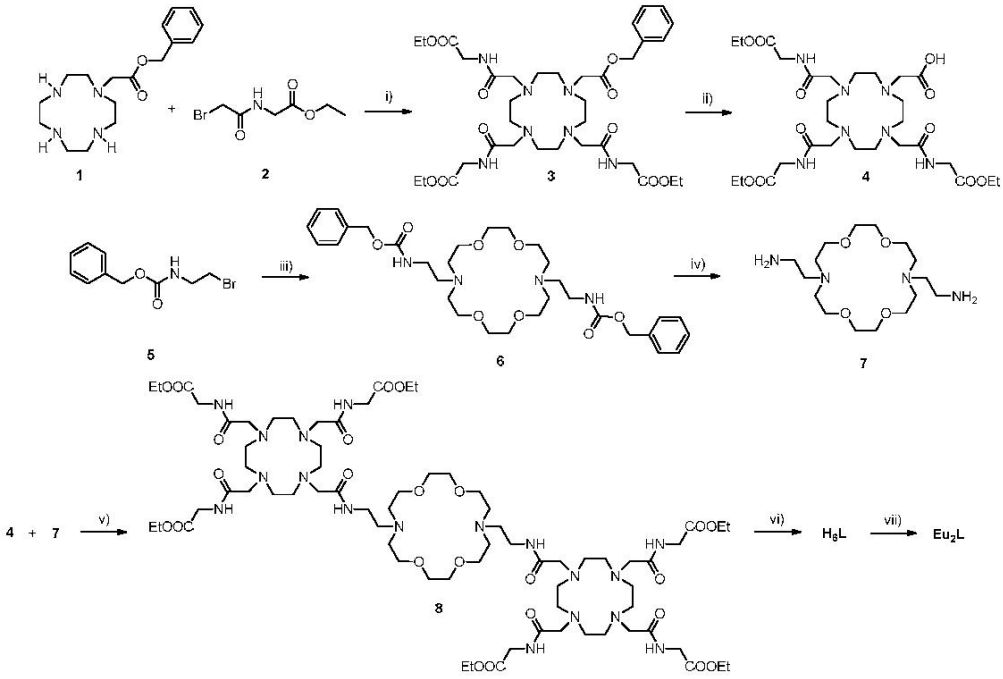

Scheme 1. Synthesis scheme of complex $\mathbf{Eu_2L}$. Reagents and conditions: (**i**) Na_2CO_3, DCM, r.t. 12 h; (**ii**) H_2/Pt, DMF, r.t., 12 h; (**iii**) MeCN, Cs_2CO_3, 65 °C, 4.5 h; (**iv**) H_2/Pt, EtOH, r.t., 4 h; (**v**) HATU, DMF, r.t., 6 h; (**vi**) LiOH, MeOH, r.t., 12 h; (**vii**) $EuCl_3{\cdot}6H_2O/H_2O$, 50 °C, 12 h.

2.2. CEST Effect Measurements of $\mathbf{Eu_2L}$

Given that the EuDOTAM-Gly complex is a well-studied paraCEST agent, the CEST properties of its structural analogue $\mathbf{Eu_2L}$ were investigated in detail and compared accordingly [23–25]. The CEST spectra of 5 mM $\mathbf{Eu_2L}$ were recorded with 10 s irradiation time and variable saturation powers (B_1 = 2.5, 5, 10, 15, 20, 25 and 30 μT) at 25 °C and pH 7.4 (Figure 1). The CEST signal resonating at ~50 ppm was observed for $\mathbf{Eu_2L}$, corresponding to the proton exchange between Eu(III)-bound water and the

bulk water molecules. The CEST effect depends on the saturation power variation [26], resulting in a CEST effect increase from ~5% to ~60% for the increase in saturation power from 5 μT to 30 μT, respectively (Figures S1 and S2, Supplementary Materials).

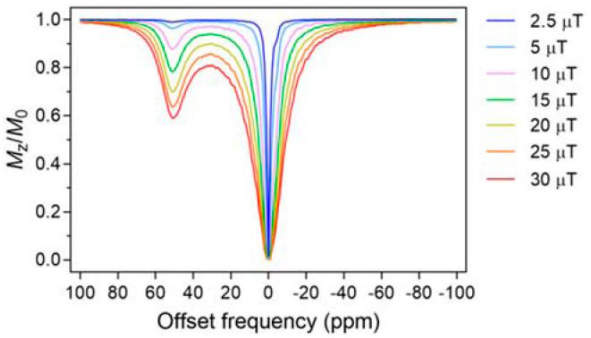

Figure 1. The CEST spectra of the complex $\mathbf{Eu_2L}$ (5 mM, irradiation time 10 s, in 50 mM HEPES with pH 7.4, 25 °C) recorded at different B_1.

Both the chemical shift of the inner-sphere bound water and the saturation efficiency of the bulk water were affected by temperature (Figure 2a). The chemical shift of the bound water pool shifted upfield with an increase in temperature (chemical shift from 57 ppm at 10 °C to 45 ppm at 40 °C). The fitting results suggested a linear-dependence between the chemical shift of the bound-water protons with temperature (Figure 2b). The observed sensitivity of the chemical shift to temperature is 0.4 ppm/°C, which is similar to that of EuDOTAM-Gly [27]. This suggested that $\mathbf{Eu_2L}$ could be used to measure temperature distribution in a living subject. The peak width of both bulk and bound water also increased with temperature (Figure 2a), owing to more rapid exchange.

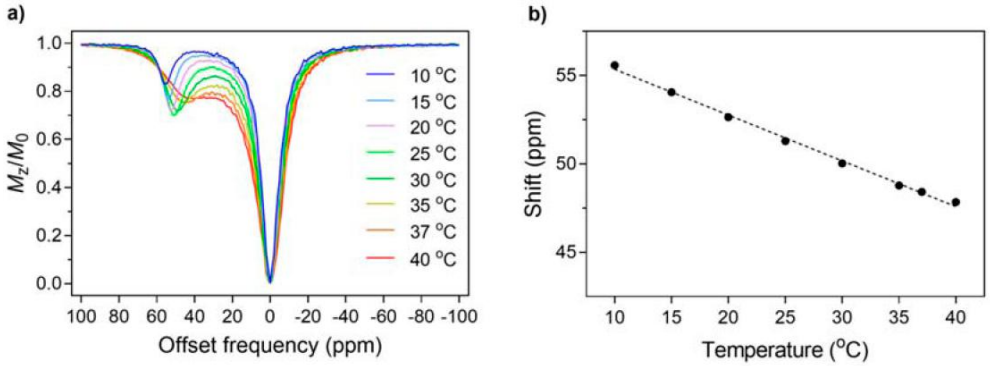

Figure 2. (**a**) The CEST spectra of 5 mM $\mathbf{Eu_2L}$ at different temperatures. (**b**) Dependence of the chemical shift of the bound water protons on temperature (pH = 7.4, B_0 = 7 T, saturation power B_1 = 20 μT, irradiation time 10 s).

The water exchange rates, k_{ex}, at different temperatures, were extracted using the quantitative CEST (qCEST) method [28]. In short, the Bloch–McConnell (BM) equations were used for fitting the experimental data, assuming a three-pool fitting model (bulk water, amide protons and the paraCEST pool). The k_{ex} values are progressively increasing as the temperature gets higher (Table 1). At 25 °C, the BM fitting three-pool model revealed the exchange rate of around 10 kHz, which corresponds to the bound-water lifetime (τ_M) of around 100 μs; this value is comparable to τ_M reported for EuDOTAM-Gly at same temperature [29]. With such properties displayed, the bismacrocyclic $\mathbf{Eu_2L}$ shows very good perspectives for future use as the paraCEST agent. Namely, owing to its bimetallic nature, $\mathbf{Eu_2L}$ can

produce the CEST signal almost twice stronger than EuDOTAM-Gly, for the same amount of the probe, while potentially having even longer retention time in tissue due to its larger size.

Table 1. The k_{ex} values of bound water molecule (5 mM complex **Eu_2L**) using the quantitative CEST (qCEST) method at different temperatures. Each temperature experiment was recorded at pH 7.4, with irradiation time of 10 s and different B_1 (2.5, 5, 10, 15, 20, 25 and 30 μT).

Temp./°C	10	15	20	25	30	35	37	40
k_{ex}/kHz	3.8 ± 0.4	4.7 ± 0.3	6.3 ± 0.3	8.9 ± 0.3	12.9 ± 0.4	18.6 ± 0.5	21.5 ± 0.5	26.7 ± 0.6

2.3. *Photophysical Characterization of Eu_2LTb*

The DA18C6 moiety in complex **Eu_2L** is also a chelator, albeit capable of binding another type of Ln(III) ion weakly [30,31]. To this end, we investigated the interaction of the **Eu_2L** with Tb(III) and the photophysical properties of the resulting hetero-trinuclear lanthanide complex **Eu_2LTb** (Figure S3, Supplementary Materials). This complex displayed mixed emission spectra in solution, which included characteristic peaks of both terbium ($^5D_4 \rightarrow {}^7F_J$) and europium ($^5D_0 \rightarrow {}^7F_J$) ions [32]. Specifically, the emission spectra of **Eu_2LTb** were recorded using excitation wavelengths ranging from 225 nm to 395 nm (Figure 3). The emission excited at 225 nm exhibited the spectrum with four characteristic signals in the visible region at 494 nm ($^5D_4 \rightarrow {}^7F_6$), 545 nm ($^5D_4 \rightarrow {}^7F_5$), 588 nm ($^5D_4 \rightarrow {}^7F_4$), and 625 nm ($^5D_4 \rightarrow {}^7F_3$), originating from the Tb(III) ion [33,34]. Concurrently, the emission excited at 395 nm resulted in the spectrum having four characteristic peaks in the visible region at 598 nm, 616 nm, 656 nm, and 702 nm, arising from the $^5D_0 \rightarrow {}^7F_J$ (J = 1, 2, 3, 4) transitions of the Eu(III) ion, respectively. Additionally, the spectra excited at 265 nm, 283 nm and 305 nm showed the combined emission peaks from both Eu(III) ($^5D_0 \rightarrow {}^7F_J$) and Tb(III) ($^5D_4 \rightarrow {}^7F_J$) transitions.

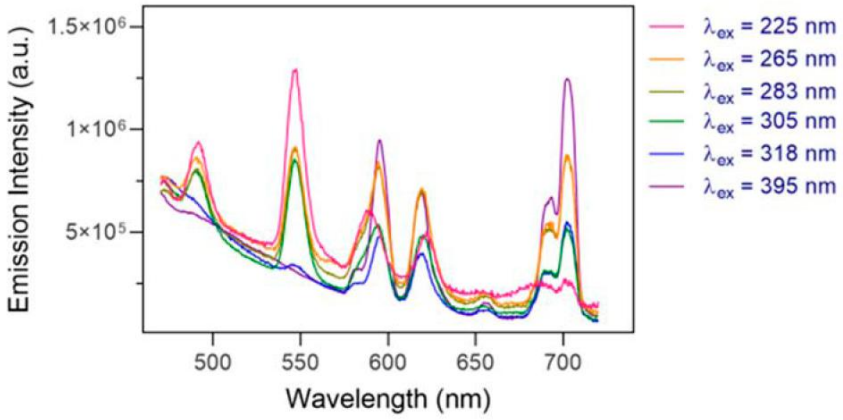

Figure 3. Luminescence spectra of 0.2 mM complex **Eu_2LTb** at 25 °C, pH 7.4 upon varying the excitation wavelength.

With the formation of **Eu_2LTb**, we sought to investigate the potential of this molecule for detection of anions. Namely, the responsiveness of coordinatively unsaturated cyclen-based Ln(III) chelates to small endogenous anions has previously been addressed by many researchers [35,36]. It is well known that the water molecules directly bound to the Eu(III) or Tb(III) ions quench luminescence efficiently due to the high energy of the O-H vibrations [37,38]. On the other hand, anions can occupy the apical position by displacing the water molecule and can circumvent the non-radiative energy quenching, giving rise to an increase in the luminescence intensity. We therefore tested whether the trismacrocyclic host **Eu_2LTb** can interact with selected biologically important anions. Thus, the interactions between **Eu_2LTb** and anions including F^-, Br^-, I^-, HCO_3^-, HPO_4^{2-}, OAc^- and

SO_4^{2-} were assessed, respectively (Figure 4). The solutions were excited at 285 nm in order to cover excitation of both Eu(III) and Tb(III), while the emission intensities were monitored in the range between 540 nm and 630 nm. The results showed no significant change in the emission intensities, except for HCO_3^- and OAc^- (Figure 4). Interestingly, HCO_3^- led to emission enhancement of Eu(III), while the OAc^- enhanced the luminescence of Tb(III), suggesting that bicarbonates preferentially bind to cyclen-derived chelates, whereas the Tb-18C6 cage dominantly interacts with acetates. Furthermore, anions F^- and HPO_4^{2-} slightly quenched the emission of Tb(III) ion only. It cannot be excluded that the latter is result of the Tb(III)-phosphate formation and precipitation of this salt, which ultimately reduces the Tb(III) centered emission intensity due to elimination of this metal ion from the solution.

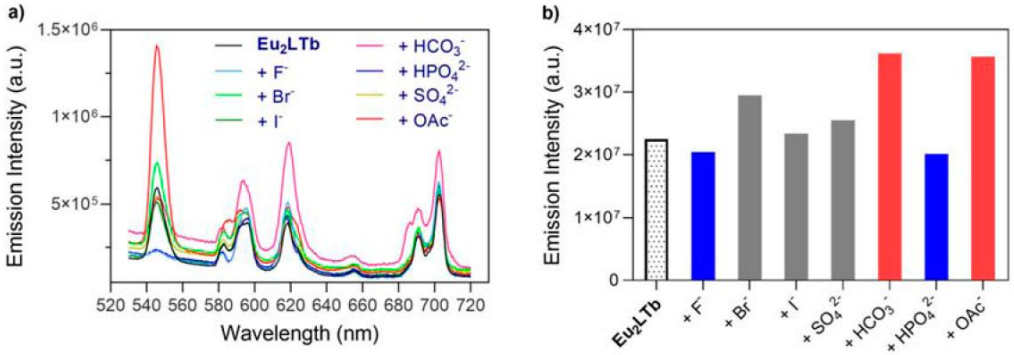

Figure 4. Luminescence selectivity studies of 0.2 mM complex **Eu_2LTb** at 25 °C, pH 7.4 with various anions (2.0 equiv.), λ_{ex} = 305 nm. (**a**) Emission spectra of **Eu_2LTb** alone and after addition of F^-, Br^-, I^-, HCO_3^-, HPO_4^{2-}, SO_4^{2-} and OAc^-. (**b**) Comparison of the recorded luminescence emission intensities monitored in the range between 540 nm and 630 nm.

3. Experimental Section

3.1. Materials

Compounds **2** and **5** were synthesized following previously reported procedures [22,24]. All other reagents and solvents were purchased from commercial sources and were used without further purification.

3.2. General Methods

Purification of synthesized compounds was performed using silica gel 60 (0.03–0.2 mm) from Carl Roth (Germany). The final ligand and metallated complexes were purified using preparative HPLC on a Varian PrepStar system equipped with the UV–vis detector model 335 and a binary pump model SD-1 manual injector, controlled by Star chromatography workstation version 6.3 software. Low resolution mass spectra were recorded on an ion trap SL 1100 system Agilent with an electrospray ionization source. High resolution mass spectra were recorded on a Bruker Daltonics APEX II (FT-ICR-MS) with an electrospray ionization source.

3.3. Synthesis

(2-Bromo-acetylamino)-acetic acid ethyl ester (**2**). A solution of 2-bromoacetyl bromide (17.4 g, 86.0 mmol) in CH_2Cl_2 (20 mL) was added dropwise to a stirred cooled solution (0 °C) of the glycine ethyl ester hydrochloride (10.1 g, 72.0 mmol) and K_2CO_3 (29.9 g, 216.0 mmol) in a mixture of CH_2Cl_2 (100 mL) and water (50 mL). The resulting solution was warmed to room temperature and stirred for 16 h, after which the organic layer was washed with water (2 × 60 mL) and brine (1 × 60 mL), dried over anhydrous Na_2SO_4, and concentrated in vacuo. The crude product was recrystallized from EtOAc to afford **2** (12.9 g, 80%) as white crystals [24]. ^{1}H-NMR ($CDCl_3$, 300 MHz): δ (ppm) 1.16–1.47 (m, 3H,

CH_3); 3.93 (s, 2H, BrCH_2); 4.06, 4.07 (d, J = 5.20 Hz, 2H, NHCH_2); 4.20, 4.23, 4.25, 4.28 (q, J = 7.18 Hz, 2H, OCH_2). ^{13}C-NMR ($CDCl_3$, 75 MHz): δ (ppm) 13.9 (CH_3); 32.0 ($BrCH_2$); 42.0 ($NHCH_2$); 61.7 (OCH_2CH_3); 168.7 (CONH); 170.4 (COO).

{4,7,10-Tris-[(ethoxycarbonylmethyl-carbamoyl)-methyl]-1,4,7,10tetraaza-cyclododec-1-yl}-acetic acid benzyl ester (**3**). The mixture of cyclen-monoacetate benzyl ester **1** (3.2 g, 10.0 mmol) and Na_2CO_3 (4.2 g, 40.0 mmol) were stirred in CH_2Cl_2 (35 mL) at room temperature for 10 min, then compound **2** in CH_2Cl_2 (9.0 g, 40.0 mmol in 15 mL) was added dropwise. The reaction mixture was stirred at room temperature for 12 h. Upon reaction completion, the reaction mixture was filtered off, the filtrate was evaporated, and the solid residue was purified by silica column chromatography using CH_2Cl_2/MeOH (*v/v*, 20:1) as the eluent to yield 2 (3.8 g, 50%) as a yellow oil. ^{1}H-NMR ($CDCl_3$, 300 MHz): δ (ppm): 1.14–1.31 (m, 9H, CH_3); 2.16–2.90 (br, 16H, NCH_2CH_2); 3.05–3.54 (br, 8H, NCH_2CO); 3.87–4.26 (br, 12H, $NHCH_2C$, OCH_2CH_3); 5.14 (s, 2H, $ArCH_2O$); 7.28–7.46 (m, 5H, Ar*H*). ^{13}C-NMR ($CDCl_3$, 75 MHz): δ (ppm): 14.3 (CH_3); 41.0, 41.1, 41.3 ($NHCH_2$); 50.6, 55.6, 57.2, 57.5, 58.3 (NCH_2); 61.4 (OCH_2CH_3); 67.0 ($ArCH_2$); 128.5, 128.8 (ArCH); 135.5 ($ArCCH_2$); 170.0, 170.2 (CONH); 172.5, 172.8 (COO); ESI-HRMS: (*m/z*) $[M + H]^+$ calcd for $C_{35}H_{56}N_7O_{11}^+$, 750.4032; found: 750.4031.

{4,7,10-Tris-[(ethoxycarbonylmethyl-carbamoyl)-methyl]-1,4,7,10tetraaza-cyclododec-1-yl}-acetic acid (**4**). The compound **3** (2.0 g, 2.7 mmol) was dissolved in DMF (25 mL). The catalyst Pd/C (10%, *w/w*, 0.2 equiv) and 10 µL of ammonia in MeOH (7 M) were added. The mixture solution was shaken in Parr apparatus in the atmosphere of H_2 (3.2 bar) for 12 h at room temperature. The resulting solution was filtered off and concentrated in vacuo to afford 4 (1.6 g, 90%) as a brown oil. ^{1}H-NMR ($CDCl_3$, 300 MHz): δ (ppm): 1.14–1.36 (br, 9H, CH_3); 2.14–3.78 (br, 24H, NCH_2); 3.79–4.26 (br, 12H, $NHCH_2$, OCH_2). ^{13}C-NMR ($CDCl_3$, 75 MHz): δ (ppm): 14.1 (CH_3); 41.2 ($NHCH_2$); 49.9, 50.5, 57.6, 57.7(NCH_2); 61.4 (OCH_2CH_3); 170.0, 170.1 (CONH); 172.1 (COO); ESI-HRMS: (*m/z*) $[M + H]^+$ calcd for $C_{28}H_{50}N_7O_{11}^+$, 660.3563; found: 660.3559.

(2-Bromo-ethyl)-carbamic acid benzyl ester (**5**). To a mixture of 2-bromoethylamine hydrogen bromide (2.0 g, 10.0 mmol) and triethylamine Et_3N (3.0 g, 30.0 mmol) in CH_2Cl_2 (40 mL), benzyl chloroformate (2.7 g, 16.0 mmol) was added in a portion-wise manner at 0 °C. The resulting mixture was stirred at 0 °C for 6 h. The mixture was then washed with aqueous $NaHCO_3$ (10%, 3 × 10 mL) and citric acid (10%, 3 × 10 mL) and dried over anhydrous Na_2SO_4. The solvent was then evaporated to obtain crude residue, which was purified by column chromatography (silica gel, hexane/EtOAc, 7:1) to afford 5 (2.3 g, 90 % yield) as a white crystal solid [22]. ^{1}H-NMR ($CDCl_3$, 300 MHz): δ (ppm): 3.01–3.56 (m, 4H, $BrCH_2$, CH_2NH); 5.04 (s, 2H, $ArCH_2$); 7.21–7.36 (br, 5H, Ar*H*). ^{13}C-NMR ($CDCl_3$, 75 MHz): δ (ppm): 31.8 ($BrCH_2$); 42.4 (CH_2NH); 66.5 ($ArCH_2$); 126.6, 127.7, 128.2 (ArCH); 136.0 ($ArCCH_2$); 155.3 (CONH).

{2-[16-(2-Benzyloxycarbonylamino-ethyl)-1,4,10,13-tetraoxa-7,16-diaza-cyclooctadec-7-yl]-ethyl}-carbamic acid benzyl ester (**6**). Cs_2CO_3 (3.9 g, 12.0 mmol) was added to a solution of 1,10-diaza-18-crown-6 (0.8 g, 3.0 mmol) in dry MeCN (15 mL). The obtained suspension was stirred for 10 min at room temperature and then **5** (1.7 g, 6.6 mmol) was added to it. The mixture was heated to 65 °C and stirred for 1.5 h after which additional amount of **5** (0.8 g, 3.1 mmol) was added and the reaction mixture was stirred for 3 h. Afterwards, the solvent was evaporated under the reduced pressure and the crude was purified by column chromatography (silica gel, CH_2Cl_2/MeOH, 100:7) to give **6** (1.6 g, 58%) as a brown oil. ^{1}H-NMR ($CDCl_3$, 300 MHz): δ (ppm): 2.43–2.98 (br, 12H, NCH_2CH_2); 3.17–3.39 (br, 4H, CH_2CH_2NH); 3.47–3.64 (br, 16H, CH_2OCH_2); 5.08 (s, 2H, $ArCH_2$); 7.21–7.45 (br, 10H, Ar*H*). ^{13}C-NMR ($CDCl_3$, 75 MHz): δ (ppm): 38.9 (CH_2NH); 53.5 (NCH_2CH_2); 66.3 ($ArCH_2$); 67.6, 68.7 (CH_2OCH_2); 127.8, 128.2, 128.5 (ArCH); 136.6 ($ArCCH_2$); 156.9 (CONH). ESI-HRMS: (*m/z*) $[M + Na]^+$ calcd for $C_{32}H_{48}N_4NaO_8^+$, 639.3364; found: 639.3376.

2-[16-(2-Amino-ethyl)-1,4,10,13-tetraoxa-7,16-diaza-cyclooctadec-7-yl]-ethylamine (**7**). The compound **6** (1.2 g, 1.9 mmol) was dissolved in EtOH (25 mL). The catalyst Pd/C (10% *w/w*, 0.2 equiv.) and 10 µL of

ammonia in MeOH (7 M) were added. The solution was shaken in Parr apparatus in the atmosphere of H_2 (3.2 bar) for 4 h at room temperature. Removal of the catalyst by filtration and evaporation of EtOH yielded the diamine **7** (0.6 g, 88%). ^{1}H-NMR (D_2O, 300 MHz): δ (ppm): 2.68–2.94 (br, 12H, NCH_2CH_2); 3.28–3.33 (br, 4H, $CH_2CH_2NH_2$); 3.48–3.81 (br, 16H, CH_2OCH_2). ^{13}C-NMR (D_2O, 75 MHz): δ (ppm): 36.9 (CH_2NH_2); 51.8, 53.9 (NCH_2CH_2); 68.2, 69.7 (CH_2OCH_2). ESI-HRMS: (*m*/*z*) $[M + H]^+$ calcd for $C_{16}H_{37}N_4O_4^+$, 349.2809; found: 349.2816.

Compound **8**. The acid **4** (1.1 g, 1.7 mmol) and HATU (1-[Bis(dimethylamino)methylene]-1H-1,2,3-triazolo[4,5-b]pyridinium 3-oxide hexafluorophosphate, Hexafluorophosphate Azabenzotriazole Tetramethyl Uronium, 0.7 g, 1.9 mmol) were subsequently added to a stirred solution of diamine **7** (0.2 g, 0.6 mmol) in dry DMF (10 mL), after which the reaction mixture was stirred for 6 h at room temperature. The solvent was removed under the reduced pressure and the residue was washed with Et_2O (3 × 10 mL), CH_2Cl_2 (3 × 10 mL) and MeOH (2 × 10 mL). The collected filtrate was concentrated in vacuo to give a yellowish oil (0.4 g, 48%). ^{1}H-NMR (CD_3OD, 300 MHz): δ (ppm): 1.23, 1.25, 1.28 (t, J = 7.50 Hz, 18H, CH_3); 3.39–3.83 (br, 64H, CH_2); 3.94–4.05 (br, 16H, OCH_2); 4.05–4.12 (br, 12H, $NHCH_2C$); 4.14–4.26 (m, 12H, $NHCH_2CO$). ^{13}C-NMR (CD_3OD, 75 MHz): δ (ppm): 14.5 (CH_3); 42.2 ($NHCH_2$); 55.2, 56.3, 62.0, 64.7, 65.3, 70.9 (NCH_2); 170.3, (CONH, COO). ESI-HRMS: (*m*/*z*) $[M + 3H]^{3+}$ calcd for $C_{72}H_{133}N_{18}O_{24}^{3+}$, 544.6575; found: 544.6575.

Compound **H_6L.** Compound **8** (300 mg, 0.2 mmol) was dissolved in MeOH (5 mL) and treated with LiOH (130 mg, 5.5 mmol) at room temperature for 12 h. After removal of LiOH by filtration, MeOH was evaporated. The crude mixture was dissolved in water and the pH was adjusted to 7 and purified by preparative HPLC. The white powder **H_6L** (120 mg, 45%) was obtained by lyophilization. ^{1}H-NMR (D_2O, 300 MHz): δ (ppm): 3.04–3.31 (br, 30H, cyclen NCH_2), 3.33–3.52 (br, 18H, cyclen NCH_2), 3.53–3.62 (br, 12H, crown ether NCH_2), 3.63–3.79 (br, 16H, crown ether OCH_2), 3.80–3.96 (br, 16H, $CONHCH_2$). ^{13}C-NMR (D_2O, 75 MHz): δ (ppm): 41.1 ($NHCH_2$); 53.2, 54.8, 55.1, 63.6 (NCH_2); 69.7 (OCH_2); 162.8, 172.8, (CONH, COOH). ESI-HRMS: (*m*/*z*) $[M - H]^-$ calcd for $C_{60}H_{105}N_{18}O_{24}^-$, 1461.7555; found: 1461.7548.

Complex **Eu_2L.** The ligand **H_6L** (100 mg, 0.07 mmol) was dissolved in MilliQ water and the pH value was set to 7. The aqueous solution of $EuCl_3{\cdot}6H_2O$ (55 mg, 0.15 mmol) was added dropwise to the ligand solution. The mixture was heated at 50 °C for 12 h and the pH of the solution was periodically adjusted to 7.0 by addition of 0.1 M NaOH solution. Then, the reaction mixture was cooled to room temperature and purified by HPLC. The yellow solid compound (84 mg, 70%) was obtained by lyophilization. ESI-HRMS: (*m*/*z*) $[M + 3H]^{3+}$ calcd for $C_{60}H_{103}Eu_2N_{18}O_{24}^{3+}$, 588.5267; found: 588.5279.

Complex **Eu_2LTb.** To a stirred solution of **Eu_2L** (40 mg, 0.02 mmol) in MilliQ water (pH~7), the aqueous solution of $TbCl_3{\cdot}6H_2O$ (10 mg, 0.03 mmol) was added dropwise while maintaining pH with 0.1 M NaOH (aq). The reaction mixture was stirred at 50 °C for 6 h. Then the solvent was reduced under the vacuum and the gray solid powder was obtained upon lyophilization. LC-MS: (*m*/*z*) $[M + H]^{2+}$ calcd for $C_{60}H_{99}Eu_2N_{18}O_{24}Tb^{2+}$, 959.3; found: 959.3.

3.4. NMR Spectroscopy

^{1}H, ^{13}C-NMR and CEST experiments were recorded on a Bruker Avance III 300 MHz spectrometer. ^{1}H and ^{13}C-NMR spectra were recorded at 25 °C, using either $CDCl_3$ or D_2O and referenced to TMS/TSP. Processing was performed using TopSpin 2.1 (Bruker GmbH) and ACD/SpecManager 9.0 (Advanced Chemistry Development, Inc., Toronto, Canada). The concentrations of **Eu_2L** and $TbCl_3$ were determined using the bulk magnetic susceptibility shift (BMS) method [39]. CEST spectra were obtained in 10% D_2O and 90% H_2O solutions of the paramagnetic complex, using a saturation time of 10 s at 7 T and different temperatures (10, 15, 20, 25, 30, 35, 37 and 40 °C) and a frequency-offset range of ± 100 ppm with 1 ppm resolution. The longitudinal and transverse relaxation times, T_1 and

T_2, were measured using the inversion-recovery and Carr–Purcell–Meiboom–Gill pulse sequences, respectively [40,41].

3.5. Optical Spectroscopy

All fluorescence spectra were recorded on a QuantaMaster™ 3 PH fluorescence spectrometer from Photon Technology International, Inc. (USA) at 25 °C and pH 7.4. Titration experiments with Tb(III) were performed by following the emission intensity at 545 nm. For the anion selectivity experiments, appropriate concentration (0.2 mM) of F^-, Br^-, I^-, HCO_3^-, SO_4^{2-}, OAc^- and HPO_4^{2-} were prepared by dilution method using HPLC grade water. All data were recorded in HEPES buffer (50 mM, pH 7.4), using the excitation wavelength at 305 nm and the slit widths of 5 nm and 1 nm for excitation and emission, respectively.

4. Conclusions

A trismacrocyclic DOTA-amide DA18C6-based ligand framework was prepared and characterized. The novel dinuclear **Eu_2L** contrast agent showed the paraCEST properties typical to that of well-known EuDOTAM-Gly probe, albeit with greater potential for stronger CEST effect due to its bismacrocyclic and dinuclear nature. Upon introduction of Tb(III) ions, the resulting trinuclear **Eu_2LTb** complex exhibited mixed luminescence emission. Moreover, the binding studies with various anions revealed specificity to HCO_3^- and OAc^- over other biologically relevant anions. The typical paraCEST signal and combined luminescence emission properties pave the way for this class of mixed macrocyclic ligands to develop further as potential dual-modal MRI/luminescence probes.

Supplementary Materials: The supplementary materials are available online. Figure S1: Change in T1 and T2 relaxation times for 5 mM **Eu_2L** with temperature at 300 MHz (50 mM HEPES, pH 7.4), Figure S2: The CEST spectra of 5 mM **Eu_2L** at different temperatures and saturation power B1, Figure S3: Emission intensity monitored at 545 nm of 0.2 mM **Eu_2L** upon titration with Tb^{3+} at 25 °C (50 mM HEPES, pH 7.4).

Author Contributions: G.W. and G.A. contributed the conceptualization and methodology. G.W. prepared the complexes and performed the measurements. G.W. and G.A. analyzed and interpreted the results, then allocated and wrote the manuscript. Both authors have read and agreed to the published version of the manuscript.

Funding: G.W. was supported by the China Scholarship Council (CSC, PhD fellowship).

Acknowledgments: The authors acknowledge the support of the China Scholarship Council (CSC, PhD fellowship).

Conflicts of Interest: The authors declare no conflict of interest.

References

1. Edelman, R.R.; Hesselink, J.R.; Zlatkin, M.B. *MRI: Clinical Magnetic Resonance Imaging*, 2nd ed.; W. B. Saunders Company: Philadelphia, PA, USA, 1996; Volume 2.
2. Zhang, K.; Cheng, Y.; Ren, W.W.; Sun, L.P.; Liu, C.; Wang, D.; Guo, L.H.; Xu, H.X.; Zhao, Y.X. Coordination-Responsive Longitudinal Relaxation Tuning as a Versatile MRI Sensing Protocol for Malignancy Targets. *Adv. Sci.* **2018**, *5*, 1800021. [CrossRef] [PubMed]
3. Helm, L.; Merbach, A.E.; Tóth, E.V. *The Chemistry of Contrast Agents in Medical Magnetic Resonance Imaging*, 2nd ed.; John Wiley & Sons Inc.: Hoboken, NJ, USA, 2013; p. 496.
4. Ward, K.M.; Aletras, A.H.; Balaban, R.S. A new class of contrast agents for MRI based on proton chemical exchange dependent saturation transfer (CEST). *J. Magn. Reson.* **2000**, *143*, 79–87. [CrossRef] [PubMed]
5. Wahsner, J.; Gale, E.M.; Rodriguez-Rodriguez, A.; Caravan, P. Chemistry of MRI Contrast Agents: Current Challenges and New Frontiers. *Chem. Rev.* **2019**, *119*, 957–1057. [CrossRef] [PubMed]
6. Evbuomwan, O.M.; Terreno, E.; Aime, S.; Sherry, A.D. CEST and PARACEST Agents for Molecular Imaging. In *The Chemistry of Molecular Imaging*; Long, N., Wong, W.T., Eds.; John Wiley & Sons: Hoboken, NJ, USA, 2014; pp. 224–243.
7. Zhang, S.R.; Merritt, M.; Woessner, D.E.; Lenkinski, R.E.; Sherry, A.D. PARACEST agents: Modulating MRI contrast via water proton exchange. *Acc. Chem. Res.* **2003**, *36*, 783–790. [CrossRef] [PubMed]

8. Heffern, M.C.; Matosziuk, L.M.; Meade, T.J. Lanthanide probes for bioresponsive imaging. *Chem. Rev.* **2014**, *114*, 4496–4539. [CrossRef]
9. Rodríguez-Rodríguez, A.; Zaiss, M.; Esteban-Gómez, D.; Angelovski, G.; Platas-Iglesias, C. Paramagnetic chemical exchange saturation transfer agents and their perspectives for application inmagnetic resonance imaging. *Int. Rev. Phys. Chem.* **2020**, *40*, 51–79.
10. Baranyai, Z.; Brucher, E.; Ivanyi, T.; Kiraly, R.; Lazar, I.; Zekany, L. Complexation Properties of *N*,*N*′,*N*″,*N*‴-[1,4,7,10-tetraazacyclododecane-1,4,7,10-tetrayltetrakis(1-oxoethane-2,1-diyl)]tetrakis[glycine] (H_4dotagl). Equilibrium, Kinetic, and Relaxation Behavior of the Lanthanide(III) Complexes. *Helv. Chim. Acta* **2005**, *88*, 604–617. [CrossRef]
11. Sherry, A.D.; Caravan, P.; Lenkinski, R.E. Primer on Gadolinium Chemistry. *J. Magn. Reson. Imaging* **2009**, *30*, 1240–1248. [CrossRef]
12. Tircso, G.; Benyo, E.T.; Garda, Z.; Singh, J.; Trokowski, R.; Brucher, E.; Sherry, A.D.; Toth, E.; Kovacs, Z. Comparison of the equilibrium, kinetic and water exchange properties of some metal ion-DOTA and DOTA-bis(amide) complexes. *J. Inorg. Biochem.* **2020**, *206*, 111042–111054. [CrossRef]
13. Bunzli, J.C. Lanthanide luminescence for biomedical analyses and imaging. *Chem. Rev.* **2010**, *110*, 2729–2755. [CrossRef]
14. Binnemans, K. Interpretation of europium(III) spectra. *Coord. Chem. Rev.* **2015**, *295*, 1–45. [CrossRef]
15. Mamedov, I.; Parac-Vogt, T.N.; Logothetis, N.K.; Angelovski, G. Synthesis and characterization of dinuclear heterometallic lanthanide complexes exhibiting MRI and luminescence response. *Dalton Trans.* **2010**, *39*, 5721–5727. [CrossRef]
16. Jones, J.E.; Amoroso, A.J.; Dorin, I.M.; Parigi, G.; Ward, B.D.; Buurma, N.J.; Pope, S.J.A. Bimodal, dimetallic lanthanide complexes that bind to DNA: The nature of binding and its influence on water relaxivity. *Chem. Commun.* **2011**, *47*, 3374–3376. [CrossRef] [PubMed]
17. Terreno, E.; Boffa, C.; Menchise, V.; Fedeli, F.; Carrera, C.; Delli Castelli, D.; Digilio, G.; Aime, S. Gadolinium-doped LipoCEST agents: A potential novel class of dual ^{1}H-MRI probes. *Chem. Commun.* **2011**, *47*, 4667–4669. [CrossRef]
18. Debroye, E.; Parac-Vogt, T.N. Towards polymetallic lanthanide complexes as dual contrast agents for magnetic resonance and optical imaging. *Chem. Soc. Rev.* **2014**, *43*, 8178–8192. [CrossRef]
19. Placidi, M.P.; Villaraza, A.J.; Natrajan, L.S.; Sykes, D.; Kenwright, A.M.; Faulkner, S. Synthesis and spectroscopic studies on azo-dye derivatives of polymetallic lanthanide complexes: Using diazotization to link metal complexes together. *J. Am. Chem. Soc.* **2009**, *131*, 9916–9917. [CrossRef]
20. Sorensen, T.J.; Tropiano, M.; Blackburn, O.A.; Tilney, J.A.; Kenwright, A.M.; Faulkner, S. Preparation and study of an f,f,f′,f″ covalently linked tetranuclear hetero-trimetallic complex—A europium, terbium, dysprosium triad. *Chem. Commun.* **2013**, *49*, 783–785. [CrossRef]
21. Faulkner, S.; Pope, S.J. Lanthanide-sensitized lanthanide luminescence: Terbium-sensitized ytterbium luminescence in a trinuclear complex. *J. Am. Chem. Soc.* **2003**, *125*, 10526–10527. [CrossRef]
22. Tseng, M.C.; Chu, Y.H. Chemoselective gas sensing ionic liquids. *Chem. Commun.* **2010**, *46*, 2983–2985. [CrossRef] [PubMed]
23. Zhang, S.; Winter, P.; Wu, K.; Sherry, A.D. A novel europium(III)-based MRI contrast agent. *J. Am. Chem. Soc.* **2001**, *123*, 1517–1518. [CrossRef] [PubMed]
24. Evbuomwan, O.M.; Kiefer, G.; Sherry, A.D. Amphiphilic EuDOTA-tetraamide complexes form micelles with enhanced CEST sensitivity. *Eur. J. Inorg. Chem.* **2012**, *2012*, 2126–2134. [CrossRef]
25. Cakic, N.; Verbic, T.Z.; Jelic, R.M.; Platas-Iglesias, C.; Angelovski, G. Synthesis and characterisation of bismacrocyclic DO3A-amide derivatives—An approach towards metal-responsive PARACEST agents. *Dalton Trans.* **2016**, *45*, 6555–6565. [CrossRef] [PubMed]
26. van Zijl, P.C.M.; Yadav, N.N. Chemical Exchange Saturation Transfer (CEST): What is in a Name and What Isn't? *Magn. Reson. Med.* **2011**, *65*, 927–948. [CrossRef] [PubMed]
27. Zhang, S.; Malloy, C.R.; Sherry, A.D. MRI thermometry based on PARACEST agents. *J. Am. Chem. Soc.* **2005**, *127*, 17572–17573. [CrossRef] [PubMed]
28. Zaiss, M.; Angelovski, G.; Demetriou, E.; McMahon, M.T.; Golay, X.; Scheffler, K. QUESP and QUEST revisited—Fast and accurate quantitative CEST experiments. *Magn. Reson. Med.* **2018**, *79*, 1708–1721. [CrossRef]

29. Dixon, W.T.; Ren, J.; Lubag, A.J.; Ratnakar, J.; Vinogradov, E.; Hancu, I.; Lenkinski, R.E.; Sherry, A.D. A concentration-independent method to measure exchange rates in PARACEST agents. *Magn. Reson. Med.* **2010**, *63*, 625–632. [CrossRef]
30. Suarez, S.; Mamula, O.; Scopelliti, R.; Donnio, B.; Guillon, D.; Terazzi, E.; Piguet, C.; Bunzli, J.C.G. Lanthanide luminescent mesomorphic complexes with macrocycles derived from diaza-18-crown-6. *New J. Chem.* **2005**, *29*, 1323–1334. [CrossRef]
31. Sazonov, P.K.; Stolyarenko, V.Y.; Shtern, M.M.; Beletskaya, I.P. Unexpected lanthanide cation selectivity of bis-β-ketovinylated diaza-18-crown-6 and open-chain diamines: Cooperative effect of the second keto group. *J. Inclusion Phenom. Macrocyclic Chem.* **2014**, *79*, 193–203. [CrossRef]
32. Gao, C.J.; Kirillov, A.M.; Dou, W.; Tang, X.L.; Liu, L.L.; Yan, X.H.; Xie, Y.J.; Zang, P.X.; Liu, W.S.; Tang, Y. Self-Assembly Synthesis, Structural Features, and Photophysical Properties of Dilanthanide Complexes Derived from a Novel Amide Type Ligand: Energy Transfer from Tb(III) to Eu(III) in a Heterodinuclear Derivative. *Inorg. Chem.* **2014**, *53*, 935–942. [CrossRef]
33. Zhang, H.X.; Chen, Z.H.; Liu, X.; Zhang, F. A mini-review on recent progress of new sensitizers for luminescence of lanthanide doped nanomaterials. *Nano Res.* **2020**, *13*, 1795–1809. [CrossRef]
34. Kaczmarek, M. Lanthanide-sensitized luminescence and chemiluminescence in the systems containing most often used medicines; a review. *J. Lumin.* **2020**, *222*, 117174. [CrossRef]
35. Parker, D.; Dickins, R.S.; Puschmann, H.; Crossland, C.; Howard, J.A. Being excited by lanthanide coordination complexes: Aqua species, chirality, excited-state chemistry, and exchange dynamics. *Chem. Rev.* **2002**, *102*, 1977–2010. [CrossRef] [PubMed]
36. Aletti, A.B.; Gillen, D.M.; Gunnlaugsson, T. Luminescent/colorimetric probes and (chemo-) sensors for detecting anions based on transition and lanthanide ion receptor/binding complexes. *Coord. Chem. Rev.* **2018**, *354*, 98–120. [CrossRef]
37. Kropp, J.L.; Windsor, M.W. Luminescence and Energy Transfer in Solutions of Rare Earth Complexes. II. Studies of Solvation Shell in Europium(III) and Terbium(III) as a Function of Acetate Concentration. *J. Phys. Chem.* **1967**, *71*, 477–482. [CrossRef]
38. Horrocks, W.D.; Sudnick, D.R. Lanthanide Ion Probes of Structure in Biology—Laser-Induced Luminescence Decay Constants Provide a Direct Measure of the Number of Metal-Coordinated Water-Molecules. *J. Am. Chem. Soc.* **1979**, *101*, 334–340. [CrossRef]
39. Corsi, D.M.; Platas-Iglesias, C.; van Bekkum, H.; Peters, J.A. Determination of paramagnetic lanthanide(III) concentrations from bulk magnetic susceptibility shifts in NMR spectra. *Magn. Reson. Chem.* **2001**, *39*, 723–726. [CrossRef]
40. Meiboom, S.; Gill, D. Modified Spin-Echo Method for Measuring Nuclear Relaxation Times. *Rev. Sci. Instrum.* **1958**, *29*, 688–691. [CrossRef]
41. Carr, H.Y.; Purcell, E.M. Effects of Diffusion on Free Precession in Nuclear Magnetic Resonance Experiments. *Phys. Rev.* **1954**, *94*, 630–638. [CrossRef]

Sample Availability: Samples of the compounds are not available from the authors.

Publisher's Note: MDPI stays neutral with regard to jurisdictional claims in published maps and institutional affiliations.

Supporting Information for

Macrocyclic Chelates Bridged by a Diaza-crown Ether: Towards Multinuclear Bimodal Molecular Imaging Probes

Gaoji Wang[1] and Goran Angelovski[1,2*]

[1] MR Neuroimaging Agents, MPI for Biological Cybernetics, Tübingen, Germany.
[2] Lab of Molecular and Cellular Neuroimaging, International Center for Primate Brain Research (ICPBR), Center for Excellence in Brain Science and Intelligence Technology (CEBSIT), Chinese Academy of Science (CAS), Shanghai 200031, PR China

*E-mail: goran.angelovski@tuebingen.mpg.de

Contents

NMR CEST experiments

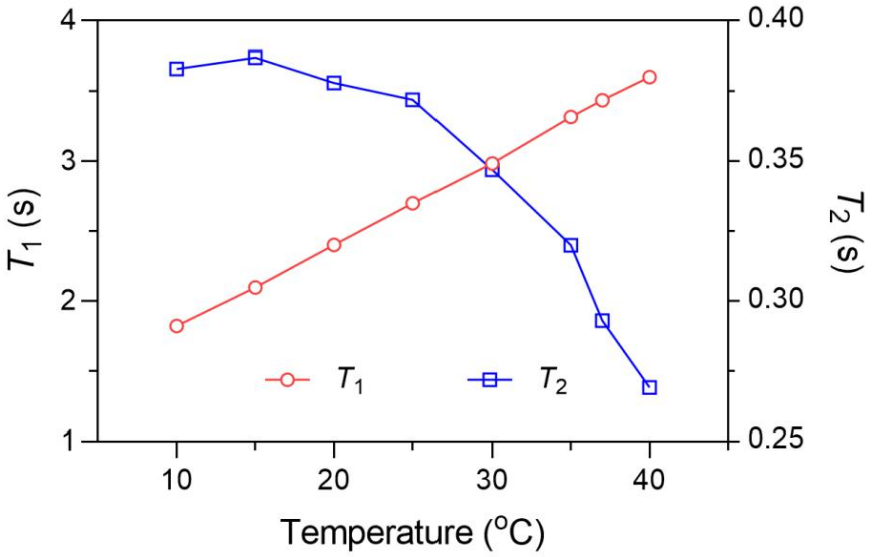

Figure S1. Change in T_1 and T_2 relaxation times for 5 mM **Eu_2L** with temperature at 300 MHz (50 mM HEPES, pH 7.4).

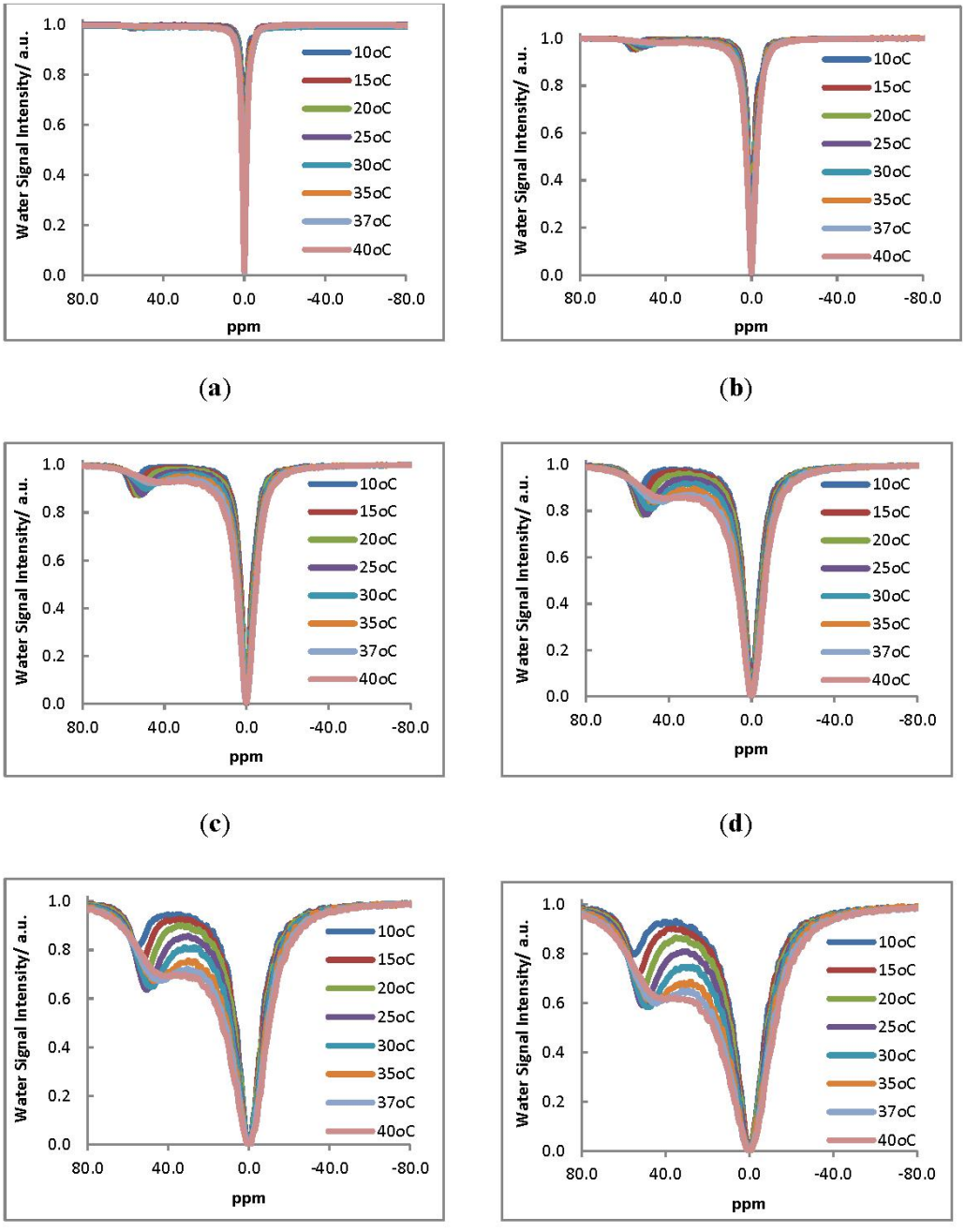

Figure S2. The CEST spectra of 5 mM **Eu_2L** at different temperatures and saturation power B_1: (a) 2.5 μT, (b) 5.0 μT, (c) 10 μT, (d) 15 μT, (e) 25 μT and (f) 30 μT.

Luminescence experiments

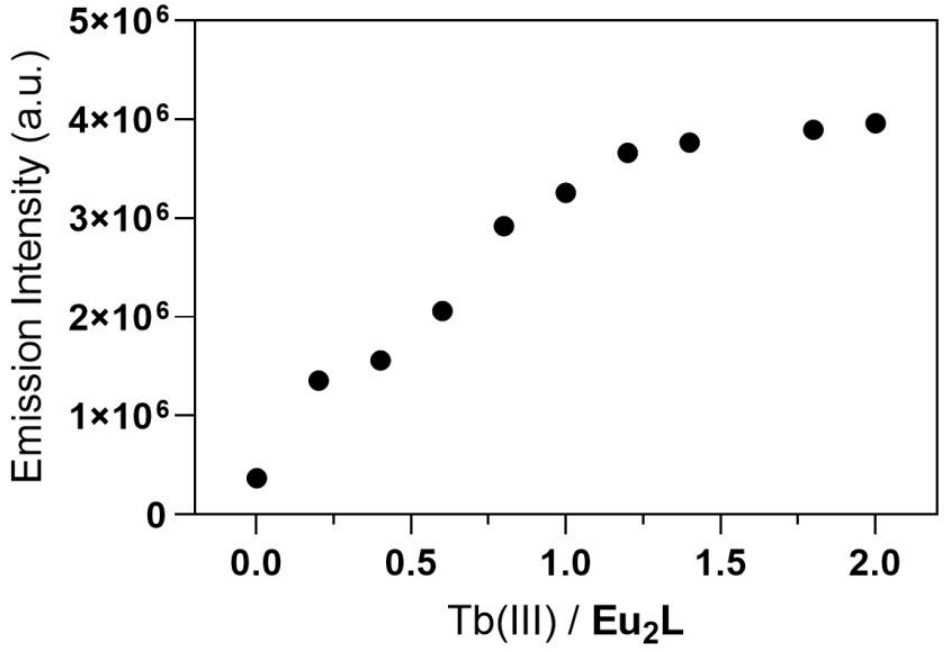

Figure S3. Emission intensity monitored at 545 nm of 0.2 mM **Eu_2L** upon titration with Tb^{3+} at 25 °C (50 mM HEPES, pH 7.4). The binding isotherm saturates after 1 equiv. of added Tb^{3+}, indicating formation of weak 1:1 complex between **Eu_2L** and Tb^{3+}.

NMR spectra

Compound **2**

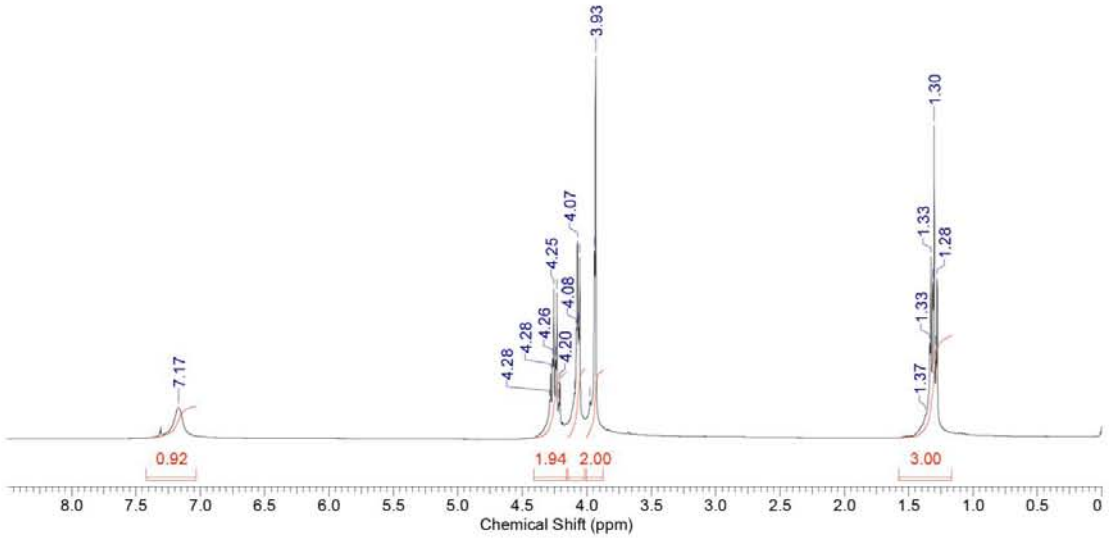

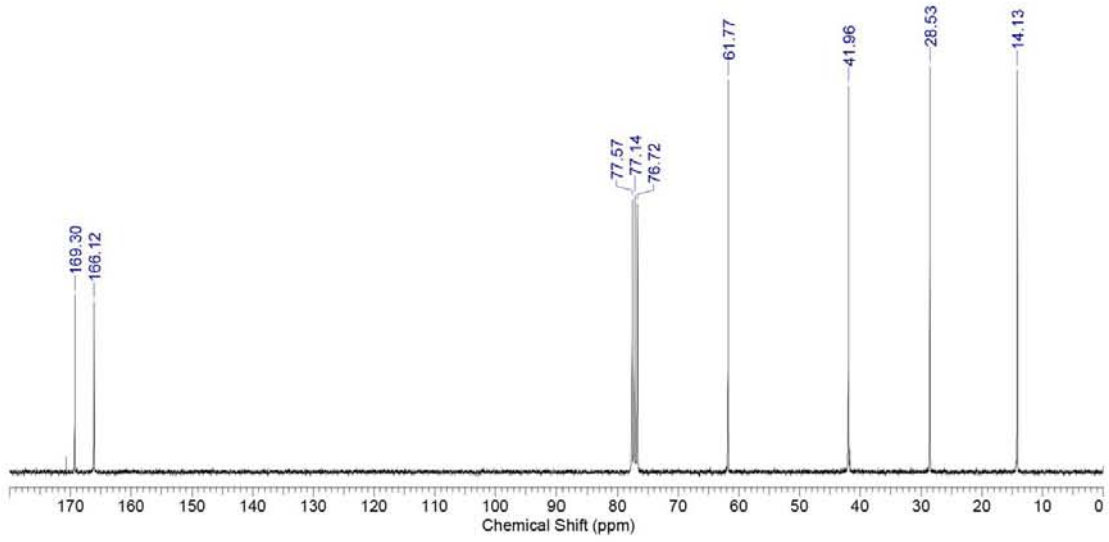

Compound **3**

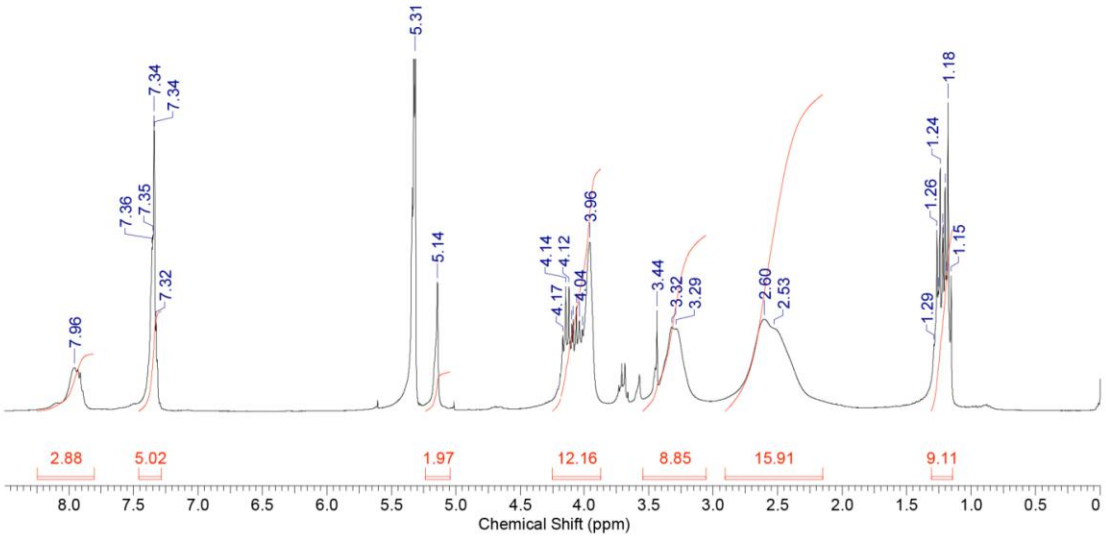
5.31
7.34
7.34
7.36
7.35
7.32
7.96
5.14
4.14
4.12
4.17
4.04
3.96
3.44
3.32
3.29
2.60
2.53
1.18
1.24
1.26
1.15
1.29
2.88
5.02
1.97
12.16
8.85
15.91
9.11
Chemical Shift (ppm)

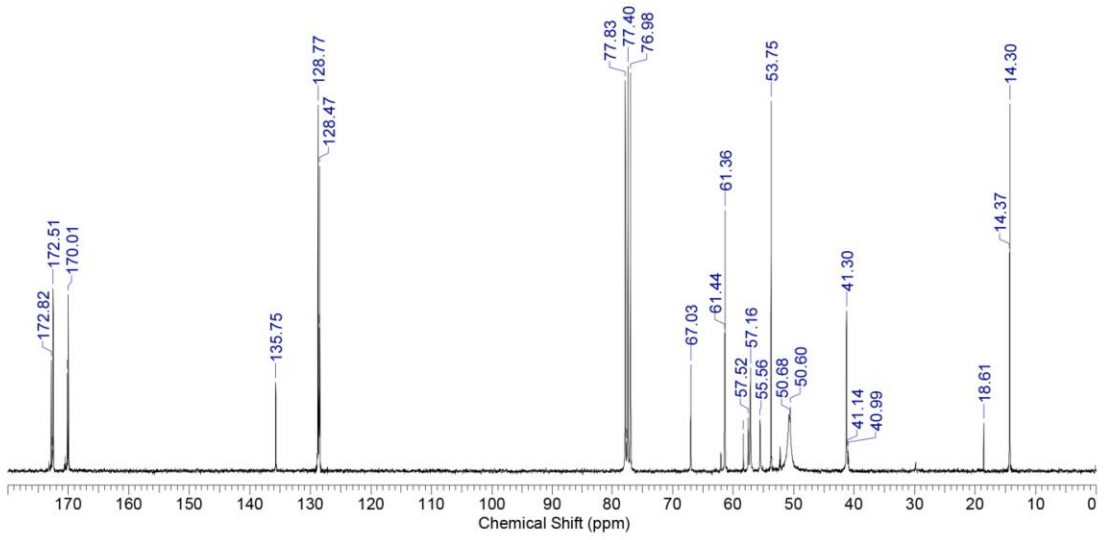
77.83
77.40
76.98
128.77
128.47
53.75
14.30
61.36
14.37
172.82
172.51
170.01
135.75
67.03
61.44
57.16
41.30
57.52
55.56
50.68
50.60
41.14
40.99
18.61
Chemical Shift (ppm)

Compound **4**

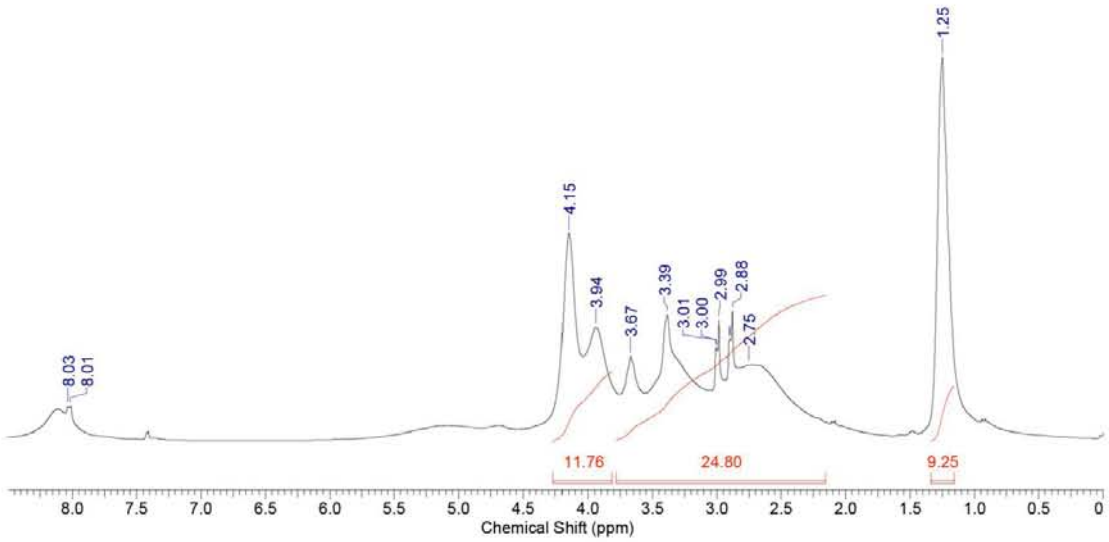
1.25
4.15
3.94
3.67
3.39
3.01
3.00
2.99
2.88
2.75
8.03
8.01
11.76
24.80
9.25
Chemical Shift (ppm)

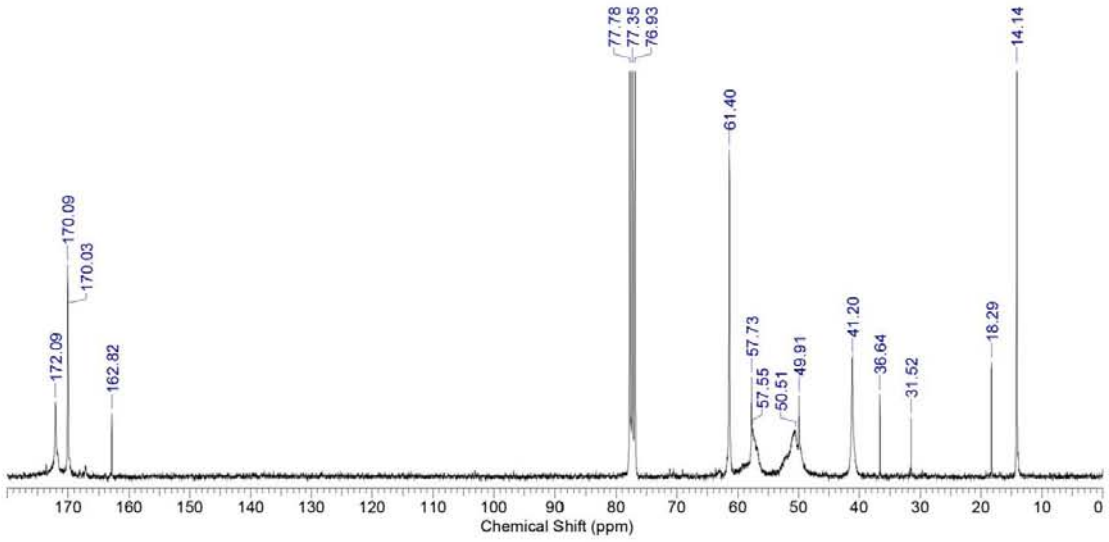
77.78
77.35
76.93
14.14
61.40
170.09
170.03
172.09
162.82
57.73
57.55
50.51
49.91
41.20
36.64
31.52
18.29
Chemical Shift (ppm)

Compound **5**

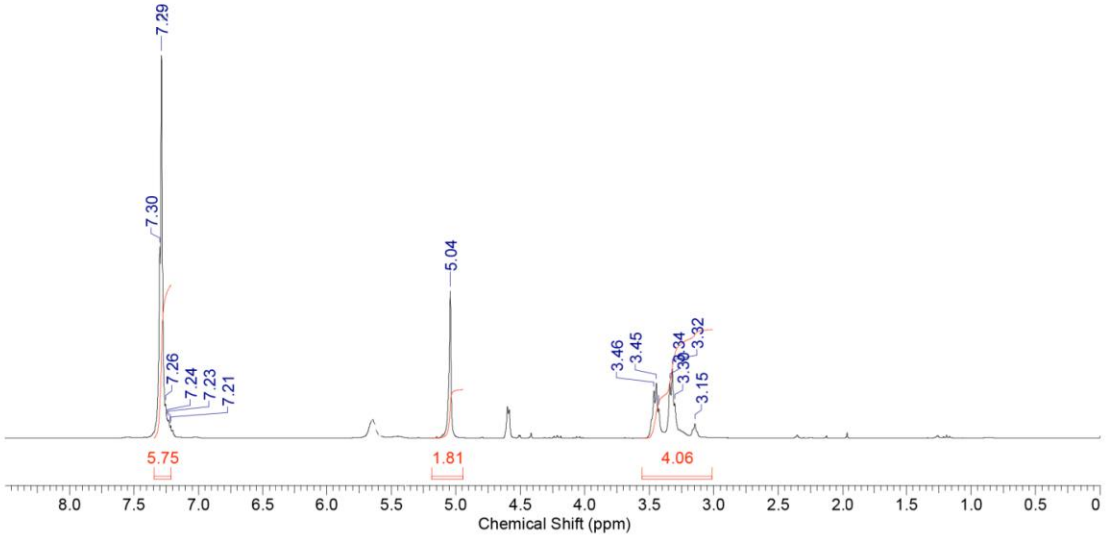
7.29
7.30
5.04
7.26
7.24
7.23
7.21
3.46
3.45
3.34
3.32
3.15
5.75
1.81
4.06
Chemical Shift (ppm)

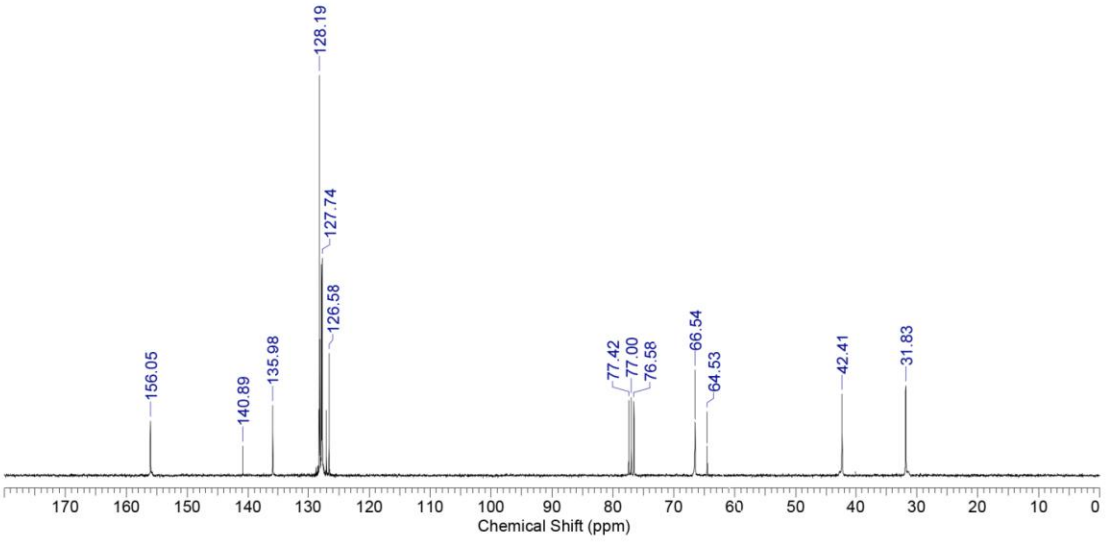
128.19
127.74
126.58
156.05
140.89
135.98
77.42
77.00
76.58
66.54
64.53
42.41
31.83
Chemical Shift (ppm)

Compound **6**

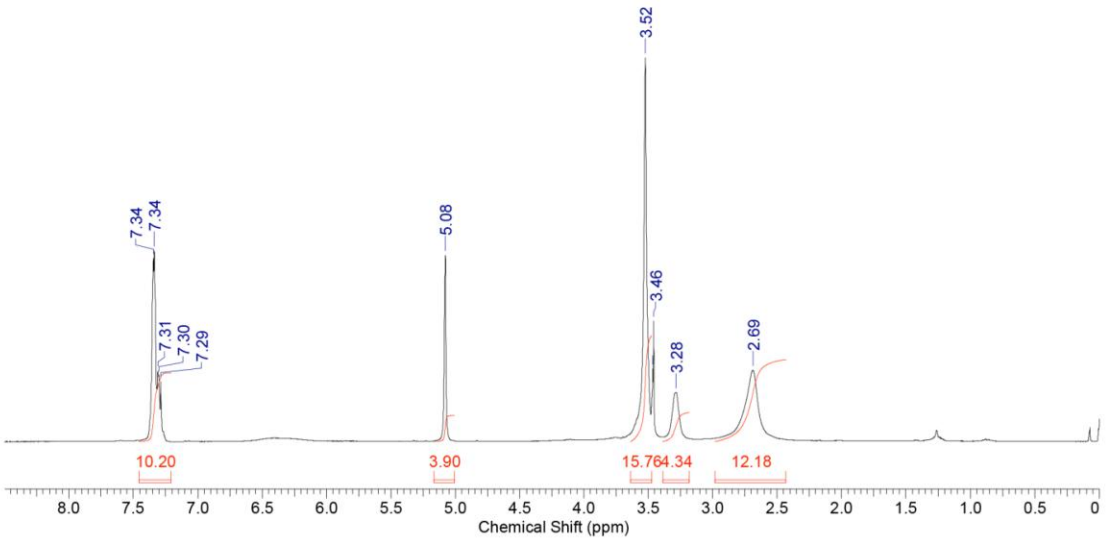
3.52
7.34
7.34
5.08
3.46
7.31
7.30
7.29
3.28
2.69
10.20
3.90
15.76
4.34
12.18
8.0 7.5 7.0 6.5 6.0 5.5 5.0 4.5 4.0 3.5 3.0 2.5 2.0 1.5 1.0 0.5 0
Chemical Shift (ppm)

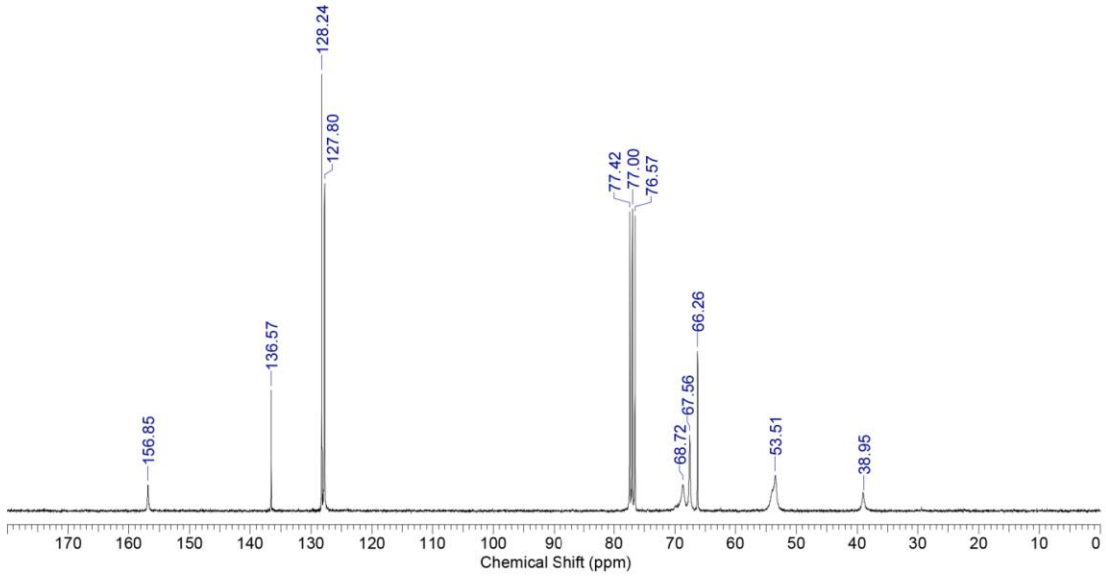
128.24
127.80
77.42
77.00
76.57
136.57
66.26
67.56
68.72
156.85
53.51
38.95
170 160 150 140 130 120 110 100 90 80 70 60 50 40 30 20 10 0
Chemical Shift (ppm)

Compound **7**

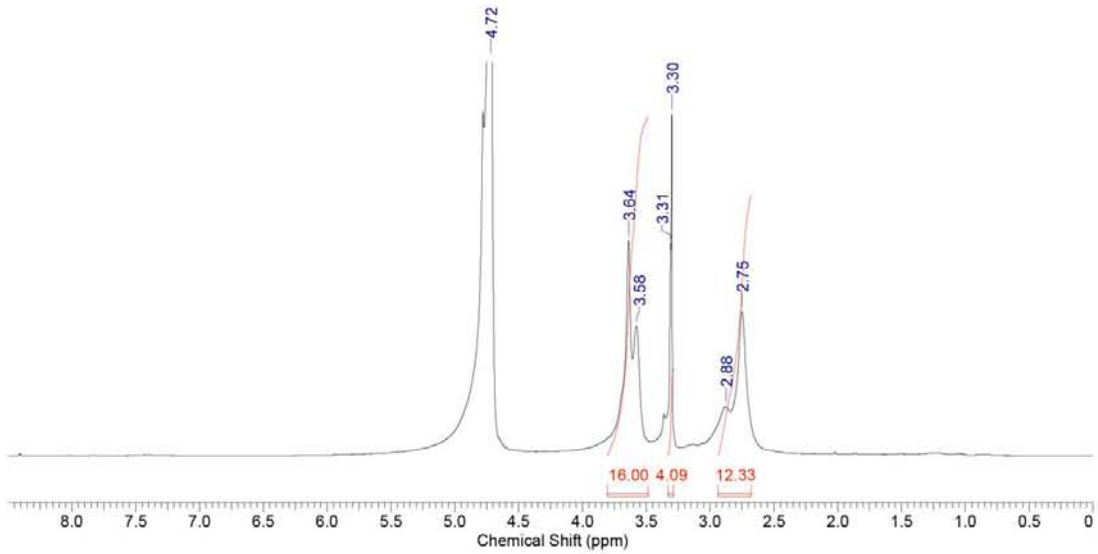
4.72
3.30
3.64
3.31
3.58
2.75
2.88
16.00
4.09
12.33
8.0 7.5 7.0 6.5 6.0 5.5 5.0 4.5 4.0 3.5 3.0 2.5 2.0 1.5 1.0 0.5 0
Chemical Shift (ppm)

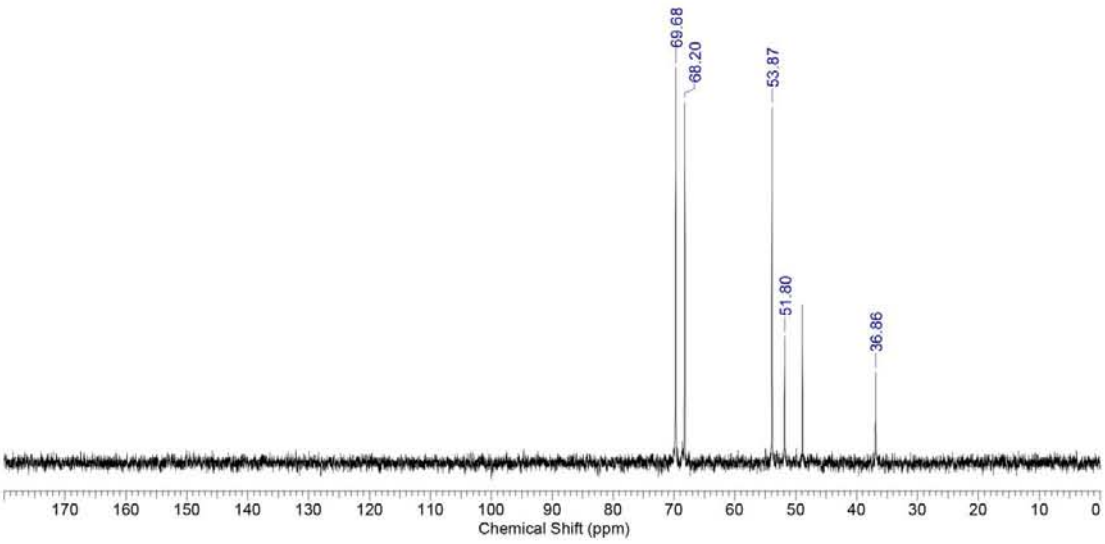
69.68
68.20
53.87
51.80
36.86
170 160 150 140 130 120 110 100 90 80 70 60 50 40 30 20 10 0
Chemical Shift (ppm)

Compound **8**

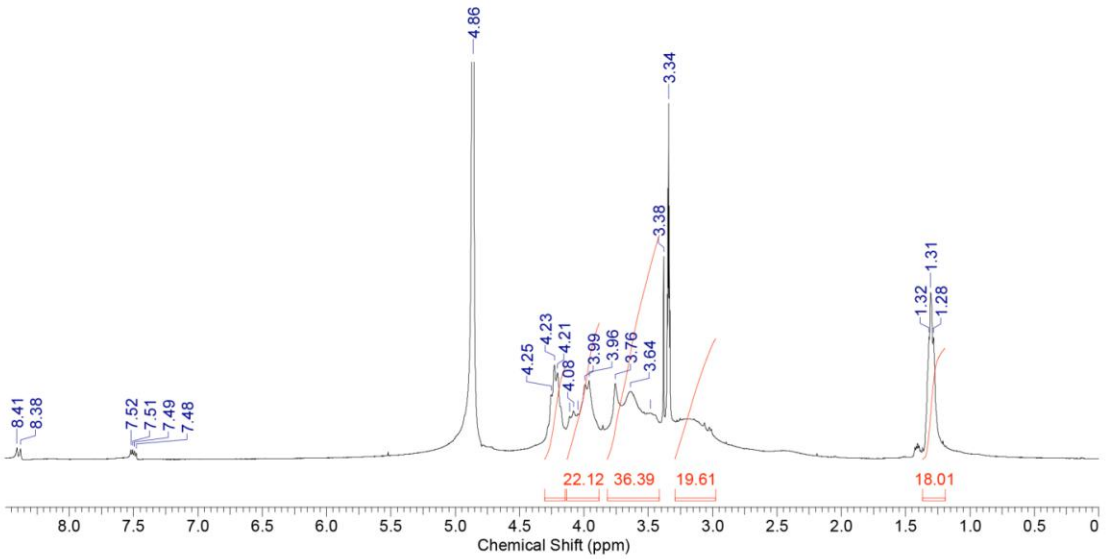
4.86
3.34
3.38
1.32
1.31
1.28
4.25
4.23
4.21
4.08
3.99
3.96
3.76
3.64
8.41
8.38
7.52
7.51
7.49
7.48
22.12
36.39
19.61
18.01
Chemical Shift (ppm)

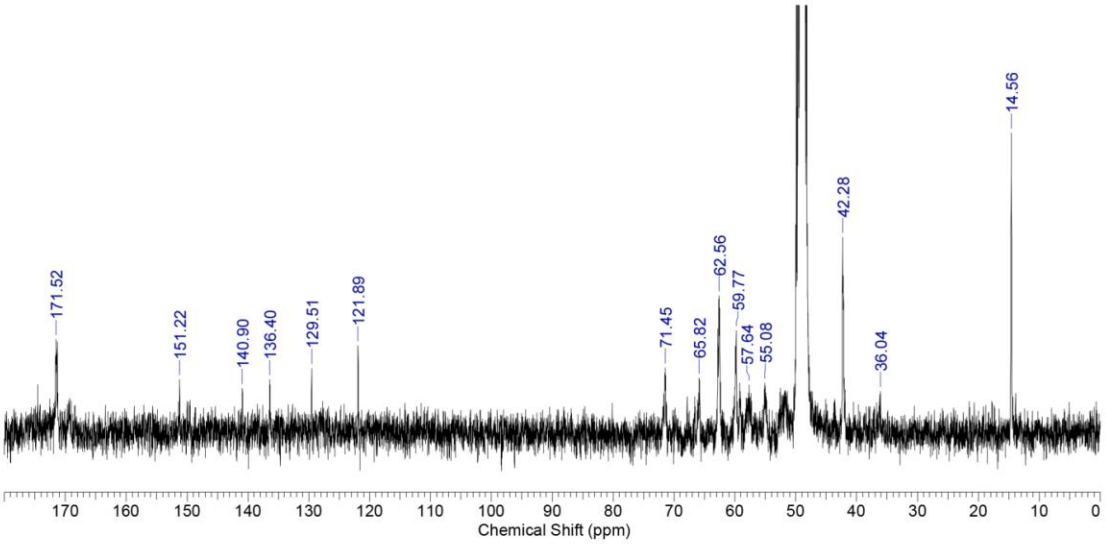
171.52
151.22
140.90
136.40
129.51
121.89
71.45
65.82
62.56
59.77
57.64
55.08
42.28
36.04
14.56
Chemical Shift (ppm)

Compound **H_6L**